THÈSE

En vue de l'obtention du

DOCTORAT DE L'UNIVERSITÉ DE TOULOUSE

Délivré par : *l'Université Toulouse 3 Paul Sabatier (UT3 Paul Sabatier)*

Présentée et soutenue le *28/09/2018* par :
Maria **KAZAKOVA**

Modèles dispersifs de propagation de vagues: Problèmes numériques et modélisation

JURY

SYLVIE BENZONI-GAVAGE	Université de Lyon	Présidente
CHRISTOPHE BESSE	Université de Toulouse 3	Examinateur
MATTHIAS EHRHARDT	Bergische Universität Wuppertal	Rapporteur
SONIA FLISS	ENSTA ParisTech	Examinatrice
SERGEY GAVRILYUK	Aix-Marseille Université	Examinateur
DAVID LANNES	Université de Bordeaux	Rapporteur
PASCAL NOBLE	INSA Toulouse	Directeur de Thèse

École doctorale et spécialité :
> *MITT : Domaine Mathématiques : Mathématiques appliquées*

Unité de Recherche :
> *Institut de Mathématiques de Toulouse (UMR 5219)*

Directeur de Thèse :
> *Pascal NOBLE*

Rapporteurs :
> *David LANNES* et *Matthias EHRHARDT*

Abstract

Key words:
water waves, shallow water, dispersive models, vorticity, artificial boundary conditions

Water waves propagation is a complex physical process. The direct numerical simulation using Navier-Stokes/Euler equations is a time-consuming and mathematically complicated solution. A good description of large-scale phenomena can be obtained by using relatively simple approximate models. However, if we are interested in a precise description of wave profiles, advanced modelling approaches are required. Once the model is derived, it needs to be solved numerically, and one faces another kind of challenges related to numerical simulations.

The first part of the present thesis is devoted to the modelling of surface and internal ocean waves propagation, including dispersive effects and dynamics of the vorticity. In the framework of shallow water hypothesis, two models are derived. Both models involve additional equations for the vorticity evolution. To include the internal waves propagation, first, we consider a system of two immiscible fluids with constant densities. It represents a simple model of the ocean where the upper layer corresponds to the (thin) layer of fluid above the thermocline whereas the lower layer is under the thermocline. The second model includes a surf zone phenomenon. Shearing and turbulence effects in breaking waves are taken into account by a vorticity generation. Both models are governed by dispersive systems and reduce to a classical Green-Naghdi model in the case of vanishing vorticity. Additionally, an algorithm for the numerical resolution of the second model is proposed, and the validation by experimental results is performed.

When dispersive/non-hydrostatic effects are taken into account, this usually leads to more accurate models of wave propagation like Green-Naghdi equations, or the two models derived in the first part, for example. The counterpart is that such a type of models requires advanced numerical techniques. In particular, one of the main issues is to define boundary conditions allowing the simulation of wave propagation in infinite physical space but on bounded numerical domains. In the second part of the present research, we focus on a definition of such boundary conditions for the Green-Naghdi equations. Artificial boundary conditions are first proposed for the linearized system. Then we address a hyperbolic system recently proposed to approximate the Green-Naghdi equations. A relatively simple structure of this new hyperbolic system allows for successful applications of Perfect Matched Layer (PML) techniques in order to deal with artificial numerical boundaries. Numerical tests are performed to validate the proposed approaches. In result, we have a correct description of numerical boundaries for non-linear cases. We have shown that the PML equations can be applied to the nonlinear system. Both approaches are then reformulated to solve the problem of injecting propagating waves in a computational domain.

Résumé

Mots clés:

propagation de vagues, eaux peu profondes, modèles dispersifs, vorticité, conditions aux limites artificielles

La propagation des vagues est un phénomène complexe. La simulation directe de ce phénomène à l'aide des équations d'Euler ou de Navier Stokes à surface libre sont complexes et très coûteuses numériquement. Si certains phénomènes aux grandes échelles sont bien décrits par des modèles réduits plus simples à simuler numériquement, des modèles plus avancés sont nécessaires pour décrire des échelles plus fines.

La première partie de cette thèse est consacrée aux modèles prenant en compte les effets de vorticité. Deux modèles moyennés sur la profondeur sont dérivés sous l'hypothèse d'eau peu profonde. Le premier concerne la propagation des ondes de surface et des ondes internes dans le cadre d'un système de deux fluides non miscibles. Le deuxième est un modèle de propagation des ondes côtières. Les effets turbulents sont pris en compte à travers l'équation de vorticité. Un algorithme numérique est construit pour la validation du second modèle et des comparaisons avec des résultats expérimentaux sont proposées.

Dans la deuxième partie on s'intéresse à l'étude des conditions aux limites. Les problèmes initialement posés dans l'espace infini demandent des conditions aux limites spéciales pour le traitement numérique. On s'intéresse ici au cas des équations de Green-Naghdi. Dans un premier temps, des conditions aux limites transparentes sont dérivées, et des validations numériques sont proposées. Les tests montrent que des conditions aux limites similaires peuvent s'appliquer pour des ondes rentrantes. Dans un deuxième temps, on considère une technique de relaxation pour un système Green-Naghdi mis sous forme d'un système hyperbolique. En particulier, ce formalisme nous permet d'appliquer la technique de Perfect Mached Layers (PML) pour traiter les ondes sortantes et rentrantes.

Remerciements

Ces travaux de thèse ont été effectués à l'Université Toulouse III dans l'équipe MIP de l'Institut de Mathématiques de Toulouse, sous la direction de Pascal Noble, professeur à l'INSA de Toulouse.

Je tiens tout d'abord à remercier mon directeur de thèse, Pascal Noble. Tout au long de ces trois années, j'ai pu apprécier sa vision de la recherche, ses nombreuses compétences mathématiques et sa capacité à voir l'essentiel des problèmes. Je le remercie pour m'avoir laissé la possibilité de choisir les sujets qui m'intéressent et la confiance placée en moi; je le remercie à la fois pour ses conseils sur la recherche, mais aussi à propos de la vie en France en general qui m'ont toujours servi.

Je remercie chaleureusement David Lannes pour avoir accepté d'être rapporteur de cette thèse et d'avoir fait part de mon jury, pour sa relecture très attentive, et ses remarques qui m'ont permis de beaucoup clarifier la présentation des résultats. Je le remercie pour son intérêt constant sur mes thématiques de recherche et ses réactions positives aux conférences où j'ai eu la possibilité de présenter mes travaux. Je remercie très sincèrement Matthias Ehrhardt qui a également accepté d'être rapporteur. Merci pour les discussions fructueuses que nous avons pu avoir sur les questions ouvertes et les voies possibles pour les résoudre. Merci également pour avoir fait la route depuis Berlin pour faire partie de mon jury. C'est un veritable honneur pour moi qu'un tel duo ait pu examiner mes travaux sur ce sujet.

Je remercie très sincèrement Sylvie Benzoni-Gavage de m'avoir fait l'honneur participer au jury de thèse. Je lui suis reconnaissante pour l'intérêt porté à mes travaux. Je remercie Christophe Besse pour avoir accepté de faire part de mon jury et partagé avec moi ses compétences, notamment au niveau des tests numériques sur les conditions aux limites artificielles.

Je remercie très chaleureusement Sergey Gavriluyk qui suit mon parcours scientifique depuis le début. Je le remercie particulièrement de m'avoir fait part de ce projet de thèse à Toulouse. Je ne regretté pas de lui avoir fait confiance sur le fait que l'équipe toulousainne est une belle équipe et que je m'entendrai bien avec eux. Et je remercie sincèrement Sergey pour ses discussions scientifiques toujours très motivantes. Merci d'avoir affronté les imprévus liés au trajet ferroviaire pour participer à mon jury de thèse.

Je remercie vivement Sonya Fliss pour sa participation dans mon jury. Je lui suis reconnaissante de m'avoir donné la possibilité de rejoindre l'équipe POEMS pour les années prochaines à l'occasion de mes recherches post doctorales sur un nouveau projet passionnant. Je rajoute un merci à Maryna Kochanovska pour sa participation à la préparation de ce nouveau projet.

Je remercie très chaleureusement Gaël Richard pour mon initiation à la recherche sur les

vagues cotières qui s'est révélée être un sujet très passionnant avec beaucoup de questions ouvertes, et qui a pris une place importante dans mes travaux de thèse. Et je remercie Gaël pour m'avoir fait confiance et pour tous ses conseils, son aide dans la préparation des présentations et tous les heures consacrées aux expériences numeriques qui nous ont permis de boucler le travail sur un modèle très prometteur en termes d'applications.

Je remercie mes collègues Jean-Paul Vila, Rémy Baraille, Fred Couderc et Florent Chazel pour m'avoir communiqué leur passion sur les problèmes en mecanique des fluides et leur motivation. C'était un honneur pour moi de faire part de cette belle equipe.

Je tiens à remercier Jean-Michel Roquejoffre et Violaine Roussier-Michon pour l'organisation regulière du groupe du travail au cours duquel j'ai pu présenter les avancées de mes travaux de thèse. Il s'agit d'une execellente opportunité pour s'exercer à présenter ses résultats et apprendre à bien motiver ses objectifs scientifiques.

Je voudrais aussi exprimer mes sincères remerciements à mes collègues de Novossibirsk, et notamment Sergey Golovin, pour mon introduction dans ce monde scientifique, pour sa confiance en mes capacités et un soutien appuyé à ma décision de venir en France.

Je voudrais aussi exprimer mon amitié aux personnes avec qui j'ai eu le plaisir de partager ses années de thèse au département du GMM de l'INSA de Toulouse où l'ambiance est très agréable, tant d'un point de vue scientifique que personnel. Merci particulièrement à Léo pour avoir pu compter sur toi tout le long de ma thèse, pour ton soutien dans la dernieère phase de ma thèse, nos joggings et nos seances à la salle. Je remercie Romain pour nos TPs et ton sens de l'humour que j'apprécie beaucoup. Merci à Victor, Clémentine, Melisande, Lorick et Sandrine, et Sandrine, Jessica, Robin et Willy et tous les members du GMM de l'INSA, sans vous tous l'ambiance du laboratoire ne serait pas si fantastique. Et un merci à Ilya pour nos discussions scientifiques toujours fructueuses.

Pour la fin je garde des remerciements personnels à mes amis et ma famille. Je remercie mes copains toulousains qui ont partagé ces années avec moi. Seb, Daisy, Matt, Sarah, Alex et Marc, merci pour avoir été à mes côtés pour m'écouter, m'apprendre le français et la gastronomie (même si la raclette en été c'est un peu tsoin-tsoin), pour les promenades et nos sessions du sport. Je vous remercie pour m'avoir formé à vos références humoristiques et à comprends les gens qui parlent très vite, et plein d'autres choses que moi même je ne remarque plus.

Je remercie Zeinab et Tillmann. Les deux personnes que j'ai eu de la chance rancontrer dès mon arrivé en France, et qui sont restées avec moi jusqu'à mon départ de Toulouse. Ravie d'avoir pu découvrir Toulouse et franchir les barrières administratives à vos côtés, c'était beaucoup plus simple et plus sympa ensemble.

Je remercie mes amis de longue date Ksenia, Anna, Alyona et Masha. Anna-let, je te remercie pour ton soutien et nos voyages. Je remercie mes copines Maya, Ira et Liza pour avoir trouvé le temps de venir partager des petits épisodes de ma vie toulousaine. Je souhaite exprimer toute ma reconnaissance à ma famille. Merci pour votre soutien et votre confiance. Mecri à vous tous de vous sentir si proches malgre la distance.

Mes derniers remerciements - mais peut-être les plus essentielles - vont à Arnaud. Pour son soutien, pour ses encouragements constants. Tu m'as fourni un appui inestimable au cours des derniers mois de ma thèse.

Я очень благодарна мои верным друзьям. Спасибо за безусловную поддержку Ксю-

ше, Маше, Ане и Алёнке, простоту и юмор с которыми вы научили меня (а я может быть вас) подходить к любой непонятной задаче. Спасибо Ane-let, за поддержку, за советы, за наши путешествия, за твоё участие в моей жизни. Спасибо Майке, Иринке и Лизе, что нашли возможность разделить со мной эпизод, хоть и совсем коротенький, моей тулузской жизни. Спасибо вам всем, что несмотря на то, что мы далеко, мы все же близко.

Я хочу выразить мою самую глубокую признательность моей семье за их поддержку и ободрения. Спасибо за вашу веру в меня. Мама, папа, бабушка, дедушка, Наташа, Лёша, Таня, Дима, Костя, Фёдор и Илья, я знаю, в любой ситуации вы меня поддержите.

A vous tous...

Merci

Table of contents

Introduction

The mathematical description of fluid motions needs to be grounded in physical laws. Essential assumptions about mass, momentum and energy conservation form a basis for the following derivation of mathematical equations of the medium motion. The description, understanding, or even prediction of medium behaviour comes then from the mathematical analysis of the equations, usually partial differential equations (PDE), or less often ordinary differential equations (ODE).

We are interested in the present research in the derivation of mathematical models of dispersive wave propagation and particular numerical issues related to such models. The principal purpose of the first part of the present thesis is to include additional physical effects into classical dispersive wave models in order to describe correctly wave profiles. The second part deals with particular numerical issues related to numerical boundaries. The discretization of dispersive models requires in particular special boundary conditions allowing the simulation of wave propagation in infinite (or very large) physical space but on bounded numerical domains. In the second part such conditions are derived for some particular models.

Before proceeding to central topics, we consider briefly in this introduction classical well-known general theoretical results and notions which we rely on in the following chapters of the present research. Further analysis of the recently proposed studies including results focusing on particular problems is proposed in each of the two parts of the present thesis.

Focus on the Euler equations

We consider first the derivation of the equations of motion ([80], [32]). The moving fluid is described by a law of the particles motion of the form $\vec{x} = \vec{x}(t, \vec{\xi})$, where $\vec{\xi}$ is an initial position of the particles,

$$\vec{x}\Big|_{t=0} = \vec{\xi}, \text{ and the fluid velocity is defined as } \mathbf{v} = \frac{\partial \vec{x}(t, \vec{\xi})}{\partial t}.$$

To complete the fluid motion description, the pressure $\mathbf{p}$ and density $\boldsymbol{\rho}$ need to be defined as well.

There exist two classical approaches to the motion description. The *Lagrangian specification* consists in the observation of each fluid particle moving in space and time. All unknown quantities are related to the Lagrangian coordinate $\vec{\xi}$ (note that $\vec{\xi}$ is constant for a given parcel during the media motion and when we need to consider the domain as a whole, $\vec{\xi}$ has the role of being the independent, spatial coordinate): velocity $\mathbf{v} = \mathbf{v}(t, \vec{\xi})$,

pressure $\mathbf{p} = \mathbf{p}(t, \vec{\xi})$, etc. In the *Eulerian specification*, all quantities are represented as a function of the spatial position $\vec{x}$: $\mathbf{v} = \mathbf{v}(t, \vec{x})$, $\mathbf{p} = \mathbf{p}(t, \vec{x})$, etc. In most cases it is more convenient to use Eulerian description for the stationary ($\mathbf{v} = \mathbf{v}(\vec{x})$) and potential motions ($\mathbf{v} = \nabla\varphi$). We will consider only Eulerian description $\vec{x} = (x, y, z)$, although, in some cases the Lagrangian one is preferable.

The integral conservation laws are written for the mass, momentum and energy in the form

$$\frac{d}{dt} \int_{\Omega(t)} \boldsymbol{\rho} \, d\Omega + \int_{\partial\Omega(t)} \boldsymbol{\rho}\mathbf{v} \cdot \vec{n} \, d\Sigma = 0,$$

$$\frac{d}{dt} \int_{\Omega(t)} \boldsymbol{\rho}\mathbf{v} \, d\Omega + \int_{\partial\Omega(t)} \left(\boldsymbol{\rho}\mathbf{v}(\mathbf{v} \cdot \vec{n}) - \mathcal{P} \cdot \vec{n} \right) d\Sigma = \int_{\Omega(t)} \boldsymbol{\rho}\vec{g} \, d\Omega, \tag{1}$$

$$\frac{d}{dt} \int_{\Omega(t)} \boldsymbol{\rho} \left(\frac{|\mathbf{v}|^2}{2} + \boldsymbol{\rho}\vec{g}z \right) d\Omega + \int_{\partial\Omega(t)} \left(\boldsymbol{\rho} \frac{|\mathbf{v}|^2}{2} - \mathcal{P} + \boldsymbol{\rho}\vec{g}z \right) (\mathbf{v} \cdot \vec{n}) \, d\Sigma = 0,$$

where $\Omega(t)$ is a fluid volume with smooth boundary $\partial\Omega$, n is the unit outward normal to $\partial\Omega$ and $\cdot$ denotes scalar product. It is supposed that the volume $\Omega(t)$ experiences a resulting force which includes external forces and internal surface forces defined by a tension vector $\mathcal{P} \cdot \vec{n}$. We consider here the case where external action is limited to the the gravity forces, and $\vec{g} = (0, 0, -g)$. However, as external forces, we can also consider the Coriolis force, or forces resulting from the bottom motion of wind action.

The modelling of the term $\nabla \cdot \mathcal{P}$ depends on the media properties. Generally, $\mathcal{P}$ is supposed to be a function of the Cauchy's strain tensor D defined as

$$D = \frac{1}{2} \left(\frac{\partial\mathbf{v}}{\partial\vec{x}} + \frac{\partial\mathbf{v}}{\partial\vec{x}}^{\top} \right),$$

where $\top$ stands for transposition. However, in the case of incompressible *perfect (non-viscid) fluid*, the tension tensor is written simply $\mathcal{P} = -\mathbf{p}\mathcal{I}$, where $\mathcal{I}$ is the identity tensor.

In order to write the system of integral laws (1) as a system of PDEs, we use the *Reynolds transport theorem* [107] (originally found in [115]), which for an arbitrary differentiable function f reads

$$\frac{d}{dt} \int_{\Omega(t)} f \, d\Omega = \int_{\Omega(t)} \left(\frac{\mathrm{D}f}{\mathrm{D}t} + f\nabla \cdot \mathbf{v} \right) d\Omega.$$

Above we employed the widely used notation in fluid mechanics for the *material derivative*

$$\frac{\mathrm{D}f}{\mathrm{D}t} = \frac{\partial f}{\partial t} + \mathbf{v} \cdot \nabla f. \tag{2}$$

Finally, it leads to the well-known system of Euler equations for incompressible flows:

$$\begin{cases} \nabla \cdot \mathbf{v} = 0, \\[2mm] \dfrac{\partial\boldsymbol{\rho}}{\partial t} + \mathbf{v}\nabla \cdot \boldsymbol{\rho} = 0, \\[2mm] \dfrac{\partial\mathbf{v}}{\partial t} + (\mathbf{v} \cdot \nabla)\mathbf{v} = -\dfrac{1}{\boldsymbol{\rho}}\nabla p - g\vec{e}_z. \end{cases} \tag{3}$$

The system (3) is closed. The energy conservation law follows from mass and momentum equations. On the contrary, for compressible flows, one needs to close the system with a state equation.

In the present study, we consider incompressible constant-density flows ($\boldsymbol{\rho} = \rho = const$), and the Euler system is written even easier:

$$\begin{cases} \nabla \cdot \mathbf{v} = 0, \\[2mm] \dfrac{\partial \mathbf{v}}{\partial t} + (\mathbf{v} \cdot \nabla)\mathbf{v} = -\dfrac{1}{\rho}\nabla p - g\vec{e}_z. \end{cases} \tag{4}$$

To study the fluid motions, the system (4) generally needs to be completed with initial and boundary conditions. The consistent initial data for the velocity are given as

$$\mathbf{v}(t, \vec{x})\Big|_{t=0} = \mathbf{v}_0(\vec{x}), \text{ such that } \nabla \cdot \mathbf{v}_0(\vec{x}) = 0.$$

Different common types of boundaries might be considered in applications:

1. Rigid walls (impermeability condition):

   $$(\mathbf{v} - V) \cdot \vec{n}\,\Big|_{\Gamma} = 0, \text{ where } V \text{ is a velocity of the moving boundary } \Gamma.$$

   If the rigid boundary is given by the equation $F(t, \vec{x}) = 0$, then

   $$V = -\frac{F_t}{|\nabla F|} \ (F_t \text{ denotes the time derivative}).$$

2. Boundary between two fluids (fluid-fluid interface):

   a. Kinematic condition ($\mathbf{v}_I$, $\mathbf{v}_{II}$ are velocities of the two fluids at the boundary Γ):

   If the interface is described by $F(t, \vec{x}) = 0$, then the conditions are

   $$F_t + \mathbf{v}_I \cdot \nabla F = \mathbf{v}_{II} \cdot \vec{n},$$
   $$F_t + \mathbf{v}_{II} \cdot \nabla F = \mathbf{v}_I \cdot \vec{n}.$$

   b. Dynamic condition ($\mathbf{p}_I$, $\mathbf{p}_{II}$ are pressures of the two fluids at the interface Γ):

   $$\mathbf{p}_I = \mathbf{p}_{II};$$

3. Free-surface condition:

   a. Kinematic condition:

   If the free surface is described by $z = h(t, \vec{x})$, then

   $$\frac{\mathrm{D}F(t, \vec{x})}{\mathrm{D}t}\Big|_{\Gamma} = 0, \text{ where } F(t, \vec{x}) = h(t, \vec{x}) - z;$$

   b. Dynamic condition:

   $$\mathbf{p} = 0 \text{ (if atmospheric pressure is normalized to zero).}$$

The principal challenge in solving problems with free surfaces and fluid interfaces lies in the determination of the unknown boundary where the conditions are established.

In the description of the fluid motion, one of the important quantities is defined as the curl of the flow velocity $\mathbf{v}$, namely ($\vec{x} = (x, y, z)$, indices denote derivatives)

$$\boldsymbol{\omega} = \nabla \times \mathbf{v} = \nabla \times \begin{pmatrix} u \\ v \\ w \end{pmatrix} = \begin{pmatrix} w_y - v_z \\ u_z - w_x \\ v_x - u_y \end{pmatrix}, \tag{5}$$

and referred to as *vorticity*. Vorticity field describes the rotating motion of the fluid. The knowledge of the vorticity distribution allows for the velocity reconstruction in some cases.

The Lagrange theorem [54] reads as: *In a perfect barotropic fluid moving in potential field, the volume of fluid that is initially irrotational remains irrotational.*

In order to demonstrate this mathematically, we provide the equation for the vorticity evolution. Applying 'curl' operator to the momentum equation and using the mass conservation law, one finds the *vorticity equation*

$$\frac{\partial \boldsymbol{\omega}}{\partial t} + (\mathbf{v} \cdot \nabla)\boldsymbol{\omega} - (\boldsymbol{\omega} \cdot \nabla)\mathbf{v} = 0.$$

The term $(\boldsymbol{\omega} \cdot \nabla)\boldsymbol{\omega}$ relates to a vorticity advection by the velocity field, while the term $(\mathbf{v} \cdot \nabla)\boldsymbol{\omega}$ represents rotation and stretching of vortex lines. However, there are no terms which relate to the vorticity generation. Nevertheless, the effect of viscosity implies the diffusion of vorticity in the fluid, in addition to advection, since the Laplace operator $\Delta\boldsymbol{\omega}$ appears in the equation. Moreover, vorticity may be generated if the external force field is not a potential.

The Euler system of equations is well studied in particular cases. First, the integral relations such as Bernoulli and Cauchy-Lagrange integrals can be derived as corollaries of the energy conservation law [80], [54]. Furthermore, effective mathematical tools are developed for studying *potential flows*, where $\nabla \times \mathbf{v} = 0$ (see, for example, §9, [80]). It implies that one can define the *potential* φ as $\mathbf{v} = \nabla\varphi$. If the flow is two-dimensional, the stream function ψ is introduced as $\mathbf{v} = (-\partial\psi/\partial x, \partial\psi/\partial y)$. Then powerful tools of the theory of functions of a complex variable can be applied to the holomorphic function $\mathcal{F} = \varphi + i\psi$ (i is the imaginary unit) in order to simplify the analysis of flow characteristics. Classes of exact solutions are provided for many different physical conditions.

The Euler equations involve different physics beyond them when different external force fields are considered. The domain of application is vast, from small-scale effects, such as surface tension, or boundary layer, to large scale ocean wave propagation, for example.

Water Waves

When waves propagate under the gravity action, dispersive effects are observed. In water waves theory the dispersion is related to the frequency dispersion, which means that the velocity of wave propagation depends on its wavelength.

When gravity water waves are studied mathematically, the linear theory is used as a first approximation. Let us consider a potential flow. The equations for the potential φ are obtained from equations of motion and boundary conditions discussed above (the motion over a flat bottom $z = 0$ is assumed, and the free surface displacement is defined as

$z = h(t, x, y))$

$$\Delta \varphi = 0,$$

$$\frac{\partial \varphi}{\partial z} = 0, \quad z = 0,$$

$$\frac{\partial h}{\partial t} + \frac{\partial \varphi}{\partial x}\frac{\partial h}{\partial x} + \frac{\partial \varphi}{\partial y}\frac{\partial h}{\partial y} = \frac{\partial \varphi}{\partial z}, \quad z = h(t, x, y),$$

$$\frac{\partial \varphi}{\partial t} + \frac{1}{2}|\nabla \varphi|^2 + gh = 0, \quad z = h(t, x, y).$$

(6)

The momentum equation is replaced by the Cauchy-Lagrange integral which is used for the pressure definition. Therefore the dynamic boundary condition is written as above. This mathematical system is referred to as *Cauchy-Poisson problem*. For more details on this and other models and methods, we refer to [54].

The fundamental issue of water wave problem is that the free surface is unknown, and the boundary condition is an additional equation to solve.

The *dispersion relation* relating the frequency and the wavenumber is defined by the linear analysis (which is also referred to as *Stokes linear theory* [128]). The system is linearized around the state $\varphi = 0$, $h = const$. The solution is constructed in the form of wave packets:

$$\varphi(t, x, y) = \Phi(z)exp\{i(kx + ly - \omega t)\},$$
$$h(t, x, y) = H(z)exp\{i(kx + ly - \omega t)\}.$$

The functional dependence between frequency ω and magnitude of the wave number $m = \sqrt{k^2 + l^2}$ is defined as ([128], [79, §228]):

$$\omega^2(k) = gm \tanh(mh)$$

(7)

where tanh denotes the hyperbolic tangent.

Even though the Euler equations are studied well, they remain very costly from a numerical point of view (whether for small and large scale oceanic simulation), since the equations need to be resolved in a fully $3D$ statement. Therefore, more simple approximate models are required. The dispersion relation (7) is used as a criterion to evaluate the dispersion property of an approximate model and determine its limits of validity.

On a shallow-water approximation

In the present thesis, we consider approximate depth-average models derived under the hypothesis of *long water waves* (or *shallow water hypothesis*). It is assumed that the characteristic wavelength L is much larger than the characteristic water depth H. The parameter $\mu = H/L$ is called *dispersion parameter* and plays an essential role in the approximate model derivations. The hypothesis $\mu \ll 1$ corresponds to small water depth or very long waves. The consideration of different orders of the system expansion with respect to μ allows for a simplification of the equations, while keeping still some significant physical effects in this specific regime. The *depth-average procedure* (mathematically, corresponds to the integration from the bottom to the free surface with respect to z, see e.g. [81]) allows to reduce the dimension of the problem. Thus, approximate systems couple the equations

for the average velocity and free surface elevation. In this context, approximate models in a two-dimensional space (x, z) are commonly referred to as a one-dimensional (1D) models, because z is not included explicitly. Similarly, two-dimensional depth-average (2D) models correspond to the physical space (x, y, z).

Let us first consider classical examples of such models. The velocity is supposed to be uniform over the depth for the models considered below. We limit ourseves to the 1D models only, the generalization to the 2D case is following the same lines.

Many asymptotic models were proposed in the last decades for the coastal wave propagation under hypothesis made on μ. The first approximation of lower order with respect to μ is the well-known nonlinear shallow water (Saint-Venant) equations ($h(t, x)$ is the free-surface elevation as before, $u(t, x)$ – depth-average velocity)

$$\begin{cases} \dfrac{\partial h}{\partial t} + \dfrac{\partial hu}{\partial x} = 0, \\[2mm] \dfrac{\partial hu}{\partial t} + \dfrac{\partial}{\partial x}\left(hu^2 + \dfrac{gh^2}{2}\right) = 0. \end{cases} \tag{8}$$

De Saint Venant first proposed this model in 1871 [39], and it was established later that the model (8) could be derived from the depth-average Euler equations as a model of order $\mathcal{O}(\mu^2)$. This system is hyperbolic and prescribes discontinuous solutions for some initial datum. Moreover, the dispersion relation is linear and no frequency dispersion is observed for the solutions, and pressure distribution is supposed to be hydrostatic. However, in the context of coastal ocean flows this model (fully justified in [81]) prescribes non-dispersive wave behaviour relatively well [25].

As we see, significant simplifications come from the assumptions of shallow water (as a consequence of hydrostatic pressure) and uniform velocity. This leads us to a next class of approximate equations, commonly referred to as Boussinesq type models. The pressure is now supposed non-hydrostatic, though, the weakly dispersive and weakly nonlinear effects are included. The terms of order $\mathcal{O}(\mu^3)$ are neglected, and an additional hypothesis of small wave amplitude a is made. The new small *nonlinearity parameter* $\varepsilon = a/H$ is introduced, which is supposed to be small $\varepsilon = \mathcal{O}(\mu)$. A review of the different type of such models can be found in [93], [82].

The natural generalization of weakly nonlinear Boussinesq models is to derive a fully-nonlinear model. The one derived by Serre in [124] for the 1D case, or the 2D model presented in [57], is now referred to as the *Green-Naghdi model* or the *fully nonlinear Boussinesq model*. The terms of third order are neglected again, but no hypothesis on the wave amplitude is made, see e.g. [81] for details. The system couples again the equations for free surface and depth-averaged velocity

$$\begin{cases} \dfrac{\partial h}{\partial t} + \dfrac{\partial hu}{\partial x} = 0, \\[2mm] \dfrac{\partial hu}{\partial t} + \dfrac{\partial}{\partial x}\left(hu^2 + \dfrac{gh^2}{2} + h^2\dfrac{\mathrm{D}^2 h}{\mathrm{D}t^2}\right) = 0, \end{cases} \tag{9}$$

where $\mathrm{D}/\mathrm{D}t$ denotes again the material derivative (2). A mathematical justification of the Green-Naghdi model is given in [97] and in [4], [81]. The dispersive properties of

the system (9) fit well to the ones obtained by Stokes which we discussed above. Being rigorously justified and having good dispersive properties, the Green-Naghdi model became very attractive in applications to shallow-water flows [21], [86], [43], [84]. Moreover, Green-Naghdi equations admit a solution of a particular form referred to as *solitary wave*. It is a travelling wave propagating in time without deformation (observed firstly by Russell [121]). The existence of such a type of wave results from the balance between nonlinear and dispersive effects.

Additionally, the effects of topography can be included in all classes of approximate models discussed above.

Dispersive properties and turbulent motions

Generally speaking, during the derivation of the simplest model (8) the dispersive/non-hydrostatic effects were neglected. The two classes of approximate models discussed next are successful attempts to include essential physical effects such as dispersion into the model; while keeping, however, a relatively simple equations structure compared to the full Euler system.

The next step is to include a non-uniform velocity distribution assumption into the modelling. It should be noticed that the vorticity $\boldsymbol{\omega}$ defined previously by (5) is neglected in all the models described above due to the assumptions made when the models are derived. However, the vorticity effects are directly related to turbulent flows. Therefore for the modelling of turbulent motions, we must get rid of irrotational flow hypothesis. The Part I is devoted to the derivation of models taking into account vorticity dynamics. The first model is designed to apply to the surf zone wave propagation, where the wave breaking takes place, and flows are clearly turbulent. The second model considers internal waves propagation, where in order to include the interactions between surface waves and currents we allow for a general (or constant) vorticity.

If the velocity is assumed to be non-uniform over the depth, then an additional small term is included in the velocity decomposition, and a closure is required. This closure can be found from additional relations such as the energy conservation law or the vorticity equation as it is proposed in [117], [29].

More specifically, the non-uniform velocity assumption can be interpreted as *shearing effects*. These effects can be added directly to the non-dispersive system (8) as it was done in [137], and generalized with empirical dissipation in [117], [118]. The systems considered in these studies are hyperbolic, and vorticity generation is related to the shocks (discontinuities) formation. The vorticity equation is derived from the energy conservation law. These models provide a good description of hydraulic jumps and roll waves.

A non-uniform velocity profile is added to the dispersive models of Green-Naghdi type in [29], where several fully nonlinear models in the presence of vorticity are derived for the cases of constant vorticity in $1D$, general vorticity in $1D$ and $2D$; the terms up to $\mathcal{O}(\mu^4)$ are kept. This work deals with a conservative framework: to close the system the vorticity equation is used, which as we saw does not include terms related to the vorticity creation. However, the dispersive properties are better than the one of the Green-Naghdi model since higher order terms are included. Another distinctive feature of the proposed models
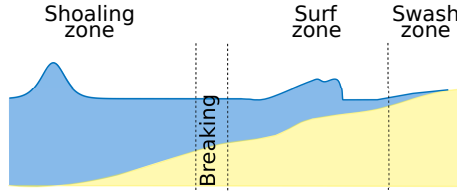
Figure 1: Wave propagation on a coastal zone.

is a coupling between surface waves and underlying currents retained in the framework of depth-averaged equations.

In [119] a dispersive model including the shearing effect is derived. Unlike the derivation in [29], this model allows for turbulence generation in the solitary wave propagation due to an additional distinction between shearing and turbulence based on the scales (these terms are of the same order with respect to μ in [29]). Therefore, additional terms are neglected. In Chapter 1 of the present thesis, we follow this idea in order to derive an approximate depth-average model for the description of surf zone propagation (Figure 1), where the vorticity and dispersive effects play an essential role. The wave breaking is a complex physical phenomenon which is hard to incorporate in the context of depth-average models. The main issue is to take into account dissipation effects and especially to find a way to include the vorticity generation during breaking in the context of dispersive models. For this purpose, following the idea found in [117], [118], a new variable *enstrophy* related to the second moment of the velocity fluctuation with respect to the vertical coordinate is added. Turbulent viscosity hypothesis governs the generation of the enstrophy. The final system couples the balance equations for mass and momentum with a transport equation for the enstrophy. Dissipation is empirically added, which leads to the introduction of constant empirical parameters. A numerical algorithm is constructed for this new model, and comparisons are performed with experimental data for solitary wave propagation over different mild slope topographies. Empirical laws for the parameters included in the model are proposed.

In Chapter 2, the one-layer models derived in [29] are generalized to the case of two-layer fluids. This study aims at taking into account the internal waves propagation in the presence of vorticity. We consider a two-layer flow of inviscid incompressible and immiscible fluids of constant densities. It corresponds to a simple model of wave propagation in the ocean, where the upper layer corresponds to the (thin) layer of fluid above the thermocline whereas the lower layer is under the thermocline (see Figure 2). The derivation is performed in the case of constant and general vorticity in $1D$. We reformulate the proposed model for constant vorticity as the Euler-Lagrange equations, following the considerations in [14] for the two-layer irrotational flow.

The Green-Naghdi equations are central in the present thesis. Both models derived in the first part reduce to the classical Green-Naghdi equations in the case of vanishing vorticities (or enstrophy). The models derived in the first part include some additional physical effects; however, they have a relatively close structure with the Green-Naghdi model (9). The second part is entirely devoted to particular numerical issues appearing when the system (9) is solved numerically.
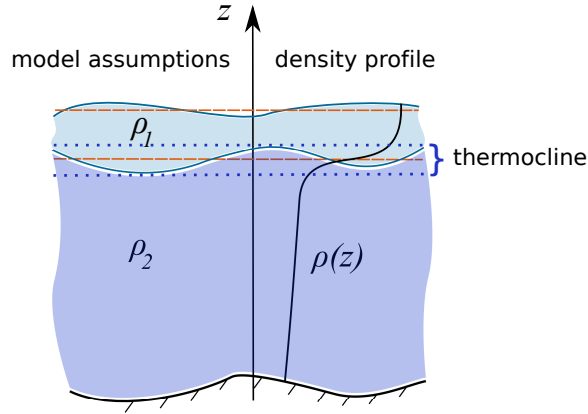
Figure 2: Modelling assumption and profile of the density distribution $\rho(z)$.

On particular boundary conditions

Part II deals with numerical issues which appear when dispersive models are integrated numerically. Common boundary conditions were discussed above. However, generally in the applications, we are interested in imposing a particular type of numerical conditions which are referred to as *transparent (or artificial) boundary conditions* (see, e.g. [46]), which are generally much harder to handle numerically.

Mathematical models for dispersive wave propagation are set on infinite domains. For real ocean waves, one can imagine a very large propagation domain as well. However, when the equations are solved numerically, one has to confine the numerical domain and deal with artificial numerical boundaries (see, Figure 3). The natural question of interest is how to impose the conditions for incoming and/or outgoing waves. This numerical issue also appears when different models are applied to describe wave propagation, and artificial boundary conditions are required in order to couple different models.

Mathematically, this numerical problem is formulated as follows: given an initial data compactly supported, one searches for suitable boundary conditions so that the solution computed with these boundary conditions approximates well on the bounded domain the solution set on the whole space. This issue is independent of the numerical algorithm used for the discretization, though the number of conditions may vary from one method to another. Dispersive models like the system (9), or other models discussed above, represent a significant challenge for this issue since they include high order derivatives.

Several techniques are used for now to deal with boundary conditions for simulations of systems set initially on unbounded domains. In Part II we consider two approaches in application to Green-Naghdi-type systems. First, in Chapter 3, transparent boundary conditions are constructed for the system (9) linearized around the steady state $h = h_0$, $u = 0$. We derive first continuous boundary conditions using the Laplace transform. These conditions are non-local in time and turn to be difficult to implement numerically. Then, following the approach proposed for example in [17] for the Airy equation, we start directly from the discretization of the equations set on the whole space and mimic the approach in the continuous case: the Laplace transform is replaced by its discrete counterpart, the $\mathcal{Z}$-transform. The technique is validated numerically for outgoing waves with different initial
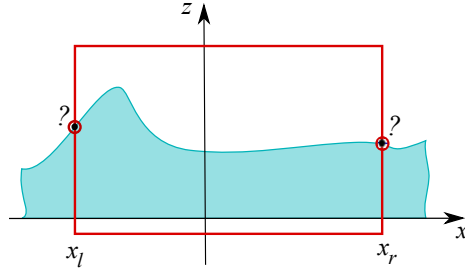
Figure 3: Numerical domain restriction for problem initially set on a infinite domain.

data. In addition, we show how to apply the proposed approach to a wave generation problem and investigate the accuracy of the proposed method with numerical tests. The derived conditions provide a good approximation of the solution on the original unbounded domain and permit to generate incoming waves. Unfortunately, these conditions may not be applied directly to the nonlinear Green-Naghdi (9), and a more complex strategy is needed. For example, one can imagine to adapt our strategy to linear equations with variable coefficients and then adopt a fixed point strategy.

In order to provide suitable conditions for the nonlinear case, in Chapter 4 we focus on a new hyperbolic formulation of the system (9) recently proposed in [49]. This new model represents a significant improvement in the simulations of dispersive waves since it is hyperbolic. It may also lead to simplifications of the construction of transparent boundary conditions, and if so this new system might be particularly promising for further applications in ocean wave modelling. Unfortunately, the proposed system does not admit a Riemann invariants form, and another approach needs to be proposed. We apply a technique which is referred to as *Perfectly Matched Layers (PML)*. In this case, no specific conditions are given on the artificial boundary, but the equations are modified inside small layers around the computational domain in such a way to ensure the wave amplitude decay and reflections are as small as possible inside the layers. These equations include generally several parameters. In Chapter 4, we are interested in the derivation of PML equations for this new Green-Naghdi system. The derivation of the PML equations and numerical validations for the linear case are provided first. We propose a preliminary stability result through an energy estimation of the solution of the resulting linear PML equations. Generalization in the weakly nonlinear case are partially justified, and then the proposed approach is successfully confirmed numerically. For the strongly nonlinear solitary waves, only small reflections are observed. The optimization of the parameters values, however, is left for the future work.

Outline

Finally, we emphasize briefly the main issues addressed in the present research:

- Part I is answering the question how to include the vorticity effects in the derivation of dispersive depth-average models. For the breaking waves, mechanisms of vorticity generation and energy dissipation are included in order to describe correctly the wave profiles. Then, internal gravity waves are modelled in the presence of vorticity effects.

- Part II deals with boundary conditions for Green-Naghdi type models in order to provide a proper procedure for the simulations of incoming and outgoing waves.

In the Annex Chapter A we examine the existence of a solitary wave solution for the hyperbolic extended formulation of the Green-Naghdi system derived in [49].

In Conclusions and Outlook the obtained results are summarised and perspectives for the future research are proposed.

Part I

Vorticity

Introduction : Vorticity effects

In the present part, we aim to derive dispersive shallow water models where vorticity effects are included. This leads to a natural generalization of the Green-Naghdi equations, applied in order to extend its validity to the regions where rip currents or wave breaking appear.

The classical hyperbolic nonlinear shallow water model [39], mathematically justified in [106, 4], is widely used for ocean wave propagation. However, in coastal regions, dispersive effects play a significant role and require an advanced modelling approach. The Green-Naghdi model [57, 124] is generally used for this purpose. Certainly, there are other models which consider dispersion effects, and we refer to [15] for a review. However, the Green-Naghdi model has relatively good dispersive properties with respect to the linear Stokes theory. Contrary to well-known one directional dispersive models as Korteweg–de Vries (KdV), or Benjamin-Bona-Machony equations, the Green-Naghdi model predicts bidirectional wave motion, which is physically more relevant. Moreover, unlike Boussinesq equations [23], the Green-Naghdi equations admit a closed form for solitary wave solutions. In [4], this model is reformulated using the Zakharov approach [150] with the non-local Dirichlet-Neumann operator. Fundamental properties of this operator allow for a rigorous justification of the model. For all of these reasons, the Green-Naghdi model is very popular for the numerical simulation of coastal wave propagation; for different numerical methods we refer for example to [35, 86, 22, 45, 83, 43].

It is known that the Green-Naghdi equations represent a depth-average second order approximation of the classical Euler equation under a shallow water hypothesis. The expansion is performed with respect to the dispersive parameter $\mu \ll 1$, defined as the ratio between the characteristic water depth H and the characteristic wavelength L. Therefore the associated dispersive relation slightly differs from the classical one and might be corrected in order to improve the dispersive properties. This question received a lot of attention recently. A fully dispersive model for small wave steepness is developed in [82], using correction terms in the expansion of the Dirichlet-Neumann operator. This model has the same dispersion relation than the one of the full water wave problem derived by Stokes. However, this model is valid in shallow water regimes with less precision than the Green-Naghdi equations. Another approach is considered in [22] where a small corrective term with some constant parameter is added artificially. This term is consistent with the approximation order of the model. The optimization of the constant parameter is proposed in order to have a dispersion relation close to the Stokes theory. Unfortunately, the inversion of the non-local in time operator is computationally time-consuming. This drawback, which is typically encountered in numerical methods used to integrate the Green-Naghdi system (or more generally, dispersive systems), was overcome in [83], where a time independent operator consistent with the approximation order of the model was introduced.

Another weakness of the Green-Naghdi model is an assumption of irrotational flow made during the model derivation. As a consequence, the vorticity effects are not included, and

the model is not valid any more in regions of vortical currents, for example, in the shoaling zone where wave breaking takes place or in cases of underlying current. The relation between vortex flows and surface wave propagation needs to be understood in order to extend the validity of the models.

During the past decade, there has been an increase of interest for the derivation of models with vorticity effects. In all these studies, it is supposed that the velocity profile is not uniform over the depth and therefore the depth-average procedure becomes more complicated. The Green-Naghdi equations are still able to describe the vertical vorticity conservation up to the order of approximation (see [31]). However, when a general vorticity is included, an additional term appears in the momentum equation, and a closure is needed [see 29, for details]. The *vorticity equation* is chosen as a closure in [29]. It follows from this equation that, if no empirical terms are added, the vorticity is conserved and transported. A more restrictive strategy is applied in [154], where a polynomial velocity profile is assumed, and a similar approach coupled with a shallow water hypothesis can be found in [109]. Despite a simplification assumption on the velocity profile, in this case, the $2D$ velocity field is truly $2D$, and equations need to be solved in the vertical direction. Rather, the essential feature of the model derived in [29] is that a non-uniform velocity profile with general vorticity is taken into account in the framework of a depth-averaged model, and therefore a physical $2D$ (or $3D$) flow is resolved in the $1D$ (or $2D$) statement. It is shown numerically in [84] that in the context of this model, new effects in wave-current interactions are possible.

A similar dispersive model derived in [119] generalizes the idea applied in [137], [117], [118] for the hyperbolic system with shearing effects. In order to allow for vorticity generation, a scaling analysis is performed with an additional distinction between shearing and turbulence, which is reminiscing the Reynolds decomposition for the velocity field. The new quantity related to the second moment of the velocity fluctuation is introduced and called enstrophy by analogy with thermodynamics. This model predicts the appearance of turbulence through the variation of the enstrophy.

In Chapter 1, a model capable to take wave breaking into account is derived. Following the idea found in [119] we use a filtering method as in the classical large-eddy simulation approach (instead of the Reynolds decomposition used in [119]). The energy transfer rate from the filtered scales towards the residual scales is assumed almost equal to the dissipation, and the empirical closure for the dissipation is proposed using a turbulent viscosity hypothesis. Then we apply a standard depth-average procedure. This procedure results in a nonlinear model having the same dispersive properties as the Green-Naghdi equation, capable to describe wave shoaling and surf zone propagation in the same time. The model features three empirical parameters, and closure relations are proposed for all of them. These dependencies give a predictive character to the model which is suitable for further developments. Numerical algorithms and validation by experimental results of the literature are proposed.

In Chapter 2, a generalization of the approach found in [29] is considered. In order to include the internal wave propagation, we consider a two-layer fluid with constant densities of each layer. This system represents a preliminary approximation of real density distribution in the ocean. Internal waves are a subsurface analogue of the familiar surface waves

that break on beaches. The breaking of internal waves, because of their strong vertical and horizontal currents, and the turbulent mixing, has a great impact on a panoply of oceanic processes (for experimental results we refer to [99]). It is then important to allow for vorticity effects when internal wave propagation models are derived.

There is a considerable variety of internal wave propagation models in the literature, as far as the possible scaling regimes in nature are numerous. We refer only to some studies performed under the shallow water (long wave) hypothesis. A weakly-nonlinear two-layer model is derived in [33], and then generalized to the fully nonlinear case in [34]. These models are compared with experimental observations and direct numerical simulations with the full Euler system in [27]. In [20], the two-layer full Euler system model is reduced to a system which involves a non-local operator under a rigid lid and flat bottom assumptions; the models mentioned above are recovered by an asymptotic expansion of this operator. The non-hydrostatic effects are also added in [42] in the regime of a medium amplitude. A Lagrangian approach is applied to the derivation of a two-layer generalization of the classical Green-Naghdi model in [14]. All models are derived under the assumption of irrotationality of the flow.

In the present work, we allow for the presence of constant vorticity and derive a $1D$ fully nonlinear model of the same approximation order $\mathcal{O}(\mu^3)$ as the classical Green-Naghdi equations. The model with a lower order than the Green-Naghdi model is derived in the case of a general vorticity. The terms related to vorticity are involved in the momentum equations, and only one vorticity equation is added in each layer in order to close the system. On the contrary, for the model derived in [29], the vorticity effects contribute to the averaged momentum by a cascade of equations following from the same vorticity equation since higher order terms are included.

Chapter 1

Modelling shoaling and breaking waves on a mild sloping beach

Mathematical modelling of coastal wave propagation is a quite challenging issue since it is difficult to describe in the same model the dispersive effects in the shoaling zone and the energy dissipation of breakers in the surf zone. As it is impractical to solve the full Navier-Stokes system over any significant domain, approximate models must be used. Many asymptotic models were proposed in the last decades for the coastal wave propagation. Some of them are dispersive, although there are some attempts to use hyperbolic models. Although some the existing models provide a very good agreement for non breaking solitary waves, models that describe correctly the free surface of breaking waves are rare.

The first attempt to describe a surf zone wave propagation was made in the context of the nonlinear shallow-water equations, also called the Saint-Venant equations [39]. In [98] Meyter & Taylor reviewed analytic solutions of the shallow-water equations over a beach. Stocker presented perhaps the first numerical solution of the shallow-water equations for a sloping beach using the method of characteristics (see [127]). His method produces quite accurate results for the simple cases. Freeman & Le Méhauté [51] and later Iwasaki & Togashi [66] improved this method. However when the characteristic lines cross at the breaking point the wave evolution has to be treated in a different manner. Further for non-uniformly sloping beaches, this method is cumbersome.

In order to be able to calculate the wave breaking Hibbert & Peregrine proposed in [62] a groundbreaking method based on the numerical solution of the nonlinear shallow-water equations in their conservative form. This method gives physically realistic results. However it is not very robust in the run-up phase [134]. Furthermore, it is important to take into account a large energy dissipation following the wave breaking. Consequently in subsequent version of this algorithm [108, 76, 75, 74] artificial dissipative terms such as viscosity and friction are added for an accurate wave amplitude description. Titov & Synolakis [141] proposed a numerical method without any ad-hoc parameters for wave

---

shoaling which describes very well the run-up of breaking and non-breaking waves but unfortunately, it does not model correctly the free surface.

Indeed the non-linear shallow-water equations give a rather good description of breaking waves representing them as shocks, and the run-up simulations generally give accurate results. However due to the absence of dispersive effects the wave profile is not described particularly in the shoaling zone. Moreover this model predicts that all waves break, which is obviously incorrect. Thereby, a more relevant modelling of wave shoaling before breaking is based on various Boussinesq type models [25]. Non-breaking numerical solutions for the Boussinesq equations are reviewed by Liu [91]. Since the 1990's considerable efforts were made to improve the dispersive properties of the Boussinesq model [94, 104, 147].

Most of Boussinesq models are derived in the assumption of a weak nonlinearity (the wave amplitude is much smaller than the characteristic water depth). The natural idea is to use a fully nonlinear model, as the one derived by Serre [124] and Su & Gardner [130] in the one-dimensional (1D) case, or the two-dimensional (2D) fully nonlinear model presented by Green & Naghdi in [57]. This model can be derived from the Euler equations as an asymptotic model in the shallow water regime without any hypothesis on the wave amplitude [see e.g. 81]. This fully-nonlinear model has better dispersive properties than the Boussinesq equations, and the water wave profile is better described. Except for being formulated in terms of the velocity vector at an arbitrary level, the equations of Wei [147] mentioned above are basically equivalent to the 2D Green-Naghdi equations. In fact the Green-Naghdi equations are often known in the literature as the fully-nonlinear Boussinesq type model.

However the weakly nonlinear or fully nonlinear Boussinesq type equations do not include dissipation due to the wave breaking, and thus become invalid in the surf zone. To extend the validity of those equations, Heitner & Housner [61] introduced an artificial viscosity term into the momentum balance equation. This approach was followed by many researchers. Zelt [151] used an eddy viscosity formulation together with a Lagrangian Boussinesq model. The inclusion of this term in the momentum equation helps to control the energy dissipation, and it must be calibrated with experiments. Similar techniques were used in [95] and [146]. Another close idea is to use the so-called roller models which include dissipation through an extra convective term in the momentum equation [see for example 131, 133, 37]. In this case additional terms are included not only in the momentum equation, but also in the mass balance equation and the thickness of the roller region has to be estimated. For the recent advances on the roller model development we refer to [24], [145], [40].

In the so-called switching or hybrid approach the dispersive terms are suppressed in the breaking regions. Contrary to the nonlinear shallow-water system the Boussinesq equations do not admit discontinuities because they are dispersive. The removal of the dispersive terms reduces the system to the nonlinear shallow water equations. This relatively simple idea was developed in many studies [for example 142, 125, 22, 140, 43, 44, 69, 50].

Generally speaking, two large groups of methods can be distinguished. The first one includes additional terms such as viscous terms or rotational effects and the second one uses hybrid methods. In both approaches some parameters need to be calibrated. Moreover some criteria must be defined to initiate or terminate the breaking process. Generally

those criteria are based on different empirical relations. For example the breaking process is activated if the wave local energy dissipation forms a peak, or if the wave slope reaches a critical value.

Detailed analysis of the different approaches cited above and an estimation of the influence of the numerical dissipation can be found in [70]. The authors highlight that despite the absence of an explanation for the physical meaning of the coefficients in the eddy viscous terms, this approach shows little sensitivity to the grid, while hybrid methods are not very robust and lead to numerical instabilities that depend on the mesh size.

The aim of the present study is to derive a dispersive model which resolves the large-scale turbulence. In most models the turbulence is not resolved but modelled with a turbulent viscosity hypothesis. In some models, this turbulent viscosity is calculated with a turbulent kinetic energy for which a transport equation with source terms is solved ([105, 152]). It is often assumed a local balance between production and dissipation, especially in the case of a mixing-length approach ([105]), which is not assured in a breaking wave.

A common assumption for the Boussinesq type model, and for the Green-Naghdi model as well, is that the horizontal velocity component is uniform or almost uniform over the whole water depth. For the modelling of the flow with turbulent structures this hypothesis is not correct, since considerable velocity fluctuations are observed.

An alternative approach is to get rid entirely of any velocity profile assumptions by adding a new variable to the equations. The addition of an extra variable implies to add also an equation to the model. This new equation is given by the averaged kinetic energy equation. Svendsen & Madsen ([132]) use the energy as the extra variable and solved the energy equation. However because they divided vertically the flow into a turbulent region and a non-turbulent region both having a variable thickness, an assumption on velocity profile is still needed. In this case, this profile was a third-order polynomial. Moreover the pressure was taken hydrostatic, and therefore no dispersive effects are included. A 2D hyperbolic model of shear flows without any velocity profile assumption was derived in [137] from the Euler equations also with the assumption of a hydrostatic pressure. When augmented with dissipation ([117], [118]) it gives an excellent description of roll waves and classical hydraulic jumps. The addition of a non-hydrostatic correction to the pressure and thus of dispersive effects was proposed in the conservative case in [29] and [119]. Gavrilyuk *et al.* (2016) first included both dissipative and dispersive effects in the framework of this approach with a two-layer model, the upper turbulent layer including shearing effects and the irrotational lower layer being described by the Green-Naghdi model. In the present work this method is extended to include dissipation and dispersion in a one-layer model.

The chapter is organised as follows, in section 1.1 the filtered equations are presented. Then the depth-average model is derived in section 1.2 and the empirical laws for the eddy viscosity and the turbulent dissipation are discussed in section 1.3. The last two sections deal with numerical tests. The numerical implementation is presented in section 1.4. In section 1.5 the model is validated by comparison with experimental results.

1.1 Filtered conservation equations

We study the propagation of coastal waves from the shoaling zone to the shoreline. The flow can be highly turbulent, especially in the breaking zone and thereafter in the surf zone. An suitable model of turbulence is thus needed to capture important physical features of the breaking waves.

The classical approach to turbulence is based on the Reynolds decomposition. The velocity field is written as the sum of the mean velocity and of the turbulent fluctuation. The mean kinetic energy of the flow can be decomposed into the kinetic energy of the mean flow and the turbulent kinetic energy. Turbulent processes usually remove energy from the mean flow and transfer it to the fluctuating velocity field. This transfer is called production since most of the time it refers to a loss of the mean kinetic energy and a production of turbulent kinetic energy.

The turbulent motions range in size from large scales, which are of the order of the characteristic lengthscales of the flow, to small scales. According to the energy cascade hypothesis ([120]) and to the Kolmogorov hypothesis ([77]), the production transfers energy first to the large-scale motions. This energy is then transferred to smaller and smaller scales until the Kolmogorov scales where the energy is dissipated by viscous processes. The large scales contain most of the energy and are therefore called the energy-containing range. The dissipating small scales are called the dissipation range. Between these two ranges, at sufficiently high Reynolds numbers lies the inertial subrange where the lengthscales are high enough so that the viscous effects are negligible but small enough compared to the lengthscales of the flow such that there is almost no production. In the inertial subrange, the energy is transferred by inviscid processes toward the smaller scales. Another feature of turbulent motions according to Kolmogorov hypothesis is that the large eddies are anisotropic whereas the small eddies are isotropic.

We use an approach similar to the large-eddy simulation (LES) method. The velocity field $\boldsymbol{v}$ is filtered to decompose the velocity into a filtered velocity field $\overline{\boldsymbol{v}}$ and a residual velocity field $\boldsymbol{v}^r$

$$\boldsymbol{v} = \overline{\boldsymbol{v}} + \boldsymbol{v}^r.$$

The difference between the Reynolds decomposition and this filtering operation is that the former decomposes the velocity field into a non-turbulent (mean) field and a turbulent field whereas in the latter the filtered velocity field includes the large-scale turbulence and the residual velocity field includes the small-scale turbulence. Ideally, the filtering operation is a low-pass filter that allows to resolve turbulent motions of a scale greater than some specified length chosen in the inertial subrange. It follows that the anisotropic energy-containing range is in the filtered field and that the isotropic dissipation range is in the residual field. Another difference with the Reynolds decomposition is that, in general, the filtered residual velocity is not equal to zero i.e. $\overline{\boldsymbol{v}^r} \neq 0$, although if the filter is a projector such as the sharp spectral filter, $\overline{\overline{\boldsymbol{v}}} = \overline{\boldsymbol{v}}$ and $\overline{\boldsymbol{v}^r} = 0$ (for more details on all this approach, see [111]).

The filtering operation is applied to the Navier-Stokes equations of an incompressible fluid of density ρ and kinematic viscosity ν. The filter is supposed to be homogeneous. The

filtered continuity equation becomes simply

$$div\,\overline{\boldsymbol{v}} = 0.$$

The filtered momentum equation is

$$\frac{\partial \overline{\boldsymbol{v}}}{\partial t} + \mathbf{div}\,(\overline{\boldsymbol{v} \otimes \boldsymbol{v}}) = \boldsymbol{g} - \frac{1}{\rho}\,\mathbf{grad}\,\overline{p} + \nu\Delta\overline{\boldsymbol{v}}$$

where $\overline{p}$ is the filtered pressure and $\otimes$ the tensorial product. The residual stress tensor is defined by

$$\boldsymbol{\sigma}^r = -\rho\,(\overline{\boldsymbol{v} \otimes \boldsymbol{v}} - \overline{\boldsymbol{v}} \otimes \overline{\boldsymbol{v}})\,.$$

The residual kinetic energy is defined from the trace of this tensor as

$$k^r = -\frac{\operatorname{tr}\boldsymbol{\sigma}^r}{2\rho}. \tag{1.1}$$

The residual stress tensor can be decomposed into an isotropic part and a deviatoric anisotropic part $\boldsymbol{A}^r$ as

$$\boldsymbol{\sigma}^r = -\frac{2}{3}\rho k^r \boldsymbol{I} + \boldsymbol{A}^r.$$

The tensor $\boldsymbol{I}$ is the identity tensor. The residual stress tensor is then modelled by a turbulent-viscosity hypothesis. This usual hypothesis implies that there is no backscatter in the model i.e. the energy is transferred only from the large scales toward the small scales. Denoting by $\overline{\boldsymbol{D}}$ the filtered strain rate tensor defined by

$$\overline{\boldsymbol{D}} = \frac{1}{2}\left[\mathbf{grad}\,\overline{\boldsymbol{v}} + (\mathbf{grad}\,\overline{\boldsymbol{v}})^{\top}\right], \tag{1.2}$$

the anisotropic residual stress tensor is written

$$\boldsymbol{A}^r = 2\rho\nu_T\overline{\boldsymbol{D}}, \tag{1.3}$$

where ν_T is a turbulent viscosity. The isotropic part of the residual stress tensor is then absorbed into a modified pressure which is denoted simply by p to simplify the notations and which is

$$p = \overline{p} + \frac{2}{3}\rho k^r.$$

The filtered momentum equation is finally written

$$\frac{\partial \overline{\boldsymbol{v}}}{\partial t} + \mathbf{div}\,(\overline{\boldsymbol{v}} \otimes \overline{\boldsymbol{v}}) = \boldsymbol{g} - \frac{1}{\rho}\mathbf{grad}p + \mathbf{div}\left(2\,\nu_T\overline{\boldsymbol{D}}\right) + \nu\Delta\overline{\boldsymbol{v}}.$$

The filtered specific kinetic energy is

$$\overline{e}_k = \frac{1}{2}\overline{\boldsymbol{v} \cdot \boldsymbol{v}}.$$

It follows from the definition (1.1) that

$$\overline{e}_k = e_f + k^r,$$

where e_f is the kinetic energy of the filtered velocity field

$$e_f = \frac{1}{2}\overline{\boldsymbol{v}} \cdot \overline{\boldsymbol{v}}.$$

Writing $\boldsymbol{g} = -\mathbf{grad}\, e_p$, the latter satisfies the equation

$$\frac{\partial e_f}{\partial t} + \mathrm{div}\left(e_f \overline{\boldsymbol{v}} + \frac{p\overline{\boldsymbol{v}}}{\rho} - \frac{\overline{\boldsymbol{v}} \cdot \boldsymbol{A}_r}{\rho} - 2\nu\overline{\boldsymbol{v}} \cdot \overline{\boldsymbol{D}} + e_p\overline{\boldsymbol{v}} \right) = -\varepsilon_f - P^r$$

where

$$\varepsilon_f = 2\nu\overline{\boldsymbol{D}} : \overline{\boldsymbol{D}}$$

and

$$P^r = 2\nu_T\overline{\boldsymbol{D}} : \overline{\boldsymbol{D}}.$$

The dot and the colon mean the dot product and the double dot product respectively. For a very high Reynolds number, the terms involving the molecular viscosity can be neglected. This is the case of the term ε_f which represents the viscous dissipation from the filtered velocity field. Most of the viscous dissipation processes take place in the dissipation range and thus in the residual velocity field. The dominant dissipative term in the equation for e_f is P_r which represents an energy transfer from the filtered motions towards the residual motions i.e. from the large scales towards the small scales. Since most of the energy is contained in the energy-containing range, the mean kinetic energy $\langle e \rangle$ is almost equal to the mean kinetic energy of the filtered velocity field $\langle e_f \rangle$ (the brackets denote the Reynolds averaging). The dissipation due to the mean flow being negligible at high Reynolds numbers, the dissipation of the mean kinetic energy is almost entirely due to the dissipation of the turbulent kinetic energy, usually denoted by ε and called simply dissipation. Consequently, the mean dissipation of $\langle e_f \rangle$, denoted by $\langle P_r \rangle$ is nearly equal to the dissipation. This also implies the equality of the dissipation of the mean residual kinetic energy and its rate of production ([89], see also [111], [63])

$$\langle P^r \rangle \simeq \varepsilon. \tag{1.4}$$

The classical closure of this approach is due to [126] who modelled the eddy viscosity by analogy with the mixing-length hypothesis. We do not follow this path because the filtered equations will be averaged over the fluid depth. We will use instead a simpler closure by assuming that the turbulent viscosity is uniform over the water depth but otherwise variable in space and time. The empirical law chosen for this eddy viscosity is discussed in section 1.3.

1.2 Averaged conservation equations

1.2.1 Governing equations

We study the particular case of a two-dimensional flow over a variable bottom. The notations are presented in Figure 1.1. The components of the velocity field are u in the horizontal direction Ox and w in the vertical direction Oz. The bottom topography is
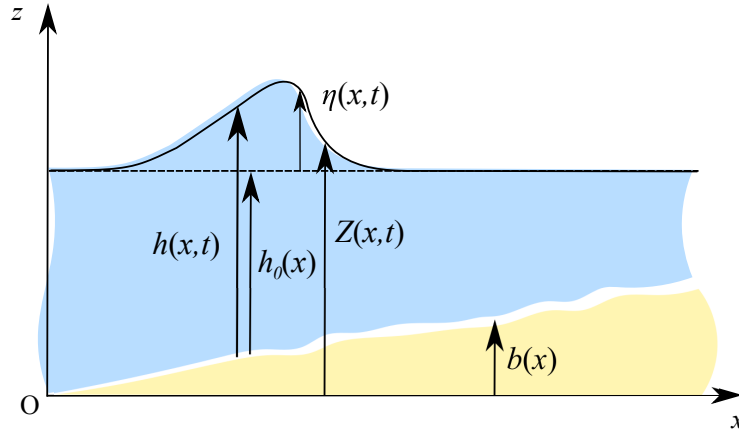
Figure 1.1: Scheme of the flow, where $h(x,t)$ is the water depth, $\eta(t,x)$ is the free-surface elevation, $b(x)$ denotes the bottom topography $\big(Z(x,t) = h(t,x) + b(x)\big)$, horizontal water level is denoted by $h_0(x)$.

measured by its elevation $b(x)$ over a horizontal datum. The elevation of the free surface over this horizontal datum is $Z(x,t)$ while the water depth is $h(x,t) = Z(x,t) - b(x)$. The still water depth is denoted by $h_0(x)$ and the water elevation over this level is $\eta(x,t)$. In the case of a solitary wave, the amplitude a of the wave is defined as the maximum value of the elevation i.e. $a = max\,\eta(x,t)$.

The filtered mass conservation equation is

$$\frac{\partial \overline{u}}{\partial x} + \frac{\partial \overline{w}}{\partial z} = 0.$$

The filtered momentum balance equation writes in the Ox direction

$$\frac{\partial \overline{u}}{\partial t} + \frac{\partial \overline{u}^2}{\partial x} + \frac{\partial \overline{uw}}{\partial z} = -\frac{1}{\rho}\frac{\partial p}{\partial x} + \frac{1}{\rho}\left(\frac{\partial A^r_{xx}}{\partial x} + \frac{\partial A^r_{xz}}{\partial z}\right) + \nu\left(\frac{\partial^2 u}{\partial x^2} + \frac{\partial^2 u}{\partial z^2}\right)$$

and in the Oz direction

$$\frac{\partial \overline{w}}{\partial t} + \frac{\partial \overline{uw}}{\partial x} + \frac{\partial \overline{w}^2}{\partial z} = -g - \frac{1}{\rho}\frac{\partial p}{\partial z} + \frac{1}{\rho}\left(\frac{\partial A^r_{xz}}{\partial x} + \frac{\partial A^r_{zz}}{\partial z}\right) + \nu\left(\frac{\partial^2 w}{\partial x^2} + \frac{\partial^2 w}{\partial z^2}\right).$$

The balance equation for the kinetic energy of the filtered motions can be written

$$\frac{\partial}{\partial t}\left(\frac{\overline{u}^2}{2} + \frac{\overline{w}^2}{2}\right)$$
$$+ \frac{\partial}{\partial x}\left[\overline{u}\left(\frac{\overline{u}^2}{2} + \frac{\overline{w}^2}{2} + gz\right) + \frac{pu}{\rho} - \frac{A^r_{xx}u}{\rho} - \frac{A^r_{xz}w}{\rho} - \frac{\tau_{xx}u}{\rho} - \frac{\tau_{xz}w}{\rho}\right]$$
$$+ \frac{\partial}{\partial z}\left[\overline{w}\left(\frac{\overline{u}^2}{2} + \frac{\overline{w}^2}{2} + gz\right) + \frac{pw}{\rho} - \frac{A^r_{xz}u}{\rho} - \frac{A^r_{zz}w}{\rho} - \frac{\tau_{xz}u}{\rho} - \frac{\tau_{zz}w}{\rho}\right] = -\varepsilon_f - P^r.$$

In this equation, the filtered viscous stress tensor is $\boldsymbol{\tau} = 2\rho\nu\overline{\boldsymbol{D}}$. The components of the involved symetrical tensors are defined as

$$\boldsymbol{A}^r = A^r_{xx}\boldsymbol{e_x} \otimes \boldsymbol{e_x} + A^r_{xz}\boldsymbol{e_x} \otimes \boldsymbol{e_z} + A^r_{xz}\boldsymbol{e_z} \otimes \boldsymbol{e_x} + A^r_{zz}\boldsymbol{e_z} \otimes \boldsymbol{e_z}$$

and

$$\boldsymbol{\tau} = \tau_{xx}\boldsymbol{e_x} \otimes \boldsymbol{e_x} + \tau_{xz}\boldsymbol{e_x} \otimes \boldsymbol{e_z} + \tau_{xz}\boldsymbol{e_z} \otimes \boldsymbol{e_x} + \tau_{zz}\boldsymbol{e_z} \otimes \boldsymbol{e_z},$$

$\boldsymbol{e_x}$ and $\boldsymbol{e_z}$ are the unit vectors in the Ox and Oz directions.

The boundary conditions are the no-penetration condition at the bottom

$$w(b) = u(b)b',$$

where $b' = \mathrm{d}b/\mathrm{d}x$, the kinematic boundary condition at the free surface

$$w(Z) = \frac{\partial h}{\partial t} + u(Z)\frac{\partial Z}{\partial x}$$

and the dynamic boundary condition at the free surface

$$(\boldsymbol{\sigma} \cdot \boldsymbol{n})(Z) = 0, \tag{1.5}$$

where $\boldsymbol{\sigma} = -p\boldsymbol{I} + \boldsymbol{A}^r + \boldsymbol{\tau}$ is the Cauchy stress tensor and where $\boldsymbol{n}$ is the unit normal vector at the free surface.

1.2.2 Scaling

The model is derived within the scope of the shallow-water approximation. If h_0^* is a reference value of the still-water depth and if L is a characteristic length of variation of the flow parameters in the horizontal direction, then there is a small parameter

$$\mu = \frac{h_0^*}{L} \ll 1.$$

The equations are then written in dimensionless form. The dimensionless quantities are denoted by a tilde symbol. The following scaling is classical for this situation ([8]):

$$\tilde{x} = \frac{x}{L}, \quad \tilde{z} = \frac{z}{h_0^*}, \quad \tilde{u} = \frac{\overline{u}}{\sqrt{gh_0^*}}, \quad \tilde{w} = \frac{\overline{w}}{\mu\sqrt{gh_0^*}}, \quad \tilde{t} = \mu t\sqrt{\frac{g}{h_0^*}}, \quad \tilde{h} = \frac{h}{h_0^*}, \quad \tilde{p} = \frac{p}{\rho g h_0^*}.$$

For the viscous stress tensor, the scaling is

$$\tilde{\tau}_{xx} = \frac{L\tau_{xx}}{\rho\nu\sqrt{gh_0^*}} \quad \tilde{\tau}_{zz} = \frac{L\tau_{zz}}{\rho\nu\sqrt{gh_0^*}} \quad \tilde{\tau}_{xz} = \frac{h_0^*\tau_{xz}}{\rho\nu\sqrt{gh_0^*}}.$$

The Reynolds number is defined by $Re = h_0^*\sqrt{gh_0^*}/\nu$. The turbulent viscosity is supposed to be of $O(\mu)$ and it is written in dimensionless form as in [8]:

$$\tilde{\nu}_T = \frac{\nu_T}{\mu h_0^*\sqrt{gh_0^*}}. \tag{1.6}$$

Consequently the components of the deviatoric part of the residual stress tensor are scaled as

$$\tilde{A}_{xx}^r = \frac{A_{xx}^r}{\mu^2\rho g h_0^*} \quad \tilde{A}_{zz}^r = \frac{A_{zz}^r}{\mu^2\rho g h_0^*} \quad \tilde{A}_{xz}^r = \frac{A_{xz}^r}{\mu\rho g h_0^*}.$$

We can write

$$\tilde{A}_{xx}^r = 2\tilde{\nu}_T\frac{\partial\tilde{u}}{\partial\tilde{x}} \quad \tilde{A}_{zz}^r = -\tilde{A}_{xx}^r \quad \tilde{A}_{xz}^r = \tilde{\nu}_T\left(\frac{\partial\tilde{u}}{\partial\tilde{z}} + \mu^2\frac{\partial\tilde{w}}{\partial\tilde{x}}\right).$$

The dimensionless mass conservation equation is simply

$$\frac{\partial \tilde{u}}{\partial \tilde{x}} + \frac{\partial \tilde{w}}{\partial \tilde{z}} = 0. \tag{1.7}$$

The momentum equation in the Ox direction becomes in dimensionless form

$$\frac{\partial \tilde{u}}{\partial \tilde{t}} + \frac{\partial \tilde{u}^2}{\partial \tilde{x}} + \frac{\partial \tilde{u}\tilde{w}}{\partial \tilde{z}} = -\frac{\partial \tilde{p}}{\partial \tilde{x}} + \mu^2 \frac{\partial \tilde{A}_{xx}^r}{\partial \tilde{x}} + \frac{\partial \tilde{A}_{xz}^r}{\partial \tilde{z}} + \frac{\mu}{Re}\frac{\partial \tilde{\tau}_{xx}}{\partial \tilde{x}} + \frac{1}{\mu Re}\frac{\partial \tilde{\tau}_{xz}}{\partial \tilde{z}}. \tag{1.8}$$

In the Oz direction, the momentum equation can be written as

$$\mu^2 \left(\frac{\partial \tilde{w}}{\partial \tilde{t}} + \frac{\partial \tilde{u}\tilde{w}}{\partial \tilde{x}} + \frac{\partial \tilde{w}^2}{\partial \tilde{z}} \right) = -1 - \frac{\partial \tilde{p}}{\partial \tilde{z}} + \mu^2 \frac{\partial \tilde{A}_{xz}^r}{\partial \tilde{x}} + \mu^2 \frac{\partial \tilde{A}_{zz}^r}{\partial \tilde{z}} + \frac{\mu}{Re}\frac{\partial \tilde{\tau}_{xz}}{\partial \tilde{x}} + \frac{\mu}{Re}\frac{\partial \tilde{\tau}_{zz}}{\partial \tilde{z}}. \tag{1.9}$$

It follows from the chosen scaling that the dimensionless viscous dissipation in the filtered velocity field can be defined as $\tilde{\varepsilon}_f = h_0^* \varepsilon_f/(g\nu)$ and that the dimensionless energy transfer toward the residual motion is $\tilde{P}^r = P^r/(\mu g \sqrt{gh_0^*})$. The dimensionless energy equation can then be written

$$\frac{\partial}{\partial \tilde{t}} \left(\frac{\tilde{u}^2}{2} + \mu^2 \frac{\tilde{w}^2}{2} \right)$$
$$+ \frac{\partial}{\partial \tilde{x}} \left[\tilde{u} \left(\frac{\tilde{u}^2}{2} + \mu^2 \frac{\tilde{w}^2}{2} + \tilde{z} \right) + \tilde{p}\tilde{u} - \mu^2 \left(\tilde{A}_{xx}^r \tilde{u} + \tilde{A}_{xz}^r \tilde{w} \right) - \frac{\mu}{Re}\left(\tilde{\tau}_{xx}\tilde{u} + \tilde{\tau}_{xz}\tilde{w} \right) \right]$$
$$+ \frac{\partial}{\partial \tilde{z}} \left[\tilde{w} \left(\frac{\tilde{u}^2}{2} + \mu^2 \frac{\tilde{w}^2}{2} + \tilde{z} \right) + \tilde{p}\tilde{w} - \tilde{A}_{xz}^r \tilde{u} - \mu^2 \tilde{A}_{zz}^r \tilde{w} - \frac{1}{\mu Re}\tilde{\tau}_{xz}\tilde{u} - \frac{\mu}{Re}\tilde{\tau}_{zz}\tilde{w} \right]$$
$$= -\frac{1}{\mu Re}\tilde{\varepsilon}_f - \tilde{P}^r. \tag{1.10}$$

The boundary conditions are also written in dimensionless form with $\tilde{b} = b/h_0^*$ and $\tilde{Z} = Z/h_0^*$. If we assume that b varies horizontally on a characteristic length of $O(L)$, then $\tilde{b}' = b'/\mu$. The no-penetration condition on the bottom and the kinematic condition at the free surface read simply

$$\tilde{w}(b) = \tilde{u}(b)\tilde{b}' \quad \tilde{w}(Z) = \frac{\partial \tilde{h}}{\partial \tilde{t}} + \tilde{u}(Z)\frac{\partial \tilde{Z}}{\partial \tilde{x}},$$

whereas the dynamic boundary condition at the free surface (1.5) gives two scalar equations

$$\tilde{A}_{xz}^r(Z) + \left[\tilde{p}(Z) - \mu^2 \tilde{A}_{xx}^r(Z) \right] \frac{\partial \tilde{Z}}{\partial \tilde{x}} = 0, \tag{1.11}$$

$$\tilde{p}(Z) - \mu^2 \tilde{A}_{zz}^r(Z) + \mu^2 \tilde{A}_{xz}^r(Z)\frac{\partial \tilde{Z}}{\partial \tilde{x}} = 0. \tag{1.12}$$

There is no surface tension and no shear stress condition imposed at the free surface.

The filtered equations are averaged over the depth. For any quantity a, its average value over the depth is denoted by $\langle\langle \cdot \rangle\rangle$ and defined as

$$\langle\langle a \rangle\rangle = \frac{1}{h} \int_{b(x)}^{Z(x,t)} a \, \mathrm{d}z.$$

The averaged horizontal velocity is denoted by $U = \langle\langle \overline{u} \rangle\rangle$ and in dimensionless form $\tilde{U} = \langle\langle \tilde{u} \rangle\rangle$. The filtered horizontal velocity is decomposed as

$$\overline{u}(x, z, t) = U(x, t) + u'(x, z, t).$$

Equivalently, $u = U + u' + u^r$. The term u' represents the deviation of the filtered horizontal velocity from its averaged value. It includes the anisotropic large-scale turbulence which contains most of the turbulent energy and the depth variations of the Reynolds-averaged velocity field (shearing effects). On the other hand, the residual velocity field u^r includes the isotropic small-scale turbulence where most of the dissipation takes place. The model is derived in the hypothesis of a weakly turbulent (and weakly sheared) flow which means that u' is of $O(\mu)$. This hypothesis is very similar in effect as the hypothesis of a weakly-sheared flow (Teshukov 2007) with a value of Teshukov's exponent β is equal to 1. Therefore we write

$$\tilde{u}(x, z, t) = \tilde{U}(x, t) + \mu \tilde{u}'(x, z, t).$$

In the following derivation of the model, all terms of an order up to $O(\mu^2)$ will be kept and the terms of $O(\mu^3)$ will be neglected.

The Reynolds number is supposed to be high enough so that all viscous terms can be neglected. This hypothesis is usual for this kind of problems (see for example [8]). It can be written $Re = O(\mu^{-3})$. The terms of $O(\mu/Re)$ are then of $O(\mu^4)$. The terms of $O(1/(\mu Re))$ involve $\tilde{\tau}_{xz}$ whose dominant term is $\partial \tilde{u}/\partial \tilde{z}$. Since $\partial \tilde{U}/\partial \tilde{z} = 0$, $\tilde{\tau}_{xz}$ is in fact of $O(\mu)$ and the terms of $O(1/(\mu Re))$ are of $O(\mu^3)$ and therefore negligible. The term $\tilde{\varepsilon}_f$ is negligible for the same reason.

The effect of the hypothesis of a weakly turbulent flow can also be applied to the scaling of $\overline{\boldsymbol{D}}$ and P^r. In $\overline{\boldsymbol{D}}$ the dominant component is normally, in dimensionless form

$$\tilde{D}_{xz} = \frac{1}{2} \left(\frac{\partial \tilde{u}}{\partial \tilde{z}} + \mu^2 \frac{\partial \tilde{w}}{\partial \tilde{x}} \right). \tag{1.13}$$

However, $\partial \tilde{u}/\partial \tilde{z} = \mu \partial \tilde{u}'/\partial \tilde{z}$. This implies that

$$\tilde{P}^r = \frac{P^r}{\mu^3 g \sqrt{g h_0^*}}. \tag{1.14}$$

Consequently, the last term in (1.10) writes in fact $-\mu^2 \tilde{P}^r$. It is thus of $O(\mu^2)$ and must be kept.

As in [144], the shear stress on the bottom is neglected and this implies a free-slip condition at the sea bed. The whole deviatoric residual stress tensor is neglected on the bottom i.e. $\boldsymbol{A}^r(b) \simeq 0$.

1.2.3 Averaging procedure

To simplify the notations, the tilde are dropped in this section dealing entirely with dimensionless quantities. Averaging the mass conservation equation (1.7) over the depth, taking into account the boundary conditions, gives

$$\frac{\partial h}{\partial t} + \frac{\partial h U}{\partial x} = 0. \tag{1.15}$$

The continuity equation (1.7) allows us to find an expression for the vertical filtered velocity

$$w = (z - b)\frac{\dot{h}}{h} + Ub' + O(\mu),$$ (1.16)

where the dot symbol is the different notation for the material derivative (see Introduction, (2)) along the average flow

$$\dot{h} = \frac{\partial h}{\partial t} + U\frac{\partial h}{\partial x}.$$ (1.17)

The momentum equation in the Oz direction (1.9) gives first

$$\frac{\partial p}{\partial z} = -1 - \mu^2(z - b)\frac{\ddot{h}}{h} - \mu^2\frac{\mathrm{D}b'U}{\mathrm{D}t} + \mu^2\frac{\partial A^r_{xz}}{\partial x} + \mu^2\frac{\partial A^r_{zz}}{\partial z}.$$

and then, with the dynamic boundary condition (1.12), an expression of the pressure

$$p = Z - z - \mu^2\frac{\ddot{h}}{h}\left[\frac{z^2 - Z^2}{2} - b(z - Z)\right] - \mu^2\frac{\mathrm{D}b'U}{\mathrm{D}t}(z - Z)$$
$$+ \mu^2\frac{\partial}{\partial x}\int_Z^z A^r_{xz}\mathrm{d}z + \mu^2 A^r_{zz}.$$ (1.18)

In these expressions, both the notations $\mathrm{D}a/\mathrm{D}t$ and $\dot{a}$ denote the material derivative of a quantity a along the average flow (see (1.17)). With the dynamic boundary condition (1.11) and since we took $A^r(b) \simeq 0$, the integration of the pressure terms and of the residual stress terms gives

$$-\int_b^Z \frac{\partial p}{\partial x}\mathrm{d}z + \int_b^Z \mu^2\frac{\partial A^r_{xx}}{\partial x}\mathrm{d}z + \int_b^Z \frac{\partial A^r_{xz}}{\partial z}\mathrm{d}z$$
$$= -\frac{\partial}{\partial x}\int_b^Z p\,\mathrm{d}z - p(b)b' + \mu^2\frac{\partial}{\partial x}\int_b^Z A^r_{xx}\mathrm{d}z.$$

The integration of the pressure leads to

$$\int_b^Z p\,\mathrm{d}z = \frac{h^2}{2} + \mu^2\frac{h^2\ddot{h}}{3} + \mu^2\frac{h^2}{2}\frac{\mathrm{D}b'U}{\mathrm{D}t} + \mu^2\int_b^Z \mathrm{d}z\frac{\partial}{\partial x}\int_Z^z A^r_{xz}\mathrm{d}z + \mu^2\int_b^Z A^r_{zz}\mathrm{d}z.$$ (1.19)

We can write

$$\int_Z^z A^r_{xz}\mathrm{d}z = \int_Z^z \nu_T\frac{\partial u}{\partial z}\mathrm{d}z + O(\mu^2).$$

Since the turbulent viscosity is uniform over the fluid depth,

$$\int_Z^z \nu_T\frac{\partial u}{\partial z}\mathrm{d}z = \nu_T(u - u(Z)).$$

The hypothesis of a weakly turbulent flow implies that $u - u(Z) = O(\mu)$. The corresponding term in (1.19) is thus of $O(\mu^3)$ and negligible. Then

$$\int_b^Z A^r_{xx}\mathrm{d}z = -\int_b^Z A^r_{zz}\mathrm{d}z.$$

With the expression of A^r_{xx}, we get

$$\int_b^Z A^r_{xx}\mathrm{d}z = 2\nu_T\int_b^Z \frac{\partial u}{\partial x}\mathrm{d}z.$$

The hypothesis of a weakly turbulent flow allows us to write $u(Z) = U + O(\mu)$ and $u(b) = U + O(\mu)$. This leads to

$$\int_b^Z A_{xx}^r \mathrm{d}z = 2\nu_T h \frac{\partial U}{\partial x}.$$

The calculation of the pressure at the sea bed gives

$$p(b)b' = hb' + \mu^2 h b' \left(\frac{\ddot{h}}{2} + \frac{\mathrm{D}b'U}{\mathrm{D}t} \right).$$

Finally the integration of the right-hand side of equation (1.8) gives

$$-\int_b^Z \frac{\partial p}{\partial x} \mathrm{d}z + \int_b^Z \mu^2 \frac{\partial A_{xx}^r}{\partial x} \mathrm{d}z + \int_b^Z \frac{\partial A_{xz}^r}{\partial z} \mathrm{d}z$$

$$= -\frac{\partial}{\partial x} \left(\frac{h^2}{2} + \mu^2 \frac{h^2 \ddot{h}}{3} + \mu^2 \frac{h^2}{2} \frac{\mathrm{D}b'U}{\mathrm{D}t} - 4\nu_T h \frac{\partial U}{\partial x} \right) - hb' - \mu^2 h b' \left(\frac{\ddot{h}}{2} + \frac{\mathrm{D}b'U}{\mathrm{D}t} \right).$$

Taking into account the boundary conditions, the integration of the left-hand side of equation (1.8) leads to

$$\int_b^Z \left(\frac{\partial u}{\partial t} + \frac{\partial u^2}{\partial x} + \frac{\partial uw}{\partial z} \right) \mathrm{d}z = \frac{\partial hU}{\partial t} + \frac{\partial}{\partial x} \left(h \langle\langle u^2 \rangle\rangle \right).$$

The treatment of $\langle\langle u^2 \rangle\rangle$ is the same as in [117]. First, $\langle\langle u^2 \rangle\rangle$ is written $U^2 + \mu^2 \langle\langle u'^2 \rangle\rangle$ since, by definition, $\langle\langle u' \rangle\rangle = 0$. Second, a new variable, φ, called enstrophy, is defined as

$$\varphi := \frac{\langle\langle u'^2 \rangle\rangle}{h^2}.$$

The averaged momentum equation can finally be written

$$\frac{\partial hU}{\partial t} + \frac{\partial}{\partial x} \left(hU^2 + \mu^2 h^3 \varphi + \frac{h^2}{2} + \mu^2 \Pi + \mu^2 \Pi' \right) = -hb' - \mu^2 f' + O(\mu^3) \qquad (1.20)$$

where

$$\Pi = \frac{h^2 \ddot{h}}{3} - 4\nu_T h \frac{\partial U}{\partial x}, \qquad (1.21)$$

$$\Pi' = \frac{h^2}{2} \frac{\mathrm{D}b'U}{\mathrm{D}t} \qquad (1.22)$$

and

$$f' = hb' \left(\frac{\ddot{h}}{2} + \frac{\mathrm{D}b'U}{\mathrm{D}t} \right). \qquad (1.23)$$

We will say that the sea bed has a mild slope if b varies horizontally on a characteristic length of $O(\mu L)$. In this case, the terms in $\mu^2 \Pi'$ and $-\mu^2 f'$ become of $O(\mu^3)$ and are negligible. The averaged momentum equation reduces to

$$\frac{\partial hU}{\partial t} + \frac{\partial}{\partial x} \left(hU^2 + \mu^2 h^3 \varphi + \frac{h^2}{2} + \mu^2 \frac{h^2 \ddot{h}}{3} - 4\nu_T h \frac{\partial U}{\partial x} \right) = -hb' + O(\mu^3). \qquad (1.24)$$

Since the model features three variables h, U and φ, three equations are needed. Two equations are provided by the averaged mass conservation equation and by the averaged

momentum equation and the third equation is the averaged energy equation. With the boundary conditions, we can integrate

$$\int_b^Z \left[\frac{\partial}{\partial t} \frac{u^2}{2} + \frac{\partial}{\partial x} \frac{u^3}{2} + \frac{\partial}{\partial z} \frac{wu^2}{2} \right] \mathrm{d}z = \frac{\partial}{\partial t} \left(\frac{h}{2} \langle\langle u^2 \rangle\rangle \right) + \frac{\partial}{\partial x} \left(\frac{h}{2} \langle\langle u^3 \rangle\rangle \right).$$

We expand as above $\langle\langle u^2 \rangle\rangle = U^2 + \mu^2 h^2 \varphi$. The same method yields $\langle\langle u^3 \rangle\rangle = U^3 + 3\mu^2 h^2 U \varphi + O(\mu^3)$. As in [137], the hypothesis of weakly turbulent flows allows us to neglect $\langle\langle u'^3 \rangle\rangle$ and thus to close the problem. Another integration combined with the boundary conditions and with the expression (1.16) of the vertical velocity leads to

$$\mu^2 \int_b^Z \left[\frac{\partial}{\partial t} \frac{w^2}{2} + \frac{\partial}{\partial x} \frac{uw^2}{2} + \frac{\partial}{\partial z} \frac{w^3}{2} \right] \mathrm{d}z$$
$$= \mu^2 \frac{\partial}{\partial t} \left(\frac{h\dot{h}^2}{6} + \frac{hU^2 b'^2}{2} + \frac{hb'U\dot{h}}{2} \right) + \mu^2 \frac{\partial}{\partial x} \left[U \left(\frac{h\dot{h}^2}{6} + \frac{hU^2 b'^2}{2} + \frac{hb'U\dot{h}}{2} \right) \right].$$

With the expression (1.18) of the pressure and with the boundary conditions, we get

$$\int_b^Z \left[\frac{\partial}{\partial x} \left(uz + pu - \mu^2 A_{xx}^r u - \mu^2 A_{xz}^r w \right) + \frac{\partial}{\partial z} \left(wz + pw - A_{xz}^r u - \mu^2 A_{zz}^r w \right) \right] \mathrm{d}z$$
$$= \frac{\partial}{\partial t} \left(\frac{h^2}{2} \right) + \frac{\partial}{\partial x} \left[U \left(h^2 + \mu^2 \frac{h^2 \ddot{h}}{3} + \mu^2 \frac{h^2}{2} \frac{\mathrm{D}b'U}{\mathrm{D}t} - \mu^2 4\nu_T h \frac{\partial U}{\partial x} \right) \right] + hb'U.$$

The averaged value of P^r over the depth is estimated by the averaged value over the depth of its mean value (in the Reynolds sense) $\langle P^r \rangle$. Then the approximation (1.4) gives

$$\langle\langle P^r \rangle\rangle \simeq \langle\langle \varepsilon \rangle\rangle. \tag{1.25}$$

Physically, this means that the energy dissipation of the model is mostly due to the dissipation of the turbulent kinetic energy in the dissipation range i.e. in the small scales. The expression of $\langle\langle \varepsilon \rangle\rangle$ is discussed in section 1.3. The averaged energy equation can finally be written

$$\frac{\partial}{\partial t} \left[h \left(e + \mu^2 e' \right) \right] + \frac{\partial}{\partial x} \left[hU \left(e + \mu^2 e' \right) + U \left(\mu^2 h^3 \varphi + \frac{h^2}{2} + \mu^2 \Pi + \mu^2 \Pi' \right) \right]$$
$$= -hb'U - \mu^2 h \langle\langle \varepsilon \rangle\rangle + O(\mu^3) \quad (1.26)$$

where Π and Π' are given by (1.21) and (1.22) respectively and where

$$e = \frac{U^2}{2} + \mu^2 \frac{h^2 \varphi}{2} + \mu^2 \frac{\dot{h}^2}{6} + \frac{h}{2}; \quad e' = \frac{b'^2 U^2}{2} + \frac{\dot{h}}{2} b'U. \tag{1.27}$$

The factor μ^2 in front of $h \langle\langle \varepsilon \rangle\rangle$ comes from the hypothesis of a weakly turbulent flow as explained at the end of section 1.2.2 (see relation (1.14)). In the case of a mild slope, e' and Π' become negligible and the energy equation reduces to

$$\frac{\partial he}{\partial t} + \frac{\partial}{\partial x} \left[hUe + U \left(\mu^2 h^3 \varphi + \frac{h^2}{2} + \mu^2 \Pi \right) \right] = -hb'U - \mu^2 h \langle\langle \varepsilon \rangle\rangle + O(\mu^3). \tag{1.28}$$

1.2.4 Enstrophy equation

The model is composed of the mass equation (1.15), the momentum equation (1.20 or 1.24 for a mild slope) and the energy equation (1.26 or 1.28 for a mild slope). From these three equations, an evolution equation for the enstrophy can be derived. From equation (1.20), we first obtain the equation

$$\frac{\partial}{\partial t}\frac{hU^2}{2} + \frac{\partial}{\partial x}\frac{hU^3}{2} + U\frac{\partial}{\partial x}\left(\mu^2 h^3\varphi + \frac{h^2}{2} + \mu^2\Pi + \mu^2\Pi'\right) = -hb'U - \mu^2 Uf'. \qquad (1.29)$$

Subtracting this equation from equation (1.26) leads to

$$\frac{\partial}{\partial t}\left(\mu^2\frac{h^3\varphi}{2} + \mu^2\frac{h\dot{h}^2}{6} + \frac{h^2}{2} + \mu^2 he'\right)$$

$$+ \frac{\partial}{\partial x}\left[\mu^2\frac{h^3 U\varphi}{2} + \frac{h^2 U}{2} + \mu^2\frac{hU\dot{h}^2}{6} + \mu^2 hUe' + U\left(\mu^2 h^3\varphi + \frac{h^2}{2} + \mu^2\Pi + \mu^2\Pi'\right)\right]$$

$$- U\frac{\partial}{\partial x}\left(\mu^2 h^3\varphi + \frac{h^2}{2} + \mu^2\Pi + \mu^2\Pi'\right) = -\mu^2\langle\langle\varepsilon\rangle\rangle + \mu^2 Uf'.$$

The mass equation implies that

$$\dot{h} = -h\frac{\partial U}{\partial x}.$$

The following equalities are satisfied

$$\frac{\partial he'}{\partial t} + \frac{\partial}{\partial x}\left(hUe' + U\Pi'\right) = U\frac{\partial\Pi'}{\partial x} + Uf',$$

$$\frac{\partial}{\partial t}\frac{h\dot{h}^2}{6} + \frac{\partial}{\partial x}\left(\frac{hU\dot{h}^2}{6} + U\frac{h^2\ddot{h}}{3}\right) = U\frac{\partial}{\partial x}\frac{h^2\ddot{h}}{3},$$

$$\frac{\partial}{\partial t}\frac{h^2}{2} + \frac{\partial h^2 U}{\partial x} = U\frac{\partial}{\partial x}\frac{h^2}{2}$$

and

$$\frac{\partial}{\partial t}\frac{h^3\varphi}{2} + \frac{\partial}{\partial x}\frac{3h^3 U\varphi}{2} - U\frac{\partial}{\partial x}\left(h^3\varphi\right) = \frac{h^3}{2}\frac{\mathrm{D}\varphi}{\mathrm{D}t}.$$

The evolution equation of the enstrophy can finally be written

$$\frac{\partial h\varphi}{\partial t} + \frac{\partial hU\varphi}{\partial x} = \frac{8\nu_T}{h}\left(\frac{\partial U}{\partial x}\right)^2 - \frac{2}{h^2}\langle\langle\varepsilon\rangle\rangle. \qquad (1.30)$$

The enstrophy φ is related to the averaged large-scale turbulent kinetic energy and to the shearing effects of the Reynolds-averaged flow. The above equation shows that it is created by the effect of the turbulent viscosity and dissipated by the dissipation of the turbulent kinetic energy. The latter takes place in the small scales after the energy had been transferred from the large scales.

The underlying conservative hyperbolic system has the mathematical structure of the Euler equations of compressible fluids. For this system, the enstrophy is analogous to the entropy. If this hyperbolic system had to be resolved, the appearance of discontinuities would impose to solve the mass, momentum and energy equations since these discontinuities would conserve the energy and would create enstrophy. Because of the diffusive and

dispersive terms of our model, no discontinuity can arise. It is thus equivalent in theory to solve the mass, momentum and energy equations or to solve the mass, momentum and enstrophy equation. However, in practice, the enstrophy equation (1.30) is much simpler than the energy equation (1.26). The enstrophy equation has no dispersive term and no term depending on the topography. Numerically, this equation is much easier to handle than the energy equation. The substitution of the enstrophy equation for the energy equation in order to solve numerically the equations was already made in [84] for the dispersive model including terms up to $O(\mu^3)$ but no dissipation nor viscosity. Take care of the notation differences since their μ is for us μ^2 and the quantity they denote by $\tilde{E}$ is $h\varphi$.

1.3 Dissipation and eddy viscosity

The closure of the model composed of equations (1.15), (1.20) (or (1.24)) and (1.30) requires to know the dissipation $\langle\langle\varepsilon\rangle\rangle$ and the eddy viscosity ν_T. We can assume that these quantities can depend on h and on the enstrophy φ but not on the average velocity U in order to satisfy easily the principle of Galilean invariance [11] (φ is a Galilean invariant quantity). Including a dependence on U would in fact requires a dependence on a velocity difference $U - v^*$ where v^* would be a suitable velocity. The only obvious choice for v^* would be the bottom velocity but it is difficult to explain a dependence on the bottom velocity while the turbulent and viscous processes close to the bottom are completely neglected in this model. Another choice for the turbulent viscosity would be a dependence on h and g writing $\nu_T = C_\nu h\sqrt{gh}$ as in [103], where C_ν is a dimensionless constant. However such an expression would imply that the turbulent viscosity is greater where the depth is greater, thus in the shoaling zone, and smaller where the wave breaks and in the surf zone whereas the opposite variation would be expected. This would make the model highly dependent on the breaking criterion. It seems much more preferable to be inspired by the models using a dependence of the viscosity with the turbulent kinetic energy.

With a dependence on h and φ only, a dimensional analysis shows that

$$\nu_T = C_p h^2 \sqrt{\varphi},$$

where C_p is a dimensionless quantity, and that

$$\langle\langle\varepsilon\rangle\rangle = \frac{C_r}{2} h^2 \varphi^{3/2} \tag{1.31}$$

where C_r is another dimensionless quantity. Note that C_p can be interpreted as the inverse of a Reynolds number R such that

$$\nu_T = \frac{h^2 \sqrt{\varphi}}{R}. \tag{1.32}$$

With these choices, the model has the mathematical structure of the turbulent-kinetic-energy model (TKE or $k - \ell_m$) proposed by [78] and [113] who suggested to base the turbulent viscosity and the dissipation on the turbulent kinetic energy and the mixing length. In our model, the enstrophy and the water depth replace the turbulent kinetic energy and the mixing length respectively (the turbulent kinetic energy is in fact homogeneous to $h^2\varphi$)

with the difference that the problem of completeness of the TKE model does not apply to this model since h is variable of the model and does not need to be specified.

Another difference is that, although the equation of the enstrophy is analogous to the equation of the turbulent kinetic energy of the TKE model, the mass equation (1.15) shows that our model is analogous to the equations of a compressible fluid (the water depth h being the analogous of the density).

The relation (1.31) implies that the dimensionless form of $\langle\langle \varepsilon \rangle\rangle$ is

$$\langle\langle \tilde{\varepsilon} \rangle\rangle = \frac{\langle\langle \varepsilon \rangle\rangle}{\mu^3 g \sqrt{g h_0^*}}. \tag{1.33}$$

This is in accordance with (1.14). The relation (1.32) is also in agreement with the scaling (1.6) of the eddy viscosity. It follows that the quantities C_p, R and C_r are all of $O(1)$. In this approach the scaling and the dependence of the turbulent viscosity have a clear physical meaning and interpretation. There is no need to impose a variation of the turbulent viscosity with the depth which would greatly complicate the model for a doubtful benefit. The viscous terms are needed for their diffusive role and to create enstrophy. The only important thing is to be able to predict the value of the eddy viscosity in all cases and the hypothesis of a viscosity which is constant over the depth is sufficient for this purpose as it is shown in the following sections.

1.4 Numerical resolution

In this section, the proposed model is validated by comparison with experimental results. Finally, the resulting system for mild slope topography can be written as ($L \leq \infty$ denotes the length of the flow domain)

$$\begin{cases} \dfrac{\partial h}{\partial t} + \dfrac{\partial hU}{\partial x} = 0, & \forall x \in [0, L], \, t > 0 \\[2mm] \dfrac{\partial hU}{\partial t} + \dfrac{\partial}{\partial x}\left(hU^2 + \dfrac{gh^2}{2} + h^3\varphi + \dfrac{h^2\ddot{h}}{3} \right) = \dfrac{\partial}{\partial x}\left(\dfrac{4}{R}h^3\sqrt{\varphi}\dfrac{\partial U}{\partial x} \right) - ghb', \\[2mm] \dfrac{\partial h\varphi}{\partial t} + \dfrac{\partial hU\varphi}{\partial x} = \dfrac{8h\sqrt{\varphi}}{R}\left(\dfrac{\partial U}{\partial x} \right)^2 - C_r h^3 \varphi^{3/2}. \end{cases} \tag{1.34}$$

We focus here on numerical tests for this system, intended to determine general laws for the empirical constants appearing in the model. It should be mentioned that the proposed system (1.34) can be treated in the same manner as the Green-Naghdi system. Consequently, the same techniques as the ones used for the Green-Naghdi equations can be applied for all challenging issues such as the evaluation of the high-order derivatives, or the preservation of the steady states. In the last two decades, the Green-Naghdi system has received much of attention due to its improved dispersive properties. Many different approaches have been applied to the one-dimensional system. A finite-difference method is proposed in [7, 6]. A finite-volume method is developed in [35, 36], [86] and [49]. A pseudo-spectral approach is applied in [45]. Hybrid methods are implemented in [30], [22]

Numerical animations are available https://www.math.univ-toulouse.fr/~mkazakov

and [140]. For continuous finite element methods and discontinuous Galerkin methods we refer to [101, 102] for the former, and to [109], [41], and [43] for the latter. Two-dimensional numerical studies can be found in [86], [125], [6], [83], [112],[50] and [44]. In this study, we focus only on one-dimensional equations to validate the proposed model.

The numerical integration of the Green-Naghdi equations generally includes an elliptic operator inversion. The change of variables proposed in [86] allows a splitting of the numerical resolution into two steps. Firstly, the system is rewritten as a hyperbolic system of equations and treated with a Godunov's type method. Then an elliptic equation for the velocity is solved. We adopted this strategy for the model (1.34) due to its straightforward realization.

1.4.1   Numerical scheme

Following [86], we introduce the new variables

$$K = U + \frac{1}{3h}\frac{\partial(h^2\dot{h})}{\partial x}, \tag{1.35}$$

$$\alpha = -\frac{2}{3}h^3\frac{\partial(hU)}{\partial x}. \tag{1.36}$$

Under this change of variables the system (1.34) can be rewritten in the following form:

$$\begin{cases} \dfrac{\partial h}{\partial t} + \dfrac{\partial hU}{\partial x} = 0,, & \forall x \in [0,L],\, t > 0 \\[2mm] \dfrac{\partial hK}{\partial t} + \dfrac{\partial}{\partial x}\left(hUK + \dfrac{gh^2}{2} + h^3\varphi + \alpha\right) = \dfrac{\partial}{\partial x}\left(\dfrac{4}{R}h^3\sqrt{\varphi}\dfrac{\partial U}{\partial x}\right) - ghb', \\[2mm] \dfrac{\partial h\varphi}{\partial t} + \dfrac{\partial hU\varphi}{\partial x} = \dfrac{8h\sqrt{\varphi}}{R}\left(\dfrac{\partial U}{\partial x}\right)^2 - C_r h\varphi^{3/2}. \end{cases} \tag{1.37}$$

The idea to replace the variable u by K was firstly used in [28] for a Hamiltonian formulation of the Green-Naghdi model.

1.4.2   Hyperbolic system

For the discretization of (1.37), we use a Godunov's type method since this system is hyperbolic. The viscous and topography source terms being not stiff an explicit algorithm can be applied. However, the influence of viscosity on the time discretization step should be taken into account. The flow domain is discretized with time and space steps δt, δx, respectively. Noting the vector of unknowns $\mathbf{V}_i^n = (h_i^n, hK_i^n, h\varphi_i^n)^\top$, where index i corresponds to the space cell $x_i = i\delta x$, and n correspond to the time instant $t^n = n\delta t$, we write the second order in space and time numerical scheme,

$$\overline{\mathbf{V}}_i = \mathbf{V}_i^n + \frac{\delta t}{2\delta x}\left(\mathbf{F}(V_{i-1/2}^n) - \mathbf{F}(V_{i+1/2}^n)\right) + \frac{\delta t}{2}\mathbf{S}(V_i^n), \quad i = 1,..,L/\delta x.$$

This step is repeated twice in conformity with the *Runge-Kutta time scheme* of the second order (RK2), i.e.:

$$\overline{\overline{\mathbf{V}}}_i = \overline{\mathbf{V}}_i + \frac{\delta t}{2\delta x}\left(\mathbf{F}(\overline{V}_{i-1/2}) - \mathbf{F}(\overline{V}_{i+1/2})\right) + \frac{\delta t}{2}\mathbf{S}(\overline{V}_i).$$

Finally, the solution is updated as

$$\mathbf{V}_i^{n+1} = \frac{1}{2} \left(\mathbf{V}_i^n + \overline{\overline{\mathbf{V}}}_i \right) \tag{1.38}$$

The fluxes are calculated with respect to inter-cell values (with indexes $i \pm 1/2$) by using an approximate Harten-Lax-van Leer (HLL) Riemann solver [143], [88] (n in time index is omitted to show that fluxes for the intermediate state $\overline{V}$ are calculated in the same manner):

$$\mathbf{F}_{i\pm1/2} = \mathcal{F}^{hll} \left(\left(\mathbf{V}_{i\pm1/2} \right)^\ell, \left(\mathbf{V}_{i\pm1/2} \right)^r \right).$$

Left and right cell value $\left(\mathbf{V}_{i\pm1/2} \right)^{\ell,r}$ are reconstructed with a second order $MUSCL$ approximation [143], [88]. In the HLL solver the eigenvalues associated to the non-dissipative part of the system (1.34)

$$\lambda_1 = U, \quad \lambda_{2,3} = U \pm \sqrt{gh + 3h^2\varphi}$$

are used.

In case of zero viscosity the time step δt is restricted by the classical Courant–Friedrichs–Lewy (CFL) condition, which is a necessary condition for stability,

$$\delta t < CFL \cdot \frac{\delta x}{\lambda_{max}},$$

where λ_{max} is the maximum eigenvalue calculated in each time layer. But in the case of non zero viscous source term for the stability of algorithm we are obliged to choose a more restrictive time step

$$\delta t < CFL \cdot min \left(\frac{\delta x}{\lambda_{max}}, \frac{R\,\delta x^2}{4} \right).$$

For the further validation of the model (1.34) it is not a very restrictive condition, but one should imagine a more efficient algorithm for the numerical realization of concrete applications, implying an implicit treatment of viscous terms, for example.

The source term $\mathbf{S}(\overline{V}_i)$ is discretized with a standard finite-difference second order approach. However, the topography term in the momentum equation should be discretized in a special manner to preserve a steady state $h + b = const$, $U = K = 0$, $\varphi = 0$, otherwise the scheme is not well-balanced (which means here does not preserve the so called *lake at rest* steady state). Following the idea found in [12], we obtain an appropriate discretization of the topography source term by considering the reduction of the system (1.37) for $h = const$, $U = K = 0$, $\varphi = 0$:

$$(ghb')_i = -\frac{g}{2} \left(h_{i-1/2} \right)^- + \frac{g}{2} \left(h_{i+1/2} \right)^+,$$

where $\left(h_{i\pm1/2} \right)^\pm$ are the reconstructed values obtained with the condition of a constant steady water level, namely $h_i + b_i = h_{i+1} + b_{i+1}$. Generally speaking, the well-balanced reconstruction described above results in changing the fluxes $\mathbf{F}_{i\pm1/2}^n$, and adding a correction cell-centred source term for the second order approximation. That procedure gives us an exact steady state conservation (for the detailed proof see [12]).

1.4.3   Elliptic equation

Once the (h_i^{n+1}, hK_i^{n+1}) is computed, the velocity field is defined by solving the equation (1.35). We rewrite this equation in terms of hu and hK

$$hK = hu - \frac{1}{3}\frac{\partial}{\partial x}\left(h^2\frac{\partial(hu)}{\partial x}\right) + \frac{1}{6}\frac{\partial}{\partial x}\left(hu\frac{\partial h^2}{\partial x}\right),$$

which leads to the equation

$$\frac{\partial^2(hu)}{\partial x^2} + A\frac{\partial(hu)}{\partial x} + B(hu) + C = 0,$$

with

$$A = \frac{1}{2h^2}\frac{\partial h^2}{\partial x}, \quad B = -\frac{1}{2h^2}\left(6 + \frac{\partial^2 h^2}{\partial x^2}\right),$$

$$C = \frac{3}{h^2}hK.$$

This equation is solved at the end of each time step, using the following finite-difference discretization (index $n+1$ is omitted over all variables)

$$\left(\frac{1}{\delta x^2} + \frac{A_i}{2\delta x}\right)(hu)_{i+1} + \left(B_i - \frac{2}{\delta x^2}\right)(hu)_i + \left(\frac{1}{\delta x^2} - \frac{A_i}{2\delta x}\right)(hu)_{i-1} + C_i = 0,$$

where

$$A_i = \frac{1}{2h_i^2}\frac{h_{i+1}^2 - h_{i-1}^2}{2\delta x}, \quad B_i = -\frac{1}{2h_i^2}\left(6 + \frac{h_{i+1}^2 - h_i^2 + h_{i-1}^2}{\delta x^2}\right)$$

$$C_i = \frac{3}{h_i^2}(hK)_i.$$

This results in the inversion of a three-diagonal matrix, which is done with the tridiagonal matrix algorithm, also known as Thomas algorithm [123] (originally described in [138]). Obviously, this step is the most time-consuming of all numerical algorithm.

Boundary conditions for both, hyperbolic and elliptic steps, must be imposed. We use the Dirichlet boundary conditions for the Riemann invariants $I_{l,r}$ by analogy with the nonlinear shallow water equations, defined as

$$I_{r,l} = K \pm \sqrt{gh}.$$

This information allows for a definition of the water depth at inflow and outflow boundaries.

1.4.4   Solitary wave propagation over a flat bottom

The numerical scheme is validated in the case of the classical soliton solution. The Green-Naghdi system admits an exact solution which corresponds to a wave propagating without deformation. This solution was found by Su & Gardner [130] and coincides with the expression derived by Rayleigh (see [114]). This particular kind of solitary wave was first observed by Russell ([121]). The model (1.34) admits also such a type of solution on a flat horizontal bottom in the absence of dissipation. The exact expressions for the water depth

h^{ex}, the fluid velocity U^{ex} and the enstrophy φ^{ex} were derived in a more general case in [119]. In this particular case, these expressions reduce to $\varphi^{\mathrm{ex}} = \varphi_0 = \mathrm{constant}$,

$$\frac{h^{\mathrm{ex}}}{h_0^*} = 1 + \frac{2\tilde{a}\left(Fr^2 - 1 - 3\tilde{\varphi}\right)}{Fr^2 - 1 - (3 + \tilde{a}^2)\tilde{\varphi} + \left[Fr^2 - 1 - (3 - \tilde{a}^2)\tilde{\varphi}\right]\cosh\left[\kappa\left(x - c_0 t - x_0\right)/h_0^*\right]} \quad (1.39)$$

and

$$U^{\mathrm{ex}} = c_0\left(1 - \frac{h_0^*}{h^{\mathrm{ex}}}\right), \quad (1.40)$$

where x_0 is the initial abscissa of the wave maximum depth position, h_0^* is the still water depth at an infinite distance from the wave, c_0 is the celerity of the soliton, $\tilde{a} = \delta = a/h_0^*$ its dimensionless amplitude (and the nonlinearity parameter), $Fr = |c_0|/\sqrt{gh_0^*}$ a Froude number representing the dimensionless wave celerity, $\tilde{\varphi} = \varphi h_0^*/g$ the dimensionless enstrophy and where

$$\kappa = \sqrt{\frac{3}{Fr^2}\left(Fr^2 - 1 - 3\tilde{\varphi}\right)}. \quad (1.41)$$

The celerity of the soliton can be written

$$c_0 = \sqrt{(h_0^* + a)\left[g + \varphi\left(3h_0^* + a\right)\right]}. \quad (1.42)$$

The dimensionless amplitude of the wave $\tilde{a}$ is

$$\tilde{a} = \frac{1}{2\tilde{\varphi}}\left[-(1 + 4\tilde{\varphi}) + \sqrt{(1 + 4\tilde{\varphi})^2 + 4\tilde{\varphi}\left(Fr^2 - 1 - 3\tilde{\varphi}\right)}\right]. \quad (1.43)$$

This soliton solution reduces to the one of the 1D Green-Naghdi equations, if $\varphi_0 = 0$. If $\varphi_0 \neq 0$, this solution describes a wave with a smaller amplitude for the same Froude number compared to Green-Naghdi solitary wave. The depth profile of a soliton calculated for $Fr = 1.095$, $h_0^* = 1\mathrm{m}$ and $\varphi_0 = 0.05\mathrm{s}^{-2}$ is presented in Figure 1.2 (a) where it is compared to the depth profile of the classical soliton ($\varphi_0 = 0$) for the same reference water depth and Froude number. The main effect of the enstrophy is to decrease the soliton amplitude.

The proposed numerical scheme preserves the dynamics of the solitary waves (see figure 1.2 (c)). This case is used to study the convergence of the algorithm. We define the error function of the approximation as a discrete version of the norm error. Let us first denote

$$e_n = |\; h(t_n, \cdot) - h_{ex}(t_n, \cdot)\;|_{L_2},$$

for all time step t_n. Then the discrete norm is defined as

$$L_\infty^{err} = \max_{0 < n \leq N}\left(e_n\right).$$

The accuracy of the numerical scheme is of second order in space if

$$L_\infty^{err} \leq C_x^\infty \delta x^2,$$

where C_x^∞ is a constant depending on the reference solution. This condition is numerically verified (see Figure 1.2 (b)).
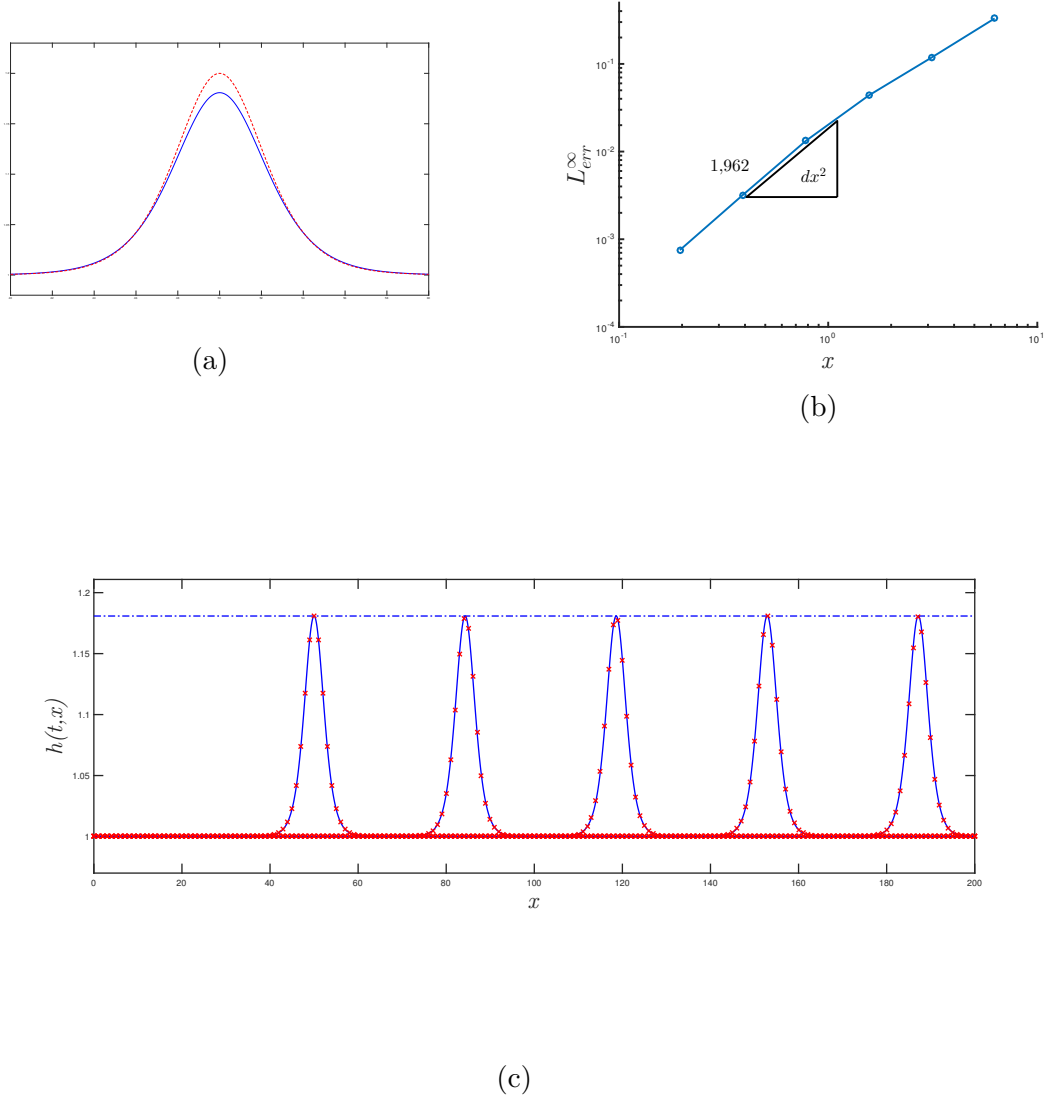
(a)

(b)

(c)

Figure 1.2: Propagation of the solitary wave (1.39) for $Fr = 1.095$, $\varphi_0 = 0.05\text{s}^{-2}$, (*a*) comparison between (1.39) (solid line) and exact Green-Naghdi solution (dashed line), (*b*) L^{err}_∞ error in a logarithmic scale for the free surface elevation for different space discretization, (*c*) solitary wave (solid line) propagation compared to the exact solution (1.39) (crosses) for different time instant $t = 0s$, $t = 10s$, $t = 20s$, $t = 30s$, $t = 40s$.

1.4.5   Virtual enstrophy breaking criteria

The nonlinearity parameter of the initial waves is defined by $\delta = a^*/h_0^*$ where a^* is the initial amplitude of the wave and where h_0^* is the still water level at the initial position of the wave. When $\delta < 0.05$ the model (1.34) can be applied directly without any modification. The breaking position is described correctly due to the sudden growth of enstrophy from a very small value at the beginning of the wave propagation to a large value in the breaking region. An example of a solitary wave with $\delta = 0.048$ propagating on a constant slope equal to $\mathrm{tg}\beta = 1/60$ is presented in Figure 1.4 (a), where the maximal value of the enstrophy is given as a function of the position during the wave propagation. This is a simulation of an experiment of Hsiao *et al.* ([64]) whose geometrical characteristics are presented in Figure 1.3. In this case, the still water depth at the initial position was $h_0^* = 1.2$m. The values of the parameters of the model are $C_r = 0.48$ and $R = 6$ and these values can be used for all solitary waves with $\delta < 0.05$ on this slope. The increase of enstrophy corresponds to the breaking point since it implies also a brutal increase of the large-scale turbulent energy and a diminution of the wave amplitude. As shown in Figure 1.4 (a), the enstrophy keeps a very small value from the beginning of the wave propagation until the breaking region where the sudden increase takes place. In the shoaling zone the values of the enstrophy range from $10^{-7}\mathrm{s}^{-2}$ to $10^{-4}\mathrm{s}^{-2}$ whereas in the surf zone, the enstrophy is in the order of $1\mathrm{s}^{-2}$ or $10\mathrm{s}^{-2}$, thus several orders of magnitude higher. This evolution is also presented in Figure 1.4 (b) with another scale showing that the enstrophy is much smaller than $10^{-3}\mathrm{s}^{-2}$ in the shoaling zone. The extreme steepness of the enstrophy curve at the breaking point shows that the enstrophy is a relevant quantity to characterize the wave breaking.

However, for solitary waves with a nonlinearity greater than about 0.05, the initial evolution of the enstrophy causes an important attenuation of the wave amplitude. The evolution of the maximum value of the enstrophy for a solitary wave with a nonlinearity parameter $\delta = 0.137$ and the conditions of Hsiao *et al.* (2008) with $h_0^* = 2.2$m is presented in Figure 1.4 (a). The increase of φ just before the breaking point is rapid but it is less steep than for $\delta = 0.048$. With the different scale presented in Figure 1.4 (b), it can be seen that the maximum value of φ increases first from its initial value $10^{-9}\mathrm{s}^{-2}$ to a constant value of about $0.2 \cdot 10^{-3}\mathrm{s}^{-2}$ corresponding to the part of the propagation over a horizontal bottom. When the wave arrives over the sloping bottom (see Figure 1.3), the maximum value of the enstrophy is no longer constant and increases until the wave breaking. Although the maximum value of φ in the shoaling zone is small, it is several orders of magnitude greater than for $\delta = 0.048$. The enstrophy is still a relevant quantity for breaking but its values are not small enough before breaking to be entirely negligible and this is the cause of the wave attenuation. Therefore, in such conditions the enstrophy must not be created in the shoaling zone. This implies that the turbulent viscosity should be activated only when the breaking is likely to occur and that a breaking criterion is needed for these waves.

There exist several breaking criteria based on empirical relations for the horizontal velocity, the free-surface gradient or the local energy dissipation (see e.g. [22]), for other criteria we refer to [69], [13], or [43]. Although most of those criteria can be adapted to our model, we introduce a new criterion specific to this model and based on the sudden increase of the enstrophy at the breaking point. The idea is to calculate the enstrophy produced by
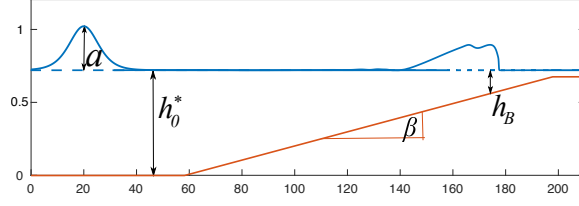
Figure 1.3: Experiment setup. A solitary wave of amplitude a in the fluid of depth h_0^* at rest propagates over a topography with incline β, a_B is the breaking amplitude, h_B is the breaking depth.
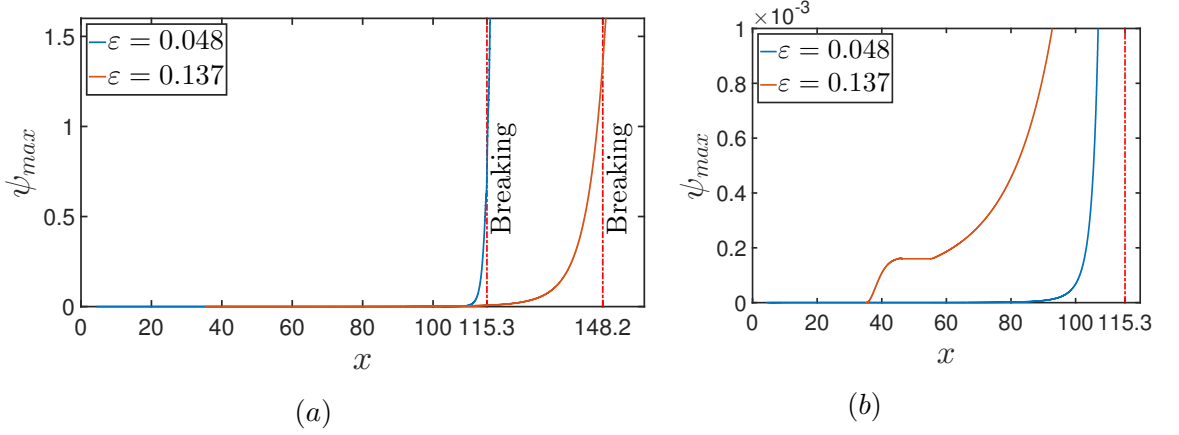

Figure 1.4: Evolution of the maximal value of the enstrophy for the different values of the nonlinearity parameter $\delta = 0.048$, $\delta = 0.137$, (a) propagation until the wave breaking defined in the experiment (vertical lines), (b) detailed zoom on the initial values of virtual enstrophy.

the wave while preventing any feedback on the wave's characteristics to avoid the spurious amplitude attenuation. A new quantity denoted by ψ is introduced. It follows the same equation as the real enstrophy φ except that the turbulent viscosity is always activated. This new quantity, homogeneous to the enstrophy, represents the amount of enstrophy that the wave is potentially able to create and therefore it is called virtual enstrophy. The virtual enstrophy undergoes a sudden increase when the wave is about to break and this can be used to characterize the breaking point. The eddy viscosity in the equation of the real enstrophy is set equal to zero as long as the virtual enstrophy did not reach a threshold value ψ_0. This means that there is no enstrophy creation before the breaking point and thus no amplitude attenuation in the shoaling zone. The cell where ψ becomes equal to ψ_0 is the beginning of the breaking process.

Moreover, the experiments and the numerical simulations show that the vorticity generation and the turbulence generation take place during breaking in approximately the same front region of the wave ([90], [26],[72]). A depth-averaged model cannot describe all the details of the breaking process. The vorticity and turbulence generation during the steepening of the free surface is taken into account by an enstrophy creation caused by the production term in the enstrophy equation (1.30). When the free surface steepens, $(\partial U/\partial x)^2$ and con-

sequently the production term increases and enstrophy is created. However the particular generation mechanism that takes place at the front side of the crest cannot be captured by a depth-averaged model. The information on the sign of $\partial U/\partial x$ is lost in the production term. Consequently enstrophy can be produced not only at the front side of the wave but also at the rear side, particularly if the wave profile is weakly asymetrical. In the case of a soliton, the wave profile is completely symetrical. In the absence of a description of the generation of vorticity and turbulence on the front surface of the wave, there is a production on both sides of the crest. A sloping bottom creates some asymmetry in the wave but this does not always prevent an enstrophy production in the rear of the wave. This gives the grounds for the introduction of a second element of breaking criterion. We allow for an enstrophy production only at the front side of a wave. This condition is equivalent to $\dot{h} < 0$ since the mass equation implies that the material derivative of the water depth is $\dot{h} = -h\partial U/\partial x$. The front part of the wave is thus defined as $\dot{h} > 0$. There are many cases where this condition is needless and, even when it is useful, its omission causes only a transient problem that is rapidly corrected by the action of the dissipation. However, since its implementation is easy, it seems that there is no reason not to include it.

To formalize what has been said, until the condition $\max\limits_{x} \psi(t,x) < \psi_0$ is satisfied we calculate the numerical solution of the system

$$\begin{cases} \dfrac{\partial h}{\partial t} + \dfrac{\partial hU}{\partial x} = 0, \\[2mm] \dfrac{\partial hK}{\partial t} + \dfrac{\partial}{\partial x}\left(hUK + \dfrac{gh^2}{2} + \alpha \right) = -ghb', \qquad \begin{aligned} &\forall t < t^*, \forall x \in [0,L] : \\ &\max\limits_{x} \psi(t,x) < \psi_0, \end{aligned} \\[2mm] \dfrac{\partial h\psi}{\partial t} + \dfrac{\partial (hU\psi)}{\partial x} = G_p \dfrac{8h\sqrt{\psi}}{R}\left(\dfrac{\partial U}{\partial x} \right)^2 - C_r h\psi^{3/2}, \end{cases} \qquad (1.44)$$

where $G_p = 0$, if $\partial U/\partial x > 0$. Further, the enstrophy $\varphi(t,x)$ is activated after the time instant t^* such that $\max\limits_{x} \psi(t^*,x) > \psi_0$, and the system (1.44) is extended to

$$\begin{cases} \qquad\qquad \dfrac{\partial h}{\partial t} + \dfrac{\partial hU}{\partial x} = 0, \\[2mm] \forall t > t_*, \qquad \dfrac{\partial hK}{\partial t} + \dfrac{\partial}{\partial x}\left(hUK + \dfrac{gh^2}{2} + h^3\varphi + \alpha \right) = \dfrac{\partial}{\partial x}\left(\dfrac{4}{R}h^3\sqrt{\varphi}\dfrac{\partial U}{\partial x} \right) - ghb', \\[2mm] \forall x \in [0,L] \quad \dfrac{\partial h\psi}{\partial t} + \dfrac{\partial (hU\psi)}{\partial x} = G_p\dfrac{8h\sqrt{\psi}}{R}\left(\dfrac{\partial U}{\partial x} \right)^2 - C_r h\psi^{3/2}, \\[4mm] \qquad\quad \forall t > t_*, \\[1mm] \forall x \in \bigcup\limits_{\ell=t^*}^{t}\{x : \max\limits_{x} \psi(\ell,x) > \psi_0\}, \quad \dfrac{\partial h\varphi}{\partial t} + \dfrac{\partial (hU\varphi)}{\partial x} = G_p\dfrac{8h\sqrt{\varphi}}{R}\left(\dfrac{\partial U}{\partial x} \right)^2 - C_r h\varphi^{3/2}. \end{cases}$$

$$(1.45)$$

An appropriate criteria for the virtual enstrophy critical value ψ_0 is proposed further, based on comparison with experiments. The advantage of the proposed criteria is that it does not depend on discrete parameters and its implementation is straightforward. It is necessary to make clear that from the form of the equation for $\psi(t,x)$ (respectively $\varphi(t,x)$) only a

non-zero initial distribution must be given for $\psi(t,x)$ ($\varphi(t,x)$). Numerical tests show that even tiny value $10^{-12} - 10^{-9}$ are sufficient for a further evolution of $\psi(t,x)$ ($\varphi(t,x)$). One can notice a similarity with common turbulence modelling.

Propagation of a soliton in a constant water depth

The evolution of the virtual enstrophy for a solitary wave propagating over a flat bottom is studied now. We show numerically that the virtual enstrophy is a bounded function for different initial wave conditions. Considering the solitary wave defined with (1.39), (1.40) with φ_0 equal to an infinitesimal value, we establish several dependences. The maximal value of $\psi(t,x)$ is bounded for different Reynolds numbers, nonlinearity parameters and initial depths, and it depends on the initial wave amplitude. For strongly nonlinear waves the maximal value is bigger than for weakly nonlinear waves (Figure 1.5 (a)). This maximal value is also bigger if R is smaller or if the depth h_0 is greater (Figure 1.5 (b) (c)). This guides us in the definition of the critical value ψ_0. Moreover, it is known that a soliton cannot physically exist if the nonlinearity parameter of the wave is greater than some limit value. The most commonly accepted limit value is $\delta = 0.78$ (McCowan 1894). For a nonlinearity greater than this limit, the wave breaks and dissipation appears. On this first point we base our further investigation on the criteria for virtual enstrophy. Moreover, the dependence on the initial water depth points that a dimensionless critical value ψ_0 must be found. Generally speaking, for the systems (1.44), (1.45) three parameters C_r, R and dimensionless ψ_0 should be defined. We base our criteria on comparison with experiments, and numericals tests are proposed in the next section. In addition, as was mentioned before the initial distribution of the enstrophy is non zero, we have checked numerically that the maximal value of $\psi(t,x)$ does not depend on this initial value if it is small enough.

1.5 Application to a mild-slope topography

We study now the waves propagation over a mild-slope topography. The recent experimental research [64] is used to validate the model (1.34). In these experiments a solitary wave is generated with a high-resolution wavemaker and it propagates in a channel $300\,\text{m}$ long, $5.0\,\text{m}$ wide and $5.2\,\text{m}$ deep. A plane beach with a slope equal to $\text{tg}\beta = 1/60$ starts 50m after the wavemaker. The setup is shown on Figure 1.3. The study of wave shoaling and wave breaking is presented for different values of the nonlinearity parameter δ ranging from 0.019 to 0.338, and initial depth $h_0^* = 1.2\,\text{m}, 2.2\,\text{m}, 2.9\,\text{m}$. The breaking position is given for each test case, and time series of wave propagation are available. The localization of breaking points is a quite challenging issue. Moreover the definition of the breaking point itself can have several interpretations. For example, the amplitude is dramatically decreasing for strongly nonlinear waves when breaking occurs. In the works of [64] the breaking points are defined as the location where the front of the leading wave becomes near vertical tangent and bubbles subsequently appear. We can interpret it physically as a turbulent energy increase, that is to say an enstrophy growth in the proposed approach. This idea allows us to determine an appropriate value for the limit virtual enstrophy ψ_0, in order to have a good agreement with experimental breaking points. It is clear that the viscosity
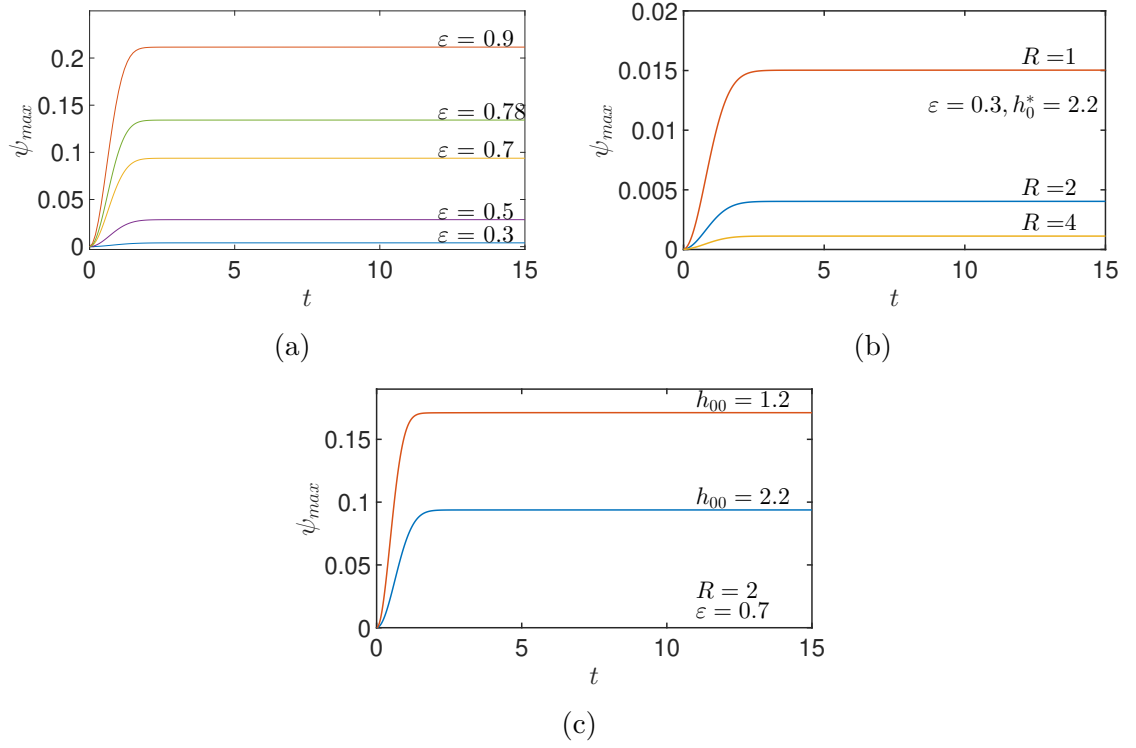
Figure 1.5: Dependence of maximal value of $\psi_{max} = \max\limits_{x} \psi(t, x)$ on different parameters of the solitary wave solution (a) $R = 2$, $h_0^* = 1, 2m$, for $\delta = 0.3 - 0.8$, (b) $\delta = 0.3$, $h_0^* = 2.2m$, for $R = 1, 2, 4$, (c) $R = 2$, $\delta = 0.7$, for $h_0^* = 1.2m, 2.2m$

δ	h_0^*, m	δ	h_0^*, m	δ	h_0^*, m	δ	h_0^*, m	δ	h_0^*, m
0.048	1.2	0.248	1.2	0.0195	2.2	0.120	2.2	0.019	2.9
0.112	1.2	0.2875	1.2	0.054	2.2	0.137	2.2	0.086	2.9
0.227	1.2	0.338	1.2	0.069	2.2	0.152	2.2		

Table 1.1: The test conditions of solitary waves up a mild sloping beach.

added to the model is responsible for the amplitude decrease after breaking; therefore this enables to define the Reynolds number value R. Tests are made for different initial depths and initial nonlinearity parameters (see Table, 1.1). We conclude on the next definition for the parameters:

$$\psi_0 = \frac{g}{h_0^*}\widetilde{\psi}_0, \quad \widetilde{\psi}_0 = \begin{cases} \left(0.1 + \dfrac{0.031}{\delta}\right), & \delta > 0.05, \\ 0, & \delta < 0.05, \end{cases} \qquad R = \begin{cases} 1.7, & \delta > 0.05, \\ 6, & \delta < 0.05, \end{cases} \tag{1.46}$$

The constant $C_r = 0.48$ is taken for all numerical tests. Choosing a constant Reynolds number for all tests lead to a good agreement on the wave profile after breaking. The value ψ_0, as discussed in subsection 1.4.5, depends on h_0^* and δ, so we propose dimensionless value $\widetilde{\psi}_0$, which depends on the nonlinearity parameter δ. As we mentioned above, no criteria is needed for small values $\delta < 0,05$, the evolution of the enstrophy during wave shoaling is very small and does not influence the wave amplitude. The breaking position is in a good agreement as well.

1.5.1 Experimental comparison

We provide several comparisons based on the time series experimental data, using the parameters given above by (1.46). The numerical breaking position is defined as the moment when the virtual enstrophy criterion $\max_x \psi > \psi_0$ is satisfied. For the given breaking points in [64], the simulation errors are of order $0.2 - 1\,m$. This can be explained by the fact that the development of bubbly layer takes some time from the beginning of the breaking process, as well as the evolution of the enstrophy in the model, but one can imagine that a non-zero level of enstrophy corresponds to bubble generation. Numerical results are presented on Figures 1.6, 1.7, 1.8. The numerical and experimental profiles are in good agreement, and the breaking positions defined by ψ_0 is in agreement with the experimental ones. The enstrophy profiles corresponding to the wave propagation are shown in the same figures. For the test case 1.6 $\delta = 0.048$, no breaking criterion is applied, however the enstrophy stays very small at initial times of the wave motion. For the test cases 1.7, 1.8 the nonlinearity parameter δ is equal to 0.137 and 0.086 respectively, and the criterion is therefore used. It provides that enstrophy stays very small and a good agreement on the amplitude is reached at the initial times of the wave propagation.

Note that after the criterion activation, the wave amplitude decreases but not immediately. One can imagine to define the breaking position as a moment when the amplitude starts to decrease (note that the same remark is made on the difficulties to define the breaking position in [64], and finally the experimental breaking position is defined with the

	experiment	ψ_0	decrease of a
figure 1.6	$116.7\,m$	$-$	$115.85\,m$
figure 1.7	$148\,m$	$148.2\,m$	$149.05\,m$
figure 1.8	$193\,m$	$192.7\,m$	$193.5\,m$

Table 1.2: Correspondence of breaking positions found in experiments, defined by the virtual enstrophy criteria and by the decreasing of the wave amplitude.
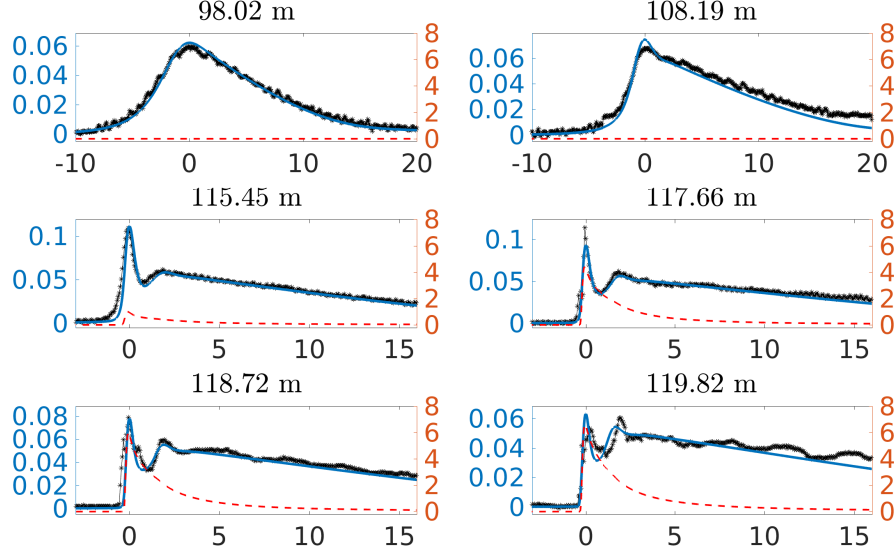

Figure 1.6: Comparison of numerical (blue line) with experimental (black line) time series for the free surface evolution $h_0^* = 1.2\,m$, $\delta = 0.048$. Enstrophy evolution is shown in red.

amplitude decrease as well). In this case the numerical breaking points are in correspondence with the experimental ones as well (see table 1.2). This definition works even if no criteria is given as in the cases of small nonlinearity parameter.

No attempt is made here to improve the dispersive properties. The model is fully nonlinear and has the same dispersive properties as the equations of Green-Naghdi. Its dispersive properties are thus better than those of weakly-nonlinear Boussinesq models. However the dispersive properties can be improved in the same way as those of the Green-Naghdi model as in [22] or [83]. Because in this part the standard dispersive properties of the Green-Naghdi system are kept, a small deviation to the experimental profiles in the shoaling zone can sometimes be observed. For example, in Figure 1.8 the calculated wave amplitude is smaller than the experimental one at $x = 192.36$m just before the breaking point.

The model predictions on the evolution of the wave amplitude are compared to the power-law of Synolakis & Skjelbreia [135]:

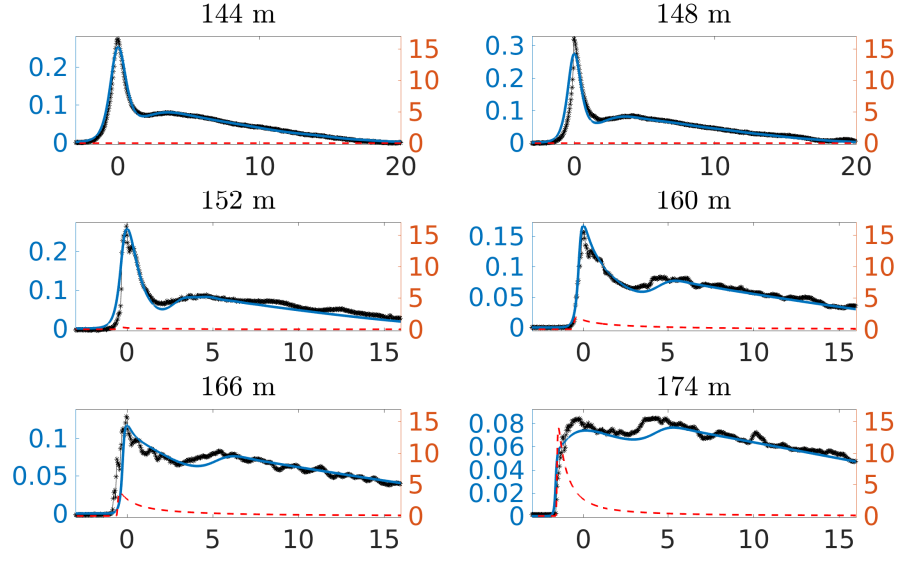$$\frac{\eta_{max}}{h_b} \sim \left(\frac{h}{h_b}\right)^n \qquad (1.47)$$

Figure 1.7: Comparison of numerical (blue line) with experimental (black line) time series for the free surface evolution $h_0^* = 2.2\,m$, $\delta = 0.137$. Enstrophy evolution is shown in red.
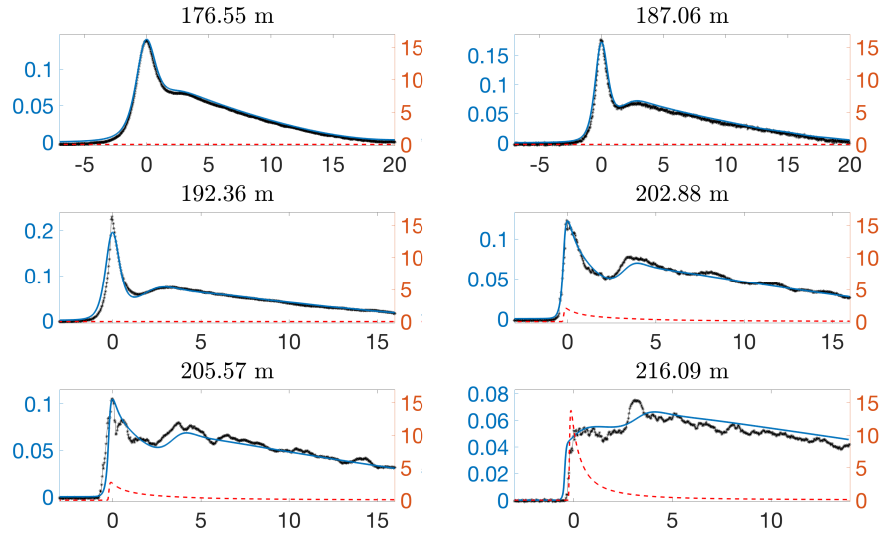

Figure 1.8: Comparison of numerical (blue line) with experimental (black line) time series for the free surface evolution $h_0^* = 2.9\,m$, for $\delta = 0.086$. Enstrophy evolution is shown in red.
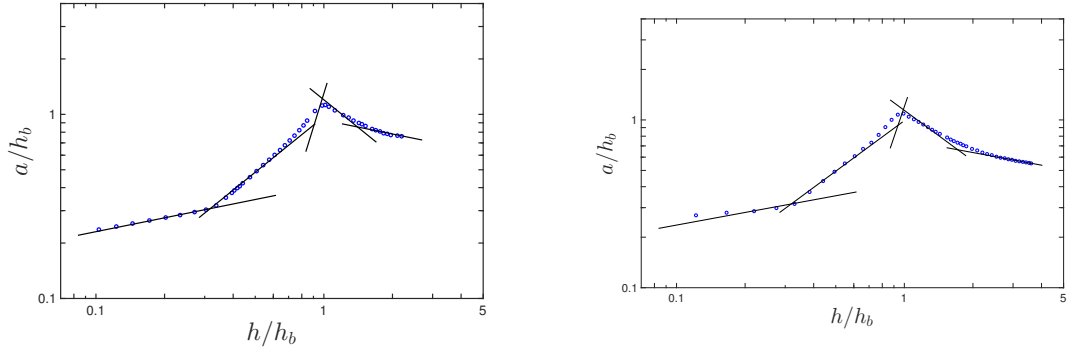
Figure 1.9: Evolution of the maximal amplitude in numerical tests (points) for a solitary wave with (left) $h_0^* = 1.2\,m$, $\delta = 0.338$ (right) $h_0^* = 2.2\,m$, $\delta = 0.152$, solid line represents theoretic slopes according to the law (1.47).

where $n = -1/4$ (Green's law) for the zone of gradual shoaling, $n = -1$ (Boussinesq's law) for the zone of rapid shoaling, $n = 4$ for the zone of rapid decay and $n = 1$ for the zone of gradual decay, respectively, as proposed by [135]. In [139] and [64] the existence of a fifth zone where $n = 1/4$ after the zone of gradual decay is shown. The numerical results are in good agreement with the experimental results and with the values of the exponent of the law (1.47) in each zone including in the fifth zone where we find a value of the exponent n close to $1/4$ (see Figure 1.9). The curve is a little bit less sharp than the experimental one at the breaking point. This is probably due to the dispersive properties of the model which are identical to the Green-Naghdi equations and which are not optimal as it is explained above. It results that the amplitude is slightly underestimated just before the breaking point. In all other regions, the predicted wave amplitude evolution is very similar to the experimental results of [64].

The other law proposed in [58] permits to confirm that the breaking position is defined correctly with the criteria (1.46). We have:

$$\frac{h_b}{h_0^*} = \frac{0.149}{(S_0/\delta)^{0.523}}, \quad \text{for } S_0 < 0.30, \tag{1.48}$$

where the slope parameter $S_0 = 1.521\,(tg\beta)\,/\sqrt{\delta}$ is related to the nonlinearity of the initial wave and the topography angle. On the whole this law was also confirmed by the experiments of Hsiao *et al.* (2008). The comparison of the breaking depths predicted by our model with this law are presented in Figure 1.10. Our numerical results are very close to the experimental results of Hsiao *et al.* (2008). There is an overall agreement with the law (1.48). The deviations follow exactly the same trends as the experimental measures. In particular, as noted by Hsiao *et al.* (2008), the law (1.48) under-predicts slightly the breaking water depth for $S_0/\delta < 2$. This small deviation has the greatest value, both in the experiments and in the numerical simulations, for S_0/δ close to 1. Conversely, for large values of S_0/δ (between 9 and 10), the numerical results are smaller than the values predicted by the law (1.48). In the experiments of Hsiao *et al.* (2008), most values of h_b/h_0^* for S_0/δ between 9 and 10 are also smaller than the predictions of this law. This comparison
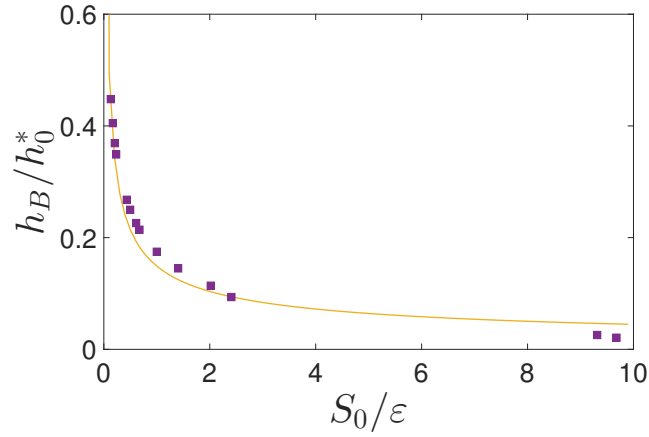
Figure 1.10: Comparison of the numerical breaking depth (points) with prediction by (1.48).

shows that the model gives an accurate prediction of the breaking depth and position, in a very good agreement with the experiments.

Finally we have checked whether the model prescribes a good velocity of the propagating solitary wave. The resulting plot is given in Figure 1.11, for the initial wave with $\delta = 0.152$ on $2.2\,m$ depth channel.

1.5.2   Wave transformation over different slopes

The influence of the slope on the values of the virtual enstrophy threshold ψ_0 and on R is studied based on recent experimental works [52] and [59], for various slope angles ($\beta = 1°, 3°, 6°$ and $11°$) and a nonlinearity parameter ranging from 0.2 to 0.7. The value of the bottom slope angle in the experiments studied above is $\beta = 0.95°$, which is very close to $\beta = 1°$. The numerical tests confirm that the proposed laws for ψ_0 and R give also satisfactory predictions for the case $\beta = 1°$ of [59]

However numerical tests show that these values are not valid for other slope angles. Since the increase of virtual enstrophy is faster if R is smaller, a given breaking point can be obtained with different sets of values for ψ_0 and R. The wave breaks later if ψ_0 or R are increased. However, given the steepness of the variation of the virtual enstrophy near the breaking point (see Figure 1.4), the threshold value ψ_0 has a much smaller effect on the breaking position than R. The value of ψ_0 must be strongly modified to change significantly the breaking point. It is therefore more practical to keep the same value of ψ_0 as above and to suppose that only R depends on the slope. This choice is also simpler to implement in the numerical scheme because in this case R is locally determined by the bathymetry. According to our numerical tests, supposing that R depends on the slope but not ψ_0 is not only the simplest choice but it works also better.

We based our final laws for virtual enstrophy limit and R on the measurement of breaking depths and positions from [64] and [59], and the analysis of a soliton over a plane horizontal bottom with the nonlinearity limit ($\delta = 0.78$). The following expressions are
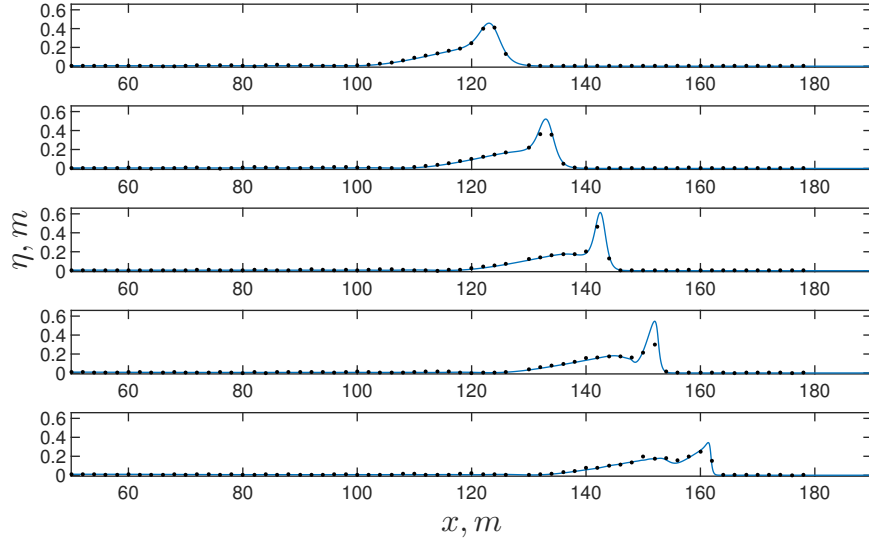
Figure 1.11: Comparison of numerical (solid line) space wave propagation with experimental data (points) for an initial wave with $\delta = 0.152$, $h_0^* = 2.2\,m$.
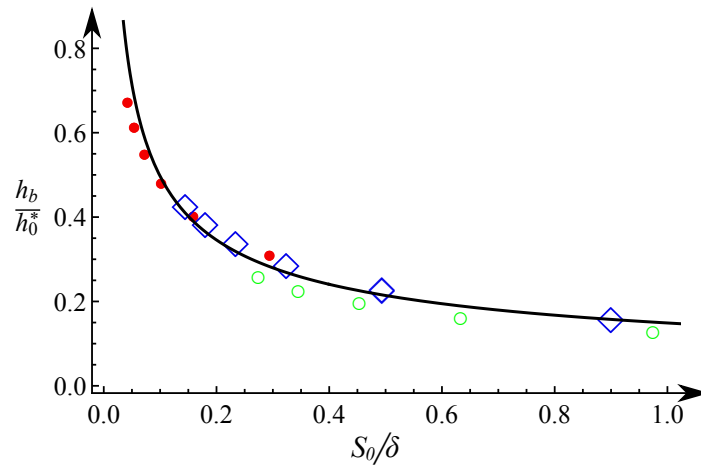

Figure 1.12: Numerical results for $\beta = 1°$ ($\bullet$), $\beta = 3°$ ($\diamond$) and $\beta = 6°$ ($\circ$) and comparison with the law (1.48) (solid curve).

proposed:

$$\psi_0 = \left(0.1 + \frac{0.031}{\delta}\right) \frac{g}{h_0^*} \quad \text{for } \delta > 0.05, \tag{1.49}$$

and

$$R = 0.85 + 60 \operatorname{tg} \beta. \tag{1.50}$$

If $\delta < 0.05$, then $\psi_0 = 0$ and $R = 6$. Predictions obtained with these expressions for β equal to $1°$, $3°$ and $6°$ and δ equal to 0.2, 0.3, 0.4, 0.5, 0.6 and 0.7 are compared to the law 1.48 proposed in [58] in Figure 1.12. The results are in good agreement with the law (1.48). The deviations are of the same order as those found in [58]. The case $\delta = 0.2$ and $\beta = 6°$ has $S_0 = 0.36$ and is not shown since the breaking type is a surging breaker ([58]) and the law (1.48) does not apply.

1.6 Conclusion

We derived a unified model which is capable to describe the breaking of a solitary wave in a surf zone. Mechanism of wave breaking is related to the appearance of turbulent structures. It is taken into account by introducing a new variable (enstrophy) in addition to water depth and average velocity of the flow. The enstrophy generation is governed by a turbulent viscosity hypothesis. Initially, filtered conservation equations are given, and the averaging with respect to depth is then made. The final system is a system of balance equations for mass, momentum and energy. In the resulting system, we choose to replace the energy balance law with the enstrophy transport equation as this system is dispersive and no shock solutions can arise. The system written in this form is more convenient for numerical implementation. The proposed model includes three empirical parameters, namely Reynolds number R, dissipation parameter C_r and virtual enstrophy limit value ψ_0 which are defined through comparison with experiments. Numerical tests are conducted for a significant range of values of the initial wave nonlinearity $\delta = 0.01 - 0.7$ and for different slopes of the mild topography ($0.95°$, $1°$, $3°$, $6°$, $11°$). It is established that the parameter R depends on the topography of the problem, and the limit value ψ_0 is related to the nonlinearity of the initial wave. The proposed empirical laws seem to define well the model parameters, as confirmed by preliminary works on $2D$ simulations [116].

In conclusion, we define some directions for the future research. The proposed model gives a good description of waves propagating over a mild topography. Therefore it should be promising to study if the method can be successfully applied to non-uniform topographies, including dry zones. However, a more robust numerical algorithm should be constructed for such a purpose. Investigations of the enstrophy evolution in the case of wave packets or cnoidal waves propagation should provide a better understanding of the waves influence at the coast. Furthermore, an additional study might be required to define the enstrophy limit value to terminate breaking process. In the present study, no additional criterion was used since it was not needed for the investigated experimental cases. However, it is important to note that enstrophy decreases to a small value after breaking and we suppose (at least in some cases) that no stopping criterion is needed. The verification is left for the future. One of the advantages of the proposed approach is the possibility to

capture an essential physical behaviour with such a simple depth-average model without any criterion for weakly-nonlinear waves. However, a breaking criterion is required for the simulations of the propagation of strongly nonlinear waves. One of the perspectives of this approach is to find a way to get rid of the breaking criterion once for all. Of course, the DNS for the Euler equations or the Navier-Stokes system could be applied, but it is a very time-consuming solution.

There are two main numerical issues related to the studied system of equations. The first one is the discretization of the high-order derivatives corresponding to the dispersive effects, and the second one is dealing with numerical boundaries. And if the numerical algorithm used in the present chapter is an appropriate way to treat the dispersive effects simply enough, the proposed boundary conditions are not very robust. In the case of a short channel as for the last experimental study we are obliged to introduce a long extension of the numerical area to prevent unphysical reflections in the numerical domain. This issue takes place usually when one deals with dispersive equations. There is no uniform strategy to treat such problem in the case of nonlinear dispersive equations. We address this question in the application to the Green-Naghdi equation in Part II of the present work.

Chapter 2

Two-layer asymptotic model for the wave propagation in the presence of vorticity

In the present study, we consider a simple two-layer representation of the ocean wave propagation. The upper layer corresponds to the (thin) layer of fluid above the thermocline, whereas the lower layer is below the thermocline. The densities of the layers are assumed to be constant. Even in this simple setting, using the full Euler system is computationally too expensive. Hypothesis such as shallowness, vanishing vorticity and hydrostatic pressure are usually made to obtain two-layer shallow water models that are mathematically more manageable. However, such models cannot describe the propagation of both internal and free surface waves correctly, while non-hydrostatic effects are not included. The present chapter aims to derive a two-layer dispersive model considering regimes from medium to large vorticities in shallow water flows. Such assumptions allow taking into account the interaction between both surface and interface waves and underlying currents. Following [29], we derive a model in the conservative framework. No assumptions are made on the velocity profiles in the layers, which leads to additional variables. The closure is found using the vorticity equations. The derivation is very similar to the one presented in Chapter 1, except that the creation of the vorticities is not addressed here. This chapter concerns the model derivation; the numerical study is left for future research.

2.1 Euler equations

We consider a two-layer flow of inviscid incompressible and immiscible fluids of constant densities ρ_1, ρ_2, under a stable stratification assumption $\rho_1 > \rho_2$. The flow area is bounded by a free surface $z = \zeta_1(\vec{x}, t)$ above and by a nonuniform bottom $z = -h_{2_0} + \zeta_2(\vec{x}, t)$ below (see Figure 2.1), h_{0_i} denotes the reference free surface and bottom levels. Hereafter quantities with index '1' correspond to the upper layer, and index '2' to the lower one.

We introduce the following notations for the velocities and pressure fields, respectively,
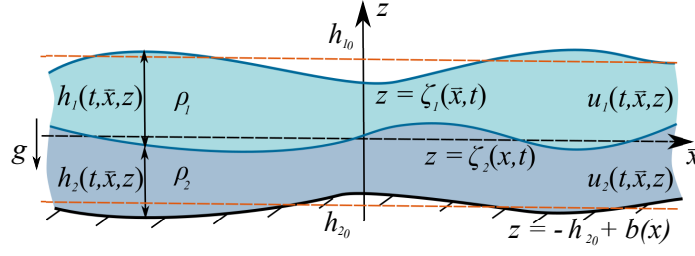
Figure 2.1: Scheme of the two-layer flow in the gravity field.

$V_i = (\vec{u}_i(t, \vec{x}, z), w_i(t, \vec{x}, z))$, $\vec{u}_i(t, \vec{x}, z) = (u_i(t, \vec{x}, z), v_i(t, \vec{x}, z))$ and p_i, $i = 1, 2$. We will skip the arguments when confusion is not possible. The governing equations are given by the full two-layer Euler system:

$$\begin{cases} (V_i)_t + V_i \cdot \nabla_{\vec{x},z} V_i = -\dfrac{1}{\rho_i} \nabla_{\vec{x},z} p_i - g e_z, \\ \nabla_{\vec{x},z} \cdot V_i = 0, \end{cases} \qquad (\vec{x}, z) \in \mathbb{R}^3, t > 0, \quad (i = 1, 2) \qquad (2.1)$$

which is complemented with the kinematic boundary conditions:

$$\begin{cases} \zeta_{1_t} + \vec{u}_1\big|_{z=h_{1_0}+\zeta_1} \cdot \nabla \zeta_1 &=& w_1\big|_{z=h_1^0+\zeta_1}, \\ \zeta_{2_t} + \vec{u}_1\big|_{z=\zeta_2} \cdot \nabla \zeta_2 &=& w_1\big|_{z=\zeta_2}, \\ \zeta_{2_t} + \vec{u}_2\big|_{z=\zeta_2} \cdot \nabla \zeta_2 &=& w_2\big|_{z=\zeta_2}, \\ \vec{u}_2\big|_{z=-h_{2_0}+b} \cdot \nabla b &=& w_2\big|_{z=-h_{2_0}+b(x)}, \end{cases} \qquad (2.2)$$

and the dynamic boundary conditions:

$$p_1\big|_{z=h_{1_0}+\zeta_1} = 0, \quad p_1\big|_{z=\zeta_2} = p_2\big|_{\zeta_2}. \qquad (2.3)$$

The gravity acceleration is denoted by g. Hereandafter, the indices t, x, z denote the derivatives, while $i = 1, 2$ corresponds to the layers. The gradient operator $\nabla_{\vec{x},z}$ is divided into horizontal and vertical parts.

It is well known that under assumptions of shallowness, vanishing vorticity and hydrostatic pressure, the model (2.1) can be reduced to the two-layer shallow water model; by construction, the dispersive/non-hydrostatic effects are not included. In [14, 42] such effects are taken into consideration in the context of a two-layer model, though the hypothesis of vanishing vorticity is made. We aim to include dispersive terms and non-hydrostatic pressure components in the derivation of the depth-averaged system. For that purpose, we follow the strategy [29, 119]. We reduce the full two-layer Euler equations (2.1) to a non-dimensional depth-average system that describes the evolution of the fluid heights, the horizontal momentums and other average quantities, as pressure contributions and velocity fluctuation tensors, which can be formally called 'Reynolds tensors' by analogy with the turbulent theory. This system is exact but requires closure relations, since no assumptions on velocities fluctuations are made. In what follows, we derive models of different orders

of approximation in the case of constant and general vorticities. To find the closure relations, following the strategy found in [29] for the one-layer model, we define shear velocities as horizontal vorticity contributions to the horizontal velocity fields (for irrotational flow these contributions are zero, and the system is closed). The pressure gradients and velocity fluctuations can be represented in terms of the shear velocities. By using vorticity and incompressible equations, we find equations for shear velocities, and therefore the system becomes closed. This technique is very reminiscent to the one applied in Chapter 1, except that we are using the vorticity equation instead of the energy equation. Moreover, the dissipation effects and vorticity creation included in Chapter 1 are now dropped. We include the influence of underlying currents on surface and interface wave propagation in the conservative framework. The difference with the one-layer derivation lies in the additional terms which are responsible for the interaction between the layers.

2.2 Asymptotic analysis

2.2.1 Dimensionless form of the averaged equations

We introduce the following dimensionless parameters:

$$\rho = \frac{\rho_1}{\rho_2} > 1, \quad \varepsilon_1 = \frac{a_1}{h_{1_0}}, \quad \varepsilon_2 = \frac{a_2}{h_{1_0}}, \quad \mu = \frac{h_{1_0}^2}{L^2}, \quad \delta = \frac{h_{1_0}}{h_{2_0}}, \quad \beta = \frac{a_B}{h_{1_0}}, \tag{2.4}$$

where several characteristic quantities are specified: the typical amplitudes a_1 of the surface waves and a_2 of the internal waves, the typical amplitude of the bottom variations a_B, the typical depths h_{1_0} and h_{2_0} of two layers and the typical wavelength L.

Parameters ε_1 and ε_2 are the nonlinearity parameters. The parameter μ is the shallowness, or dispersion parameter, determining which wave scales are taken into account. In order to avoid confusion we emphasize the difference with the notations used in Chapter 1.

We are interested in shallow water flows and therefore we assume that the shallowness parameter is small, $\mu \ll 1$, but no smallness assumption is made for the nonlinearity parameters ε_1, ε_2, allowing for large-amplitude waves.

We define the dimensionless variables (with tildes) as follows:

$$\tilde{x} = \frac{x}{L}, \quad \tilde{z} = \frac{z}{h_{1_0}}, \quad \tilde{\zeta}_1 = \frac{\zeta_1}{a_1}, \quad \tilde{\zeta}_2 = \frac{\zeta_2}{a_2}, \quad \tilde{b} = \frac{b}{a_B}. \tag{2.5}$$

The dimensionless velocities, time and pressure fields are given by:

$$\tilde{\vec{u}}_i = \frac{\vec{u}_i}{\varepsilon_i \sqrt{gh_{1_0}}}, \quad \tilde{w}_i = \frac{w_i L}{h_{1_0} U_i}, \quad \tilde{p}_i = \frac{p_i}{\rho_i gh_{1_0}}, \quad \tilde{t} = \frac{t\sqrt{gh_{1_0}}}{L}, \quad (i = 1, 2), \tag{2.6}$$

In terms of dimensionless variables, the Euler equations take the form (tildes are omitted):

$$\begin{cases} (V_i)_t + \varepsilon_i V_i \cdot \nabla_{\vec{x},z} V_i = -\dfrac{R_i}{\varepsilon_i M}(\nabla_{\vec{x},z} p_i + e_z), \\[2mm] \nabla_{\vec{x},z} \cdot V_i = 0, \end{cases} \tag{2.7}$$

where $M = (0, 0, \mu)^\top$, $e_z = (0, 0, 1)^\top$, $R_1 = 1$, $R_2 = \rho$, coupled with the dimensionless boundary conditions. Hereafter, the index $i = 1, 2$ corresponds to the layer parameters.

The vertical averaged values of the horizontal velocity components are introduced as

$$\overline{u}_1 = \frac{1}{h_1} \int_{\varepsilon_2 \zeta_2}^{1+\varepsilon_1 \zeta_1} \vec{u}_1 \; dz, \quad \overline{u}_2 = \frac{1}{h_2} \int_{-\frac{1}{\delta}+\beta b(x)}^{\varepsilon_2 \zeta_2} \vec{u}_2 \; dz, \tag{2.8}$$

where $h_1 = 1 + \varepsilon_1 \zeta_1 - \varepsilon_2 \zeta_2$ and $h_2 = \varepsilon_2 \zeta_2 + \frac{1}{\delta} - \beta b(x)$ are the variable layer depths.

Therefore the velocity field decompositions can be given by:

$$\vec{u}_1 = \overline{u}_1 + \sqrt{\mu} \vec{u}_1^*(t, \vec{x}, z), \quad \vec{u}_2 = \overline{u}_2 + \sqrt{\mu} \vec{u}_2^*(t, \vec{x}, z). \tag{2.9}$$

No assumptions on the velocity fluctuations $\vec{u}_i^*$ are made, which means that no velocity profiles are assumed. In the terminology of [137], or [117], we consider weakly sheared flows.

The system of depth-averaged equations is obtained by integrating the system (2.7) over z and taking into account the boundary conditions (2.2), (2.3) in dimensionless form,

$$\begin{cases} (h_i)_t + \varepsilon_i \nabla \cdot (h_i \overline{u}_i) = 0, \\\\ (h_i \overline{u}_i)_t + \varepsilon_i \nabla \cdot (h_1 \overline{u}_i \otimes \overline{u}_i) + \varepsilon_i \mu \nabla \cdot \left(\int_{A_i}^{B_i} \vec{u}_i^* \otimes \vec{u}_i^* dz \right) + \frac{R_i}{\varepsilon_i} \int_{A_i}^{B_i} \nabla p_i dz = 0, \\\\ (w_i)_t + \varepsilon_i (u_i \nabla \cdot) w_i + \varepsilon_i w_i (w_i)_z = -\frac{1}{\mu \varepsilon_i} (R_i (p_i)_z + 1), \end{cases} \tag{2.10}$$

where $\nabla = (\partial_x, \partial_y)$ is a two-dimensional operator, and

$$A_1 = \varepsilon_2 \zeta_2, \quad B_1 = 1 + \varepsilon_1 \zeta_1, \quad A_2 = -\frac{1}{\delta} + \beta b(x), \quad B_2 = \varepsilon_2 \zeta_2, \tag{2.11}$$

denote the upper and lower layer boundaries.

The system (2.10) is exact and couples the equations for depths h_i and average velocities $\overline{u}_i$. However, a closure for 'Reynolds tensors' and pressure terms:

$$\int_{A_i}^{B_i} \vec{u}_i^* \otimes \vec{u}_i^* \; dz, \quad \frac{R_i}{\varepsilon_i} \int_{A_i}^{B_i} \nabla p_i$$

in terms of $\overline{u}_i$, h_i is required.

In the Chapter 1 the procedure is similar; the new variable enstrophy is added and the energy conservation law is used. Now, in order to find a closure we introduce dimensionless vorticities $\Omega_i = \nabla \times u_i$. Taking into account (2.9), we represent Ω_i as:

$$\Omega_i = \frac{\varepsilon_i \sqrt{g h_{1_0}}}{h_{1_0}} \sqrt{\mu} \begin{pmatrix} -\tilde{v}_{iz}^* + \sqrt{\mu} \tilde{w}_{iy} \\ \tilde{u}_{iz}^* - \sqrt{\mu} \tilde{w}_{ix} \\ \nabla^{\perp} \cdot \tilde{\vec{u}}_i \end{pmatrix} \equiv \frac{\varepsilon_i \sqrt{g h_{1_0}}}{h_{1_0}} \sqrt{\mu} \begin{pmatrix} \vec{\omega}_h^i \\ \omega_v^i \end{pmatrix}, \tag{2.12}$$

where the orthogonal operator $\nabla^{\perp}$ is defined as $\nabla^{\perp} = (-\partial_y, \partial_x)$, and we divide the vorticity fields into horizontal $\vec{\omega}_h^i$, and vertical ones ω_v^i, $i = 1, 2$.

Velocity fields decompositions

Now we can find representations for the velocity fields in terms of vorticities. Indeed, an integration of the continuity equations leads to the following expressions for the vertical velocities components in terms of horizontal velocities:

$$
\begin{aligned}
w_1 &= -\nabla \cdot [\overline{u}_1(z - \varepsilon_2\zeta_2)] - \sqrt{\mu}\,\nabla \cdot \int_{\varepsilon_2\zeta_2}^z \vec{u}_1^* dz + \frac{\varepsilon_2}{\varepsilon_1}\zeta_{2_t}, \\
w_2 &= -\nabla \cdot \left[\overline{u}_2\left(z - \beta b(x) + \frac{1}{\delta}\right)\right] - \sqrt{\mu}\,\nabla \cdot \int_{\beta b(x)-\frac{1}{\delta}}^z \vec{u}_2^* dz,
\end{aligned}
\tag{2.13}
$$

using the boundary conditions.

The definition of the vorticities (2.12) gives the equations for the components of the horizontal velocity fields:

$$
\partial_z \vec{u}_i^* = \sqrt{\mu}\,\nabla w_i - (\vec{\boldsymbol{\omega}}_h^i)^\perp.
\tag{2.14}
$$

Integrating (2.14) and taking into account the expressions for vertical velocities (2.13) yields (we use $\partial_z \vec{u}_i^* = \partial_z \overline{u}_i$)

$$
\vec{u}_1^* = \sqrt{\mu}\left(\int_z^{1+\varepsilon_1\zeta_1} \nabla\nabla \cdot [\overline{u}_1(z - \varepsilon_2\zeta_2)]\right)^* + \mu\left(\int_z^{1+\varepsilon_1\zeta_1} \nabla\nabla \cdot \int_{\varepsilon_2\zeta_2}^z \vec{u}_1^*\right)^*
$$

$$
- \sqrt{\mu}\left(\int_z^{1+\varepsilon_1\zeta_1} \frac{\varepsilon_2}{\varepsilon_1}\nabla\zeta_{2_t}\right)^* + \left(\int_z^{1+\varepsilon_1\zeta_1} (\vec{\boldsymbol{\omega}}_h^1)^\perp\right)^*, \quad (2.15)
$$

$$
\vec{u}_2^* = \sqrt{\mu}\left(\int_z^{\varepsilon_2\zeta_2} \nabla\nabla \cdot \left[\overline{u}_2\left(z - \beta b(x) + \frac{1}{\delta}\right)\right]\right)^* + \mu\left(\int_z^{\varepsilon_2\zeta_2} \nabla\nabla \cdot \int_{-\frac{1}{\delta}+\beta b(x)}^z \vec{u}_2^*\right)^*
$$

$$
+ \left(\int_z^{\varepsilon_2\zeta_2} (\vec{\boldsymbol{\omega}}_h^2)^\perp\right)^*. \quad (2.16)
$$

We introduce the operators T_i, $i = 1, 2$, defined as:

$$
T_1 V = \int_z^{1+\varepsilon_1\zeta_1} \nabla\nabla \cdot \int_{\varepsilon_2\zeta_2}^z V, \qquad T_2 V = \int_z^{\varepsilon_2\zeta_2} \nabla\nabla \cdot \int_{-\frac{1}{\delta}+\beta b(x)}^z V,
$$

$$
T_1^* V = (T_1 V)^*, \quad T_2^* V = (T_2 V)^*,
$$

and the shear velocities which represent the contribution of the horizontal vorticities to the horizontal velocities:

$$
\vec{u}_{1sh} = \int_z^{1+\varepsilon_1\zeta_1} (\vec{\boldsymbol{\omega}}_h^1)^\perp, \quad \vec{u}_{2sh} = \int_z^{\varepsilon_2\zeta_2} (\vec{\boldsymbol{\omega}}_h^2)^\perp,
\tag{2.17}
$$

so that the expressions (2.15), (2.16) can be rewritten as

$$
(1 - \mu T_1^*)\vec{u}_1^* = \vec{u}_{1sh}^* + \sqrt{\mu}\left(T_1^* \overline{u}_1 - \nabla\zeta_{2_t}\left(-z + \frac{1 + \varepsilon_1\zeta_1 + \varepsilon_2\zeta_2}{2}\right)\right),
$$

$$(1 - \mu T_2^*)\vec{u}_2^* = \vec{u}_{2sh}^* + \sqrt{\mu}\left(T_2^*\overline{u}_2\right).$$

These expressions are exact, however for the model derivation we will use approximate expressions. Applying the operators $(1 + \mu T_i^*)$ on both sides of each identity, we obtain the approximations

$$\vec{u}_1^* = (1 + \mu T_1^*)\vec{u}_{1sh}^* + \sqrt{\mu}\left(T_1^*\overline{u}_1 - \nabla\zeta_{2_t}\left(-z + \frac{1 + \varepsilon_1\zeta_1 + \varepsilon_2\zeta_2}{2}\right)\right) + \mathcal{O}(\mu^{3/2}), \quad (2.18)$$

$$\vec{u}_2^* = (1 + \mu T_2^*)\vec{u}_{2sh}^* + \sqrt{\mu}\left(T_2^*\overline{u}_2\right) + \mathcal{O}(\mu^{3/2}). \quad (2.19)$$

Recalling the velocity field decompositions (2.9), we can write first order approximations of the complete velocity fields u_i:

$$u_1 = \overline{u}_1 + \sqrt{\mu}u_{1sh}^* + \mathcal{O}(\mu), \quad u_2 = \overline{u}_2 + \sqrt{\mu}u_{2sh}^* + \mathcal{O}(\mu), \quad (2.20)$$

and second order approximations:

$$u_1 = \overline{u}_1 + \sqrt{\mu}u_{1sh}^* + \mu\left(T_1^*\overline{u}_1 - \nabla\zeta_{2_t}\left(-z + \frac{1 + \varepsilon_1\zeta_1 + \varepsilon_2\zeta_2}{2}\right)\right) + \mu^{3/2}T_1^*u_{1sh}^* + \mathcal{O}(\mu^2),$$

$$u_2 = \overline{u}_2 + \sqrt{\mu}u_{2sh}^* + \mu\left(T_2^*\overline{u}_2\right) + \mu^{3/2}T_2^*u_{2sh}^* + \mathcal{O}(\mu^2).$$
(2.21)

Significantly, even at first order $\mathcal{O}(\mu)$ the velocity field is coupled with vorticities effects, and layer velocities depend on z. We also note that the model includes a coupling between the layers through the interface dynamical condition, which leads to a term with an explicit dependence on z in the upper velocity field representations (2.21). Finally, if the shear velocities are known then the system is closed. The next step is to define the equations for the shear velocities evolution.

Equations for the shear velocities

The vorticity in each layer is transported in the absence of viscous and dissipation effects. These assumptions are physically relevant in some flow regimes. The vorticity equations are found by applying the curl operator to the momentum equations

$$\boldsymbol{\omega}_t^i + \varepsilon_i(\vec{u_i}\nabla_{x,z})\boldsymbol{\omega}_h^i = \varepsilon_i\boldsymbol{\omega}_h^i\nabla u_i + \frac{\varepsilon_i}{\sqrt{\mu}}\boldsymbol{\omega}_v^i(u_i)_z. \quad (2.22)$$

We derive first the equation for the shear velocity in the upper layer u_{1sh}^*. Recalling the definition of u_{1sh} (2.17), we integrate the upper layer equation (2.22),($i = 1$) with respect to z over the interval $(z, 1 + \varepsilon_1\zeta_1)$:

$$\partial_t u_{1sh} + \varepsilon_1\overline{u}_1 \cdot \nabla u_{1sh} + \varepsilon_1 u_{1sh} \cdot \nabla\overline{u}_1 - (\varepsilon_1\nabla \cdot (\overline{u}_1(z - \varepsilon_2\zeta_2)) - \varepsilon_2\zeta_{2t})\partial_z u_{1sh} = \mathcal{O}(\varepsilon_1\sqrt{\mu}). \quad (2.23)$$

The following vectorial identity is used above

$$(\nabla \cdot \mathbf{A})\mathbf{B} + \mathbf{B}^{\perp} \cdot \nabla\mathbf{A}^{\perp} + (\nabla^{\perp} \cdot \mathbf{A})\mathbf{B} = \mathbf{B} \cdot \mathbf{A}.$$

Then we integrate the equation (2.23) once again over the layer depth, in order to find the equation for the average component $\overline{u_{1sh}}$. Subtracting one from another gives us the following equation for u_{1sh}^*:

$$\partial_t u_{1sh}^* + \varepsilon_1 \overline{u}_1 \cdot \nabla u_{1sh}^* + \varepsilon_1 u_{1sh}^* \cdot \nabla \overline{u}_1 - \left(\varepsilon_1 \nabla \cdot (\overline{u}_1(z - \varepsilon_2 \zeta_2)) - \varepsilon_2 \zeta_{2t} \right) \partial_z u_{1sh}^* = \mathcal{O}(\varepsilon_1 \sqrt{\mu}). \quad (2.24)$$

Analogously, we obtain the equation for the shear velocity of the lower layer:

$$\partial_t u_{2sh}^* + \varepsilon_2 \overline{u}_2 \cdot \nabla u_{2sh}^* + \varepsilon_2 u_{2sh}^* \cdot \nabla \overline{u_2} - \left(\varepsilon_2 \nabla \cdot \left(\overline{u}_2 \left(z - \beta b(x) + \frac{1}{\delta} \right) \right) \right) \partial_z u_{2sh}^* = \mathcal{O}(\varepsilon_2 \sqrt{\mu}). \quad (2.25)$$

It is should be noted that the order $\mathcal{O}(\varepsilon_i \sqrt{\mu})$ of equations obtained in this section is not enough to derive the models of order $\mathcal{O}(\mu^2)$ in the case of general vorticities. Then more precise equations are needed for the shear velocities in order to derive a Green-Naghdi model of order $\mathcal{O}(\mu^2)$. This derivation is left for future work. In the case of a general vorticity, a model of intermediate order $\mathcal{O}(\mu^{3/2})$ is proposed.

Pressure fields closures

The pressure field is represented in terms of the velocities by integrating the vertical components of the Euler equations (2.10). Taking into account the dynamic boundary conditions (2.3) we have:

$$\frac{1}{\varepsilon_1} \nabla p_1 = \nabla \int_z^{1+\varepsilon_1 \zeta_1} \left(-\frac{1}{\varepsilon_1} \partial_z p_1 \right) dz =$$

$$\nabla \zeta_1 + \mu \nabla \int_z^{1+\varepsilon_1 \zeta_1} \left(w_{1t} + \varepsilon_1 (u_1 \nabla \cdot) w_1 + \varepsilon_1 w_1 w_{1z} \right) dz, \quad (2.26)$$

$$\frac{\rho}{\varepsilon_2} \nabla p_2 = \nabla \left(\int_z^{\varepsilon_2 \zeta_2} \left(-\frac{\rho}{\varepsilon_2} \partial_z p_2 \right) dz + \frac{\rho}{\varepsilon_2} p_1 \big|_{\varepsilon_2 \zeta_2} \right) =$$

$$= \nabla \zeta_2 + \mu \nabla \int_z^{\varepsilon_2 \zeta_2} \left(w_{2t} + \varepsilon_2 (u_2 \nabla \cdot) w_2 + \varepsilon_2 w_2 w_{2z} \right) dz + \nabla \left(\frac{\rho}{\varepsilon_2} p_1 \big|_{\varepsilon_2 \zeta_2} \right). \quad (2.27)$$

The first terms on the right-hand sides in both representations are related to the hydrostatic pressure. An expansion for non-hydrostatic terms will be found in the next section in the case of constant vorticities.

Generally speaking, the required closures are already constructed. The algorithm for the solution can be outlined as follows:

- The shear velocities u_{1sh}^*, u_{1sh}^* are defined by equations (2.24), (2.25);

- Using the equations (2.18), (2.19) the velocity fluctuations $\vec{u}_1^*$, $\vec{u}_2^*$ are calculated;

- The horizontal velocity fields are reconstructed using (2.20), or (2.21) depending on the approximation order of the model; the vertical velocities are specified by (2.13);

- The pressure field contributions are determined from (2.27), (2.26) using the vertical velocities w_1, w_2.

However, the order of the equations (2.24), (2.25) for shear velocities must be consistent with the model order, and therefore sometimes more precise equations than (2.24), (2.25) are needed. Moreover, the main issue encountered in the derivations is the calculation of the pressure contributions with (2.27), (2.26). We will limit ourselves only to some special cases. First we consider the constant vorticity case, and derive a model of the same order as the classical Green-Naghdi equations. Then we turn to the general vorticity case and derive a model of lower order.

2.3 Constant vorticities 1d case

We consider a one-dimensional depth-averaged approach, which means that we consider the plane (x, z), and velocities have only two non-zero components. In this case, only one component of each vorticity is non-zero, and we assume that these components remain constant for all time:

$$\Omega_i = \begin{pmatrix} 0 \\ \omega_i \\ 0 \end{pmatrix}, \quad \omega_i = \partial_z \vec{u}_i^* - \sqrt{\mu}\partial_x w_i \equiv const.$$

The horizontal vorticity fields are then written as $(\omega_h^i)^\perp = -(\omega_i, 0)^\top$. The shear velocities defined by (2.17) are calculated explicitly without using the equations (2.24), (2.25). One obtains

$$u_{ish} = \int_{A_i}^{B_i} (\omega_h^i)^\perp dz = -\omega_i \left(B_i - z - \frac{h_i}{2} \right), \tag{2.28}$$

where A_i, B_i are boundaries of the layers defined above by (2.11). Therefore, the vertical velocities are defined with (2.13):

$$w_1 = \partial_x(\overline{u}_1(z - \varepsilon_2\zeta_2)) + \frac{\sqrt{\mu}}{2}\partial_x \left(\omega_1 \left(z - \varepsilon_2\zeta_2 \right) \left(1 + \varepsilon_1\zeta_1 - z \right) \right) + \frac{\varepsilon_2}{\varepsilon_1}\zeta_{2_t},$$

$$w_2 = \partial_x \left(\overline{u}_2 \left(z - \beta b(x) + \frac{1}{\delta} \right) \right) + \frac{\sqrt{\mu}}{2}\partial_x \left(\omega_2 \left(z - \varepsilon_2\zeta_2 \right) \left(\beta b(x) - \frac{1}{\delta} - z \right) \right). \tag{2.29}$$

2.3.1 'Reynolds tensor' contributions for the constant vorticity case

Using velocity field reconstructions (2.20) and shear velocities (2.28) calculated above, we define the 'Reynold tensors' with second order approximation $\mathcal{O}(\mu^2)$. For the upper layer

one has

$$\varepsilon_1\mu\partial_x \int_{\varepsilon_2\zeta_2}^{1+\varepsilon_1\zeta_1} |u_1^*|^2 dz = \varepsilon_1\mu\partial_x \int_{\varepsilon_2\zeta_2}^{1+\varepsilon_1\zeta_1} |u_{1sh}^*|^2\, dz + 2\varepsilon_1\mu^{3/2}\partial_x \int_{\varepsilon_2\zeta_2}^{1+\varepsilon_1\zeta_1} u_{1sh}^* T_1\overline{u}_1\, dz$$

$$- 2\varepsilon_2\mu^{3/2}\partial_x \left(\zeta_{2_t} \int_{\varepsilon_2\zeta_2}^{1+\varepsilon_1\zeta_1} u_{1sh}^*(1+\varepsilon_1\zeta_1 - z) dz \right) =$$

$$\frac{\varepsilon_1\mu}{12}\omega_1^2(h_1^3)_x - \frac{\varepsilon_1\mu^{3/2}}{12}\omega_1\partial_x\left(h_1^3(h_1\partial_x^2\overline{u}_1 - 4\varepsilon_2\partial_x\zeta_2\partial_x\overline{u}_1 - 2\varepsilon_2\partial_x^2\zeta_2\overline{u}_1)\right) + \frac{\varepsilon_1\mu^{3/2}}{6}\omega_1\partial_x(h_1^3\zeta_{2_t}). \tag{2.30}$$

Likewise, for the lower layer we obtain

$$\varepsilon_2\mu\partial_x \int_{-\frac{1}{\delta}+\beta b(x)}^{\varepsilon_2\zeta_2} |u_2^*|^2 dz =$$

$$\frac{\varepsilon_2\mu}{12}\omega_2^2(h_2^3)_x - \frac{\varepsilon_2\mu^{3/2}}{12}\omega_2\partial_x\left(h_2^3(h_2\partial_x^2\overline{u}_2 - 4\beta b'(x)\partial_x\overline{u}_2 - 2\beta b''(x)\overline{u}_2)\right). \tag{2.31}$$

Therefore, for the constant vorticity case, the required closure relations for the 'Reynold tensors' are calculated directly, without shear velocities equations. Moreover, these terms are defined only in terms of h_i, u_i and on the other known parameters such as a bottom parametrisation $b(x)$ and constant vorticities ω_i.

2.3.2   Pressure contributions

In order to compute the pressure contributions, we represent the vertical velocity (2.29) in the following form:

$$w_1 = f_1(x,t) + zg_1(x,t), \quad w_2 = f_2(x,t) + zg_2(x,t).$$

Here $f_i(x,t)$, $g_i(t,x)$ are defined as:

$$f_1(x,t) = \frac{\varepsilon_2}{\varepsilon_1}\zeta_{2_t} + \varepsilon_2\partial_x(\overline{u}_1\zeta_2) - \frac{\sqrt{\mu}}{2}\omega_1(\varepsilon_1\varepsilon_2\partial_x(\zeta_1\zeta_2) + \varepsilon_2\zeta_{2_x}),$$

$$g_1(x,t) = \frac{\sqrt{\mu}}{2}\omega_1\partial_x(\varepsilon_1\zeta_1 + \varepsilon_2\zeta_2) - \partial_x\overline{u}_1,$$

$$f_2(x,t) = \beta\partial_x(\overline{u}_2 b(x)) - \frac{1}{\delta}\partial_x\overline{u}_2 - \frac{\sqrt{\mu}}{2}\omega_2\left(\varepsilon_2\beta\partial_x(\zeta_2 b(x)) - \frac{1}{\delta}\varepsilon_2\zeta_{2_x}\right),$$

$$g_2(x,t) = \frac{\sqrt{\mu}}{2}\omega_2\partial_x(\varepsilon_2\zeta_2 + \beta b(x)) - \partial_x\overline{u}_2.$$

Using such notations, the pressure integrals take the form:

$$\frac{1}{\varepsilon_1} \int_{\varepsilon_2\zeta_2}^{1+\varepsilon_1\zeta_1} \nabla p_1 \, dz = h_1 \zeta_{1_x}$$

$$+ \mu \left(\varepsilon_2 \zeta_{2_x} h_1 \left(\frac{\mathrm{D}_1 f_1}{\mathrm{D}_1 t} + \varepsilon_1 f_1 g_1 + \frac{1}{2} \left(\frac{\mathrm{D}_1 g_1}{\mathrm{D}_1 t} + \varepsilon_1 g_1^2 \right) (1 + \varepsilon_1 \zeta_1 + \varepsilon_2 \zeta_2) \right) \right.$$

$$+ \partial_x \left(\frac{h_1^2}{2} \left(\frac{\mathrm{D}_1 f_1}{\mathrm{D}_1 t} + \varepsilon_2 \zeta_2 \frac{\mathrm{D}_1 g_1}{\mathrm{D}_1 t} + \varepsilon_1 f_1 g_1 + \varepsilon_1 \varepsilon_2 \zeta_2 g_1^2 \right) + \frac{h_1^3}{3} \left(\frac{\mathrm{D}_1 g_1}{\mathrm{D}_1 t} + \varepsilon_1 g_1^2 \right) \right) \bigg)$$

$$- \mu^{3/2} \omega_1 \varepsilon_1 \left(\frac{h_1^3}{12} \varepsilon_2 \zeta_{2_x} \partial_x^2 \overline{u}_1 + \partial_x \left(\frac{h_1^3}{12} \left(\partial_x f_1 + \left(1 + \varepsilon_1 \zeta_1 - \frac{h_1}{2} \right) \partial_x g_1 \right) + \frac{h_1^4}{24} \partial_x g_1 \right) \right),$$
$$(2.32)$$

$$\frac{1}{\varepsilon_2} \int_{-\frac{1}{\delta}+\beta b(x)}^{\varepsilon_2\zeta_2} \nabla p_2 \, dz = h_2 \zeta_{2_x}$$

$$+ \mu \left(\beta b'(x) h_2 \left(\frac{\mathrm{D}_2 f_2}{\mathrm{D}_2 t} + \varepsilon_2 f_2 g_2 + \frac{1}{2} \left(\frac{\mathrm{D}_2 g_2}{\mathrm{D}_2 t} + \varepsilon_2 g_2^2 \right) \left(\varepsilon_2 \zeta_2 - \frac{1}{\delta} + \beta b(x) \right) \right) \right.$$

$$+ \partial_x \left(\frac{h_2^2}{2} \left(\frac{\mathrm{D}_2 f_2}{\mathrm{D}_2 t} - \left(\frac{1}{\delta} - \beta b(x) \right) \frac{\mathrm{D}_2 g_2}{\mathrm{D}_2 t} + \varepsilon_2 f_2 g_2 - \varepsilon_2 \left(\frac{1}{\delta} - \beta b(x) \right) g_2^2 \right) + \frac{h_2^3}{3} \left(\frac{\mathrm{D}_2 g_2}{\mathrm{D}_2 t} + \varepsilon_2 g_2^2 \right) \right) \bigg)$$

$$- \mu^{3/2} \omega_2 \varepsilon_2 \partial_x \left(\frac{h_2^3}{12} \beta b'(x) \partial_x^2 \overline{u}_2 + \partial_x \left(\frac{h_2^3}{12} \left(\partial_x f_2 + \left(\varepsilon_2 \zeta_2 - \frac{h_2}{2} \right) \partial_x g_2 \right) + \frac{h_2^4}{24} \partial_x g_2 \right) \right),$$
$$(2.33)$$

with the material derivative operators given by:

$$\frac{\mathrm{D}_1 f}{\mathrm{D}_1 t} = \partial_t f + \varepsilon_1 \overline{u}_1 \partial_x f, \quad \frac{\mathrm{D}_2 f}{\mathrm{D}_2 t} = \partial_t f + \varepsilon_2 \overline{u}_2 \partial_x f. \tag{2.34}$$

Thus, gathering the 'Reynolds tensors' (2.30), (2.31) and pressure contributions (2.32), (2.33), we finally obtain a model of first order $\mathcal{O}(\mu)$:

$$\begin{cases}
h_{1_t} + \varepsilon_1 (h_1 \overline{u}_1)_x = 0, \\[2mm]
(h_1 \overline{u}_1)_t + \varepsilon_1 (h_1 \overline{u}_1^2)_x + \dfrac{\mu \varepsilon_1}{12} \omega_1 (h_1^3)_x + h_1 \zeta_{1_x} + \dfrac{1}{6} \mu h_1 \mathcal{M}_{\varepsilon_1 \varepsilon_2} = 0, \\[2mm]
h_{2_t} + \varepsilon_2 (h_2 \overline{u}_2)_x = 0, \\[2mm]
(h_2 \overline{u}_2)_t + \varepsilon_2 (h_2 \overline{u}_2^2)_x + \dfrac{\mu \varepsilon_2}{12} \omega_2 (h_2^3)_x + h_2 \zeta_{2_x} + \\[2mm]
\qquad\qquad \displaystyle\int_{-\frac{1}{\delta}+\beta b(x)}^{\varepsilon_2\zeta_2} \nabla \left(\dfrac{\rho}{\varepsilon_2} p_1 \bigg|_{\varepsilon_2 \zeta_2} \right) + \dfrac{1}{6} \mu h_2 \mathcal{M}_b = 0,
\end{cases} \tag{2.35}$$

where the terms of order μ are the constant vorticity terms and the terms $\mathcal{M}_{\varepsilon_1\varepsilon_2}$ and $\mathcal{M}_b$ are defined as follows

$$\mathcal{M}_{\varepsilon_1\varepsilon_2} = 3\varepsilon_1\varepsilon_2\bar{u}_1^2\mathcal{G}(h_1,\zeta_1,\zeta_2) + 2h_1^2(\varepsilon_1\bar{u}_{1_x}\bar{u}_{1_{xx}}\bar{u}_{1_{txx}})$$
$$+ \bar{u}_1\mathcal{T}_1(\bar{u}_1) + 6\varepsilon_2\zeta_{1_x}(\zeta_{2_{tt}} + \varepsilon_1\zeta_{2_x}\bar{u}_{1_t}) + 3h_1\mathcal{T}_2(\bar{u}_1),$$

$$\mathcal{M}_b = 3\beta\varepsilon_2\bar{u}_2^2\mathcal{B}(h_2,b) + \varepsilon_2\bar{u}_2\mathcal{R}_1(\bar{u}_2) + 6\beta b'(\beta b' + h_{2_x})\bar{u}_{2_t} + h_2\mathcal{R}_2(\bar{u}_2).$$

In calligraphic here we denote the following operators:

$$\mathcal{T}_1(V) = -6\varepsilon_1 h_{1_x}(\varepsilon_1\zeta_{1_x}\partial_x V + h_1\partial_{xx}V) + \partial_x V(6\varepsilon_1^3(\zeta_{1_x})^2) + 9\varepsilon_1\varepsilon_2 h_1\zeta_{2_{xx}}) -$$
$$2\varepsilon_1 h_1^2\partial_{xxx}V + 12\varepsilon_1\varepsilon_2\zeta_{1_x}\zeta_{2_{tx}} + 6\varepsilon_2 h_1\zeta_{2_{txx}},$$

$$\mathcal{T}_2(V) = 2\varepsilon_1^2(\partial_x V)^2\zeta_{1_x} + \varepsilon_2\zeta_{2_{xx}}\partial_t V - 2h_{1_x}\partial_{tx}V + 2\varepsilon_2\partial_x V\zeta_{2_{tx}} + \varepsilon_2\zeta_{2_{ttx}},$$

$$\mathcal{R}_1(V) = (6\beta^2(b')^2 + 6\beta b'h_{2_x} + 9h_2\beta b'')\partial_x V - 6h_2 h_{2_x}\partial_x^2 V - 2h_2^2\partial_x^3 V,$$

$$\mathcal{R}_2(V) = 6\varepsilon_2(\beta b' + h_{2_x})(\partial_x V)^2 + 3\beta b''\partial_t V - 6h_{2_x}\partial_{tx}V + h_2(2\varepsilon_2\partial_x V\partial_{xx}V - 2\partial_{txx}V),$$

$$\mathcal{G}(h_1,\zeta_1,\zeta_2) = 2\varepsilon_1\zeta_{1_x}\zeta_{2_{xx}} + h_1\zeta_{2_{xxx}},$$

$$\mathcal{B}(h_2,b) = 2(\beta b' + h_{2_x})b'' + h_2 b'''.$$

The interface pressure term is defined as:

$$\int_{-\frac{1}{\delta}+\beta b(x)}^{\varepsilon_2\zeta_2} \nabla\left(\frac{\rho}{\varepsilon_2}p_1\Big|_{\varepsilon_2\zeta_2}\right) dz = \frac{\rho}{\varepsilon_2}h_{1x} + \rho\frac{\varepsilon_1}{\varepsilon_2}\mu^{3/2}\partial_x\left(\frac{h_1^3}{12}\omega_1 B_{1x}\right)$$

$$+ \rho\frac{\varepsilon_1}{\varepsilon_2}\mu\partial_x\left(h_1\left(\frac{\mathrm{D}_1 A_1}{\mathrm{D}_1 t} + \varepsilon_1 A_1 B_1\right) + h_1\left(\frac{\mathrm{D}_1 B_1}{\mathrm{D}_1 t} + \varepsilon_1 B_1^2\right)(1 + \varepsilon_1\zeta_1 + \varepsilon_2\zeta_2)\right) \quad (2.36)$$

A generalized Green-Naghdi model of second order $\mathcal{O}(\mu^2)$ in the presence of constant vorticity can be written directly from the contribution (2.30), (2.31), (2.32), (2.33) with the additional interface term (2.36).

2.4 1d Equations with general vorticity.

In the present section, we derive the $1D$ equations in the presence of general vorticities in each layer. As already discussed, the calculation of the pressure contributions for the model of order $\mathcal{O}(\mu^2)$ are cumbersome, and additional terms in the shear velocity equations need to be added. Here, we limit ourselves to the derivation of a model of intermediate order $\mathcal{O}(\mu^{3/2})$. Assuming that medium wave amplitudes are considered ($\varepsilon = \sqrt{\mu}$) like in the case of the classical Boussinesq equations, we drop the $\mathcal{O}(\mu^2)$ terms. The vorticities are not included in the pressure terms at this order, however the pressure is non hydrostatic it each layer. Moreover, the pressure contributions are calculated explicitly, and the result coincides with the one calculated before, for the constant vorticity case without taking into account the vorticity terms (see Subsection 2.3.2).

The 'Reynolds tensor' contributions are written in terms of shear velocities, and closure relations are needed. We have

$$\varepsilon_1 \mu \partial_x \int_{\varepsilon_2\zeta_2}^{1+\varepsilon_1\zeta_1} |u_1^*|^2 dz = \varepsilon_1 \mu \partial_x \int_{\varepsilon_2\zeta_2}^{1+\varepsilon_1\zeta_1} |u_{1sh}^*|^2 dz + \mathcal{O}(\mu^{3/2}),$$

$$\varepsilon_2 \mu \partial_x \int_{-\frac{1}{\delta}+\beta b(x)}^{\varepsilon_2\zeta_2} |u_2^*|^2 dz = \varepsilon_2 \mu \partial_x \int_{-\frac{1}{\delta}+\beta b(x)}^{\varepsilon_2\zeta_2} |u_{2sh}^*|^2 dz + \mathcal{O}(\mu^{3/2}).$$

We introduce the general vorticities E^1, E^2 defined as:

$$E^1 = \int_{\varepsilon_2\zeta_2}^{1+\varepsilon_1\zeta_1} |u_{1sh}^*|^2 dz, \quad E^2 = \int_{-\frac{1}{\delta}+\beta b(x)}^{\varepsilon_2\zeta_2} |u_{2sh}^*|^2 dz.$$

In order to find the closure relations, we use the equations for the shear velocities (2.24), (2.25) derived with the order $\mathcal{O}(\varepsilon_i \sqrt{\mu})$.

Multiplying each equation (2.24), (2.25) by u_{ish}, respectively, upon integration over the layer depths, we obtain the equations for E^1, E^2:

$$E_t^1 + \varepsilon_1 \bar{u}_1 E_x^1 + 3\varepsilon_1 \bar{u}_{1_x} E^1 = \mathcal{O}(\varepsilon_1 \sqrt{\mu}), \tag{2.37}$$

$$E_t^2 + \varepsilon_2 \bar{u}_2 E_x^2 + 3\varepsilon_2 \bar{u}_{2_x} E^2 = \mathcal{O}(\varepsilon_2 \sqrt{\mu}). \tag{2.38}$$

Then, the closure is found by adding the two additional equations (2.37), (2.38) to the model. Since E^1, E^2 appear only in the terms of order $\mathcal{O}(\mu)$, the order of the approximate equation (2.37), (2.38) is enough for the derivation of a model of order $\mathcal{O}(\mu^{3/2})$.

Following [29] we introduce the operators

$$\mathbf{T}_1(V) = \frac{1}{3h_1}\partial_x\left(h_1^3\partial_x V\right) + \varepsilon_2\zeta_{2_x}h_1\partial_x V, \tag{2.39}$$

$$\mathbf{Q}_1(V) = \frac{2}{3h_1}\partial_x\left(h_1^3(\partial_x V)^2\right) + 2\varepsilon_2\zeta_{2_x}h_1\left(\partial_x V\right)^2, \tag{2.40}$$

for the equations in the upper layer, and the operators

$$\mathbf{T}_2(V) = \frac{1}{3h_2}\partial_x\left(h_1^3\partial_x V\right), \tag{2.41}$$

$$\mathbf{Q}_2(V) = \frac{2}{3h_2}\partial_x\left(h_2^3(\partial_x V)^2\right), \tag{2.42}$$

for the lower layer. The final system reads as follows,

$$
\begin{cases}
h_{1_t} + \varepsilon_1 \partial_x \left(h_1 \overline{u}_1 \right) = 0, \\[2mm]
\left(1 + \dfrac{\mu}{2} \mathbf{T}_1 \right) \dfrac{\mathrm{D}_1 \overline{u}_1}{\mathrm{D}_1 t} - \dfrac{\mu \varepsilon_1}{2} \mathbf{Q}_1 (\overline{u}_1) + \\[3mm]
\qquad\qquad \mu \varepsilon_1 \zeta_{1_x} \dfrac{\mathrm{D}_1^2 \zeta_1}{\mathrm{D}_1 t^2} + \dfrac{\mu h_1}{2} \partial_x \left(\dfrac{\mathrm{D}_1 \zeta_1}{\mathrm{D}_1 t} + \dfrac{\varepsilon_2}{\varepsilon_1} \dfrac{\mathrm{D}_1 \zeta_{2_t}}{\mathrm{D}_1 t} \right) + \dfrac{\mu \varepsilon_1}{h_1} E^1 + \zeta_{1_x} = 0, \\[3mm]
E_t^1 + \varepsilon_1 \overline{u}_1 E_x^1 + 3 \varepsilon_1 \overline{u}_{1_x} E^1 = 0, \\[2mm]
h_{2_t} + \varepsilon_2 \partial_x \left(h_2 \overline{u}_2 \right) = 0, \\[2mm]
\left(1 + \dfrac{\mu}{2} \mathbf{T}_2 \right) \dfrac{\mathrm{D}_2 \overline{u}_2}{\mathrm{D}_2 t} - \dfrac{\mu \varepsilon_2}{2} \mathbf{Q}_2 (\overline{u}_2) + \\[3mm]
\qquad\qquad \mu \varepsilon_2 h_{2_x} \dfrac{\mathrm{D}_2 \zeta_2}{\mathrm{D}_2 t} + \dfrac{\mu h_2}{2} \partial_x \left(\dfrac{\mathrm{D}_2 \zeta_2}{\mathrm{D}_2 t} + \beta b_x \dfrac{\mathrm{D}_2 \overline{u}_2}{\mathrm{D}_2 t} \right) + \dfrac{\mu \varepsilon_2}{h_2} E^2 + \mathcal{P}_{int} = 0, \\[3mm]
E_t^2 + \varepsilon_2 \overline{u}_2 E_x^2 + 3 \varepsilon_2 \overline{u}_{2_x} E^2 = 0,
\end{cases}
\tag{2.43}
$$

where the interface pressure contribution $\mathcal{P}_{int}$ is the same as previously defined by (2.36). By introducing the operators (2.39)-(2.42) we aim to write the model in a formulation close to the one used for the numerical study of the Green-Naghdi equations in [21], [43], or [83], for example. The methods considered in these works are constructed for an efficient treatment of high order derivatives coming with dispersive effects, using a similar operator form of the Green-Naghdi system. Another strategy, used to overcome the numerical difficulties related to dispersive effects, found in [86], is applied in Chapter 1. In order to allow for the application of the second strategy to the case of constant vorticity, in the next section we follow the Lagrangian approach proposed in [14] for a two-layer model derivation in the absence of vorticity effects. We provide preliminary derivations for the Euler-Lagrange equations and corresponding additional conservation laws with constant vorticities in each layer.

2.5   Lagrangian approach: Constant vorticity $1d$ case.

The equations in the case of constant vorticity in each layer can be obtained by applying the Hamiltonian principle to the master Lagrangian $\mathcal{L}$ of the two-layer system. Following the approach described in [14], we define the Lagrangian for the two-layer system as:

$$
\mathcal{L} = \int_{\mathbb{R}^2} \int_{-\frac{1}{\delta}}^{\varepsilon_2 \zeta_2} \left(\dfrac{\varepsilon_2^2}{2} \left(|\vec{u}_2|^2 + \mu w_2^2 \right) - z \right) dx dz + \int_{\mathbb{R}^2} \int_{\varepsilon_2 \zeta_2}^{1 + \varepsilon_1 \zeta_1} \left(\dfrac{\rho \varepsilon_1^2}{2} \left(|\vec{u}_1|^2 + \mu w_1^2 \right) - \rho z \right) dx dz.
$$

We introduce the same dimensionless variables (2.5), (2.6). Integrating and dropping the $\mathcal{O}(\mu^{3/2})$ terms, the following approximate expression for $\mathcal{L}$ is obtained:

$$
\mathcal{L} = \int_{\mathbb{R}^2} T^2 - W^2 \left(h_2, \dfrac{\mathrm{D}_2 h_2}{\mathrm{D}_2 t} \right) dz + \int_{\mathbb{R}^2} T^1 - W^1 \left(h_1, h_2, \dfrac{\mathrm{D}_1 h_1}{\mathrm{D}_1 t}, \dfrac{\mathrm{D}_1 h_2}{\mathrm{D}_1 t} \right) dz,
\tag{2.44}
$$

where the kinetic energies T^i and the potentials $W^i\left(h_i, \dfrac{D_i h_i}{D_i t}\right)$ are defined as follows:

$$T^2 = \frac{\varepsilon_2^2}{2}|\overline{u}_2|^2 h_2, \quad T^1 = \frac{\rho\varepsilon_1^2}{2}|\overline{u}_1|^2 h_1,$$

$$W^2\left(h_2, \frac{D_2 h_2}{D_2 t}\right) = \frac{h_2(h_2 - 2/\delta)}{2} - \frac{\varepsilon_2^2}{2}\left(\frac{\mu\varepsilon_2}{12 h_2}\omega_2^2(h_2^3) + \mu\frac{h_2}{3}\left(\frac{D_2 h_2}{D_2 t}\right)^2\right),$$

$$W^1\left(h_1, h_2, \frac{D_1 h_1}{D_1 t}, \frac{D_1 h_2}{D_1 t}\right) = \frac{\rho h_1(h_1 + 2 h_2 - 2/\delta)}{2}$$
$$- \frac{\rho\varepsilon_1^2}{2}\left(\frac{\mu\varepsilon_1}{12 h_1}\omega_1^2(h_1^3) + \mu h_1\left(\frac{D_1(h_1 + h_2)}{D_1 t}\right)^2 \frac{D_1 h_2}{D_1 t} + \mu h_1\left(\frac{D_1 h_1}{D_1 t}\right)^2\right).$$

The dimensionless parameters used above are defined earlier by (2.4). The horizontal velocity decompositions (2.9) are taken into account, and the velocities $\overline{u}_1$, $\overline{u}_2$ denote again the depth-average horizontal velocities (see (2.8)).

The corresponding Euler-Lagrange equations lead to the equations for the system motion. By adding the mass conservation laws

$$(h_1)_t + \varepsilon_1 \partial_x(h_1 \overline{u}_1) = 0,$$

$$(h_2)_t + \varepsilon_2 \partial_x(h_2 \overline{u}_2) = 0,$$

(2.45)

as constraint relations to the action integral, we construct the momentum conservation equations. We first introduce the notations

$$\rho_1 = h_1, \rho_2 = \rho h_2.$$

For the upper layer, we find the following momentum equation

$$\frac{D_1 \overline{u}_1}{D_1 t} + \partial_x\left(\frac{\rho_1}{\rho} + \rho_2 + \frac{\mu\varepsilon_1^2}{8\rho^2}\omega_1^2 \rho_1^2\right)$$

$$-\partial_x\left(\mu\varepsilon_1^2\left(\frac{1}{2}\left(\frac{D_1\rho_2}{D_1 t}\right)^2 + \frac{1}{2}\frac{D_1\rho_1}{D_1 t}\frac{D_1\rho_2}{D_1 t} + \frac{1}{6\rho}\left(\frac{D_1\rho_1}{D_1 t}\right)^2\right) - \rho_1\mu\varepsilon_1^2\left(\frac{1}{2}\frac{D_1^2\rho_2}{D_1 t^2} + \frac{1}{3\rho}\frac{D_1^2\rho_1}{D_1 t^2}\right)\right) +$$

$$\mu\varepsilon_1^2\left(\left(\frac{1}{2}\frac{D_1^2\rho_2}{D_1 t^2} + \frac{1}{3\rho}\frac{D_1^2\rho_1}{D_1 t^2}\right)\rho_{1x} + \left(\frac{1}{2}\frac{D_1\rho_2}{D_1 t} + \frac{1}{3\rho}\frac{D_1\rho_1}{D_1 t}\right)\frac{D_1\rho_{1x}}{D_1 t}\right)$$

$$+\mu\varepsilon_1^2\left(\left(\frac{D_1^2\rho_2}{D_1 t^2} + \frac{1}{2}\frac{D_1^2\rho_1}{D_1 t^2}\right)\rho_{2x} + \left(\frac{D_1\rho_2}{D_1 t} + \frac{1}{2}\frac{D_1\rho_1}{D_1 t}\right)\frac{D_1\rho_{2x}}{D_1 t}\right)$$

$$+\overline{u}_{1x}\mu\varepsilon_1^2\left[\left(\frac{1}{2}\frac{D_1\rho_2}{D_1 t} + \frac{1}{3\rho}\frac{D_1\rho_1}{D_1 t}\right)\rho_{1x} + \left(\frac{D_1\rho_2}{D_1 t} + \frac{1}{2}\frac{D_1\rho_1}{D_1 t}\right)\rho_{2x}\right] = 0,$$

(2.46)

and the equation in the lower layer reads

$$\frac{D_2 \overline{u}_2}{D_2 t} + \partial_x \left(\rho_1 + \rho_2 + \frac{\mu \varepsilon_2^2}{8} \omega_2^2 \rho_2^2 \right)$$

$$- \partial_x \left(\frac{1}{6} \mu \varepsilon_2^2 \left(\frac{D_2 \rho_2}{D_2 t} \right)^2 - \frac{1}{3} \rho_2 \mu \varepsilon_2^2 \frac{D_2^2 \rho_2}{D_2 t^2} - \rho_1 \mu \varepsilon_1^2 \left(\frac{D_1^2 \rho_2}{D_1 t^2} + \frac{1}{2} \frac{D_1^2 \rho_1}{D_1 t^2} \right) \right)$$

$$+ \mu \varepsilon_2^2 \left(\frac{1}{3} \frac{D_2^2 \rho_{2_x}}{D_2 t^2} + \frac{1}{3} \frac{D_2 \rho_2}{D_2 t} \frac{D_2 \rho_{2_x}}{D_2 t} \right) + \frac{1}{3} \overline{u}_{2x} \mu \varepsilon_2^2 \frac{D_2 \rho_2}{D_2 t} \rho_{2x} = 0. \tag{2.47}$$

One property of variational structure of the obtained system is that total momentum and energy conservation can be derived. One obtains the two conservation laws:

$$(\rho_1 \overline{u}_1 + \rho_2 \overline{u}_2)_t + \left(\rho_1 \overline{u}_1^2 + \rho_2 \overline{u}_2^2 + \frac{\mu}{12} \left(\frac{\varepsilon_1^2 \omega_1^2 \rho_1^3}{\rho^2} + \varepsilon_2^2 \omega_2^2 \rho_2^3 \right) + p \right)_x = 0,$$

$$\left(\frac{1}{2} \rho_1 \overline{u}_1^2 + \frac{1}{2} \rho_2 \overline{u}_2^2 + E \right)_t + \left(\overline{u}_1 \left(\frac{1}{2} \rho_1 \overline{u}_1^2 + F_1 \right) + \overline{u}_2 \left(\frac{1}{2} \rho_2 \overline{u}_2^2 + F_2 \right) \right)_x = 0, \tag{2.48}$$

where the "pressure" p, "internal energy" E, and energy fluxes F_1, F_2 are defined as follows

$$p = \frac{1}{2} \left(\frac{\rho_1^2}{\rho} + \rho_1 \rho_2 + \rho_2^2 \right) + \frac{1}{3} \rho_2^2 \mu \varepsilon_2^2 \frac{D_2^2 \rho_2}{D_2 t^2} + \mu \varepsilon_1^2 \rho_1 \left(\frac{\rho_1}{2} + \rho_2 \right) \frac{D_1^2 \rho_2}{D_1 t^2} + \mu \varepsilon_1^2 \left(\frac{\rho_1}{3\rho} + \frac{\rho_2}{2} \right) \frac{D_1^2 \rho_1}{D_1 t^2},$$

$$E = \frac{\rho_2}{2} \left(\rho_2 - \frac{2}{\delta} \right) + \frac{\rho_1}{2} \left(\frac{\rho_1}{\rho} + 2 \left(\rho_2 - \frac{1}{\delta} \right) \right) + \frac{\mu}{24} \left(\frac{\varepsilon_1^2 \rho_1^3 \omega_1^2}{\rho^2} + \varepsilon_2^2 \rho_2^3 \omega_2^2 \right)$$

$$+ \frac{1}{6} \mu \rho_2 \varepsilon_2^2 \left(\frac{D_2 \rho_2}{D_2 t} \right)^2 + \frac{1}{6\rho} \mu \rho_1 \varepsilon_1^2 \left(\frac{D_1 \rho_1}{D_1 t} \right)^2 + \frac{1}{2} \mu \rho_1 \varepsilon_1^2 \left(\frac{D_1 \rho_2}{D_1 t} \right)^2 + \frac{1}{2} \mu \rho_1 \varepsilon_1^2 \frac{D_1 \rho_1}{D_1 t} \frac{D_1 \rho_2}{D_1 t},$$

$$F_1 = \rho_1 \left(\frac{\rho_1}{\rho} + \rho_2 + \frac{\mu \varepsilon_1^2}{8\rho^2} \omega_1^2 \rho_1^2 \right)$$

$$- \rho_1 \left(\mu \varepsilon_1^2 \left(\frac{1}{2} \left(\frac{D_1 \rho_2}{D_1 t} \right)^2 + \frac{1}{2} \frac{D_1 \rho_1}{D_1 t} \frac{D_1 \rho_2}{D_1 t} + \frac{1}{6\rho} \left(\frac{D_1 \rho_1}{D_1 t} \right)^2 \right) - \rho_1 \mu \varepsilon_1^2 \left(\frac{1}{2} \frac{D_1^2 \rho_2}{D_1 t^2} + \frac{1}{3\rho} \frac{D_1^2 \rho_1}{D_1 t^2} \right) \right),$$

$$F_2 = \rho_2 \left(\rho_1 + \rho_2 + \frac{\mu \varepsilon_2^2}{8} \omega_2^2 \rho_2^2 - \frac{1}{6} \mu \varepsilon_2^2 \left(\frac{D_2 \rho_2}{D_2 t} \right)^2 + \frac{1}{3} \rho_2 \mu \varepsilon_2^2 \frac{D_2^2 \rho_2}{D_2 t^2} + \rho_1 \mu \varepsilon_1^2 \left(\frac{D_1^2 \rho_2}{D_1 t^2} + \frac{1}{2} \frac{D_1^2 \rho_1}{D_1 t^2} \right) \right).$$

This preliminary model needs to be analysed in details. It is necessary to compare the presented model with the model (2.35). We expect that the two models coincide in the approximation order $\mathcal{O}(\mu^{3/2})$.

In order to proceed with a numerical strategy similar to the one used in Chapter 1, the following change of variables is used

$$K_1 = \overline{u}_1 + \mu \varepsilon_1^2 \left(\left(\frac{1}{2} \frac{D_1 \rho_2}{D_1 t} + \frac{1}{3\rho} \frac{D_1 \rho_1}{D_1 t} \right) \rho_{1x} + \left(\frac{D_1 \rho_2}{D_1 t} + \frac{1}{2} \frac{D_1 \rho_1}{D_1 t} \right) \rho_{2x} \right),$$

$$K_2 = \overline{u}_2 + \frac{1}{3} \mu \varepsilon_2^2 \left(\frac{D_2 \rho_2}{D_2 t} \right) \rho_{2x}.$$

The numerical study of the presented model is left for future work.

2.6 Conclusion

In the present chapter, two-layer model derivations are proposed in the case of rotational flows. The models describe free surface and interface waves propagation in the framework of depth average equations. Without irrotationality assumptions, the model requires a closure. When constant vorticities are assumed, the model is automatically closed, and we derive a second order model which reduces to the Green-Naghdi equations in the case of vanishing vorticities. However, for the general vorticity case, additional equations are needed to define the 'Reynolds tensor' and pressure contributions. The vorticity equation is used to find a closure. For the general vorticity case, we derived a weakly nonlinear model.

The natural perspective of this work is to derive a model in the case of general vorticities with better dispersive properties, in order to correct non-hydrostatic pressure terms and obtain closures in the classical Green-Naghdi order or higher. According to [29], it is possible to close the system through a cascade of equations which is consistent with the model order. It implies an additional correction for the pressure contribution terms, which is a non-trivial task. Firstly, for the sake of simplicity, one can imagine considering the rigid lid approximation (when it is assumed that the displacements of the surface are negligible compared to the interface displacements). Another direction of future research is to perform numerical simulations for the obtained models.

Part II

Boundaries

Introduction : Boundary conditions

This part is devoted to a particular numerical issue which appears when dispersive models of wave propagation are solved numerically. The physical space, where the phenomenon takes place, has generally to be limited in order to study in details some regions of interest, and boundary conditions must be imposed. Mathematically, the equations are set on an infinite space, and it is a hard problem to provide suitable boundary conditions which lead to a well-posed initial-boundary problem approximating the initial value problem.

The construction of boundary conditions (BC) for dispersive problems is recognised as being a challenging issue for numerical simulations. In particular, the problem of providing well-posed conditions is considerably complicated by a wide range of phase speeds at the boundary. Some physical settings allow for simplifications of the procedure. If we are interested in short-time simulations, the Neumann boundary conditions are appropriate. If the solution stays compactly supported for all time, periodic boundary conditions can be applied. Finally, reflecting solid wall conditions lead generally to a stable behaviour at the boundary. For examples of applications either of these boundary conditions, we refer to [86], [83], or [70].

However, in more general applications, a proper procedure for the simulation of incoming and outgoing waves is of fundamental concern. These particular type of conditions are referred to *artificial/transparent* boundary conditions as well as *open/open sea* boundary conditions. As discussed in the Introduction, the dispersive Green-Naghdi system is generally used in the context of coastal water wave propagation, and when this system is solved numerically, artificial conditions are often required. The same issue arises for the models derived in Part I. We focus in this part only on the Green-Naghdi equations, because even in this case, construction of BCs is also far from trivial.

Generally, boundary conditions are not a central subject in the literature devoted to studies on ocean waves propagation in the context of Boussinesq type and Green-Naghdi models. This is partly due to the fact that the proposed approaches are mostly heuristic and often adapted for every special case. However, we can distinguish several numerical techniques used for the Boussinesq/Green-Naghdi type models.

In [92] Madsen proposed a *relaxation technique*, where the computational domain is extended with thin relaxation zones, inside which a particular forcing of a numerical solution to a target one is applied at the end of each time step. The *sponge layer* approach firstly proposed in [65] has been followed by many others researchers (e.g. [85], [73]). The principle idea is to add an artificial damping term to the right-hand side of the momentum equation. In the original work [65], three different kinds of damping mechanism are proposed: Newtonian cooling, viscous damping and sponge filter. Also, there it is mentioned that the last one is the best for an open sea boundary condition. However, any of these terms are generally used based on what works the best. In [71], [125] it is discovered that the model used in [73] is noisy and it is partially due to the boundary condition implementation. In [153], modified sponge layers are proposed in order to obtain a more predictable behaviour

at the boundaries; it is also shown that this modified approach is practically identical to the relaxation technique, with the only significant difference that the new system is invariant with respect to the time step and, as a consequence, has a more predictable properties. All these techniques allow for the wave generation when the forcing is performed to an exact profile, and not to zero. A different approach is used in [36, 100, 21], where efficient absorbing-generating boundary conditions are implemented, using that outflow-inflow Riemann invariants might be locally conserved along the characteristics. According to [148], an ad-hoc source function added in the mass conservation law is used for the wave generation. Different types of source functions are used in the following studies, see for example [73], [70].

In this thesis, we aim to propose a more general and rigorous approach for the boundary conditions treatment in application to the Green-Naghdi system. In Chapter 3 we propose artificial boundary conditions for the equations linearized around the steady state $h = $ const, $u = 0$. In [149] continuous transparent boundary conditions are constructed for the Airy equation using the Laplace transform, and then the initial-boundary problem is discretized. Following the authors we construct continuous boundary conditions. However, the discretization of the obtained conditions is not a trivial task, and we follow the different strategy found in [17] (in application to the Airy equation). The approach consists in a direct application of the method, similar to the one used in the continuous case, to a fully discrete system. The Laplace transform is replaced by its discreet counterpart, the $\mathcal{Z}-$transform. This strategy was already successfully applied to other unidirectional wave propagation models [19, 18]. In Chapter 3, we consider two discretizations of the initial linear system on staggered and collocated grids. The procedure for the discrete boundary conditions construction involves the inversion of a nonlocal in time $\mathcal{Z}-$transform operator. In the case when a staggered grid is used, this inversion is done explicitly, while for the discretization on a collocated grid, a more sophisticated numerical inversion procedure needs to be designed. Both schemes are proved to be stable, consistent and convergent. Numerical tests are performed for Gaussian and wave packet initial data. We show that the procedure can be adapted for the wave generation. Unfortunately, tries to use the same conditions for the nonlinear Green-Naghdi system have not been successful, and further investigations are envisaged.

In order to provide a suitable boundary treatment for the nonlinear case, we apply another method, used for this issue, which is referred to as *Perfect Matched Layer (PML)* technique [16]. The idea is to surround the computational domain with thin layers where the properties of wave propagation are modified in order to have an amplitude decay and reflections as small as possible for all frequencies and angles of incidence. This leads to modifications in the original equations and allows for the absorption of outgoing waves. In Chapter 4, we consider the new hyperbolic system recently proposed in [49] to approximate the original Green-Naghdi equations. The hyperbolicity of this new system allows for a simplification of the PML technique application. Following [1], we construct the modified equations. The proposed approach is validated on different numerical tests for linear and nonlinear cases. Using the same arguments, the PML equations can be constructed to handle incoming waves. Numerical tests are provided to illustrate this procedure.

Chapter 3

Discrete transparent boundary conditions for the linearized Green-Naghdi system

In this chapter we introduce artificial boundary conditions (ABCs) for the linearized Green-Naghdi system. We will consider two spatial discretizations of the initial system either on a staggered grid or on a collocated grid, both of interest from the practical point of view.

The dimensional Green-Naghdi equations read as

$$\begin{cases} h_t + div(h\vec{u}) = 0, \\ (h\vec{u})_t + div(h\vec{u} \otimes \vec{u} + pI) = 0, \quad p = \dfrac{gh^2}{2} + \dfrac{1}{3}h^2\ddot{h}, \end{cases} \quad x \in \mathbb{R}^2, \, t > 0, \qquad (3.1)$$

where h is a fluid depth, $\vec{u}$ is a depth-averaged horizontal velocity, indexes mean the derivation with respect to t, $x \in \mathbb{R}^2$, and dot is a material derivative $\dot{h} = h_t + \vec{u} \cdot \nabla h$. The consistency result with the Euler equations can be found in [81]. The model (3.1) describes bidirectional propagation of dispersive water waves in the shallow water regime. It is physically more relevant for water wave problems than the unidirectional models like the Korteweg-de Vries equation or the Benjamin-Bona-Mahony equation which only describe small amplitude/unidirectional water waves.

The original system (3.1) is derived and set on the whole space. For practical applications, as already discussed, the area of study is restricted to a bounded domain and one has to prescribe suitable boundary conditions.

We focus here on *artificial* boundary conditions in order to let waves go out of the computational domain without reflection or to prescribe an incoming wave on a part of the domain. From a mathematical point of view, the problem is set, in both cases, as follows: given compactly supported initial data, one searches for suitable boundary conditions such that the solution computed with these boundary conditions coincide on the bounded domain with the restriction of the solution set on the whole space. One possibility to solve this problem is to compute the solution on a sufficiently large domain with, say, periodic boundary conditions. However, it is cumbersome from a numerical point of view and re-

quires the solution to remain compactly supported for all time. In particular it is untrue for large classes of dispersive equations like the Korteweg-de Vries equation or the Schrödinger equation. Moreover, the energy of the exact solution for the problem set on the whole space is conserved whereas the energy of the restricted solution should decrease. For all these reasons it is important to determine the suitable boundary conditions, which absorb the energy at the boundaries and lead to a well-posed initial boundary value problem.

A review on different techniques for the construction of such conditions for the linear and nonlinear Schrödinger equations can be found in [5]. For linear equations, the construction of the exact transparent boundary conditions (TBCs) is carried out by using Laplace transform in time and impose boundary conditions so as to obtain finite energy solutions. The inversion of those conditions yields boundary conditions that are in general nonlocal in time. For nonlinear equations, pseudodifferential or paradifferential calculus is needed to provide transparent boundary conditions in the high frequency/short time regime [5]. A numerical implementation of these boundary conditions is not straightforward: see e.g. [149] for a discretization of transparent boundary conditions for the Airy equation which requires an approximation of fractional derivatives. An alternative and fruitful approach consists in starting directly from a discretization of the equations set on the whole space and mimic the approach in the continuous case: the Laplace transform is replaced by the $\mathcal{Z}$-transform: see e.g. [17] for an application of this strategy to the Airy equation. In this chapter the inverse $\mathcal{Z}$-transform cannot be carried out explicitly and the authors implemented directly the explicit formula of the inverse transform. This procedure is not stable from a numerical point of view. Recently the same idea provided the appropriate continuous and discrete boundary conditions for other dispersive equations for unidirectional wave propagation such as the Benjamin-Bona-Mahoney (BBM) equation [18] and the mixed KDV-BBM equation [19] where an alternative, stable method is introduced to compute the inverse transform. These equations model unidirectional, small amplitude water waves: for practical applications, it is important to consider more general equations which model waves propagating possibly in all directions. We focus here on the Green-Naghdi equations which are widely used in coastal engineering to model dispersive non linear waves. In this case, classical techniques are useless (in particular factorisation of pseudo-differential operators: [5] for more details) and one has to introduce a more robust methodology.

In this chapter, we focus on a version of the model (3.1) linearized about the steady state $(h, u) := (H_0, 0) + (\eta, w)$ with $|(\eta, w)| \ll 1$. In the one-dimensional case, this linearized system is written as:

$$\begin{cases} \eta_t + w_x = 0, \\ w_t + \eta_x - \varepsilon w_{txx} = 0, \end{cases} \qquad x \in \mathbb{R}, \quad t > 0, \tag{3.2}$$

where $\varepsilon > 0$ is a dispersion parameter. We are interested in the derivation of discrete transparent boundary conditions (DTBCs) for (3.2): they should provide suitable absorbing boundary conditions for the full system (3.1) for small amplitude waves. For that purpose, we focus on two spatial discretizations by working either on a collocated grid (η, w are evaluated at the same points) or on a staggered grid (i.e. η is evaluated at the cell centre and w is evaluated at the cell faces). Both grids are used in oceanography depending on the applications: these are the so-called A (collocated) grid for compressible like flows and C

(arakawa) grids for incompressible (low Froude) flows. We use a Crank-Nicolson scheme for the time discretization. We then follow the same strategy as for the derivation of continuous transparent boundary conditions (the two strategies do not commute though): we apply the $\mathcal{Z}-$transform and identify modes which are increasing exponentially as x tends to $\pm\infty$. By restricting our attention to finite energy solutions, we impose conditions at the boundary points and then apply either explicitly or numerically the inverse $\mathcal{Z}-$transform. These conditions are in general nonlocal in time and can be cumbersome from a numerical point of view. There are various strategies to implement efficiently those DTBC. Let us mention in particular "sum of exponentials" techniques: this approach is well documented. See e.g. [9], [10], for quantum evolution equations and [17] for an application in the case of the linearized (KdV) equation.

In section 3.1, we apply the technique found in [149] to construct the exact boundary conditions for the linear system (3.2). Moreover one can notice that the system (3.2) is equivalent to a linearized version of the Boussinesq equation:

$$(w - \varepsilon w_{xx})_{tt} - w_{xx} = 0, \quad \forall x \in \mathbb{R}, \quad \forall t > 0,$$

and we focus on the construction of boundary conditions for this equation too. It is useful when we construct the discrete conditions for Crank-Nicolson time-discretization on a staggered grid: see section 3.2. As it was already mentioned the procedure of discrete boundary conditions construction involves the inversion of nonlocal-in-time $\mathcal{Z}$-transform operator, and the main reason to consider the scheme on the staggered grid is that this inversion can be done explicitly. The inversion of conditions for a scheme on a collocated grid needs to be done numerically, and a more sophisticated procedure of inversion is presented in section 3.3. Finally, in section 3.4, we present some numerical simulations to illustrate the accuracy of the proposed boundary conditions. We perform three types of simulations. The examples are inspired by works [19], [18]. We show different dispersive effects with a Gaussian and a wave packet initial data.

3.1 Exact transparent boundary conditions

In this section we show how to derive transparent boundary conditions in the continuous case and prove the absorbing property of constructed conditions.

3.1.1 Exact boundary conditions for the linearized Green–Naghdi system

We derive first the continuous boundary conditions for the system (3.2). We consider the initial value problem set on the whole space

$$\eta_t + w_x = 0, \quad \forall x \in \mathbb{R}, \forall t > 0,$$
$$w_t + \eta_x - \varepsilon w_{txx} = 0, \quad \forall x \in \mathbb{R}, \forall t > 0,$$
$$\eta(0, x) = \eta_0(x), \quad w(0, x) = w_0(x), \quad \forall x \in \mathbb{R},$$
$$\lim_{x \to \pm\infty} w(t, x) = \lim_{x \to \pm\infty} \eta(t, x) = 0,$$

where the initial data η_0, w_0 are compactly supported functions in a finite interval $[x_\ell, x_r]$. In order to construct the transparent boundary conditions at x_ℓ, x_r, we consider the "exterior" solution of the problem set on the complement of $[x_\ell, x_r] \subset \mathbb{R}$:

$$\tilde{\eta}_t + \tilde{w}_x = 0, \quad \forall x \in \mathbb{R} \setminus [x_\ell, x_r], \forall t > 0,$$

$$\tilde{w}_t + \tilde{\eta}_x - \varepsilon \tilde{w}_{txx} = 0, \quad \forall x \in \mathbb{R} \setminus [x_\ell, x_r], \forall t > 0,$$

$$\tilde{\eta}(0, x) = 0, \quad \tilde{w}(0, x) = 0, \quad \forall x \in \mathbb{R} \setminus [x_\ell, x_r], \tag{3.3}$$

$$\lim_{x \to \pm\infty} \tilde{w}(t, x) = \lim_{x \to \pm\infty} \tilde{\eta}(t, x) = 0,$$

with transmission conditions at x_ℓ, x_r (continuity with "interior" solution)

$$\tilde{\eta}(t, x_\ell) = \eta(t, x_\ell), \quad \tilde{w}(t, x_\ell) = w(t, x_\ell), \quad \tilde{\eta}(t, x_r) = \eta(t, x_r), \quad \tilde{w}(t, x_r) = w(t, x_r).$$

This problem is homogeneous in time. We can apply the Laplace transform defined as

$$\mathcal{L}(f)(s; x) = \int_0^\infty e^{-st} f(t; x) dt,$$

where s is a parameter such as $\Re(s) > 0$ (where $\Re$ denotes the real part). We obtain the ordinary differential equations:

$$s\mathcal{L}(\tilde{\eta}) + \mathcal{L}(\tilde{w}_x) = 0,$$
$$s\mathcal{L}(\tilde{w}) + \mathcal{L}(\tilde{\eta}_x) - \varepsilon s \mathcal{L}(\tilde{w}_{xx}) = 0. \tag{3.4}$$

The solutions of the system (3.4) have the from

$$\begin{pmatrix} \mathcal{L}(\tilde{w})(s, x) \\ \mathcal{L}(\tilde{\eta})(s, x) \end{pmatrix} = \alpha_+^r V^+ e^{\lambda^+ x} + \alpha_-^r V^- e^{\lambda^- x}, \quad \forall x > x_r,$$

$$\begin{pmatrix} \mathcal{L}(\tilde{w})(s, x) \\ \mathcal{L}(\tilde{\eta})(s, x) \end{pmatrix} = \alpha_+^\ell V^+ e^{\lambda^+ x} + \alpha_-^\ell V^- e^{\lambda^- x}, \quad \forall x < x_\ell,$$

where $\alpha_+^{r,\ell}$, $\alpha_-^{r,\ell}$ are constant coefficients, λ^+, λ^- are given by

$$\lambda^+ = \sqrt[+]{\frac{s^2}{1 + \varepsilon s^2}}, \quad \lambda^- = -\sqrt[+]{\frac{s^2}{1 + \varepsilon s^2}},$$

and V^+, V^- are the constant vectors:

$$V^+ = (1, -\lambda^+/s)^\top, \, V^- = (1, \lambda^+/s)^\top.$$

The number $\sqrt[+]{z}$ corresponds to the principal square root of the complex number $z \in \mathbb{C}$:

$$\forall z = \rho e^{i\theta}, \quad \theta \in]-\pi, \pi], \quad \sqrt[+]{z} = \sqrt{\rho} e^{i\theta/2}.$$

Note that the function $s \mapsto s^2/(1+\varepsilon s^2)$ maps $\{s \in \mathbb{C}, \Re(s) > 0\}$ into $\mathbb{C} \setminus \mathbb{R}^-$, therefore λ^+ has a strictly positive real part whereas λ^- has a negative one. As a result, $x \mapsto e^{\lambda^+ x}$ increases exponentially fast as $x \to \infty$. In order to have a bounded solution $\mathcal{L}(\tilde{w})(s, x), \mathcal{L}(\tilde{\eta})(s, x)$ for

all $x \geq x_r$, one must impose $\alpha_+^r = 0$. Similarly, one has $\alpha_-^\ell = 0$. The constant coefficients α_+^r, α_-^ℓ are written as:

$$2\alpha_+^r = \mathcal{L}(\tilde{w})(s, x_r) - \sqrt[+]{1 + \varepsilon s^2}\mathcal{L}(\tilde{\eta})(s, x_r) = 0,$$

$$2\alpha_-^\ell = \mathcal{L}(\tilde{w})(s, x_\ell) + \sqrt[+]{1 + \varepsilon s^2}\mathcal{L}(\tilde{\eta})(s, x_\ell) = 0.$$

By using the transmission conditions (see (3.3)) at the points x_ℓ, x_r, we then deduce a relation between $\mathcal{L}(\eta)$ and $\mathcal{L}(w)$ at the boundary points x_ℓ, x_r:

$$\mathcal{L}(w)(s, x_r) = \frac{1 + \varepsilon s^2}{\sqrt[+]{1 + \varepsilon s^2}}\mathcal{L}(\eta)(s, x_r), \quad \mathcal{L}(w)(s, x_\ell) = -\frac{1 + \varepsilon s^2}{\sqrt[+]{1 + \varepsilon s^2}}\mathcal{L}(\eta)(s, x_\ell). \quad (3.5)$$

The inversion of the Laplace transform can be carried out explicitly and finally we get the following nonlocal in time transparent boundary conditions:

$$\varepsilon w_{tx}(t, x_r) - \eta(t, x_r) = -\int_0^t \frac{\mathcal{J}_2 + \mathcal{J}_0}{2\sqrt{\varepsilon}}\left(\frac{s}{\sqrt{\varepsilon}}\right)w(t - s, x_r)ds - \sqrt{\varepsilon}w_t(t, x_r),$$

$$\varepsilon w_{tx}(t, x_\ell) - \eta(t, x_\ell) = \int_0^t \frac{\mathcal{J}_2 + \mathcal{J}_0}{2\sqrt{\varepsilon}}\left(\frac{s}{\sqrt{\varepsilon}}\right)w(t - s, x_\ell)ds + \sqrt{\varepsilon}w_t(t, x_\ell),$$

(3.6)

where $\mathcal{J}_n$ is the Bessel function of the first kind:

$$\mathcal{J}_n(t) = \frac{1}{\pi}\int_0^\pi \cos(n\tau - t\sin\tau)d\tau$$

with $n \in \mathbb{N}$. Note that there are several alternative formulations of the boundary conditions (3.6) depending on how the relations (3.5) are inverted. We have chosen the formulation that is useful to prove dissipativity of these boundary conditions set on a bounded domain.

Now we prove the following stability result.

3.1.1 Proposition. *The problem*

$$\eta_t + w_x = 0, \quad w_t + \eta_x - \varepsilon w_{txx} = 0 \quad \forall x \in]x_\ell, x_r[, \forall t > 0,$$

$$\eta(0, x) = \eta_0(x), \quad w(0, x) = w_0(x), \quad \forall x \in]x_\ell, x_r[,$$

$$\varepsilon w_{tx}(t, x_r) - \eta(t, x_r) = -\int_0^t \frac{\mathcal{J}_2 + \mathcal{J}_0}{2\sqrt{\varepsilon}}\left(\frac{s}{\sqrt{\varepsilon}}\right)w(t - s, x_r)ds - \sqrt{\varepsilon}w_t(t, x_r),$$

$$\varepsilon w_{tx}(t, x_\ell) - \eta(t, x_\ell) = \int_0^t \frac{\mathcal{J}_2 + \mathcal{J}_0}{2\sqrt{\varepsilon}}\left(\frac{s}{\sqrt{\varepsilon}}\right)w(t - s, x_\ell)ds + \sqrt{\varepsilon}w_t(t, x_\ell),$$

(3.7)

is $L^\infty(\mathbb{R}^+, H^1(\mathbb{R}) \times L^2(\mathbb{R}))$ stable: for all $t > 0$ and for all smooth solutions of (3.7), we have

$$\int_{x_\ell}^{x_r} \frac{\eta^2(t, x)}{2} + \frac{w^2(t, x)}{2} + \varepsilon\frac{(w_x(t, x))^2}{2}dx \leq \int_{x_\ell}^{x_r} \frac{\eta_0^2(x)}{2} + \frac{w_0^2(x)}{2} + \varepsilon\frac{(w_{0,x}(x))^2}{2}dx. \quad (3.8)$$

Proof. We deduce directly from the equations a derivative of the generalized kinetic energy with respect to time:

$$\frac{d}{dt}\int_{x_\ell}^{x_r}\frac{\eta^2(t,x)}{2}+\frac{w^2(t,x)}{2}+\varepsilon\frac{(w_x(t,x))^2}{2}dx = \Big[w(t,x)\left(\varepsilon w_{tx}(t,x)-\eta(t,x)\right)\Big]_{x_\ell}^{x_r},$$

where the brackets denote a jump of the function between x_ℓ and x_r. By integrating this equation with respect to the time variable on the interval $(0,t)$, one obtains:

$$\int_{x_\ell}^{x_r}\frac{\eta^2(t,x)}{2}+\frac{w^2(t,x)}{2}+\varepsilon\frac{(\partial_x w(t,x))^2}{2}dx - \int_{x_\ell}^{x_r}\frac{\eta_0^2(x)}{2}+\frac{w_0^2(x)}{2}+\varepsilon\frac{(\partial_x w_0(x))^2}{2}dx$$
$$= \int_0^t w(s,x_r)(\varepsilon w_{tx}-\eta)(s,x_r)ds - \int_0^t w(s,x_\ell)(\varepsilon w_{tx}-\eta)(s,x_\ell)ds =: J_r - J_\ell$$

if $J_r \le 0$ and $J_\ell \ge 0$ then the inequality (3.8) is satisfied. Let us consider J_r first: by substituting the boundary condition (3.6), one obtains

$$J_r = -\int_0^t \left(\frac{\mathcal{J}_2+\mathcal{J}_0}{2\sqrt{\varepsilon}}\left(\frac{\cdot}{\sqrt{\varepsilon}}\right)*w(s,x_r)+\sqrt{\varepsilon}w_t(s,x_r)\right)w(s,x_r)ds, \qquad (3.9)$$

where $*$ denotes time convolution. Next, we fix $T > 0$ and denote $W(t) = w(t,x_r)1_{[0,T]}(t)$. One has

$$w'(t) = W'(t) + W(T)\delta_{t=T}.$$

Substitution into the formula (3.9) for J_r gives

$$J_r = -\int_0^\infty \left(\frac{\mathcal{J}_2+\mathcal{J}_0}{2\sqrt{\varepsilon}}(\frac{\cdot}{\sqrt{\varepsilon}})*W(s)+\sqrt{\varepsilon}W'(s)\right)W(s,x_r)ds - \sqrt{\varepsilon}W(T)^2.$$

By applying Plancherel's identity [110], one finds:

$$J_r = -\frac{1}{2\pi}\Re\int_{\mathbb{R}} \sqrt[4]{1-\varepsilon\xi^2}|\widehat{W}|^2(\xi)d\xi - \sqrt{\varepsilon}|W(T)|^2,$$
$$- \int_{-1/\sqrt{\varepsilon}}^{1/\sqrt{\varepsilon}}\sqrt{1-\varepsilon\xi^2}|\widehat{W}|^2(\xi)d\xi - \sqrt{\varepsilon}|W(T)|^2 \le 0.$$

Similarly, one proves that $J_\ell \ge 0$ which concludes the proof of the proposition. $\qquad\square$

3.1.2 Exact boundary conditions for the linearized Boussinesq equation

We can obtain alternative transparent boundary conditions. Indeed, the system (3.2) is equivalent to the linearized Boussinesq equation:

$$(w-\varepsilon w_{xx})_{tt} - w_{xx} = 0, \quad \forall x \in \mathbb{R}, \forall t > 0. \qquad (3.10)$$

We consider the initial value problem set on the whole space

$$(w-\varepsilon w_{xx})_{tt} - w_{xx} = 0, \quad \forall x \in \mathbb{R}, \forall t > 0$$
$$w(0,x) = w_0(x), \quad w_t(0,x) = v_0(x), \quad \forall x \in \mathbb{R}$$
$$\lim_{x\to\infty} w(t,x) = \lim_{x\to-\infty} w(t,x) = 0,$$

where the initial data w_0, v_0 are compactly supported in $[x_\ell, x_r]$. The problem set on the complement of the interval $[x_\ell, x_r] \subset \mathbb{R}$ reads as:

$$(\tilde{w} - \varepsilon \tilde{w}_{xx})_{tt} - \tilde{w}_{xx} = 0, \quad \forall x \in \mathbb{R}, \forall t > 0,$$

$$\tilde{w}(0, x) = 0, \quad \tilde{w}_t(0, x) = 0, \quad \forall x \in \mathbb{R} \setminus [x_\ell, x_r],$$

$$\tilde{w}(t, x_\ell) = w(t, x_\ell), \quad \tilde{w}(t, x_r) = w(t, x_r), \quad \forall t > 0,$$

$$\tilde{w}_x(t, x_\ell) = w_x(t, x_\ell), \quad \tilde{w}_x(t, x_r) = w_x(t, x_r), \quad \forall t > 0,$$

$$\lim_{x \to \infty} \tilde{w}(t, x) = \lim_{x \to -\infty} \tilde{w}(t, x) = 0.$$

By applying the Laplace transform, one finds:

$$s^2 \Big(\mathcal{L}(w)(s, x) - \varepsilon \mathcal{L}(w)_{xx}(s, x) \Big) - \mathcal{L}(w)_{xx}(s, x) = 0.$$

We are searching again for the solution decaying at infinity: this gives us one condition on the left boundary and one on the right one for the function $\mathcal{L}(w)$:

$$\mathcal{L}(w_x)(s, x_r) = -\frac{s}{\sqrt[+]{1 + \varepsilon s^2}} \mathcal{L}(w)(s, x_r), \quad \mathcal{L}(w_x)(s, x_\ell) = \frac{s}{\sqrt[+]{1 + \varepsilon s^2}} \mathcal{L}(w)(s, x_\ell).$$

The inversion of the Laplace transform can be found explicitly and finally we get

$$
w_x(t, x_r) = \frac{1}{\varepsilon} \int_0^t \mathcal{J}_1 \left(\frac{s}{\sqrt{\varepsilon}} \right) w(t - s, x_r) ds - \frac{1}{\sqrt{\varepsilon}} w(t, x_r),
$$
$$
w_x(t, x_\ell) = -\frac{1}{\varepsilon} \int_0^t \mathcal{J}_1 \left(\frac{s}{\sqrt{\varepsilon}} \right) w(t - s, x_\ell) ds + \frac{1}{\sqrt{\varepsilon}} w(t, x_\ell),
$$
(3.11)

with $\mathcal{J}_n(t) = \frac{1}{\pi} \int_0^\pi \cos(n\tau - x \sin(\tau)) d\tau$. An alternative formulation of these boundary conditions is given by

$$
\left(1 + \varepsilon \frac{\partial^2}{\partial t^2} \right) w_x(t, x_r) = -\int_0^t \frac{\mathcal{J}_2 + \mathcal{J}_0}{2\sqrt{\varepsilon}} \left(\frac{t - s}{\sqrt{\varepsilon}} \right) w_t(s, x_r) ds - \sqrt{\varepsilon} w_{tt}(t, x_r),
$$
$$
\left(1 + \varepsilon \frac{\partial^2}{\partial t^2} \right) w_x(t, x_\ell) = \int_0^t \frac{\mathcal{J}_2 + \mathcal{J}_0}{2\sqrt{\varepsilon}} \left(\frac{t - s}{\sqrt{\varepsilon}} \right) w_t(s, x_\ell) ds + \sqrt{\varepsilon} w_{tt}(t, x_\ell).
$$
(3.12)

For these boundary conditions, the absorbing property is fulfilled as well:

3.1.2 Proposition. *Any smooth solution of the problem*

$$(w - \varepsilon w_{xx})_{tt} - w_{xx} = 0, \quad \forall x \in [x_l, x_r], \forall t > 0$$

$$w(0, x) = w_0(x), \quad w_t(0, x) = v_0(x), \quad \forall x \in]x_\ell, x_r[$$

$$
\left(1 + \varepsilon \frac{\partial^2}{\partial t^2} \right) w_x(t, x_r) = -\int_0^t \frac{\mathcal{J}_2 + \mathcal{J}_0}{2\sqrt{\varepsilon}} \left(\frac{t - s}{\sqrt{\varepsilon}} \right) w_t(s, x_r) ds - \sqrt{\varepsilon} w_{tt}(t, x_r),
$$
(3.13)
$$
\left(1 + \varepsilon \frac{\partial^2}{\partial t^2} \right) w_x(t, x_\ell) = \int_0^t \frac{\mathcal{J}_2 + \mathcal{J}_0}{2\sqrt{\varepsilon}} \left(\frac{t - s}{\sqrt{\varepsilon}} \right) w_t(s, x_\ell) ds + \sqrt{\varepsilon} w_{tt}(t, x_\ell),
$$

satisfies for all $t > 0$ the following estimate:

$$\int_{x_\ell}^{x_r} \left((w_t)^2 + (w_x)^2 + \varepsilon \ (w_{tx})^2 \right) (t,x) dx \le \int_{x_\ell}^{x_r} \left(v_0^2 + (w_{0,x})^2 + \varepsilon \ (v_{0,x})^2 \right) dx.$$

Proof. The proof is carried out in the same manner as Proposition 3.1.1. The time-derivative of the generalized kinetic energy in this case reads

$$\frac{d}{dt} \int_{x_l}^{x_r} \left(\frac{(w_t)^2}{2} + \frac{(w_x)^2}{2} + \varepsilon \frac{(w_{tx})^2}{2} \right) (t,x) dx = \left[w_t(t,x) \Big(\varepsilon w_{xtt}(t,x) + w_x(t,x) \Big) \right]_{x_l}^{x_r},$$

where the brackets denote a jump of the function. Integrating over the time interval $(0,t)$ yields:

$$\int_{x_l}^{x_r} \left(\frac{(w_t)^2}{2} + \frac{(w_x)^2}{2} + \varepsilon \frac{(w_{tx})^2}{2} \right) (t,x) dx - \int_{x_l}^{x_r} \left(\frac{(v_0)^2}{2} + \frac{(w_{0,x})^2}{2} + \varepsilon \frac{(v_{0,x})^2}{2} \right) dx$$
$$= \int_0^t \Big(w_t(\varepsilon w_{xtt} + w_x) \Big)(s,x_r) ds - \int_0^t \Big(w_t(\varepsilon w_{xtt} + w_x) \Big)(s,x_l) ds =: J_r - J_l.$$

If $J_r \le 0$, $J_l \ge 0$ then the inequality is satisfied. Let us first consider J_r using the boundary condition

$$J_r = \int_0^t w_t(s,x_r)(\varepsilon w_{xtt} + w_x)(s,x_r) ds$$
$$= -\int_0^t w_t(s,x_r) \left(\frac{\mathcal{J}_2 + \mathcal{J}_0}{2\sqrt{\varepsilon}}(\frac{\cdot}{\sqrt{\varepsilon}}) * w_t(s,x_r) + \sqrt{\varepsilon} w_{tt}(s,x_r) \right) ds.$$

Next, we fix $T > 0$ and denote $W(t) = w_t(t,x_r) \cdot 1_{[0,T]}(t)$. Then, one has

$$w_{tt} = W_t + W(T) \delta_{t=T}.$$

We can then write J_r as

$$J_r = -\int_0^\infty W(s) \left(\frac{\mathcal{J}_2 + \mathcal{J}_0}{2\sqrt{\varepsilon}}(\frac{\cdot}{\sqrt{\varepsilon}}) * W(s) + \sqrt{\varepsilon} W_t(s) \right) ds - \sqrt{\varepsilon} W(T)^2$$
$$= -\frac{1}{2\pi} \int_{\mathbb{R}} \Re \sqrt[4]{1 - \varepsilon\xi^2} |\widehat{W}|^2(\xi) d\xi - \sqrt{\varepsilon} |W(T)|^2 \le 0.$$

The estimate of J_ℓ is carried out similarly which concludes the proof of the proposition.   □

The discretization of the conditions (3.6) or the conditions (3.11) is not a trivial task. In the next section, we show how to obtain a consistent discretization of the boundary conditions which is compatible with the discrete numerical scheme used to carry out the simulation of the model (3.2). The proofs of consistency with the continuous conditions are carried out in the sections 3.2, 3.3.

3.2   Discrete transparent boundary conditions: Staggered grid

In this section we derive discrete artificial boundary conditions for the linearized Green-Naghdi system (3.2). In order to construct these conditions, we follow the strategy of

[17] and [18] and consider directly the problem on the fully discretized equations. In this section, we focus on a spatial discretization on a staggered grid and a Crank-Nicolson time discretization. A staggered grid is a setting for the spatial discretization, in which the unknowns are evaluated at the different space positions, i.e. $w_j^n \approx w(n\delta t, x_\ell + j\delta x)$, $\eta_{j+1/2}^n \approx \eta(n\delta t, x_\ell + (j+1/2)\delta x)$. The numerical scheme is written as:

$$\frac{\eta_{j+1/2}^{n+1} - \eta_{j+1/2}^n}{\delta t} + \frac{1}{2}\left(\frac{w_{j+1}^{n+1} - w_j^{n+1}}{\delta x} + \frac{w_{j+1}^n - w_j^n}{\delta x}\right) = 0,$$

$$\frac{w_j^{n+1} - w_j^n}{\delta t} - \frac{\varepsilon}{\delta t}\left(\frac{w_{j+1}^{n+1} - 2w_j^{n+1} + w_{j-1}^{n+1}}{\delta x^2} - \frac{w_{j+1}^n - 2w_j^n + w_{j-1}^n}{\delta x^2}\right)$$

$$+ \frac{1}{2}\left(\frac{\eta_{j+1/2}^{n+1} - \eta_{j-1/2}^{n+1}}{\delta x} + \frac{\eta_{j+1/2}^n - \eta_{j-1/2}^n}{\delta x}\right) = 0, \quad j \in \mathbb{Z}, \quad n \in \mathbb{N} \tag{3.14}$$

where $\delta t > 0$, $\delta x > 0$ are time and space steps. The procedure mimics what was done for the continuous case in the previous section. We assume $(w_j^0)_{j\in\mathbb{Z}}$ is compactly supported in $[1, J]$ and $\eta_{j+1/2}^0$ is compactly supported in $[1 + 1/2, J + 1/2]$ with $J \in \mathbb{N}$ such that $x_r - x_\ell = (J+1)\delta x$. We consider a solution $\tilde{\eta}_{j+1/2}^n, \tilde{w}_j^n$ of (3.14) for all $j \geq J + 1$ and $j \leq 0$ with the transmission conditions

$$\tilde{w}_{J+1}^n = w_{J+1}^n, \quad \tilde{w}_0^n = w_0^n, \quad \tilde{\eta}_{J+1/2}^n = \eta_{J+1/2}^n, \quad \tilde{\eta}_{1/2}^n = \eta_{1/2}^n.$$

and the initial conditions $\tilde{\eta}_{j+1/2}^0 = 0$, $\tilde{w}_j^0 = 0$, $\forall j \in \mathbb{Z} \setminus [1, J]$. The index $j = 0$ stands for the point $x = x_\ell$ and $j = J + 1$ stands for $x = x_r$. We first apply a discrete analogue of the Laplace transform which is referred to as $\mathcal{Z}-$transform [68]. The definition reads as follows:

$$\hat{u}(z) = \mathcal{Z}\{(u)_n\}(z) = \sum_{n\geq 0} u_n z^{-n}, \quad |z| > R > 0,$$

z is the complex variable and R is the radius of convergence of the Laurent series. Hereafter the hat will denote the result of the $\mathcal{Z}-$transform of the discrete sequences $\tilde{\eta}_{j+1/2}^n, \tilde{w}_j^n$ with respect to the time index n. The discrete system (3.14) reduces to the linear difference equation:

$$\hat{\eta}_{j+1/2} = -\frac{1}{s(z)\delta x}(\hat{w}_{j+1} - \hat{w}_j),$$

$$-\frac{\varepsilon s(z)}{\delta x^2}\hat{w}_{j-1} + s(z)\left(1 + \frac{2\varepsilon}{\delta x^2}\right)\hat{w}_j - \frac{\varepsilon s(z)}{\delta x^2}\hat{w}_{j+1} + \frac{\hat{\eta}_{j+1/2} - \hat{\eta}_{j-1/2}}{\delta x} = 0, \quad \forall j \in \mathbb{Z} \setminus [1, J] \tag{3.15}$$

where

$$s(z) = \frac{2}{\delta t}\frac{z-1}{z+1} \tag{3.16}$$

is the generator function of the Crank-Nicolson scheme. As the function $z \mapsto s(z)$ has a singularity at $z = -1$, we assume $|z| > 1$, which in turn yields $\Re(s(z)) > 0$. We can eliminate $\hat{\eta}_{j+1/2}$ from the system (3.15) so as to obtain a scalar difference equation:

$$(1+\varepsilon s^2(z))\hat{w}_{j-1} - 2\left(1 + s^2(z)\left(\varepsilon + \frac{\delta x^2}{2}\right)\right)\hat{w}_j + \left(1+\varepsilon s^2(z)\right)\hat{w}_{j+1} = 0, \quad j \in \mathbb{Z}\setminus[1, J], n \in \mathbb{N}. \tag{3.17}$$

The characteristic polynomial P associated to (3.17) is given by

$$P(r) = \left(1 + \varepsilon s^2(z)\right)r^2 - 2\left(1 + s^2(z)\left(\varepsilon + \frac{\delta x^2}{2}\right)\right)r + \left(1 + \varepsilon s^2(z)\right).$$

The roots of P are written as

$$r_\pm(z) = 1 + \frac{s^2(z)\delta x^2}{2(1 + \varepsilon s^2(z))} \pm \frac{s(z)\delta x\sqrt{\delta x^2 + 4(1 + \varepsilon s^2(z))}}{2(1 + \varepsilon s^2(z))}. \tag{3.18}$$

We show now an important separation property of $r_\pm(z)$.

3.2.1 Proposition. *The roots of the characteristic polynomial P associated with the linear difference equation* (3.17) *have the following separation property: for all $z \in \mathbb{C}$ such that $|z| > 1$, one has*

$$|r_+(z)| > 1, \quad |r_-(z)| < 1.$$

Proof. We follow the idea found in [155]. First let us show that there is no root on the unit circle. We assume that there is a root $r = e^{i\varphi}$ such that $P(r) = 0$. This equation reads

$$\left(1 + \varepsilon s^2(z)\right)e^{2i\varphi} - 2\left(1 + s^2(z)\left(\varepsilon + \frac{\delta x^2}{2}\right)\right)e^{i\varphi} + \left(1 + \varepsilon s^2(z)\right) = 0$$

and one deduces that

$$s^2(z) = -\frac{4\sin^2(\varphi/2)}{2\varepsilon(1 - \cos(\varphi)) + \delta x^2} \in \mathbb{R}^-,$$

and therefore $\Re(s) = 0$, which is in contradiction with the assumption $|z| > 1$. Therefore, there is no root of P on the unit circle.

The product of the roots is equal to one due to relation between the coefficients of P and there are no roots with modulus one. Therefore there is necessarily one root with a modulus larger than one and the other one with modulus smaller than one. In the limit $|s(z)| \to \infty$ one has $|r_+(z)| > 1$ and $|r_-(z)| < 1$. By continuity of $z \mapsto |r_\pm(z)|$ on the domain $\{z \in \mathbb{C}, |z| > 1\}$, this remains true for all $|z| > 1$. This completes the proof of the proposition. $\qquad \square$

The construction of the boundary conditions is then carried out just as in the continuous case. First note that the solution to (3.17) reads

$$\widehat{w}_j = \alpha^r_+ r_+(z)^j + \alpha^r_- r_-(z)^j, \quad \forall j \geq J,$$
$$\widehat{w}_j = \alpha^\ell_+ r_+(z)^j + \alpha^\ell_- r_-(z)^j, \quad \forall j \leq 1.$$

We search for bounded solutions as x tends to $\pm\infty$. Using the separation property shown in Proposition 3.2.1, we conclude that that $\alpha^\ell_- = 0$, and $\alpha^r_+ = 0$. These conditions are equivalent to the boundary conditions:

$$\widehat{w}_1 = r_+(z)\widehat{w}_0, \quad \widehat{w}_{J+1} = r_-(z)\widehat{w}_J. \tag{3.19}$$

Here we have the conditions for the images in the $\mathcal{Z}-$domain. In order to apply the $\mathcal{Z}-$inverse transform, we present the conditions (3.19) in the following form (we have used the explicit formula (3.16) for $s(z)$):

$$
\begin{aligned}
\widehat{w}_1 &= \left(1 + \frac{2\delta x^2(z-1)^2}{\Lambda z^2 - 2\mu z + \Lambda} + \frac{2\delta x(z-1)\sqrt{\Gamma z^2 - 2\nu z + \Gamma}}{\Lambda z^2 - 2\mu z + \Lambda}\right)\widehat{w}_0, \\
\widehat{w}_{J+1} &= \left(1 + \frac{2\delta x^2(z-1)^2}{\Lambda z^2 - 2\mu z + \Lambda} - \frac{2\delta x(z-1)\sqrt{\Gamma z^2 - 2\nu z + \Gamma}}{\Lambda z^2 - 2\mu z + \Lambda}\right)\widehat{w}_J,
\end{aligned}
\tag{3.20}
$$

where $\Lambda = 4\varepsilon + \delta t^2$, $\mu = 4\varepsilon - \delta t^2$, $\Gamma = \Lambda + \delta t^2 \delta x^2/4$, $\nu = \mu - \delta t^2 \delta x^2/4$. The inversion of the constructed conditions can be done explicitly and it is a *key aspect* in using the scheme on a staggered grid. In the next section we will show that such inversion is not possible for the scheme with collocated grid, and another strategy for the inversion should be used.

We focus on the inversion of the left boundary condition, the treatment of the right one being similar. Let us first mention a useful result for the inversion of (3.20), namely

3.2.2 Lemma. [87]
$$
\mathcal{Z}^{-1}\left(\frac{z}{\sqrt{z^2 - 2\nu z + 1}}\right) = \sum_{n=0}^{\infty} \mathcal{P}_n(\nu)z^{-n},
$$

for all $|z| > max(z_1, z_2)$, where z_1, z_2 are the roots of $z^2 - 2\nu z + 1$ and $\mathcal{P}_n(\nu)$ is the $n-$th Legendre polynomial.

In order to use this result, we write

$$
\sqrt{\Gamma z^2 - 2\nu z + \Gamma} = \sqrt{\Gamma}(z - 2v + z^{-1})\frac{z}{\sqrt{z^2 - 2vz + 1}}, \quad v = \frac{\nu}{\Gamma}.
$$

By multiplying the left boundary condition by $\Lambda z^2 - 2\mu z + \Lambda$ and by using the inverse shift property of $\mathcal{Z}-$transform, one finds

$$
\Lambda w_1^{n+1} - (\Lambda + 2\delta x^2 + 2\delta x\sqrt{\Gamma})w_0^{n+1} = 2(\mu w_1^n - (\mu + 2\delta x^2 + \delta x\sqrt{\Gamma}(v+1))w_0^n) -
$$

$$
- (\Lambda w_1^{n-1} - (\Lambda + 2\delta x^2 + 2\delta x\sqrt{\Gamma})w_0^{n-1}) + 2\delta x\sqrt{\Gamma}\left((\mathcal{P}_2 - 2v^2 + v)w_0^{n-1} + \sum_{k=2}^{n} s_k w_0^{n-k}\right).
\tag{3.21}
$$

A similar calculation gives the boundary condition on the right:

$$
\Lambda w_{J+1}^{n+1} - (\Lambda + 2\delta x^2 - 2\delta x\sqrt{\Gamma})w_J^{n+1} = 2(\mu w_{J+1}^n - (\mu + 2\delta x^2 - \delta x\sqrt{\Gamma}(v+1))w_J^n) -
$$

$$
- (\Lambda w_{J+1}^{n-1} - (\Lambda + 2\delta x^2 - 2\delta x\sqrt{\Gamma})w_J^{n-1}) - 2\delta x\sqrt{\Gamma}\left((\mathcal{P}_2 - 2v^2 + v)w_J^{n-1} + \sum_{k=2}^{n} s_k(v)w_J^{n-k}\right),
\tag{3.22}
$$

where

$$
\forall k \in \mathbb{N}: \quad s_k(v) = \mathcal{P}_{k+1}(v) - (2v+1)\mathcal{P}_k(v) + (2v+1)\mathcal{P}_{k-1}(v) - \mathcal{P}_{k-2}(v),
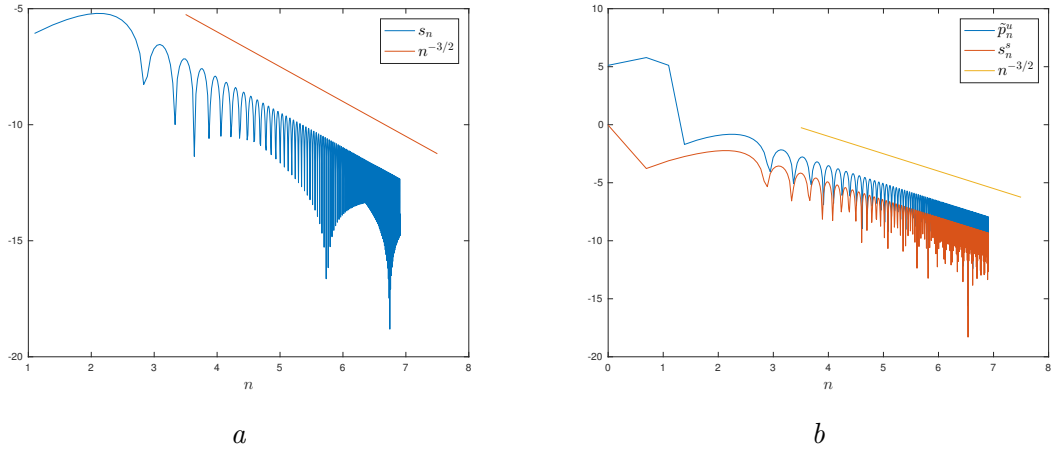$$

Figure 3.1: Coefficients of the discrete boundary conditions (3.21), (3.22) (a) and (3.35), (3.36) (b) with $\delta x = 2^{-10}$, $\delta t = 10^{-2}$, $\varepsilon = 10^{-3}$.

and $\mathcal{P}_{-1} = 0$, $\mathcal{P}_{-2} = 0$. Thus, the evaluation of n convolution coefficients requires $O(n)$ operations. In order to prove that the boundary conditions (3.21) and (3.22) are stable with respect to round off errors, we verify that the convolution coefficients $(s_n)_{n \in \mathbb{N}}$ decrease sufficiently fast. We found numerically (see Figure 3.1a) that they decrease as $O(n^{-3/2})$.

This conjecture can be proved rigorously. For that purpose, we recall that the Legendre polynomial satisfy the estimate $P_n(v) = O(n^{-1/2})$ for all $v \in]0, 1[$ (see [10] for more details) and the recurrence relation

$$(n + 1)P_{n+1}(v) = (2n + 1)v\,P_n(v) + n\,P_{n-1}(v), \qquad \forall n \in \mathbb{N} \backslash \{0\}.$$

Then, the coefficients $(s_n(v))_{n \in \mathbb{N}}$ have the alternative representation formula:

$$s_n(v) = \frac{P_{n-1}(v) - P_{n+1}(v)}{2n + 1} - \frac{P_{n-2}(v) - P_n(v)}{2n - 1}, \quad \forall n \geq 2.$$

From this relation, one finds $s_n(v) = O(n^{-3/2})$ as $n \to \infty$. This is exactly the decay rate found in convolution coefficients involved in the discrete transparent boundary conditions for the linear Schrödinger equation [10]. This estimate implies that the boundary conditions (3.21) and (3.22) are stable with respect to round off errors.

As a conclusion, the full scheme consists in boundary conditions (3.21) and (3.22) together with the interior scheme written as

$$- a_+ w_{j+1}^{n+1} + (1 + 2a_+)w_j^{n+1} - a_+ w_{j-1}^{n+1} = 2(-a_- w_{j+1}^n + (1 + 2a_-)w_j^n - a_- w_{j-1}^n)$$
$$- (-a_+ w_{j+1}^{n-1} + (1 + 2a_+)w_j^{n-1} - a_+ w_{j-1}^{n-1}), \quad 1 \leq j \leq J, n \in \mathbb{N}, \quad (3.23)$$

where

$$a_- = \frac{\varepsilon - \delta t^2/4}{\delta x^2}, \quad a_+ = \frac{\varepsilon + \delta t^2/4}{\delta x^2}.$$

The interior scheme (3.23) is second order accurate in time and in space. In what follows, we check the consistency of the boundary conditions (3.21) and (3.22).

3.2.1 Consistency and stability theorem

In order to provide a good approximation of the continuous solution of (3.10) by numerical solution of (3.23) with (3.21), (3.22), one should prove a consistency result. In what follows, we show that (3.21) and (3.22) are second order accurate in time and space.

3.2.3 Theorem. *Let w be a smooth solution of* (3.10) *which satisfies the transparent boundary conditions* (3.11). *We define the $\mathcal{Z}-$transform of $w(\cdot, x)$ for all $x \in [x_\ell, x_r]$ by*

$$\forall z \neq 0, \quad \widehat{w}(z, x) = \sum_{n=0}^{\infty} \frac{w(n\delta t, x)}{z^n}.$$

Then for all compact $K \subset \mathbb{C}^+ = \{z \in \mathbb{C}, \Re(z) > 0\}$, for all $s \in K$, we have

$$\hat{w}(e^{s\delta t}, x_\ell + \delta x) - r_+(e^{s\delta t})\hat{w}(e^{s\delta t}, x_\ell) = O(\delta t^2 + \delta x^2),$$

$$\hat{w}(e^{s\delta t}, x_r) - r_-(e^{s\delta t})\hat{w}(e^{s\delta t}, x_r - \delta x) = O(\delta t^2 + \delta x^2),$$

where $r_\pm(z)$ are defined by (3.18).

Proof. First of all, let us note that the $\mathcal{Z}-$transform, defined above, is an approximation of the Laplace transform. More precisely, for all smooth functions $f(0) = f'(0) = \cdots = f^{(k)}(0) = 0$ ($k \in \mathbb{N}$), and all $s \in \mathbb{C}^+$, we have:

$$\mathcal{L}(f)(s) = \delta t \hat{f}(e^{s\delta t}) + O(\delta t^{k+2}), \tag{3.24}$$

where s is a parameter of the Laplace transform. See [18] for a proof of this result. Recalling the definition of the roots (3.18), we have

$$\widehat{w}(z, x_\ell + \delta x) - r_+(z)\widehat{w}(z, x_\ell) =$$

$$\widehat{w}(z, x_\ell + \delta x) - \left(1 + \frac{s^2(z)\delta x^2}{2(1 + \varepsilon s^2(z))} + \frac{s(z)\delta x \sqrt{\delta x^2 + 4(1 + \varepsilon s^2(z))}}{2(1 + \varepsilon s^2(z))}\right)\widehat{w}(z, x_\ell) =$$

$$\widehat{w}(z, x_\ell + \delta x) - \widehat{w}(z, x_\ell) - \frac{s^2(z)\delta x^2}{2(1 + \varepsilon s^2(z))}\widehat{w}(z, x_\ell) - \frac{s(z)\delta x}{\sqrt{1 + \varepsilon s^2(z)}}\sqrt{1 + \frac{\delta x^2}{4(1 + \varepsilon s^2(z))}}\widehat{w}(z, x_\ell).$$

Note that the function $s(z)$ defined in (3.16) with $z = e^{s\delta t}$ is approximated as

$$s(z) = s + O(\delta t^2).$$

We then find

$$\widehat{w}(z, x_\ell + \delta x) - r_+(z)\widehat{w}(z, x_\ell) =$$
$$\delta x \left(\partial_x \widehat{w}(e^{s\delta t}, x_\ell) + \frac{\delta x}{2}\partial_{xx}\widehat{w}(e^{s\delta t}, x_\ell) - \frac{s^2\delta x}{2(1 + \varepsilon s^2)}\widehat{w}(e^{s\delta t}, x_\ell) - \frac{s}{\sqrt{1 + \varepsilon s^2}}\widehat{w}(e^{s\delta t}, x_\ell)\right)$$

$$+ O(\delta x^2 + \delta x \delta t^2) = \frac{\delta x}{\delta t}\left(\delta t\left(\partial_x\widehat{w}(e^{s\delta t}, x_\ell) - \frac{s}{\sqrt{1 + \varepsilon s^2}}\widehat{w}(e^{s\delta t}, x_\ell)\right)\right.$$

$$\left. + \delta t\frac{\delta x}{2}\left(\partial_{xx}\widehat{w}(e^{s\delta t}, x_\ell) - \frac{s^2}{1 + \varepsilon s^2}\widehat{w}(e^{s\delta t}, x_\ell)\right)\right) + O(\delta x^2 + \delta x \delta t^2).$$

By applying the relation (3.24) to the last line, we find that the first expression between the parentheses is the Laplace transform of the continuous boundary condition on the left and the second one is the Laplace transform of (3.10):

$$\widehat{w}(z, x_\ell + \delta x) - r_+(z)\widehat{w}(z, x_\ell) =$$

$$\delta x \left(\partial_x \mathcal{L}(w) - \frac{s}{\sqrt{1 + \varepsilon s^2}} \mathcal{L}(w) \right) + \frac{\delta x^2}{2} \left(\partial_{xx} \mathcal{L}(w) - \frac{s^2}{1 + \varepsilon s^2} \mathcal{L}(w) \right) + O(\delta x^2 + \delta t^2)$$

$$= O(\delta x^2 + \delta t^2).$$

This completes the proof of consistency for the boundary on the left, the proof being similar for the boundary on the right. □

Let us now prove a stability result on boundary conditions (3.21) and (3.22) similar to the stability property 3.1.2. For that purpose, we introduce the following notations: for any sequence (w_j^n), we set

$$D_x^+(w)_j^n = \frac{w_{j+1}^n - w_j^n}{\delta x}, \quad D_x^-(w)_j^n = \frac{w_j^n - w_{j-1}^n}{\delta x}$$

$$D_t^+(w)_j^n = \frac{w_j^{n+1} - w_j^n}{\delta t}, \quad D_t^-(w)_j^n = \frac{w_j^n - w_j^{n-1}}{\delta t},$$

The numerical scheme associated to (3.14) can then be written as a discretization of the linearized Boussinesq equation (3.10)

$$D_t^+ \left(D_t^- \left(w - \varepsilon D_x^+(D_x^-(w)) \right) \right)_j^n = D_x^- \left(D_x^+(w) \right)_j^n, \quad \forall j \in [1, J], \quad \forall n \geq 0. \tag{3.25}$$

Let us introduce the following discretization of the continuous energy

$$\mathcal{E}(t) = \frac{1}{2} \int_{x_\ell}^{x_r} \left((w_t)^2 + (w_{tx}^2 + (w_x)^2) \right)(t, x)dx,$$

with w as smooth solution of (3.10):

$$E^n = \frac{\delta x}{4} \left(\frac{w_0^n - w_0^{n-1}}{\delta t} \right)^2 + \frac{\delta x}{4} \left(\frac{w_{J+1}^n - w_{J+1}^{n-1}}{\delta t} \right)^2 + \frac{\delta x}{2} \sum_{j=1}^{J} \left(\frac{w_j^n - w_j^{n-1}}{\delta t} \right)^2$$

$$+ \frac{\delta x}{2} \sum_{j=0}^{J} \left(D_x^+(\frac{w^n + w^{n-1}}{2})_j \right)^2 + \left(\frac{D_x^+(w)_j^n - D_x^+(w)_j^{n-1}}{\delta t} \right)^2.$$

We prove the following proposition

3.2.4 Proposition. *Assume $(w_j^n)_{j \in [0, J+1], n \in \mathbb{N}}$ is a solution of (3.25) with boundary conditions (3.21) and (3.22). Then one has $E^N \leq E^1$ for all $N \in \mathbb{N}\backslash\{0\}$.*

In order to prove this proposition, we state the following result on a discrete analogue of integration by parts, called "summation by parts"

3.2.5 Lemma. *For all sequences* $(v_j)_{j \in [1,J+1]}, (w_j)_{j \in [1,J+1]}$, *one has*

$$\sum_{j=1}^{J} \delta x\, v_j D_x^{-} \left(D_x^{+}(w) \right)_j = - \sum_{j=0}^{J} \delta x\, D_x^{+}(v)_j\, D_x^{+}(w)_j + v_{J+1} D_x^{-}(w)_{J+1} - v_0 D_x^{+}(w)_0.$$

Proof. We follow the strategy in the proof of Proposition 3.1.2: we multiply equations (3.25) by $\dfrac{w_j^{n+1} - w_j^{n-1}}{2\delta t}$ for all $j = 1, \ldots, J$, sum over all $j = 1, \ldots, J$ and perform a discrete integration by parts. One finds

$$\frac{\tilde{E}^{n+1} - \tilde{E}^n}{\delta t} = \tag{3.26}$$

$$\frac{w_{J+1}^{n+1} - w_{J+1}^{n-1}}{2\delta t} \left\{ \varepsilon D_x^{-} \left(\frac{w^{n+1} - 2w^n + w^{n-1}}{\delta t^2} \right)_{J+1} + D_x^{-} \left(\frac{w^{n+1} + 2w^n + w^{n-1}}{4} \right)_{J+1} \right\}$$

$$- \frac{w_0^{n+1} - w_0^{n-1}}{2\delta t} \left\{ \varepsilon D_x^{+} \left(\frac{w^{n+1} - 2w^n + w^{n-1}}{\delta t^2} \right)_0 + D_x^{+} \left(\frac{w^{n+1} + 2w^n + w^{n-1}}{4} \right)_0 \right\},$$

with

$$\tilde{E}^n = \frac{\delta x}{2} \sum_{j=1}^{J} \left(\frac{w_j^n - w_j^{n-1}}{\delta t} \right)^2 + \frac{\delta x}{2} \sum_{j=0}^{J} \left(D_x^{+}(\frac{w^n + w^{n-1}}{2})_j \right)^2 + \left(\frac{D_x^{+}(w)_j^n - D_x^{+}(w)_j^{n-1}}{\delta t} \right)^2.$$

Next, we rewrite the boundary conditions (3.21) and (3.22) in a suitable form just as we did in the continuous case. Recall that these boundary conditions can be written as

$$\widehat{w}_J(z) = r_+(z)\widehat{w}_{J+1}(z), \qquad \widehat{w}_1(z) = r_+(z)\widehat{w}_0(z)$$

which are equivalent to

$$\left(\frac{(z+1)^2}{4} + \varepsilon \frac{(z-1)^2}{\delta t^2} \right) D_x^{-}(\widehat{w})_{J+1} = -\frac{\delta x}{2} \frac{(z-1)^2}{\delta t^2} \widehat{w}_{J+1} - \alpha \sqrt{z^2 - 2\beta z + 1} \frac{z-1}{\delta t} \widehat{w}_{J+1},$$

$$\left(\frac{(z+1)^2}{4} + \varepsilon \frac{(z-1)^2}{\delta t^2} \right) D_x^{+}(\widehat{w})_0 = \frac{\delta x}{2} \frac{(z-1)^2}{\delta t^2} \widehat{w}_0 + \alpha \sqrt{z^2 - 2\beta z + 1} \frac{z-1}{\delta t} \widehat{w}_0,$$

with

$$\alpha = \sqrt{\frac{1}{4} + \frac{\varepsilon}{\delta t^2} + \frac{\delta x^2}{4\delta t^2}} \quad \text{and} \quad \beta = \frac{4\varepsilon + \delta x^2 - \delta t^2}{4\varepsilon + \delta x^2 + \delta t^2} \in]-1, 1[.$$

These boundary conditions can be written alternatively as

$$\varepsilon D_x^{-} \left(\frac{w^{n+1} - 2w^n + w^{n-1}}{\delta t^2} \right)_{J+1} + D_x^{-} \left(\frac{w^{n+1} + 2w^n + w^{n-1}}{4} \right)_{J+1} =$$

$$- \frac{\delta x}{2} \frac{w_{J+1}^{n+1} - 2w_{J+1}^n + w_{J+1}^{n-1}}{\delta t^2} - \alpha \left\{ \frac{w_{J+1}^{n+1} - w_{J+1}^n}{\delta t} + \sum_{m=0}^{n} t_{n-m}(\beta) \quad D_t^{-}(w)_{J+1}^m \right\}$$

$$\varepsilon D_x^{+} \left(\frac{w^{n+1} - 2w^n + w^{n-1}}{\delta t^2} \right)_0 + D_x^{+} \left(\frac{w^{n+1} + 2w^n + w^{n-1}}{4} \right)_0 = \frac{\delta x}{2} \frac{w_0^{n+1} - 2w_0^n + w_0^{n-1}}{\delta t^2}$$

$$+ \alpha \left\{ \frac{w_0^{n+1} - w_0^n}{\delta t} + \sum_{m=0}^{n} t_{n-m}(\beta) D_t^{-}(w)_0^m \right\},$$

where $t_n(\beta)$ are defined as $t_n(\beta) = P_{n+1}(\beta) - 2\beta P_n(\beta) + P_{n-1}(\beta)$ with P_n denotes the n-th Legendre polynomial and $P_{-1} = 0$. By plugging these boundary conditions into the energy estimate (3.26), one finds

$$\frac{E^{n+1} - E^n}{\delta t} = -\alpha \frac{w_{J+1}^{n+1} - w_{J+1}^{n-1}}{2\delta t} \left\{ \frac{w_{J+1}^{n+1} - w_{J+1}^n}{\delta t} + \sum_{m=0}^{n} t_{n-m}(\beta) D_t^-(w)_{J+1}^m \right\}$$

$$-\alpha \frac{w_0^{n+1} - w_0^{n-1}}{2\delta t} \left\{ \frac{w_0^{n+1} - w_0^n}{\delta t} + \sum_{m=0}^{n} t_{n-m}(\beta) D_t^-(w)_0^m \right\}.$$

We sum this equation for all $n = 1, \ldots, N - 1$ and extend the sequences $(w_0^n)_{n \in \mathbb{N}}$ and $(w_{J+1}^n)_{n \in \mathbb{N}}$ by setting $w_0^{N+2n+1} = w_0^{N-1}$ and $w_0^{N+2n} = w_0^N$ for all $n \in \mathbb{N}$, the extension being the same for w_{J+1}^n . One finds

$$E^N - E^1 = -\alpha \delta t \sum_{n=1}^{\infty} \frac{w_{J+1}^{n+1} - w_{J+1}^{n-1}}{2\delta t} \left\{ \frac{w_{J+1}^{n+1} - w_{J+1}^n}{\delta t} + \sum_{m=0}^{n} t_{n-m}(\beta) D_t^-(w)_{J+1}^m \right\}$$

$$-\alpha \delta t \sum_{n=1}^{\infty} \frac{w_0^{n+1} - w_0^{n-1}}{2\delta t} \left\{ \frac{w_0^{n+1} - w_0^n}{\delta t} + \sum_{m=0}^{n} t_{n-m}(\beta) D_t^-(w)_0^m \right\}.$$

Then, by introducing the sequences $D_t^0 w_k^n = \dfrac{w_k^{n+1} - w_k^{n-1}}{2\delta t}$ with $k = 0, J + 1$ and by using the Plancherel formula, one obtains

$$E^N - E^1 = -\frac{\delta t}{2\pi} \int_{-\pi}^{\pi} \Re \sqrt{1 + (\varepsilon + \frac{\delta x^2}{4}) s^2(e^{i\theta})} \left(\left| \widehat{D_t^0(w)}_{J+1}(e^{i\theta}) \right|^2 + \left| \widehat{D_t^0(w)}_0(e^{i\theta}) \right|^2 \right) d\theta,$$

$$-\frac{\delta t}{2\pi} \int_{-\pi}^{\pi} \Re \sqrt{1 - \frac{4}{\delta t^2}(\varepsilon + \frac{\delta x^2}{4}) \tan^2\left(\frac{\theta}{2}\right)} \left(\left| \widehat{D_t^0(w)}_{J+1}(e^{i\theta}) \right|^2 + \left| \widehat{D_t^0(w)}_0(e^{i\theta}) \right|^2 \right) d\theta.$$

We deduce from this formula that $E^N \leq E^1$ for all $N \geq 1$ and the proof of the proposition is complete. $\qquad\square$

3.3 Discrete transparent boundary conditions: Collocated grid

In this section, we consider transparent boundary conditions associated to a spatial discretization of (3.2) on collocated grids (functions η, w are evaluated at the same points) . We keep a Crank-Nicolson time discretization, i.e. the numerical scheme reads as follows:

$$\frac{\eta_j^{n+1} - \eta_j^n}{\delta t} \quad + \quad \frac{1}{2}\left(\frac{w_{j+1}^{n+1} - w_{j-1}^{n+1}}{2\delta x} + \frac{w_{j+1}^n - w_{j-1}^n}{2\delta x} \right) = 0,$$

$$\frac{w_j^{n+1} - w_j^n}{\delta t} \quad - \quad \varepsilon \left(\frac{w_{j+1}^{n+1} - 2w_j^{n+1} + w_{j-1}^{n+1}}{\delta x^2} - \frac{w_{j+1}^n - 2w_j^n + w_{j-1}^n}{\delta x^2} \right) \qquad (3.27)$$

$$+ \quad \frac{1}{2}\left(\frac{\eta_{j+1}^{n+1} - \eta_{j-1}^{n+1}}{2\delta x} + \frac{\eta_{j+1}^n - \eta_{j-1}^n}{2\delta x} \right) = 0,$$

for all $1 \leq j \leq J$ and $n \in \mathbb{N}$. By applying the $\mathcal{Z}$−transform, the system (3.27) reduces to the second order linear difference equations ($|z| > 1$):

$$\widehat{w}_{j+1} = \widehat{w}_{j-1} - s(z)\widehat{\eta}_j,$$

$$\widehat{\eta}_{j+1} = \widehat{\eta}_{j-1} + \frac{\varepsilon\, s(z)}{\delta x^2}\widehat{w}_{j+1} - s(z)(1 + \frac{2\varepsilon}{\delta x^2})\widehat{w}_j + \frac{\varepsilon\, s(z)}{\delta x^2}\widehat{w}_{j-1}, \qquad s(z) = \frac{2}{\delta t}\frac{z-1}{z+1}. \qquad (3.28)$$

We search for a basis of solutions of this system of difference equations. We first write (3.28) as a first order system

$$\begin{pmatrix} \widehat{w}_{j+1} \\ \widehat{\eta}_{j+1} \\ \widehat{t}_{j+1} \\ \widehat{r}_{j+1} \end{pmatrix} = \begin{pmatrix} 0 & -2\delta x s(z) & 1 & 0 \\ -2\delta x s(z)(1 + 2\varepsilon/\delta x^2) & -4\varepsilon s^2(z) & 4\varepsilon s(z)/\delta x & 1 \\ 1 & 0 & 0 & 0 \\ 0 & 1 & 0 & 0 \end{pmatrix} \begin{pmatrix} \widehat{w}_j \\ \widehat{\eta}_j \\ \widehat{t}_j \\ \widehat{v}_j \end{pmatrix} := A(z) \begin{pmatrix} \widehat{w}_j \\ \widehat{\eta}_j \\ \widehat{t}_j \\ \widehat{v}_j \end{pmatrix},$$

where we have set $\widehat{t}_j = \widehat{w}_{j-1}$, $\widehat{v}_j = \widehat{\eta}_{j-1}$. The solutions of this system of difference equations have the form

$$\left(\widehat{w}_j, \widehat{\eta}_j, \widehat{t}_j, \widehat{v}_j\right)^\top = \sum_{k=1}^4 \alpha_k^r r_k^j V_k, \quad \forall j \geq J+1, \quad \left(\widehat{w}_j, \widehat{\eta}_j, \widehat{t}_j, \widehat{v}_j\right)^\top = \sum_{k=1}^4 \alpha_k^\ell r_k^j V_k, \quad \forall j \leq 0,$$

where r_k, $k = 1, 2, 3, 4$ are the roots of the characteristic polynomial P associated to the matrix $A(z)$

$$P(r) = r^4 + 4\varepsilon s^2(z)r^3 - \left(2 + 4s^2(z)(\delta x^2 + 2\varepsilon)\right) r^2 + 4\varepsilon s^2(z)r + 1, \qquad (3.29)$$

whereas V_k are the corresponding eigenvectors, and $\alpha_k^{r,\ell}$ are constant coefficients. The expressions for the roots of $P(r)$ are explicit but useless when we will have to carry out the inversion of the $\mathcal{Z}$−transform. We also do not need it to prove the following separation property.

3.3.1 Proposition. *The roots of the characteristic polynomial P given by (3.29) have the following separation property: for all $z \in \mathbb{C}$ such that $|z| > 1$, one has*

$$|r_1(z)| > 1, \quad |r_2(z)| > 1, \quad |r_3(z)| < 1, \quad |r_4(z)| < 1.$$

Here the roots are ordered as $|r_1(z)| \geq |r_2(z)| \geq |r_3(z)| \geq |r_4(z)|$.

Proof. First let us show that there is no root on the unit circle. Assume that there is a root $r = e^{i\varphi}$ of P, then the equation $P(r) = 0$ reads

$$s^2(z) = -\frac{\sin^2 \varphi}{\delta x^2 + 2\varepsilon(1 - \cos \varphi)} \in \mathbb{R}^-,$$

and thus $\Re(s(z)) = 0$ which is in contradiction with $|z| > 1$.

There remains to locate the four roots with respect to unit circle. We order the roots as follows $|r_i(z)| \geq |r_{i+1}(z)|$ with $i = 1, 2, 3$. First, note that the constant term of P is equal to 1 which means that $|r_1(z)r_2(z)r_3(z)r_4(z)| = 1$. Moreover, if r is a root of P so is r^{-1}. As a consequence we have necessarily $|r_1(z)| \geq |r_2(z)| > 1 > |r_3(z)| \geq |r_4(z)|$ and $r_3(z) = r_2(z)^{-1}$ and $r_4(z) = r_1(z)^{-1}$. $\qquad \square$

3.3.2 Remark. The characteristic equation $P(r) = 0$ can be written in the following form

$$(r - 1)^2 \left((r + 1)^2 + 4s^2(z)\varepsilon r\right) = 4s^2(z)r^2\delta x^2,$$

which can be rewritten as

$$(r - 1)^2 = \frac{4s^2(z)r^2\delta x^2}{(r + 1)^2 + 4s^2(z)\varepsilon r},$$

and so by applying the implicit function theorem, we can compute an expansion of the roots $r_{2,3}$ bifurcating form 1 at $\delta x = 0$:

$$r_2(z) = 1 + \frac{s(z)\delta x}{\sqrt{1 + \varepsilon s^2(z)}} + O(\delta x^2), \quad r_3(z) = 1 - \frac{s(z)\delta x}{\sqrt{1 + \varepsilon s^2(z)}} + O(\delta x^2).$$

A similar argument yields also an asymptotic expansion of $r_{1,4}$:

$$r_1 = -\left(1 + 2\varepsilon s^2(z)\right) - 2\sqrt{\varepsilon s^2(z)(1 + \varepsilon s^2(z))} + O(\delta x^2),$$
$$r_4 = -\left(1 + 2\varepsilon s^2(z)\right) + 2\sqrt{\varepsilon s^2(z)(1 + \varepsilon s^2(z))} + O(\delta x^2).$$

Thanks to the roots separation, we have a decomposition of the solutions space into a stable subspace $E^s(z) = \text{span}(V_3; V_4)$ of solutions decreasing to 0 as $j \to \infty$ and an unstable subspace $E^u(z) = \text{span}(V_1, V_2)$ of solutions decreasing to 0 as $j \to -\infty$. In order to obtain bounded solutions, one must impose

$$\left(\widehat{w}_{J+1}, \widehat{\eta}_{J+1}, \widehat{t}_{J+1}, \widehat{v}_{J+1}\right)^\top \in E^s(z), \quad \left(\widehat{w}_1, \widehat{\eta}_1, \widehat{t}_1, \widehat{v}_1\right)^\top \in E^u(z),$$

which is equivalent to

$$(\widehat{w}_{J+1}, \widehat{\eta}_{J+1}, \widehat{w}_J, \widehat{\eta}_J)^\top \in E^s(z), \quad (\widehat{w}_1, \widehat{\eta}_1, \widehat{w}_0, \widehat{\eta}_0)^\top \in E^u(z).$$

Let us start with the left boundary condition: the vector $(\widehat{w}_1, \widehat{\eta}_1, \widehat{w}_0, \widehat{\eta}_0)^\top$ is given by

$$\begin{pmatrix} \widehat{w}_0 \\ \widehat{\eta}_0 \\ \widehat{w}_1 \\ \widehat{\eta}_1 \end{pmatrix} = \begin{pmatrix} r_1 & r_2 & r_3 & r_4 \\ \dfrac{1 - r_1^2}{2\delta x s(z)} & \dfrac{1 - r_2^2}{2\delta x s(z)} & \dfrac{1 - r_3^2}{2\delta x s(z)} & \dfrac{1 - r_4^2}{2\delta x s(z)} \\ 1 & 1 & 1 & 1 \\ \dfrac{1 - r_1^2}{2\delta x r_1 s(z)} & \dfrac{1 - r_2^2}{2\delta x r_2 s(z)} & \dfrac{1 - r_3^2}{2\delta x r_3 s(z)} & \dfrac{1 - r_4^2}{2\delta x r_4 s(z)} \end{pmatrix} \begin{pmatrix} \alpha_1^\ell \\ \alpha_2^\ell \\ \alpha_3^\ell \\ \alpha_4^\ell \end{pmatrix}, \tag{3.30}$$

with $\alpha_3^\ell = \alpha_4^\ell = 0$. Then from (3.30) we have:

$$\widehat{\eta}_0 = \frac{1 - r_1^2}{2\delta x r_1 s(z)}\alpha_1^\ell + \frac{1 - r_2^2}{2\delta x r_2 s(z)}\alpha_2^\ell, \quad \widehat{\eta}_1 = \frac{1 - r_1^2}{2\delta x s(z)}\alpha_1^\ell + \frac{1 - r_2^2}{2\delta x s(z)}\alpha_2^\ell.$$

In order to determine α_1^ℓ, α_2^ℓ, we use the remaining two equations of (3.30). We set $r_1 + r_2 = S^u$ and $r_1 r_2 = P^u$: the left boundary conditions are given by

$$(1 + P^u)\widehat{w}_1 = S^u\widehat{w}_0 - 2\delta x P^u s(z)\widehat{\eta}_0,$$
$$2\delta x \, s(z)\widehat{\eta}_1 + S^u\widehat{w}_1 = (1 + P^u)\widehat{w}_0. \tag{3.31}$$

The derivation of the right boundary conditions are carried out with the same method. We set $r_3 + r_4 = S^s$ and $r_3 r_4 = P^s$. The right boundary conditions are given by:

$$
\begin{aligned}
(1 + P^s)\widehat{w}_{J+1} &= S^s \widehat{w}_J - 2\delta x\, P^s s(z)\widehat{\eta}_J, \\
2\delta x\, s(z)\widehat{\eta}_{J+1} + S^s \widehat{w}_{J+1} &= (1 + P^s)\widehat{w}_J.
\end{aligned}
\tag{3.32}
$$

The coefficients of the boundary conditions (3.31), (3.32) contain a singularity at $z = -1$, which in turn implies that the expansion coefficients for S^s, P^s, S^u, P^u decrease slowly. In order to remove this singularity, we multiply the boundary conditions (3.31), (3.32) by $(1 + z^{-1})^q$, where the power q depends on the order of a pole $z = -1$ of the coefficients. For example, as we have seen the unstable root r_1 has the following asymptotic behaviour $r_1 \sim s^2(z)$ (see Proposition 3.3.1). For stabilization, the coefficient $-2\delta x P^u s(z)$ needs to be multiplied by $(1 + z^{-1})^3$. The roots r_3, r_4 stay bounded as well as P^s and S^s and, therefore, we need to deal only with the singularity of $s(z)$, and $q = 1$. We thus consider the new unknowns $\tilde{P}^u = (1 + z^{-1})^2 P^u$ and $\tilde{S}^u = (1 + z^{-1})^2 S^u$. We set $z^{-1} = x$ and obtain the following boundary conditions with coefficients decreasing faster which ensures stability with respect to round off errors:

$$
\begin{aligned}
((1+x)^3 + (1+x)\tilde{P}^u)\widehat{w}_1 &= (1+x)\tilde{S}^u \widehat{w}_0 - \frac{4\delta x}{\delta t}(1-x)\tilde{P}^u \widehat{\eta}_0, \\
\frac{4\delta x}{\delta t}(1-x^2)\widehat{\eta}_1 + \tilde{S}^u \widehat{w}_1 &= ((1+x)^2 + \tilde{P}^u)\widehat{w}_0, \\
((1+x) + (1+x)P^s)\widehat{w}_{J+1} &= (1+x)S^s \widehat{w}_J - \frac{4\delta x}{\delta t}(1-x)P^s \widehat{\eta}_J, \\
\frac{4\delta x}{\delta t}(1-x)\widehat{\eta}_{J+1} + (1+x)S^s \widehat{w}_{J+1} &= ((1+x) + (1+x)P^s)\widehat{w}_J.
\end{aligned}
\tag{3.33}
$$

In order to invert the $\mathcal{Z}-$transform, it is required to find the coefficients in the expansions of S^s, P^s, $\tilde{S}^u$, $\tilde{P}^u$ which are defined as

$$
S^s(x) = \sum_{n\geq 0} s_n^s x^n, \quad P^s(x) = \sum_{n\geq 0} p_n^s x^n,
$$

$$
\tilde{S}^u(x) = (1+x)^2 S^u(x) = (1+x)^2 \sum_{n\geq 0} s_n^u x^n = \sum_{n\geq 0} \tilde{s}_n^u x^n,
$$

$$
\tilde{P}^u(x) = (1+x)^2 P^u(x) = (1+x)^2 \sum_{n\geq 0} p_n^u x^n = \sum_{n\geq 0} \tilde{p}_n^u x^n.
$$

We follow the procedure proposed in [19] and use the relation between the roots and coefficients of P. More precisely we have

$$
S^s + S^u = -4\varepsilon s^2(x),
$$

$$
P^u + S^u S^s + P^s = -(2 + 4s^2(x)(\delta x^2 + 2\varepsilon)),
$$

$$
P^u S^s + P^s S^u = -4\varepsilon s^2(x),
$$

$$
P^u P^s = 1.
$$

Then, the system satisfied by S^s, P^s, $\tilde{S}^u$, $\tilde{P}^u$ is given by

$$(1+x)^2 S^s + \tilde{S}^u = -16\varepsilon(1-x)^2/\delta t^2,$$

$$\tilde{P}^u + \tilde{S}^u S^s + (1+x)^2 P^s = -(2(1+x)^2 + 16(1-x)^2(\delta x^2 + 2\varepsilon)/\delta t^2),$$

$$\tilde{P}^u S^s + P^s \tilde{S}^u = -16\varepsilon(1-x)^2/\delta t^2,$$

$$\tilde{P}^u P^s = (1+x)^2.$$

By substituting the expansion of S^s, P^s, $\tilde{S}^u$, $\tilde{P}^u$ in this system, one finds for all $n \geq 1$

$$s_n^s + \tilde{s}_n^u = -(2s_{n-1}^s + s_{n-2}^s) - 16\varepsilon\sigma_n/\delta t^2,$$

$$\tilde{p}_n^u + s_0^s \tilde{s}_n^u + \tilde{s}_0^u s_n^s + p_n^s = -(2p_{n-1}^s + p_{n-2}^s) - \sum_{k=1}^{n-1} s_k^s \tilde{s}_{n-k}^u - \kappa_n,$$

$$s_0^s \tilde{p}_n^u + \tilde{p}_0^u s_n^s + p_0^s \tilde{s}_n^u + \tilde{s}_0^u p_n^s = -\sum_{k=1}^{n-1} s_k^s \tilde{p}_{n-k}^u - \sum_{k=1}^{n-1} p_k^s \tilde{s}_{n-k}^u - 16\varepsilon\sigma_n/\delta t^2,$$

$$p_0^s \tilde{p}_n^u + \tilde{p}_0^u p_n^s = -\sum_{k=1}^{n-1} p_k^s \tilde{p}_{n-k}^u + \zeta_n.$$

$$(3.34)$$

where the sequence σ_n, ζ_n, κ_n are given by formulas

$$\sigma_n = \delta_0 - 2\delta_1 + \delta_2,$$

$$\zeta_n = \delta_0 + 2\delta_1 + \delta_2,$$

$$\kappa_n = (2 + 16(\delta x^2 + 2\varepsilon)/\delta t^2)\delta_0 - (4 - 32(\delta x^2 + 2\varepsilon)/\delta t^2)\delta_1 + (2 + 16(\delta x^2 + 2\varepsilon)/\delta t^2)\delta_2,$$

and $\delta_0 = (1, 0, \ldots 0, \ldots)$, $\delta_1 = (0, 1, 0, \ldots 0, \ldots)$, $\delta_2 = (0, 0, 1, 0 \ldots 0, \ldots)$. We used the convention $s_{-1}^s = p_{-1}^s = 0$. The quantities $\tilde{s}_0^s$, $\tilde{s}_0^u$, $\tilde{p}_0^s$, $\tilde{p}_0^u$ are found directly via the roots of P for $z^{-1} = x = 0$, and the resolution of (3.34) is implemented numerically. The evaluation of the n first coefficients requires $O(n^2)$ operations. Now it remains to invert the boundary conditions (3.33). One finds on the left

$$(1 + \tilde{p}_0^u)w_1^{n+1} - \tilde{s}_0^u w_0^{n+1} + \frac{4\delta x}{\delta t}\tilde{p}_0^u \eta_0^{n+1} = -(3 + \tilde{p}_1^u + \tilde{p}_0^u)w_1^n + (\tilde{s}_1^u + \tilde{s}_0^u)w_0^n - \frac{4\delta x}{\delta t}(\tilde{p}_1^u - \tilde{p}_0^u)\eta_0^n$$

$$-3w_1^{n-1} - w_1^{n-2} - \sum_{k=1}^{n}(\tilde{p}_{k+1}^u + \tilde{p}_k^u)w_1^{n-k} + \sum_{k=1}^{n}(\tilde{s}_{k+1}^u + \tilde{s}_k^u)w_0^{n-k} - \frac{4\delta x}{\delta t}\sum_{k=1}^{n}(\tilde{p}_{k+1}^u - \tilde{p}_k^u)\eta_0^{n-k},$$

$$\frac{4\delta x}{\delta t}\eta_1^{n+1} + \tilde{s}_0^u w_1^{n+1} - (1 + \tilde{p}_0^u)w_0^{n+1} =$$

$$-\tilde{s}_1^u w_1^n + (2 + \tilde{p}_1^u)w_0^n + \frac{4\delta x}{\delta t}\eta_1^{n-1} + w_0^{n-1} - \sum_{k=1}^{n}\tilde{s}_{k+1}^u w_1^{n-k} + \sum_{k=1}^{n}\tilde{p}_{k+1}^u w_0^{n-k},$$

$$(3.35)$$

and on the right:

$$(1+p_0^s)w_{J+1}^{n+1} - s_0^s w_J^{n+1} + \frac{4\delta x}{\delta t}p_0^s \eta_J^{n+1} = -(1+p_1^s+p_0^s)w_{J+1}^n + (s_1^s+s_0^s)w_J^n - \frac{4\delta x}{\delta t}(p_1^s-p_0^s)\eta_J^n$$

$$-\sum_{k=1}^n (p_{k+1}^s+p_k^s)w_{J+1}^{n-k} + \sum_{k=1}^n (s_{k+1}^s+s_k^s)w_J^{n-k} - \frac{4\delta x}{\delta t}\sum_{k=1}^n (p_{k+1}^s-p_k^s)\eta_J^{n-k},$$

$$\frac{4\delta x}{\delta t}\eta_{J+1}^{n+1} + s_0^s w_{J+1}^{n+1} - (1+p_0^s)w_J^{n+1} = \frac{4\delta x}{\delta t}\eta_{J+1}^n - (s_0^s+s_1^s)w_{J+1}^n + (1+p_1^s+p_0^s)w_J^n$$

$$+\sum_{k=1}^n (p_{k+1}^s+p_k^s)w_J^{n-k} - \sum_{k=1}^n (s_{k+1}^s+s_k^s)w_{J+1}^{n-k}.$$

$$\tag{3.36}$$

3.3.1 Consistency theorem

We show that the discrete boundary conditions (3.35), (3.36) are consistent of order $O(\delta t^2 + \delta x^2)$.

3.3.3 Theorem. *Let η, w be a smooth solution of (3.2) and (3.6). We define the $\mathcal{Z}-$transform of $f(\cdot, x)$ for all $x \in [x_\ell, x_r]$ by*

$$\forall z \neq 0, \quad \widehat{f}(z,x) = \sum_{n=0}^\infty \frac{f(n\delta t, x)}{z^n}.$$

For all compact $K \subset \mathbb{C}^+$ and for all $\lambda \in K$:

$$(1+r_1 r_2)\widehat{w}(e^{\lambda\delta t}, x_\ell+\delta x) - (r_1+r_2)\widehat{w}(e^{\lambda\delta t}, x_\ell) + 2\delta x r_1 r_2 s(e^{\lambda\delta t})\widehat{\eta}(e^{\lambda\delta t}, x_\ell) = O(\delta t^2+\delta x^2),$$

$$2\delta x s(e^{\lambda\delta t})\widehat{\eta}(e^{\lambda\delta t}, x_\ell+\delta x) + (r_1+r_2)\widehat{w}(e^{\lambda\delta t}, x_\ell+\delta x) - (1+r_1 r_2)\widehat{w}(e^{\lambda\delta t}, x_\ell) = O(\delta t^2+\delta x^2),$$

$$(1+r_3 r_4)\widehat{w}(e^{\lambda\delta t}, x_r) - (r_3+r_4)\widehat{w}(e^{\lambda\delta t}, x_r-\delta x)$$
$$+2\delta x r_3 r_4 s(e^{\lambda\delta t})\widehat{\eta}(e^{\lambda\delta t}, x_r-\delta x) = O(\delta t^2+\delta x^2),$$

$$2\delta x s(e^{\lambda\delta t})\widehat{\eta}(e^{\lambda\delta t}, x_r) + (r_3+r_4)\widehat{w}(e^{\lambda\delta t}, x_r) - (1+r_3 r_4)\widehat{w}(e^{\lambda\delta t}, x_r-\delta x) = O(\delta t^2+\delta x^2),$$

where r_i, $i = 1,..,4$ are the roots of the polynomial (3.29) such that $|r_1| \geq |r_2| > 1 > |r_3| \geq |r_4|$.

Proof. The proof of this theorem is similar to the proof of Theorem 3.2.3. However the explicit expressions for the roots r_i are exceedingly lengthy and useless. Instead, we consider asymptotic expansions of the roots as $\delta x \to 0$. Recall that $(r_i)_{i=1,...,4}$ is expanded as

$$r_2 = 1 + \frac{s(z)\delta x}{\sqrt[4]{1+\varepsilon s^2(z)}} + O(\delta x^2), \quad r_3 = 1 - \frac{s(z)\delta x}{\sqrt[4]{1+\varepsilon s^2(z)}} + O(\delta x^2),$$

$$r_1 = -1 - 2\varepsilon s^2(z) - 2\sqrt[4]{\varepsilon s^2(z)(1+\varepsilon s^2(z))} + O(\delta x^2),$$

$$r_4 = -1 - 2\varepsilon s^2(z) + 2\sqrt[4]{\varepsilon s^2(z)(1+\varepsilon s^2(z))} + O(\delta x^2).$$

Let us denote by $e_1(\delta t, \delta x)$ the consistency error associated to the first boundary condition:

$$e_1 = (1+r_1 r_2)\widehat{w}(e^{\lambda\delta t}, x_\ell+\delta x) - (r_1+r_2)\widehat{w}(e^{\lambda\delta t}, x_\ell) + 2\delta x r_1 r_2 s(e^{\lambda\delta t})\widehat{\eta}(e^{\lambda\delta t}, x_\ell)$$

and define R_1, R_2 as

$$R_1 = -1 - 2\varepsilon s^2(z) - 2\sqrt[+]{\varepsilon s^2(z)(1 + \varepsilon s^2(z))}, \quad R_2 = \frac{s(z)}{\sqrt[+]{1 + \varepsilon s^2(z)}},$$

such that $r_1 = R_1 + O(\delta x^2)$, $r_2 = 1 + R_2\,\delta x + O(\delta x^2)$. The consistency error e_1 reads:

$$\begin{aligned}
e_1 \;&= (1 + R_1 + R_1 R_2 \delta x)\widehat{w}(e^{\lambda\delta t}, x_\ell + \delta x) \\
&\quad -(1 + R_1 + R_2\delta x)\widehat{w}(e^{\lambda\delta t}, x_\ell) + 2\delta x s(e^{\lambda\delta t})R_1\widehat{\eta}(e^{\lambda\delta t}, x_\ell) + O(\delta x^2) \\
&= \delta x \left((1 + R_1)\partial_x\widehat{w}(e^{\lambda\delta t}, x_\ell) + R_2(R_1 - 1)\widehat{w}(e^{\lambda\delta t}, x_\ell) + 2s(e^{\lambda\delta t})R_1\widehat{\eta}(e^{\lambda\delta t}, x_\ell) \right) + O(\delta x^2) \\
&= \delta x (R_1 + 1)\left(\partial_x\widehat{w} + s(e^{\lambda\delta t})\widehat{\eta} \right)(e^{\lambda\delta t}, x_\ell) + \delta x(R_1 - 1)\left(R_2\widehat{w} + s(e^{\lambda\delta t})\widehat{\eta} \right)(e^{\lambda\delta t}, x_\ell) + O(\delta x^2).
\end{aligned}$$

Recall that the function $s(z)$ with $z = e^{\lambda\delta t}$ is approximated by $s(e^{\lambda\delta t}) = \lambda + O(\delta t^2)$. By applying the relation (3.24) between $\mathcal{Z}-$transform and Laplace transform, we find that

$$\begin{aligned}
e_1 = \frac{\delta x}{\delta t}(R_1 + 1)\left(\partial_x\mathcal{L}(w) + \lambda\mathcal{L}(\eta) \right)(\lambda, x_\ell) + \\
\frac{\delta x}{\delta t}(R_1 - 1)\left(\frac{\lambda}{\sqrt[+]{1 + \varepsilon\lambda^2}}\mathcal{L}(w) + \lambda\mathcal{L}(\eta) \right)(\lambda, x_\ell) + O(\delta x^2 + \delta t^2). \quad (3.37)
\end{aligned}$$

Since η, w is a smooth solution of (3.2), one has $\partial_x\mathcal{L}(w) + \lambda\mathcal{L}(\eta) = 0$. Moreover η, w satisfies (3.6) so that $(R_2\mathcal{L}(w) + \lambda\mathcal{L}(\eta))(s, x_\ell) = 0$. As a result, one has $e_1 = O(\delta t^2 + \delta x^2)$. We proceed similarly for the other consistency errors. This concludes the proof of the proposition. $\qquad\square$

We observed numerically that the coefficients involved in (3.36) and (3.35) decrease as $n^{-3/2}$. The coefficients are plotted in Figure 3.1, b. One finds similar decay properties for the linear Korteweg-de Vries equation [19], Benjamin-Bona-Mahony equation [18] or the Schrödinger equation [46]. The discrete boundary conditions (3.36) and (3.35) are thus stable with respect to round off errors.

In the next section we will discuss the results of numerical simulations for equation (3.23) with the boundary conditions (3.21), (3.22) and for the system (3.14) with the boundary conditions (3.35), (3.36).

3.4   Numerical results

In this section we present a numerical validation of the discretized transparent boundary conditions through various tests. First we validate the boundary conditions for a Gaussian initial data. Different dispersion properties are analysed for a wave packet as initial datum. This analysis is based on the dispersion relation corresponding to the linearized Green-Naghdi equation. All test are carried out for both types of boundary conditions on a staggered and on a collocated grid. Finally, we show how to inject a (planar) wave into

---

Numerical animations are available https://www.math.univ-toulouse.fr/~mkazakov

the computational domain. To validate the efficiency of the artificial boundary conditions we perform a numerical analysis of the approximation error. The tests show second order of approximation with respect to time and space. Let us introduce first the numerical implementation of the numerical methods considered in this chapter.

3.4.1   Numerical implementation

Staggered grid

We present a numerical strategy to solve the problem on a staggered grid. The discretization (3.14) is equivalent to the scheme (3.23) and the conditions (3.21), (3.22) are written for the values of velocity $w_{0,J+1}^n$. It remains to reconstruct the values for the free surface elevations $\eta_{j+1/2}^{n+1}$, $j \in (0, J)$. By taking into account the boundary condition and setting

$$\Lambda_- = \Lambda + 2\delta x^2 - 2\delta x\sqrt{\Gamma}, \quad \Lambda_+ = \Lambda + 2\delta x^2 + 2\delta x\sqrt{\Gamma},$$

$$\mu_- = \mu + 2\delta x^2 - \delta x\sqrt{\Gamma}(v+1), \quad \mu_+ = \mu + 2\delta x^2 + \delta x\sqrt{\Gamma}(v+1),$$

the full numerical step written as a one time step method reads

$$MW^{n+1} = 2NW^n - MW^{n-1} + V^n, \quad n \in \mathbb{N},$$

where $W^{n+1} = [w_0^{n+1}, \ldots, w_{J+1}^{n+1}]^\top$ is the unknown vector, and the matrices $M, N \in M_{J+2}(\mathbb{R})$ are defined as:

$$M = \begin{bmatrix} -\Lambda_+ & \Lambda \\ -a_+ & 1+2a_+ & -a_+ \\ & \ddots & \ddots & \ddots \\ & & -a_+ & 1+2a_+ & -a_+ \\ & & & -\Lambda_- & \Lambda \end{bmatrix}, \quad N = \begin{bmatrix} -\mu_+ & \mu \\ -a_- & 1+2a_- & -a_- \\ & \ddots & \ddots & \ddots \\ & & -a_- & 1+2a_- & -a_- \\ & & & -\mu_- & \mu \end{bmatrix}.$$

The vector V^n on the right hand side has only two non-zero components:

$$V^n = \begin{bmatrix} 2\delta x\sqrt{\Gamma}\left((\mathcal{P}_2 - 2v^2 + v)w_0^{n-1} + \sum_{k=2}^n s_k(v)w_0^{n-k}\right) \\ \vdots \\ -2\delta x\sqrt{\Gamma}\left((\mathcal{P}_2 - 2v^2 + v)w_J^{n-1} + \sum_{k=2}^n s_k(v)w_J^{n-k}\right) \end{bmatrix}.$$

The matrix M is easily proved to be invertible (for δx small enough) and the solution vector at time t_{n+1} is given by

$$W^{n+1} = M^{-1}(2NW^n + V^n) - W^{n-1}, \quad n \in \mathbb{N},$$

so that the velocity components can be computed at each time step.

Once the velocity field is computed, there remains to reconstruct the values of the free-surface elevation η. This can be done by solving the first equation of (3.14). Since the velocity at iterations n and $(n+1)$ is known, one finds

$$\eta_{j+1/2}^{n+1} = \eta_{j+1/2}^n - \frac{\delta t}{2}\left(\frac{w_{j+1}^{n+1} - w_j^{n+1}}{\delta x} + \frac{w_{j+1}^n - w_j^n}{\delta x}\right).$$

Note that this equation has no influence on the velocity calculations and should be solved simply for the correct description of the water wave problem.

We need to set the initial values for the velocity W^0 at $t = 0$ and W^1 at $t = \delta t$. In order to take into account the physics of the problem the initial conditions should be imposed for the velocity W^0 and the elevation η^0. To find a value for W^1 at $t = \delta t$ we use the Taylor expansion in the vicinity of $t = 0$:

$$(w - \varepsilon w_{xx})\left.\right|_{t=\delta t} = (w - \varepsilon w_{xx})\big|_{t=0} + \delta t(w - \varepsilon w_{xx})_t\big|_{t=0} + \frac{\delta t^2}{2}(w - \varepsilon w_{xx})_{tt}\big|_{t=0} + O(\delta t^3),$$

using the continuous equations (3.2) one finds

$$(w - \varepsilon w_{xx})\big|_{t=\delta t} = \left(w - \left(\varepsilon - \frac{\delta t^2}{2}\right)w_{xx}\right)\Big|_{t=0} - \delta t\, \eta_x\big|_{t=0}. \tag{3.38}$$

The discretization of (3.38) gives the linear system for the requested value. Note that the order of approximation for values $W(t = \delta t)$ is the same as for the numerical scheme itself.

Collocated grid

We rewrite in a matrix form the discrete equations (3.27) on a collocated grid coupled with the boundary conditions derived in Section 3.3. We have:

$$\begin{bmatrix} A_+ & B_+ \\ C_+ & D_+ \end{bmatrix}\begin{pmatrix} \eta^{n+1} \\ w^{n+1} \end{pmatrix} = \begin{bmatrix} A_- & B_- \\ C_- & D_- \end{bmatrix}\begin{pmatrix} \eta^n \\ w^n \end{pmatrix} + \overline{V}^n,$$

where the matrices $A_\pm$, $B_\pm$, $C_\pm$, $D_\pm$ are block matrices in $M_{J+2}(\mathbb{R})$ defined as follows

$$A_+ = \begin{bmatrix} \tilde{p}_0^u/c & & & & \\ 0 & 1 & 0 & & \\ & \ddots & \ddots & \ddots & \\ & & 0 & 1 & 0 \\ 0 & 1/c & & 0 & 0 \end{bmatrix}, \quad B_+ = \begin{bmatrix} -\tilde{s}_0^u & 1+\tilde{p}_0^u & & \\ -c & 0 & c & \\ & \ddots & \ddots & \ddots \\ & & -c & 0 & c \\ -(1+\tilde{p}_0^u) & \tilde{s}_0^u & & 0 \end{bmatrix},$$

$$C_+ = \begin{bmatrix} 0 & 0 & & p_0^s/c & 0 \\ -c & 0 & c & & \\ & \ddots & \ddots & \ddots & \\ & & -c & 0 & c \\ 0 & & & 0 & 1/c \end{bmatrix}, \quad D_+ = \begin{bmatrix} 0 & & & -s_0^s & 1+p_0^s \\ -a & 1+2a & -a & & \\ & \ddots & \ddots & \ddots & \\ & & -a & 1+2a & -a \\ & & & -(1+p_0^s) & s_0^s \end{bmatrix},$$

and :

$$A_- = \begin{bmatrix} -(\tilde{p}_1^u - \tilde{p}_0^u)/c & & & & \\ 0 & 1 & 0 & & \\ & & \ddots & \ddots & \ddots \\ & & & 0 & 1 & 0 \\ 0 & 0 & & 0 & 0 \end{bmatrix}, \quad B_- = \begin{bmatrix} \tilde{s}_0^u + \tilde{s}_1^u & -(3 + \tilde{p}_0^u + \tilde{p}_1^u) & & \\ c & 0 & -c & \\ & \ddots & & \ddots & \ddots \\ & & & c & 0 & -c \\ 2 + \tilde{p}_1^u & -\tilde{s}_1^u & & 0 \end{bmatrix},$$

$$C_- = \begin{bmatrix} 0 & 0 & -(p_1^s - p_0^s)/c & 0 \\ c & 0 & -c & \\ & \ddots & \ddots & & \ddots \\ & c & 0 & & -c \\ 0 & & 0 & & 1/c \end{bmatrix},$$

$$D_- = \begin{bmatrix} 0 & & & (s_0^s + s_1^s) & -(1 + p_0^s + p_1^s) \\ -a & 1+2a & -a & & \\ & \ddots & \ddots & \ddots & \\ & & -a & 1+2a & -a \\ & & & 1 + p_0^s + p_1^s & -(s_0^s + s_1^s) \end{bmatrix}.$$

We have denoted $c = \delta t/(4\delta x)$ and $a = \varepsilon \delta t/\delta x^2$. It follows from the form of the boundary conditions that the vector $\vec{V}_n$ on the right hand side contains the previous time-iteration values of the functions η_j^n, w_j^n:

$$\overline{V}_0^n = -3w_1^{n-1} - w_1^{n-2} - \sum_{k=1}^{n}(\tilde{p}_{k+1}^u + \tilde{p}_k^u))w_1^{n-k} + \sum_{k=1}^{n}(\tilde{s}_{k+1}^u + \tilde{s}_k^u))w_0^{n-k} - \frac{4\delta x}{\delta t}\sum_{k=1}^{n}(\tilde{p}_{k+1}^u - \tilde{p}_k^u)\eta_0^{n-k},$$

$$\overline{V}_{J+1}^n = \frac{4\delta x}{\delta t}\eta_1^{n-1} - \sum_{k=1}^{n}\tilde{s}_{k+1}^u w_1^{n-k} + w_0^{n-1} + \sum_{k=1}^{n}\tilde{p}_{k+1}^u w_0^{n-k}$$

$$V_{J+2}^n = \frac{4\delta x}{\delta t}\sum_{k=1}^{n}(p_{k+1}^s - p_k^s)\eta_J^{n-k} - \sum_{k=1}^{n}(p_{k+1}^s + p_k^s)w_{J+1}^{n-k} + \sum_{k=1}^{n}(s_{k+1}^s + s_k^s)w_J^{n-k},$$

$$V_{2(J+2)}^n = -\sum_{k=1}^{n}(s_{k+1}^s + s_k^s)w_{J+1}^{n-k} + \sum_{k=1}^{n}(p_{k+1}^s + p_k^s)w_J^{n-k},$$

$$\overline{V}_j^n = 0, \quad j = 1,.., J, (J+3),.., 2J+3.$$

3.4.2 Gaussian initial distribution

In this section we show the numerical results when we take a Gaussian initial distribution for the free surface elevation and zero distribution for velocity

$$\eta_0(x) = \exp(-400 \times (x - 1/2)^2), \quad w_0(x) = 0,$$

whereas the computational domain $(t,x) \in [0,1] \times [0,1]$ is meshed with $N \times (J+2)$ nodes. We first show that there is no reflection on the boundaries of the computational domain.
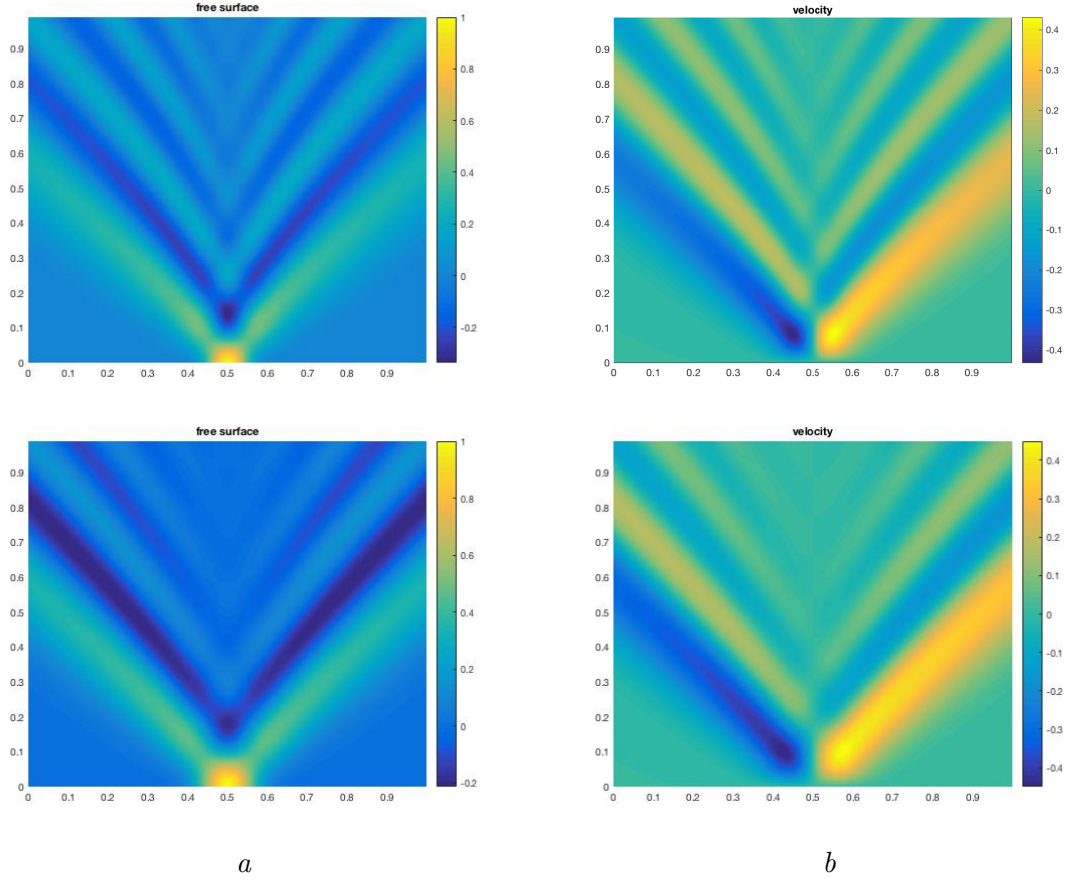
Figure 3.2: Numerical solution on a staggered (up) and collocated (down) grids: Evolution of (a) the surface elevation, (b) the fluid velocity for $\delta x = 10^{-3}$, $\delta t = 10^{-2}$, $\varepsilon = 10^{-3}$.

We present results both for staggered and collocated spatial grids. The velocity and free surface evolution are shown on the (x, t)-plane on the Figure, 3.2. Following the numerical strategy described at the beginning of this section we have reconstructed the value for $w(t = \delta t)$ from the initial datum for the method on a staggered grid.

Let us comment the computed results. Recall that the dispersion relation associated to (3.2) is written as

$$\omega^2(k) = \frac{k^2}{1 + \varepsilon k^2}. \tag{3.39}$$

There are two solutions for $\omega(k)$, that corresponds to the fact that the Green-Naghdi system describes bi-directional propagation of waves, just as we can see in Figure, 3.2. On the left Figure 3.3, the positive solution of the dispersive relation (3.39) is plotted. From the dispersive relation (3.39), we find that phase and group velocities are given by

$$v_\varphi(k) = \frac{\omega(k)}{k} = \frac{1}{\sqrt{1 + \varepsilon k^2}}, \quad v_g(k) = \frac{d\omega(k)}{dk} = \frac{1}{(1 + \varepsilon k^2)^{3/2}}.$$

The group velocity is always smaller than the phase velocity (see right Figure 3.3).
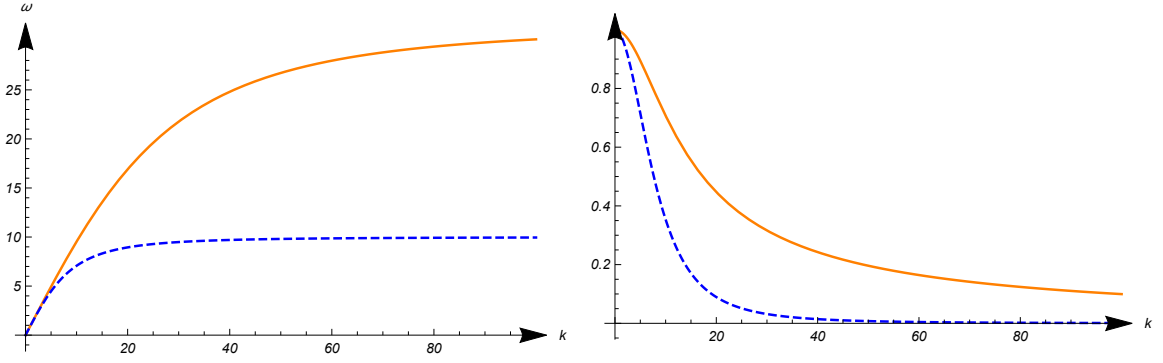
Figure 3.3: Positive solution of dispersive relation $\omega(k)$ for $\varepsilon = 10^{-4}$ (solid), $\varepsilon = 10^{-3}$ (dashed) (left) and phase (continued) and group (dashed) velocities for $\varepsilon = 10^{-3}$ (right).

3.4.3   Wave packet

In order to observe more clearly the dispersive behavior of the Green-Naghdi system, we consider the solution of (3.2) with the next initial datum

$$\eta_0(x) = \exp(-400 \times (x - 1/2)^2)\sin(20\pi x), \quad w_0(x) = 0. \tag{3.40}$$

For different values of ε, the dispersive properties are not the same. The results are presented in Figure 3.4. As dispersive effects are more important for $\varepsilon = 10^{-3}$ we have more diversity for frequency values, but for smaller value $\varepsilon = 10^{-4}$ the behaviour of the solution is closer to the solutions of the hyperbolic Saint-Venant system. Namely, the velocity profile splits into two waves travelling at speed ± 1: in this case, phase and group velocities coincide.

In order to check numerically the order of approximation of the numerical schemes, we have constructed the reference solution for the velocity. The reference solution of (3.10) can be written as

$$w_{ref}(t,x) = \mathcal{F}^{-1}\left(\xi \mapsto \cos\left(\frac{\xi t}{\sqrt{1 + \xi^2 \varepsilon}}\right)\mathcal{F}(w_0)(\xi)\right)(t,x),$$

here $\mathcal{F}$, $\mathcal{F}^{-1}$ are the Fourier and inverse Fourier transforms in space, and w_0 denotes the initial data. For the numerical test, the reference solution is calculated with periodic boundary conditions and the Fast Fourier transform. The extension of the computational domain is chosen large enough to avoid any spurious effects of the boundary conditions. The evolution of the reference solution is shown in Figure 3.5.

We define the error functions of the approximation which corresponds to the discrete version of $L_\infty^t L_2^x$ and $L_2^t L_2^x$ norms of the errors. Let us first denote

$$e_n = \mid w(t_n, \cdot) - w_{ref}(t_n, \cdot) \mid_{L_2},$$

for all time step t_n, then the discrete norms are defined as

$$L_2err = \left(\delta t \sum_{n=1}^{N}(e_n^2)\right)^{1/2}, \quad L_\infty err = \max_{0 < n \leq N}(e_n).$$

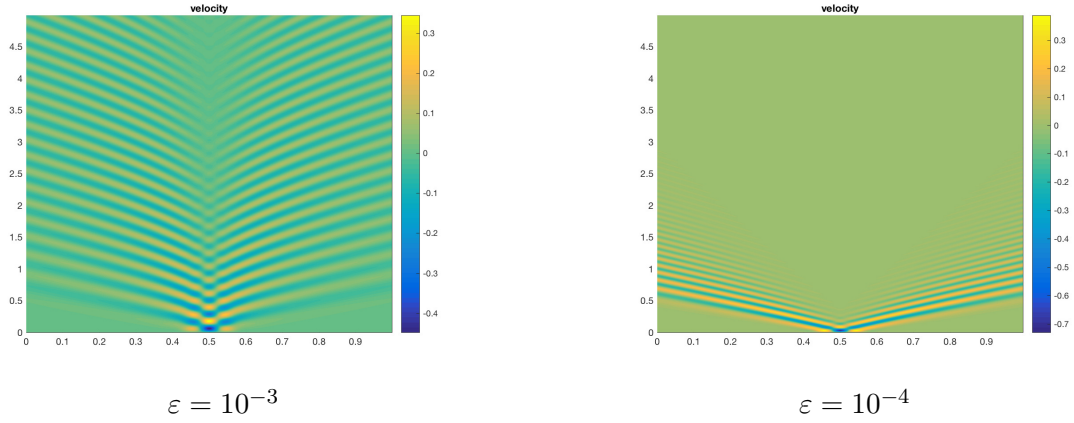$$\varepsilon = 10^{-3} \qquad\qquad\qquad\qquad \varepsilon = 10^{-4}$$

Figure 3.4: Evolution of the velocity profile for $\delta x = 10^{-3}$, $\delta t = 10^{-2}$ with (3.40) initial datum with $\varepsilon = 10^{-3}$ (left) and $\varepsilon = 10^{-4}$ (right).

The next estimates are satisfied due to the second order of accuracy for both the numerical scheme on a staggered and collocated grid

$$L_2 err = C_t^2 \delta t^2 + C_x^2 \delta x^2, \quad L_\infty err = C_t^\infty \delta t^2 + C_x^\infty \delta x^2,$$

where $C_{t,x}^2$, $C_{t,x}^\infty$ are constants depending on the reference solution. We start the analysis of the behaviour of the error functions with respect to δx. For that purpose, we take $N = 10^3$ which leads to a value for δt small enough to ensure that the dominating error term is linked to C_x . The errors are plotted in Figure 3.6. The second order accuracy with respect to the space step is satisfied. In the case of staggered grid, the space discretization induced errors that stagnate after $\delta x \leq 0.005$: in this area, the time discretization induced error dominates.

In order to check the approximation order with respect to δt, we fix $J = 2^{15}$, to take δx small enough and ensure that there is no influence of C_x^2, C_x^∞. We find the second order of approximation as well. The plots are presented in Figure 3.7. We find also in one case that the time discretization error stagnate: here the spatial discretization errors dominate.

3.4.4 Incoming wave

In this subsection we will consider the numerical test with a travelling wave entering the computational domain, which is an important real physical case. Indeed, it is still an open problem for the Green-Nagdhi equation to impose an incoming wave like a solitary wave or a cnoidal wave which can model tidal waves at the edge of the computational domain without perturbing the solution computed numerically in the domain. We follow here the method presented in [3] for the Schrödinger-Poisson system and successfully applied in [18] for the Benjamin-Bona-Mahoney equation.

Let us denote by $w^{in}(x,t) = \beta \cos(kx - \omega(k)t)$ a plane wave solution for the velocity of the linear equation (3.10). Now we are searching for the transparent boundary conditions for the linear equation with an initial data w_0 satisfying $w_0(x) = w^{in}(x)$, $\forall x \leq x_l$ and $w_0(x) = 0$, $\forall x \geq x_r$. For that purpose, we decompose w as $w(x,t) = \chi(x)w^{in}(x,t) + v(x,t)$,
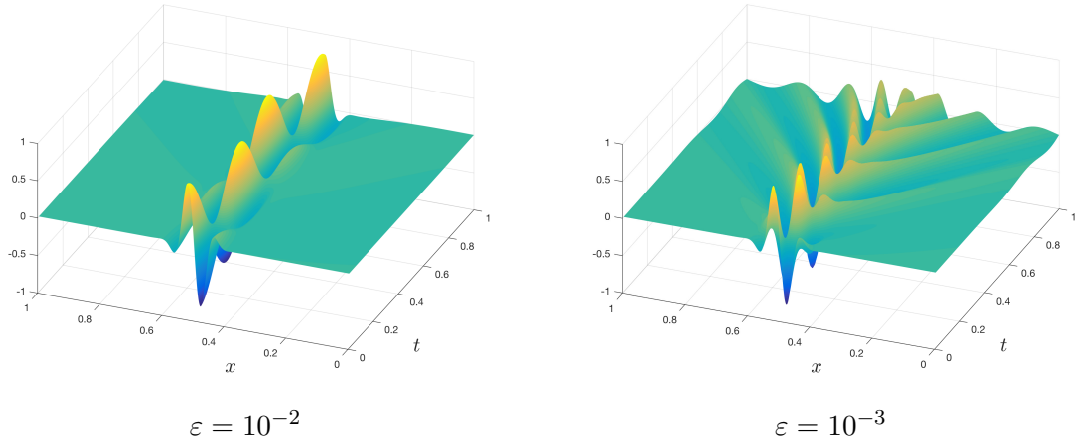
Figure 3.5: Evolution of the reference solution for $\varepsilon = 10^{-2}$ (left) and $\varepsilon = 10^{-3}$ (right).

where the cut-off function χ is defined as $\chi = 1, \forall x \le x_l$ $\chi = 0, \forall x \ge x_r$ and is smooth: its derivatives χ' is compactly supported in $[x_\ell, x_r]$. Then, the new unknown function v is compactly supported in $[x_\ell, x_r]$. One finds that v satisfies the following equation with a source term:

$$(v - \varepsilon v_{xx})_{tt} - v_{xx} = G_\varepsilon(x, t)$$

$$G_\varepsilon(x, t) = \varepsilon(\chi''(x)w_{tt}^{in}(t, x) + 2\chi' w_{xtt}^{in}(t, x)) + \chi''(x)w^{in}(t, x) + 2\chi''(x)w_x^{in}(t, x).$$

The derivation of the continuous boundary conditions for v is exactly similar to the homogeneous case ($w^{in} = 0$) discussed above, one finds

$$
\begin{aligned}
w_x(t, x_r) &= -\partial/\partial t \int_0^t \mathcal{J}_0(s/\sqrt{\varepsilon})w(t - s, x_r)ds, \\
\partial_x(w - w^{in})(t, x_l) &= \partial/\partial t \int_0^t \mathcal{J}_0(s/\sqrt{\varepsilon})(w - w^{in})(t - s, x_l)ds.
\end{aligned}
\tag{3.41}
$$

For the discrete boundary condition, we consider the problem set on a staggered grid. The procedure repeats the method proposed in the homogeneous case $w^{in} = 0$. The continuous plane wave solution is replaced by the discrete solution

$$w_{n,j}^{in} = \beta \cos(jk\delta x - n\tilde{\omega}(k)\delta t), \quad \tilde{\omega}(k) = \frac{1}{\delta t}\arccos\left(\frac{2\delta x^2 + (4\varepsilon - \delta t^2)\sin^2(k\delta x/2)}{2\delta x^2 + (4\varepsilon + \delta t^2)\sin^2(k\delta x/2)}\right),$$

and the condition on the left boundary is written as

$$\Lambda(w_1^{n+1} - [w^{in}]_1^{n+1}) - (\Lambda + \delta x^2 + 2\delta x\sqrt{\Gamma})(w_0^{n+1} - [w^{in}]_0^{n+1}) =$$

$$2(\mu(w_1^n - [w^{in}]_1^n) - (\mu + 2\delta x^2 + \delta x\sqrt{\Gamma}(v + 1))(w_0^n - [w^{in}]_0^n)) -$$

$$(\Lambda + (w_1^{n-1} - [w^{in}]_1^{n-1}) - (\Lambda + \delta x^2 + 2\delta x\sqrt{\Gamma})(w_0^{n-1} - [w^{in}]_0^{n-1})) +$$

$$2\delta x\sqrt{\Gamma}\left((\mathcal{P}_2 - 2v^2 + v)(w_0^{n-1} - [w^{in}]_0^{n-1}) + \sum_{k=2}^n s_k(w_0^{n-k} - [w^{in}]_0^{n-k})\right), \quad (3.42)$$
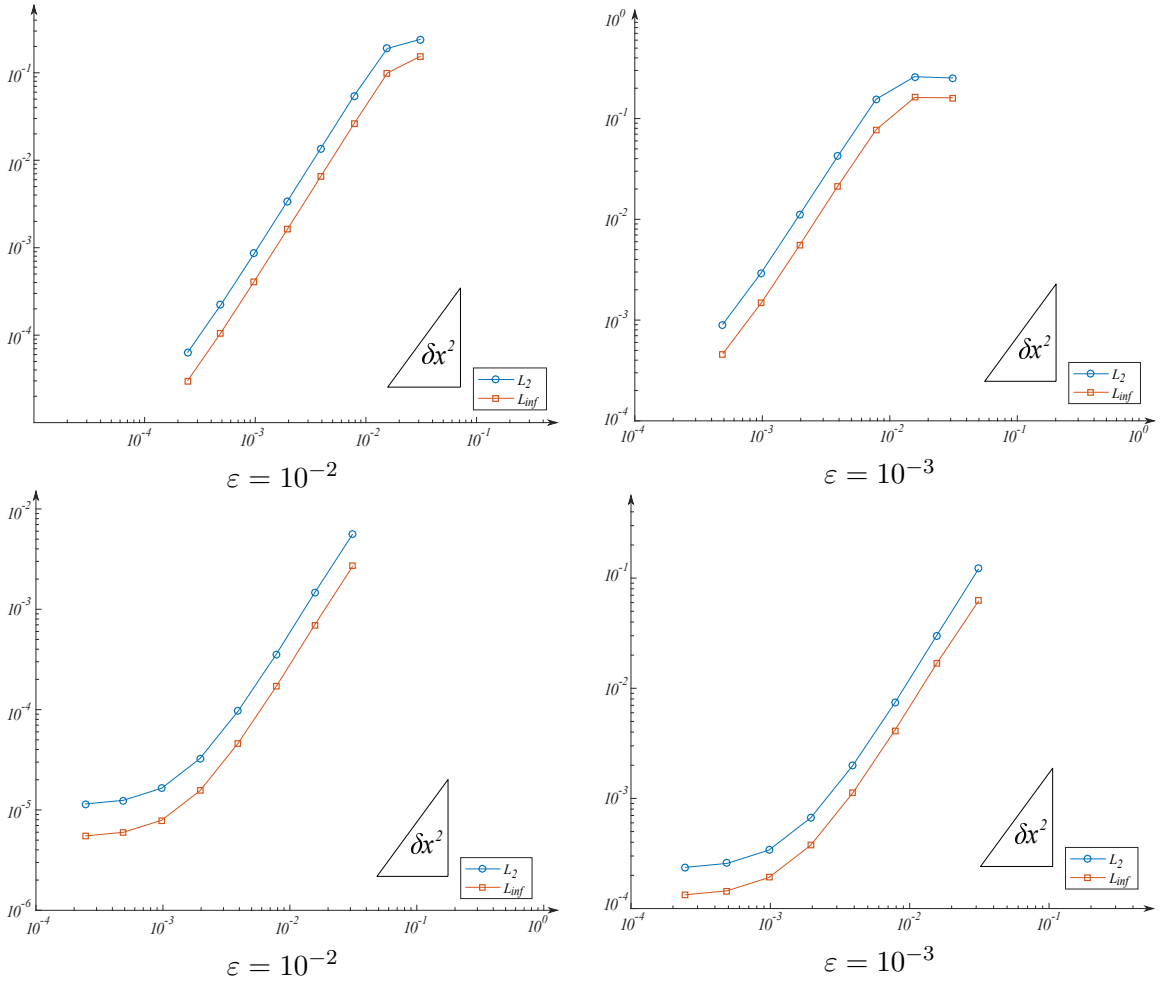
Figure 3.6: Evolution of the error functions for the numerical methods on a collocated (up) and staggered (down) grid with respect to δx.
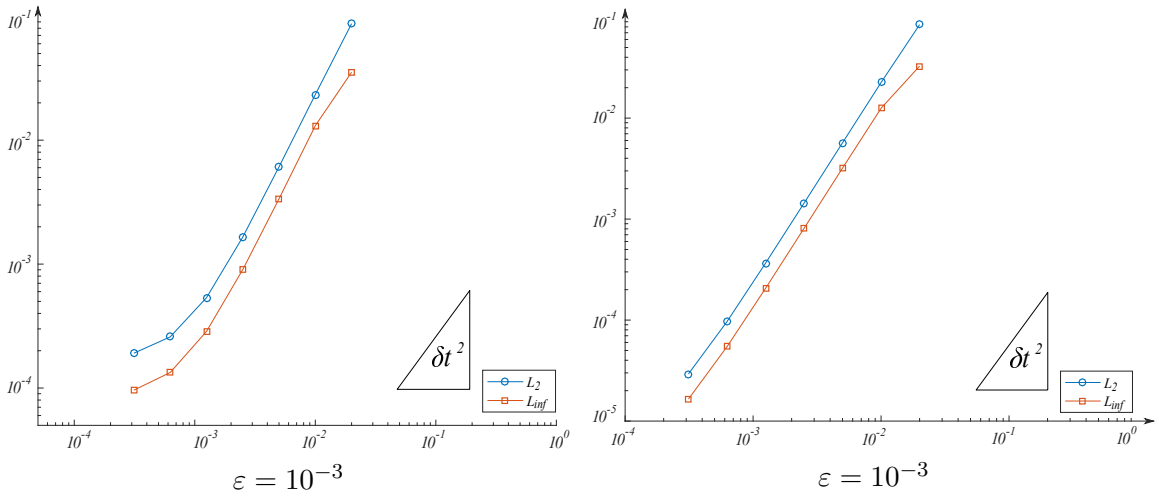

Figure 3.7: Evolution of the error functions for the numerical methods on a collocated (left) and staggered (right) grid with respect to δt.
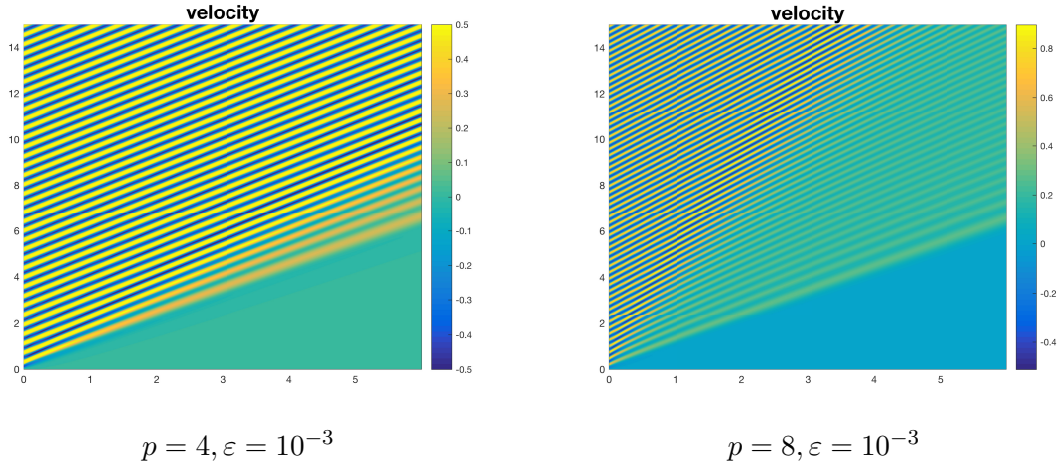
$$p = 4, \varepsilon = 10^{-3} \qquad\qquad p = 8, \varepsilon = 10^{-3}$$

Figure 3.8: Evolution of incoming wave solutions for different wave number.

whereas on the right boundary, one has:

$$\Lambda(w_{J+1}^{n+1} - [w^{in}]_{J+1}^{n+1}) - (\Lambda + \delta x^2 - 2\delta x\sqrt{\Gamma})(w_J^{n+1} - [w^{in}]_J^{n+1}) =$$

$$2(\mu(w_{J+1}^n - [w^{in}]_{J+1}^n) - (\mu + 2\delta x^2 - \delta x\sqrt{\Gamma}(v+1))(w_J^n - [w^{in}]_J^n) -$$

$$- (\Lambda(w_{J+1}^{n-1} - [w^{in}]_{J+1}^{n-1}) - (\Lambda + \delta x^2 - 2\delta x\sqrt{\Gamma})(w_J^{n-1} - [w^{in}]_J^{n-1}) -$$

$$- 2\delta x\sqrt{\Gamma}\left((\mathcal{P}_2 - 2v^2 + v)(w_J^{n-1} - [w^{in}]_J^{n-1}) + \sum_{k=2}^n s_k(v)(w_J^{n-k} - [w^{in}]_J^{n-k})\right). \quad (3.43)$$

The boundary conditions for the numerical scheme (3.27) (collocated grids) can be written in the same manner.

The numerical results are plotted in Figure 3.8. We write the wave number as $k = 2\pi p$, $p \in N$ and we present the results for different wave numbers ($p = 4, 8$). In both cases there exists a transient regime, but after the wave solution propagates correctly. We observe again the difference between phase and group velocities. Note that the characteristics in the (x, t)-plane have all a slope close to 1 in the zone after transition, which corresponds to the velocity of the waves (a coefficient preceding w_x). But a part of the energy is carried along the characteristic with the smaller slope on the border of the transient regime which corresponds to the fact that the group velocity is smaller.

3.5 Conclusion

In this chapter, we have derived exact and discrete transparent boundary conditions for the linear Green-Naghdi system for a Crank-Nicolson discretization on a staggered and a collocated grid. Both schemes are proved to be stable, consistent and convergent. The technique is validated numerically for outgoing waves with different initial data. We show

how to deal with the problem of wave generation in water wave problems and prove the accuracy of the proposed method on numerical tests.

In practice, we will have to deal with nonlinear equations. It remains an open question what are the transparent boundary conditions for this case. One can imagine to adapt our strategy to linear equations with variable coefficients and then adopt a fixed point strategy, as it was done for nonlinear Schrödinger equation in [5]. Another question of interest is to derive discrete transparent boundary conditions in the case of the two-layer Green-Naghdi equations which are used to describe internal waves propagation.

Chapter 4

Perfectly Matched Layers: Application to a relaxation system for the Green-Naghdi equations

Mathematical modelling of dispersive wave propagation in large domains requires advanced numerical techniques. In particular, as already mentioned, a much smaller numerical domain than the physical space is generally used in order to reduce the computational costs. Therefore suitable boundary conditions must be imposed. As discussed in Introduction, the dispersive Green-Naghdi system is generally used in the context of coastal water wave propagation. The same problem arises for the models derived in Part I. We focus in this chapter first on the Green-Naghdi equations, since both models obtained in the previous part reduce to this system for particular cases.

Nonlinear Green-Naghdi equations are set initially on the whole space, but when integrating numerically, one has to confine the computational domain. Naturally, in applications, we are interested in simulating incoming and outgoing waves. For ocean wave propagation, classical numerical boundaries (reflecting walls, periodic settings) are limiting. This numerical issue is not specific to fluid dynamics, one faces the same problem in acoustics, quantum mechanics, electrodynamics, optics, and the other fields implying wave propagation.

In the previous Chapter 3, transparent boundary conditions are proposed for the linearized Green-Naghdi system. The derived conditions provide a good approximation of the solution on the original unbounded domain and permit to generate incoming waves. Unfortunately, transposition of such techniques to a nonlinear setting is, up to our knowledge, still an open question.

We have already discussed methods used to resolve the difficulties with boundary conditions in the case of dispersive Green-Naghdi (more generally Boussinesq type) models. Now let us focus on a model recently proposed in [49]. The idea is to extend the Green-Naghdi

system to a hyperbolic system, introducing new variables. The equations are derived by using a Lagrangian approach. The proposed system may be interpreted as a numerical relaxation strategy for the initial Green-Naghdi equations (like the one initially proposed in [67]). The introduction of new variables allows for the reduction of the order, a more straightforward resolution. Consequently, the proposed approach resolves one of the main difficulties encountered with the dispersive terms discretization: there is no need to inverse an elliptic operator. The system can be solved with a classical Godunov-type method, supplemented by a splitting strategy for the source terms.

This new formulation is a significant improvement in the simulations of dispersive waves. However, one has to impose suitable boundary conditions, and notably when dealing with reduced numerical domains. Contrary to the original equations, the system under consideration is hyperbolic. This may allow simplifying the boundary conditions treatment, and if so this new system might be very promising for further applications in ocean wave modelling. Validations considered in [49] implied solitary wave propagation and Favre waves, more general test cases may require a proper procedure for boundary conditions. In particular, we need to propose a suitable procedure for inflow and outflow simulations, which is the primary goal of the present study.

Dealing with boundary conditions in the classical context of $1D$ hyperbolic systems the equations should be rewritten, if possible, in Riemann invariants form. Unfortunately, this is not the case for the proposed system. Moreover, the generalization of the notion of Riemann invariants for multidimensional cases is not a trivial task. Another approach needs to be proposed.

Several techniques are used for now to deal with boundary conditions for simulations of systems set initially on unbounded domains. We briefly mention two strategies which are not discussed here in details. The problem can be treated with Infinite Element Methods (IEM), and Boundary Element Methods (BEM). IEM are usually used in acoustics, where the unbounded outer region is modelled in its entirety by particular elements of infinite extent. BEM methods are used for problems for which Green's functions can be calculated.

Another approach is the construction of artificial boundary conditions (ABC), considered in the previous chapter. Engquist and Majda performed one of the first pioneering works on such a type of conditions in [48]. They applied the theory of reflection of singularities developed earlier in [96]. Since this work, many research works concerned the generalization of these conditions for different application fields. A review of these approaches can be found in [55], and another one devoted to the Schrödinger equation in [5]. In general, the construction of ABCs may be performed at the continuous level, for example in [60] where a general method for evolution problems is proposed. In [47], well-posed ABCs are found for a general hyperbolic system using pseudo-differential operators. Another possibility is to construct ABCs at a discrete level directly, as it was done recently in [18] for the Benjamin–Bona–Mahony (BBM) equation, or in [19] for the KdV-BBM equation, and in Chapter 3 for the linearized Green-Naghdi system.

Generally speaking, all those techniques give specific conditions on the artificial boundary by factorization of the differential equations into inflow and outflow parts. A different approach is referred to as absorbing layer approach. In this case, a more physical interpretation is applied: a damping medium is put around the computational domain. It leads

to modifications of the equations since the physical properties of the part of the medium where waves propagate are changed. One of the pioneering work employing such a strategy was proposed by Bérenger [16] with the Perfectly Matched Layer (PML) approach, where thin layers are introduced around the computational domain in the context of electromagnetics. Since then, this idea was followed by other researchers. A review of applications to electrodynamics is given in [136]. Particular applications to advective acoustics can be found in [2]. For linear water waves, we refer to [38] among others.

In the present study, we are interested in the derivation of PML equations for the new relaxed system introduced before. The chapter is organised as follows: the first two sections are devoted to the new relaxed Green-Naghdi system introduced in [49] and its mathematical structure. The derivation of the PML equations and numerical validations are given in the next two sections. Then we provide a preliminary stability result through an energy estimation of the solution of the resulting linear PML equations. Explanations on how to proceed in the nonlinear case are considered in section 4.6, together with nonlinear numerical tests. In the last Section, we show that using the same arguments the PML equations can be applied to the wave generation in both linear and nonlinear cases. Numerical tests are provided to illustrate the procedure.

4.1 From Green-Naghdi to a hyperbolic system

We consider a robust numerical method proposed recently in [49]. The idea is to extend the Green-Naghdi system to a hyperbolic system, using a Lagrangian approach. The one-dimensional Green-Naghdi equations are written as

$$\begin{cases} \dfrac{\partial h}{\partial t} + \dfrac{\partial (hu)}{\partial x} = 0, \\ \dfrac{\partial (hu)}{\partial t} + \dfrac{\partial}{\partial x}(hu^2 + p) = 0, \quad p = \dfrac{gh^2}{2} + \dfrac{1}{3}h^2\ddot{h}, \end{cases} \quad t > 0,\, x \in \mathbb{R}, \qquad (4.1)$$

with $\ddot{h}$ denotes the second order material derivative:

$$\dot{h} = \frac{\partial h}{\partial t} + u\frac{\partial h}{\partial x}, \quad \ddot{h} = \left(\frac{\partial}{\partial t} + u\frac{\partial}{\partial x}\right)h.$$

The system describes an evolution of the water depth $h(t,x)$ and velocity $u(t,x)$. The equations admit a variational formulation ([53], [122]) with the Lagrangian $\mathcal{L}$ defined as

$$\mathcal{L} = \int_{-\infty}^{\infty} \frac{hu^2}{2} - W(h,\dot{h})\,dx. \qquad (4.2)$$

The potential $W(h,\dot{h})$ is

$$W(h,\dot{h}) = \frac{gh^2}{2} - \frac{h\dot{h}^2}{6}.$$

The corresponding Euler-Lagrange equations lead to the dispersive Green-Naghdi equations.

The main idea used in [49] is to extend (4.2) to

$$\mathcal{L}^* = \int_{-\infty}^{\infty} \frac{hu^2}{2} + \frac{h\dot{\eta}^2}{6} - \frac{gh^2}{2} - \frac{\lambda h}{6}\left(\frac{\eta}{h} - 1\right)^2 dx, \quad \lambda = \text{const}, \qquad (4.3)$$

using a non-equilibrium variable η with the property that in equilibrium one has $\eta = h$.

The Euler-Lagrange equations then leads to the new extended system (see [49] for details):

$$\frac{\partial \mathbf{U}}{\partial t} + \frac{\partial \mathbf{F}(\mathbf{U})}{\partial x} = \mathbf{S}(\mathbf{U}), \tag{4.4}$$

where the vector functions are defined as follows

$$\mathbf{U} = (h, hu, h\eta, hw)^{\top}, \quad \mathbf{F}(\mathbf{U}) = \left(hu, hu^2 + gh^2/2 - \frac{\lambda}{3}\left(\frac{\eta}{h} - 1\right), h\eta u, hwu \right)^{\top}$$

$$\mathbf{S}(\mathbf{U}) = \left(0, 0, hw, -\lambda\left(\frac{\eta}{h} - 1\right) \right)^{\top}.$$

By construction the function $w(t, x)$ corresponds to the material derivative of water depth h.

For the definition of the value of the relaxation parameter λ, we turn to a dispersion relation analysis. For the model (4.4), the phase velocity reads

$$(v_\varphi^*(k))^2 = \frac{1}{2}\left(gh_0^3 + \frac{\lambda h_0^2}{3} + \frac{\lambda}{(kh_0)^2} \pm \sqrt{gh_0^3 + \frac{\lambda h_0^2}{3} + \frac{\lambda}{(kh_0)^2} - \frac{4gh_0\lambda}{k^2}} \right), \tag{4.5}$$

while for the original Green-Naghdi system the phase velocity is simpler and written as

$$(v_\varphi(k))^2 = \frac{3gh_0\, k^2}{3 + (kh_0)^2}. \tag{4.6}$$

The wave number is denoted by k, and $h_0 = \text{const}$ is an equilibrium water depth. For the choice of a reliable value of λ, one should pay attention to how close the values $v_\varphi^*(k)$ are to the values of $v_\varphi(k)$ for all k. In [49] it is shown that for relatively big values of λ one can guarantee a good approximation of (4.6) by (4.5).

4.2 Mathematical structure of the system

We begin with the study of hyperbolicity of the system (4.4). Generally, the homogeneous system of the form

$$\frac{\partial \mathbf{U}}{\partial t} + \frac{\partial \mathbf{F}(\mathbf{U})}{\partial x} = 0, \tag{4.7}$$

where $\mathbf{U} = \mathbf{U}(t, x)$ is the conservative state, $\mathbf{F}(\mathbf{U})$ is the flux, is *hyperbolic* if the Jacobian matrix of $\mathbf{F}(\mathbf{U})$ with respect to $\mathbf{U}$ has real eigenvalues and a set of associated eigenvectors which form a basis of $\mathbb{R}^d$, where d is the dimension of vector $\mathbf{U}$.

For the system (4.4) the Jacobian matrix $D\mathbf{F}(\mathbf{U})$ has form:

$$D\mathbf{F}(\mathbf{U}) = \begin{pmatrix} u & h & 0 & 0 \\ g + \dfrac{\lambda}{3}\dfrac{\eta^2}{h^3} & u & -\dfrac{\lambda}{3}\left(\dfrac{2\eta}{h} - 1\right) & 0 \\ 0 & 0 & u & 0 \\ 0 & 0 & 0 & u \end{pmatrix}. \tag{4.8}$$

All eigenvalues of (4.8) are real, and one is multiple. Indeed,

$$\det(D\mathbf{F} - s_i\mathbb{I}) = 0,$$

this leads to the following eigenvalues s_i:

$$s_{1,2}(\mathbf{U}) = u, \quad s_{3,4}(\mathbf{U}) = u \pm \sqrt{gh + \frac{\lambda}{3}\frac{\eta^2}{h^2}}. \tag{4.9}$$

The corresponding eigenvectors are given by

$$\mathbf{q}_1 = \begin{pmatrix} 0 \\ 0 \\ 0 \\ 1 \end{pmatrix}, \mathbf{q}_2 = \begin{pmatrix} \lambda(h-2\eta)/3 \\ 0 \\ gh + \lambda\eta^2/(3h^2) \\ 0 \end{pmatrix}, \mathbf{q}_{3,4} = \begin{pmatrix} 1 \\ \pm\sqrt{gh + \lambda\eta^2/(3h^2)} \\ 0 \\ 0 \end{pmatrix}. \tag{4.10}$$

We conclude that the system is hyperbolic since the set of eigenvectors is complete. Moreover $\nabla_{\mathbf{U}}s_{1,2} \cdot \mathbf{q}_{1,2} = 0$, where $\nabla_{\mathbf{U}}$ is the gradient with respect to dependent variables $\mathbf{U} = (h, u, \eta, w)$. It follows that the corresponding characteristic field is linear degenerated. For the other characteristics we have $\nabla_{\mathbf{U}}s_{3,4} \cdot \mathbf{q}_{3,4} < 0$ and the fields associated with $s_{3,4}$ are genuinely non-linear.

For hyperbolic equations, according to the system structure, solutions can be decomposed on inflow and outflow parts. Indeed, one can see it in the linear case. In this case, the matrix $D\mathbf{F}(\mathbf{U})$ is constant with constant eigenvalues s_i. Therefore the characteristics defined as $dx/dt = s_i$ are straight lines. The matrix $D\mathbf{F}(\mathbf{U})$ can be diagonalized in this case. Denoting by $D = diag(s_i)$ a diagonal matrix whose entries are the eigenvalues s_i, we obtain from (4.7)

$$\frac{\partial \mathbf{W}}{\partial t} + D\frac{\partial \mathbf{W}}{\partial x} = 0, \quad \mathbf{W} = L^\ell U,$$

where L^ℓ is a matrix whose row vectors are the left eigenvectors of $D\mathbf{F}(\mathbf{U})$. The part of the solution $\mathbf{W}$, constant along the characteristics with positive slopes ($s_i > 0$) define inflow part, and characteristics with negative slopes ($s_i < 0$) define outflow part, respectively. This knowledge allows deducing the number of boundary conditions. Only inflow part needs to be imposed at the left boundary and outflow at right one; initial conditions define the rest of the information. For the nonlinear case, we have similar conclusions when the system is endowed with a coordinate system of Riemann invariants. For example, in the case of nonlinear shallow water (Saint-Venant) equations nonlinear Riemann invariants can be constructed. Unfortunately, it is not always the case for a general nonlinear system.

First of all, we linearize the system (4.4) around the constant flow state $h = \tilde{h} + H_0$, $u = \tilde{u} + U_0$, $\eta = \tilde{\eta} + H_0$, $w = \tilde{w}$, in order to find the linear Riemann invariants. One obtains

$$\frac{\partial \mathbf{V}}{\partial t} + A^{dim}\frac{\partial \mathbf{V}}{\partial x} = \mathbf{S}(\mathbf{V}), \tag{4.11}$$

where $V = (\tilde{h}, \tilde{u}, \tilde{\eta}, \tilde{w})$ is a vector of the perturbations, $S(\mathbf{V}) = (0, 0, w, \lambda(\eta-h)/H_0^2)^\top$, and

A^{dim} is a square matrix defined as

$$A^{dim} = \begin{pmatrix} U_0 & 1 & 0 & 0 \\ g + \dfrac{\lambda}{3H_0} & 1 & -\dfrac{\lambda}{3H_0} & 0 \\ 0 & 0 & U_0 & 0 \\ 0 & 0 & 0 & U_0 \end{pmatrix}.$$ (4.12)

The system is simplified by elimination of h_t from the last three equations.

We introduce now nondimensional variables (denoted with primes),

$$h' = \frac{\tilde{h}}{H_0}, \quad u' = \frac{\tilde{u}}{V_0}, \quad \eta' = \frac{\tilde{\eta}}{H_0}, \quad x' = \frac{x}{L},$$

where L is the characteristic horizontal length of the flow. From the equations (4.11) we then conclude the following dimensionless form:

$$w' = \frac{L}{H_0 V_0}\tilde{w}, \quad \lambda' = \frac{\lambda}{V_0^2}, \quad t' = \frac{V_0}{L}t.$$

The nondimensional system takes the form:

$$\frac{\partial \mathbf{V}'}{\partial t'} + A\frac{\partial \mathbf{V}'}{\partial x'} = \mathbf{S}'(\mathbf{V}'),$$ (4.13)

with unknown vector $V' = (h', u', \eta', w')$ and source term $\mathbf{S}'(\mathbf{V}') = (0, 0, w, -\lambda'(\eta' - h')/\mu^2)$. To simplify the notation, primes are dropped further. The matrix A reads

$$A = \begin{pmatrix} \nu & 1 & 0 & 0 \\ \dfrac{1}{F^2} + \dfrac{\lambda}{3} & \nu & -\dfrac{\lambda}{3} & 0 \\ 0 & 0 & \nu & 0 \\ 0 & 0 & 0 & \nu \end{pmatrix}$$ (4.14)

The nondimensional quantities F and μ are respectively a Froude number, and a shallow water parameter:

$$F^2 = \frac{V_0^2}{gH_0}, \quad \mu^2 = \frac{H_0^2}{L^2}.$$

Note that the velocity is scaled with V_0 which is different from the equilibrium velocity U_0, and $\nu = U_0/V_0$ stands for the velocity ratio. In the linear case, this choice is optional, and in the sake of simplicity we take $\nu = 1$. However, the assumption $\nu \neq 1$ is useful for the PML equations construction.

We consider now the homogeneous system associated with (4.13)

$$\frac{\partial \mathbf{V}}{\partial t} + A\frac{\partial \mathbf{V}}{\partial x} = 0.$$ (4.15)

To construct the Riemann invariants in the linear case we need to derive the left eigenvectors of the matrix A (4.14). The eigenvalues are given by

$$s_{1,2} = 1, \quad s_{3,4} = 1 \pm \sqrt{\frac{1}{F^2} + \frac{\lambda}{3}}.$$ (4.16)

We have $s_{1,2,3} > 0$, and thus three characteristics propagate to the right, and $s_4 < 0$ defines one left-propagating characteristic. The corresponding left eigenvectors are written as

$$\mathbf{q}_1^\ell = \begin{pmatrix} 0 \\ 0 \\ 1 \\ 0 \end{pmatrix}, \quad \mathbf{q}_2^\ell = \begin{pmatrix} 0 \\ 0 \\ 0 \\ 1 \end{pmatrix}, \quad \mathbf{q}_{3,4}^\ell = \begin{pmatrix} -\left(\dfrac{1}{F^2} + \dfrac{\lambda}{3}\right) \\ \mp\sqrt{\dfrac{1}{F^2} + \dfrac{\lambda}{3}} \\ \dfrac{\lambda}{3} \\ 0 \end{pmatrix}. \tag{4.17}$$

The left eigenvectors form a matrix of change of variables. A standard diagonalization procedure yields:

$$(\partial_t + \partial_x)\, \eta = 0, \quad (\partial_t + \partial_x)\, w = 0,$$

$$(\partial_t + s_3 \partial_x)\left(\left(\frac{1}{F^2} + \frac{\lambda}{3}\right)h - \sqrt{-\frac{1}{F^2} + \frac{\lambda}{3}}\, u - \frac{\lambda}{3}\eta\right) = 0,$$

$$(\partial_t + s_4 \partial_x)\left(\left(\frac{1}{F^2} + \frac{\lambda}{3}\right)h + \sqrt{\frac{1}{F^2} + \frac{\lambda}{3}}\, u - \frac{\lambda}{3}\eta\right) = 0,$$

where the differential operators above correspond to the operators along the characteristic directions of the linear system. We conclude that the values $r_\eta = \eta$, $r_w = w$ and

$$r = \left(\frac{1}{F^2} + \frac{\lambda}{3}\right)h + \sqrt{\frac{1}{F^2} + \frac{\lambda}{3}}\, u - \frac{\lambda}{3}\eta \tag{4.18}$$

are constant along the characteristics corresponding to the right-propagating waves, and

$$l = \left(\frac{1}{F^2} + \frac{\lambda}{3}\right)h - \sqrt{\frac{1}{F^2} + \frac{\lambda}{3}}\, u - \frac{\lambda}{3}\eta \tag{4.19}$$

is constant along the left-propagating one.

Therefore, one finds that r, η, w define the inflow part, and l the outflow part. In order to impose boundary conditions correctly, only variables transported from the boundaries towards the interior can be freely imposed. The remaining variables will depend on this information. One can choose the Dirichlet boundary conditions for r, η, w at the left boundary, and for l at the right one.

For the linear homogeneous system, such conditions define incoming and outgoing waves exactly, and no reflection is observed. We demonstrate this numerically below, once the numerical resolution algorithm is presented. However, when the dispersion is taken into account by adding the source terms, this approach is not valid for all range of frequencies. For high-frequency range, the source terms are almost negligible. But, for the main range of interest, low-frequency range, it is not the case, and another more robust technique should be applied.

4.3 PML equations construction

Now let us focus on another more general technique for the boundary conditions which is referred to as Perfectly Matched Layers (PML). We will see that this approach can be applied to the non-homogeneous system and the nonlinear equations as well. As it was discussed in the introduction, the idea of this method is to add absorbing layers around the computational domain, where the original set of equations is modified in such a way that the waves decay in all directions. Generally, the PML technique is applied to linear systems. We are searching for the solution of the initial problem with initial data compactly supported on $[x_\ell, x_r]$. The solution is decomposed into waves going in different directions (in the present one-dimensional case to the left and the right), and then the equations are modified in a right or left thin layer, according to the wave characteristics.

We consider plane wave solutions to the system (4.15) of the form (i is the imaginary unit)

$$\mathbf{V} = \begin{pmatrix} h \\ u \\ \eta \\ w \end{pmatrix} = \mathbf{q}^j e^{i\omega(t - s_j x)} = \begin{pmatrix} q_1^j \\ q_2^j \\ q_3^j \\ q_4^j \end{pmatrix} e^{i\omega(t - s_j x)}.$$

The representation of the solution in such a form leads to the definition of s_i as inverse quantities of the eigenvalues (4.16) ($\nu \neq 1$ is supposed now):

$$s_{1,2} = \frac{1}{\nu}, \quad s_{3,4} = \frac{1}{\nu \pm \sqrt{\dfrac{1}{F^2} + \dfrac{\lambda}{3}}}.$$

The vectors $\mathbf{q}^j$ are the full set of corresponding eigenvectors defined as

$$(a) \ \mathbf{q}^1 = \begin{pmatrix} \dfrac{\lambda}{3} \\ 0 \\ \dfrac{1}{F^2} + \dfrac{\lambda}{3} \\ 0 \end{pmatrix} \quad (b) \ \mathbf{q}^2 = \begin{pmatrix} 0 \\ 0 \\ 0 \\ 1 \end{pmatrix} \quad (c) \ \mathbf{q}^{3,4} = \begin{pmatrix} \pm 1 \\ \sqrt{\dfrac{1}{F^2} + \dfrac{\lambda}{3}} \\ 0 \\ 0 \end{pmatrix}. \quad (4.20)$$

Three eigenvalues $\lambda_{1,2,3}$ correspond to the right going waves, and the last one to the only wave propagating to the left. This leads to different equations in the right and left thin layers.

4.3.1 Construction of absorbing layer equations

We add now into the computational domain $[x_\ell, x_r]$ finite width intervals $(x_\ell, x_\ell + \delta_x)$ on the left and $(x_r - \delta_x, x_r)$ on the right, where the media properties are modified in such a way that the waves propagate into those layers with amplitude decay and reflections as small as possible. Following the PML construction approach, presented in [2], we define a solution ansatz. We then modify the equations in order to make this new ansatz a solution of the problem.

To construct PML equations in the right absorbing layer, we modify the plane wave solution corresponding to three rightward propagating waves. Thus we consider the following ansatz

$$
\begin{pmatrix} h \\ u \\ \eta \\ w \end{pmatrix} = \begin{pmatrix} 0 \\ 0 \\ 0 \\ 1 + k_1(x) \end{pmatrix} e^{i\omega\left(t - \frac{x}{\nu}\right)} exp\left\{ - \int_0^{x>0} \sigma^R(\xi)d\xi \right\}, \tag{4.21}
$$

$$
\begin{pmatrix} h \\ u \\ \eta \\ w \end{pmatrix} = \begin{pmatrix} \frac{\lambda}{3}\left(1 + f_2(x)\right) \\ 0 \\ \left(\frac{1}{F^2} + \frac{\lambda}{3}\right)\left(1 + h_2(x)\right) \\ 0 \end{pmatrix} e^{i\omega\left(t - \frac{x}{\nu}\right)} exp\left\{ - \int_0^{x>0} \sigma^R(\xi)d\xi \right\} \tag{4.22}
$$

and

$$
\begin{pmatrix} h \\ u \\ \eta \\ w \end{pmatrix} = \begin{pmatrix} -\Lambda(1 + f_3(x)) \\ (\Lambda\nu - 1)(1 + g_3(x)) \\ 0 \\ 0 \end{pmatrix} e^{i\omega(t - \Lambda x)} exp\left\{ - \int_0^{x>0} \sigma^R(\xi)d\xi \right\}, \tag{4.23}
$$

where $\sigma^R(x)$ is positive a function of x and Λ denotes the eigenvalue

$$
\Lambda = \frac{1}{\nu + \sqrt{\dfrac{1}{F^2} + \dfrac{\lambda}{3}}}.
$$

A modulation of wave vectors by unknown functions f_j, g_j, h_j, k_j, $(j = 1, .., 3)$ should be defined. For this, we based on the assumption that the amplitude decay is independent on the frequency of the waves incoming in the absorbing layer.

It should be pointed out that in general, we must consider an ansatz which is an arbitrary linear combination of solutions put forward in (4.21)-(4.23). However, since we consider a linear system, we can resolve three systems independently. More explicitly, the form of the ansatzes (4.21) - (4.23) allows to split the system into three independent subsystems for $w(t, x)$ (coming from the last equation of the homogeneous system (4.15)), (h, η) (first and third equations) and (h, u) (first and second equations).

Subsystem $w(t, x)$

Firstly let us consider the substitution of (4.21) into (4.15). Only the last scalar equation for $w(t, x)$ is not trivial:

$$
w_t + U_0 w_x = S_4^w e^{i\omega\left(t - \frac{x}{\nu}\right)} exp\left\{ - \int_0^{x>0} \sigma^R(\xi)d\xi \right\} = \tilde{S}_4^w,
$$

where

$$
S_4^w = (1 + k_1(x))i\omega + \nu\left((1 + k_1(x))\left(-\frac{i\omega}{\nu} - \sigma^R\right) + k_1'(x)\right) = -\nu(1 + k_1(x))\sigma^R + k_1'(x).
$$

It is necessary to provide PML equations guaranteeing the absorption of waves of all frequencies. That is to say, S_4^w must be cast in a form that precludes the explicit appearance of ω, Λ, U_0 and only depends on the unknown functions h, u, η, w and σ^R. This leads to the choice $k_1(x) = 0$.

By referring to (4.20) (b), we obtain

$$\tilde{S}_4^w = -\nu\sigma^R(x)w.$$

Subsystem (h, u)

The substitution of (4.23) into the initial linear system gives the following subsystem for (h, u):

$$\begin{cases} h_t + \nu h_x + u_x = S_1^{hu} e^{i\omega(t-\Lambda x)} exp\left\{-\int_0^{x>0}\sigma^R(\xi)d\xi\right\} = \tilde{S}_1^{hu}, \\ \\ u_t + \left(\dfrac{1}{F^2} + \dfrac{\lambda}{3}\right)h_x + \nu u_x - \dfrac{\lambda}{3}\eta_x = S_2^{hu} e^{i\omega(t-\Lambda x)} exp\left\{-\int_0^{x>0}\sigma^R(\xi)d\xi\right\} = \tilde{S}_2^{hu}, \end{cases}$$
$$(4.24)$$

with

$$S_1^{hu} = -\Lambda^2\left(f_3(x) - g_3(x)\right) + \\ + \Lambda\left(\nu\sigma^R(f_3(x) - g_3(x)) - i\omega(f_3(x) - g_3(x)) - \nu(f_3'(x) - g_3'(x))\right) + \\ + \sigma^R(1 + g_3(x)) - g_3'(x), \quad (4.25)$$

$$S_2^{hu} = i\omega\Lambda^2\nu^2(f_3(x) - g_3(x)) + \\ + \Lambda\left(\nu^2(f_3(x) - g_3(x))\sigma^R + i\omega(f_3(x) - g_3(x))(1 - 2\nu)\right) + \\ + \nu\sigma^R(g_3(x) - 2f_3(x) - 1) + \dfrac{1 + f_3(x)}{\Lambda}\sigma^R. \quad (4.26)$$

We must express S_1^{hu}, S_2^{hu} again only in terms of unknown functions and σ^R. We first require the coefficients of Λ^2 in (4.25) to vanish, which implies $f_3 = g_3$, $\forall x \in [x_\ell, x_r]$. One obtains

$$S_1^{hu} = \sigma^R(1 + g_3(x)) - g_3'(x).$$

Therefore (with the choice $g_3 = 0$):

$$\tilde{S}_1^{hu} = -\sigma^R e^{i\omega(t-\Lambda x)} exp\left\{-\int_0^{x>0}\sigma^R(\xi)d\xi\right\} = -\sigma^R h. \quad (4.27)$$

The last equality is established by comparison with (4.20) (c).

Plugging the found condition $f_3(x) = g_3(x) = 0$ into (4.26) leads to

$$\tilde{S}_2^{hu} = -\sigma^R\dfrac{\Lambda\nu - 1}{\Lambda}e^{i\omega(t-\Lambda x)} exp\left\{-\int_0^{x>0}\sigma^R(\xi)d\xi\right\} = -\sigma^R u.$$

Subsystem (h, η)

Now we consider in the same manner the last (h, η) subsystem. Substituting the corresponding ansatz (4.22) into (4.15) we have

$$
\begin{cases}
h_t + \nu h_x + u_x = S_1^{h\eta} e^{i\omega(t-x/U_0)} e^{i\omega\left(t-\frac{x}{\nu}\right)} exp\left\{ -\int_0^{x>0} \sigma_x^R(\xi)d\xi \right\} = \tilde{S}_1^{h\eta}, \\[3mm]
u_t + \left(g + \dfrac{\bar{\lambda}}{H_0}\right) h_x + \nu u_x - \dfrac{\bar{\lambda}}{H_0}\eta_x = S_2^{h\eta} e^{i\omega\left(t-\frac{x}{\nu}\right)} exp\left\{ -\int_0^{x>0} \sigma_x^R(\xi)d\xi \right\} = \tilde{S}_2^{h\eta}, \\[3mm]
\eta_t + \nu\eta_x = S_3^{h\eta} e^{i\omega\left(t-\frac{x}{\nu}\right)} exp\left\{ -\int_0^{x>0} \sigma_x^R(\xi)d\xi \right\} = \tilde{S}_3^{h\eta},
\end{cases}
\tag{4.28}
$$

where

$$
S_1^{h\eta} = -\frac{\lambda}{3}\left(\nu(1 + f_2(x))\sigma^R + f_2'(x)\right),
\tag{4.29}
$$

$$
S_2^{h\eta} = -\frac{\lambda}{3}\left(\frac{1}{F^2} + \frac{\lambda}{3}\right)\left(\left(\frac{i\omega}{\nu} + \sigma^R\right)(f_2(x) - h_2(x)) - (f_2'(x) - h_2'(x))\right),
\tag{4.30}
$$

$$
S_3^{h\eta} = -\nu\left(\left(\frac{1}{F^2} + \frac{\lambda}{3}\right)(1 + h_2(x))\sigma^R - \left(\frac{1}{F^2} + \frac{\lambda}{3}\right)h_2'(x)\right).
\tag{4.31}
$$

Again, one needs to get the expressions only in terms of the unknown function and σ^R. It implies that $f_2 \equiv g_2 \equiv 0$. Thus we obtain $S_2^{h\eta} = 0$, and therefore $\tilde{S}_2^{h\eta} = 0$. Hence, we get

$$
S_1^{h\eta} = -\nu\frac{\lambda}{3}\sigma^R, \quad \tilde{S}_1^{h\eta} = -\nu\frac{\lambda}{3}\sigma^R e^{i\omega\left(t-\frac{x}{\nu}\right)} exp\left\{ -\int_0^{x>0} \sigma_x^R(\xi)d\xi \right\} = -\nu\sigma^R h,
$$

$$
S_3^{h\eta} = -\nu\left(\frac{1}{F^2} + \frac{\lambda}{3}\right), \quad \tilde{S}_3^{h\eta} = -\nu\left(\frac{1}{F^2} + \frac{\lambda}{3}\right)e^{i\omega\left(t-\frac{x}{\nu}\right)} exp\left\{ -\int_0^{x>0} \sigma_x^R(\xi)d\xi \right\} = -\nu\sigma^R\eta,
$$

Finally, the modified system reads:

$$
\begin{cases}
h_t + \nu h_x + u_x = -\sigma^R h, \\[3mm]
u_t + \left(\dfrac{1}{F^2} + \dfrac{\lambda}{3}\right)h_x + \nu u_x - \dfrac{\lambda}{3}\eta_x = -\sigma^R u, \\[3mm]
\eta_t + \nu\eta_x = w - \nu\sigma^R\eta, \\[3mm]
w_t + \nu w_x = -\dfrac{\lambda}{\mu^2}(\eta - h) - \nu\sigma^R w.
\end{cases}
\tag{4.32}
$$

By construction, the waves propagate with amplitude decay in the layer $(1, \delta_x > 0)$, when an appropriate positive function σ^R is chosen.

We consider now the part of the solution corresponding to the left-propagating waves. The PML equations are constructed similarly. We obtain almost the same ansatz as (4.23) for the modulated solution

$$
\begin{pmatrix} h \\ u \\ \eta \\ w \end{pmatrix} = \begin{pmatrix} -M(1 + f_3(x)) \\ (M\nu - 1)(1 + g_3(x)) \\ 0 \\ 0 \end{pmatrix} e^{i\omega(t-Mx)} exp\left\{ -\int_{x<0}^0 \sigma^L(\xi)d\xi \right\},
\tag{4.33}
$$

with the only difference that M is now given by:

$$M = \frac{1}{\nu - \sqrt{\dfrac{1}{F^2} + \dfrac{\lambda}{3}}}.$$

As a result, the strategy is similar to the one employed for the subsystem (h, u) considered above. In contrast, the sign of the derivative of $\left(-\displaystyle\int_{x<0}^{0} \sigma^L(\xi) d\xi \right)$ with respect to the integral limit x is positive due to the integration sense.

Only the two first component of the eigenvector are not zero, which leads to modifications in the two first equations only. The resulting system reads as follows:

$$\begin{cases} h_t + \nu h_x + u_x = -\sigma^L h, \\[2mm] u_t + \left(\dfrac{1}{F^2} + \dfrac{\lambda}{3} \right) h_x + \nu u_x - \dfrac{\lambda}{3} \eta_x = -\sigma^L u, \\[2mm] \eta_t + \nu \eta_x = w, \\[2mm] w_t + \nu w_x = -\dfrac{\lambda}{\mu^2}(\eta - h). \end{cases} \tag{4.34}$$

The assumption $\nu \neq 1$ is of interest only for the treatment of the non-linear case. We will suppose that the flow is stationary at the infinity (as in the case of the solitary wave propagation). In particular, it means that only the first two equations need to be modified in both right and left layers. Thus, without loss of generality, we suppose once again $\nu = 1$ for the linear case.

4.4 Linear case : numerical implementation

Gathering the left and right PML systems (4.34), (4.32), we are left with the study of the following problem

$$\frac{\partial \mathbf{V}}{\partial t} + \frac{\partial \mathbf{F}(\mathbf{V})}{\partial x} = \mathbf{S}^\sigma(\mathbf{V}), \tag{4.35}$$

with the unknown vector $\mathbf{V} = (h, u, \eta, w)^\top$, the fluxes

$$\mathbf{F} = \left(h + u, \left(\frac{1}{F^2} + \frac{\lambda}{3} \right) h + u - \frac{\lambda}{3} \eta, \eta, w \right)^\top,$$

and source terms $\mathbf{S}^\sigma = (-(\sigma^L + \sigma^R)h, -(\sigma^L + \sigma^R)u, -\sigma^R \eta + w, -\sigma^R w - \lambda(\eta - h)/\mu^2)^\top$.

Algorithm

For the discretization, we use a second order splitting method with a Crank-Nicolson scheme for the source terms. The numerical resolution consists of three steps. We use the Strang splitting strategy in time [129]; the hyperbolic part is solved by the Godunov-type. We decompose the solution operator $S(\cdot)$ associated with the discretization of the system (4.35) as follows

$$S(\delta t) = S_1(\delta t/2) S_2(\delta t) S_1(\delta t/2)$$

Numerical animations are available https://www.math.univ-toulouse.fr/~mkazakov

where S_1 corresponds to the discretization of ordinary differential equations (ODE) of the first order with respect to t with Crank-Nicolson scheme:

$$\frac{\partial \mathbf{V}}{\partial t} = \mathbf{S}^\sigma(\mathbf{V}). \tag{4.36}$$

In [49] this system of ODE is solved exactly, since it is relatively simple, the two first equations being homogeneous. In the present case, the modified system has additional source terms, and an implicit numerical scheme is used. However, there is no need to inverse a matrix at each iteration, since explicit formulas can be found for all variables.

The operator S_2 denotes the Godunov-type second-order scheme for the homogeneous system

$$\frac{\partial \mathbf{V}}{\partial t} + \frac{\partial \mathbf{F}(\mathbf{V})}{\partial x} = \mathbf{0}, \tag{4.37}$$

where we use Rusanov numerical flux definition together with $MUSCL$ reconstruction, in order to obtain a second order scheme in space. The second order time scheme is implemented using the Heun method.

For the stability of the present scheme, a CFL condition must be satisfied. The estimation for the time step comes from hyperbolic part resolution. Implicit scheme for ODE part is unconditionally stable. We must respect the following condition

$$\delta t < CFL \frac{\delta x}{\max\limits_{i}(s_i)},$$

where the eigenvalues s_i are defined by (4.16).

Initial data

The variables initialization should be consistent with the approach used for the model derivation ([49]). The assumptions made when the new variables $\eta(t,x)$, $w(t,x)$ were introduced should be satisfied when setting the initial conditions.

More precisely, in the equilibrium we have $\eta = h$, and this must be respected in the initial conditions. To define w we use the third equation of the system. Notably, if $h(t,x)$, $u(t,x)$ are given at initial time as

$$\begin{aligned} h(0,x) &= h_0(x), \\ u(0,x) &= u_0(x), \end{aligned} \tag{4.38}$$

thus, $\eta(t,x)$ and $w(t,x)$ are initialized as follows,

$$\begin{aligned} \eta(0,x) &= h_0(x), \\ w(0,x) &= -h_0(x)\frac{\partial}{\partial x}(u_0(x)). \end{aligned} \tag{4.39}$$

Boundary conditions

Once the PML equations are used, the boundary conditions might be chosen arbitrarily. One can use linearized Riemann invariant or simply Neumann boundary conditions.
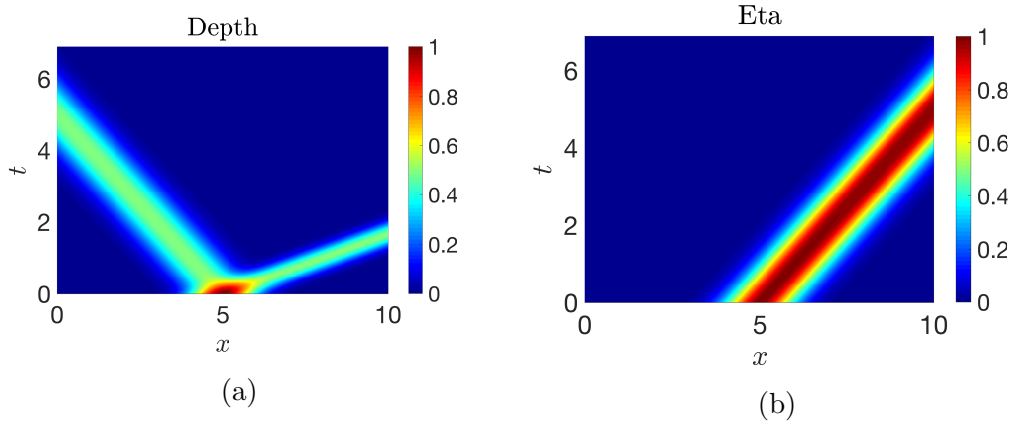
Figure 4.1: (x, t)-diagram for the depth $h(t, x)$ and $\eta(t, x)$ evolutions for non-dispersive problem ($\lambda = 0$). Initialization: $h_0(x)$ – Gaussian distribution, $u_0(x)$ – zero initial data. No PML equations used.

Numerical tests

We begin with numerical test considering the propagation of initial Gaussian distribution for water depth $h(t, x)$ with zero velocity,

$$h(0, x) = e^{-(x-D)^2}, \quad D = \text{const},$$
$$u(0, x) = 0. \tag{4.40}$$

We first set $\lambda = 0$, so there is no connection between the subsystems (h, u) and (η, w). As a result, there is no dispersion. The evolution of the water depth $h(t, x)$ describes a bi-directional wave propagation, just as in the case of nonlinear shallow water equations, whereas $\eta(t, x)$ is simply transported (see Figure 4.1). The right-propagating part of the solution moves faster since the equations are linearized around a constant flow with a positive velocity.

The parameters used for the first test are the following

$$x_\ell = 0, \quad x_r = 10,$$
$$D = 5, \tag{4.41}$$
$$CFL = 0.5, \quad \delta x = 0.02.$$

The Riemann invariants are used to impose boundary conditions as described above. The PML equations are not needed since the Riemann invariants r, l ((4.18), (4.19)) correspond to the left- and right- propagating waves exactly. As can be seen in the figure 4.2, no reflection is observed.

Now, we turn to a dispersive case. We set $\lambda = 1000$ for a good approximation of the Green-Naghdi dispersive relation. We set the dispersive parameter $\mu = 0.25$ (in the previous test for $\lambda = 0$ the value of μ is not needed). The smaller its value is, the closer the behaviour of propagating waves to the one obtained in the previous non-dispersive test. We observe now the dispersive effects appearing in the problem: the phase velocity of a wave depends now on its frequency, and more than just two waves propagate in both directions. Moreover, $\eta(t, x)$ is now relaxed to $h(t, x)$, i.e. the evolution of $\eta(t, x)$ coincides with to the
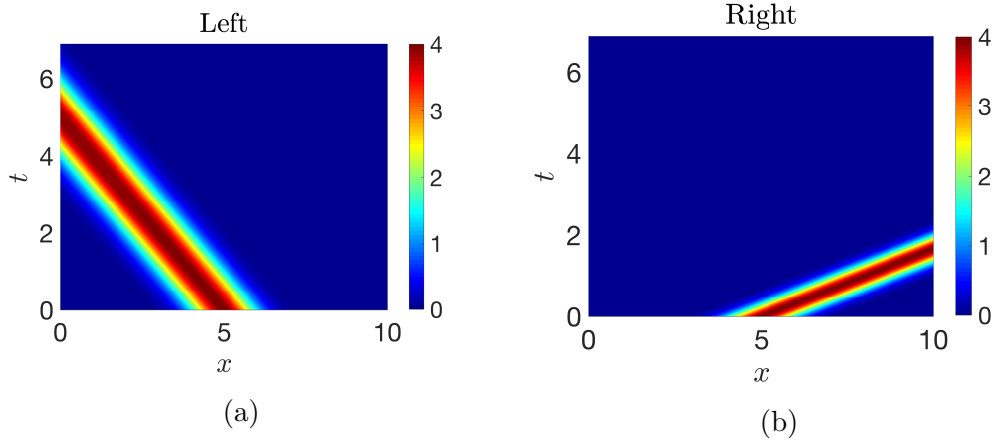
Figure 4.2: Riemann invariants propagation for non dispersive problem ($\lambda = 0$). Initialization: $h_0(x)$ – Gaussian distribution, $u_0(x)$ zero initial data. No PML used.
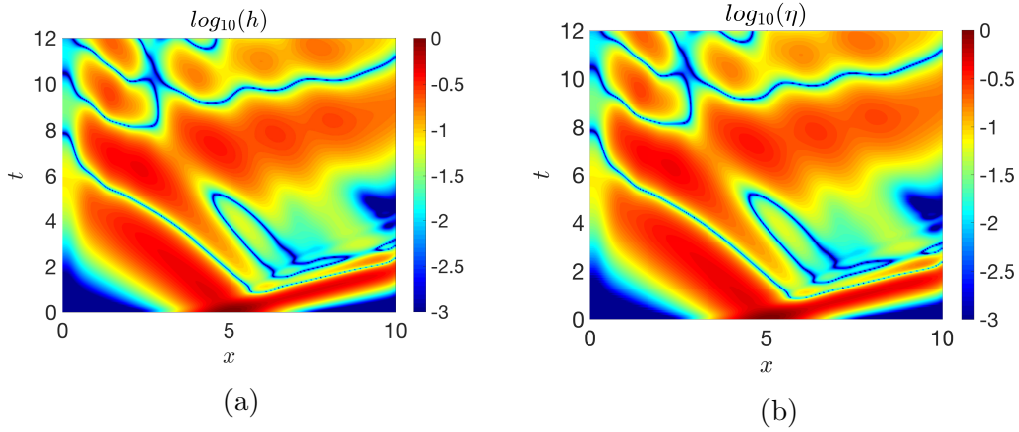

Figure 4.3: Evolution of $log_{10}(h(t, x))$ and $log_{10}(\eta(t, x))$ for dispersive problem ($\lambda = 1000$, $\mu = 0.25$). Initialization: $h_0(x)$ – Gaussian distribution, $u_0(x)$ – zero initial data. No PML used.

evolution of $h(t, x)$. In Figure 4.3, the (x, t) diagrams for the waves propagation are given. We present the results in a logarithmic scale in order to see the wave reflections properly. On the right boundary, we observe a form of stagnation effect. It can be explained by both the constant steady flow used as an equilibrium speed for the linearization and the boundary reflections. Besides, it is not clear whether the reflection on the left boundary comes from a fallible procedure for the boundary conditions, or from a residual dispersive waves propagation coming from an initial perturbation moving with the constant flow to the right. However, the Riemann invariants are not constant along the characteristics any more due to the presence of the source terms (see Figure 4.4). Moreover, the reflection is observed more clearly for both left and right propagating waves.

Moreover, the additional test shows that the reflections are observed more clearly if a smaller value is chosen for μ (see figure 4.5). In this case, the behaviour is closer to non-dispersive wave propagation, and larger wave amplitudes are observed.

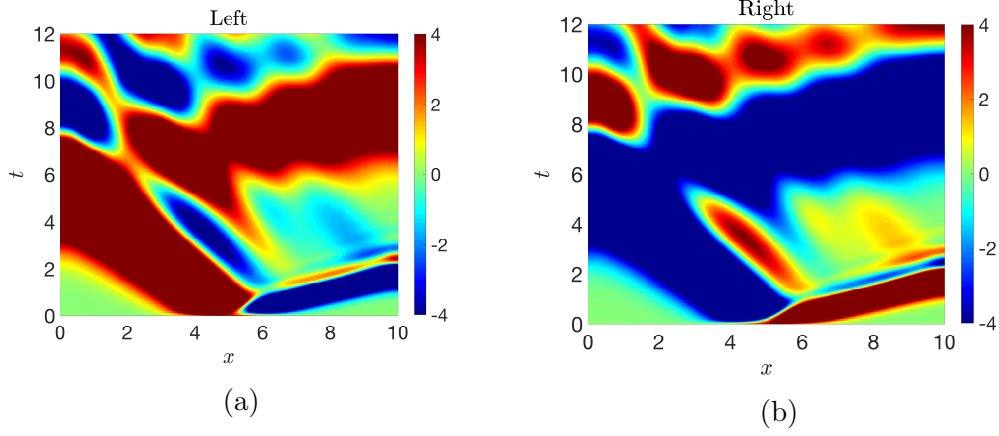We turn now to the tests of the PML equations derived in the previous section. We first

Figure 4.4: Riemann invariants propagation for dispersive problem ($\lambda = 1000$, $\mu = 0.25$). Initialization: $h_0(x)$ – Gaussian distribution, $u_0(x)$ zero initial data. No PML used.
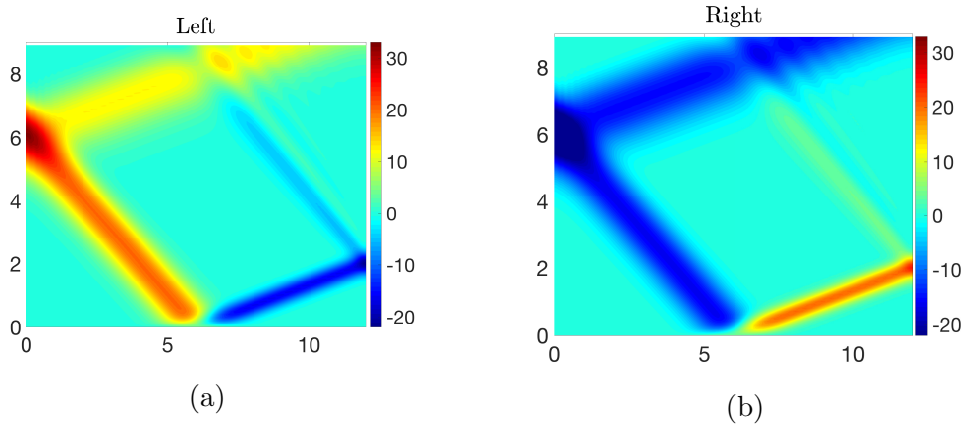

Figure 4.5: Riemann invariants propagation for dispersive problem ($\lambda = 1000$, $\mu = 0.01$). Initialization: $h_0(x)$ – Gaussian distribution, $u_0(x)$ zero initial data. No PML used.
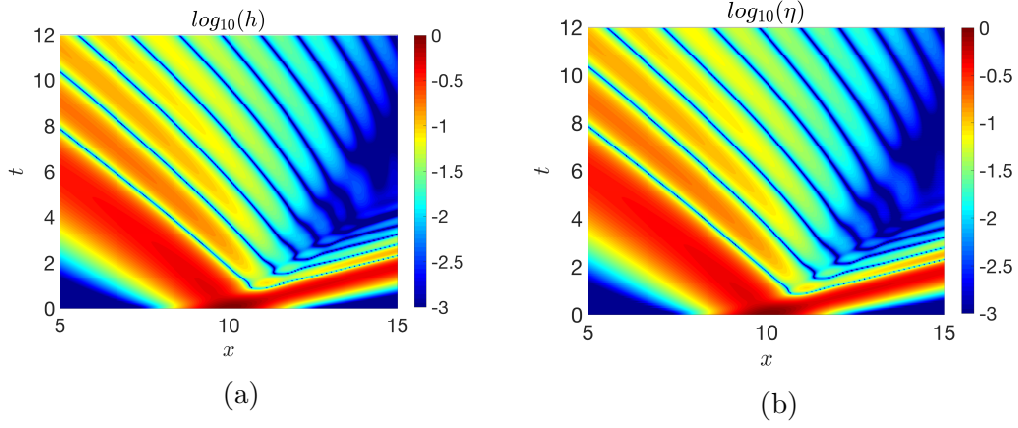
Figure 4.6: PML application: Evolution of $log_{10}(h(t,x))$ and $log_{10}(\eta(t,x))$ evolution for dispersive problem ($\lambda = 1000$). Initialization: $h_0(x)$ – Gaussian distribution, $u_0(x)$ – zero initial data

perform the same numerical test as one considered just before. The initial data are chosen as (4.40). We add in the calculation domain layers of width $\delta_x = 5$ in both directions. All parameters are the same as in the previous case, only a larger domain is considered:

$$
\begin{aligned}
x_\ell = 0, \quad x_r = 20, \\
D = 10, \\
CFL = 0.5, \quad \delta x = 0.02, \quad \mu = 0.25.
\end{aligned}
\tag{4.42}
$$

The functions $\sigma^{L,R}$ determine the amplitude decay in the intervals $[x_\ell - \delta_x, x_\ell]$ and $[x_r - \delta_x, x_r]$ respectively, and read as follows

$$
\begin{aligned}
\sigma^L(x) = \min(0, C(x - \delta_x))^p, \\
\sigma^R(x) = \max(0, C(x - \delta_x))^p.
\end{aligned}
\tag{4.43}
$$

This form for $\sigma^{L,R}$ is standard for PML schemes, and we will use those representations for all further tests. For the current test, we set $C = 0.1$, $\delta_x = 5$, $p = 2$. Generally speaking, δ_x might be chosen differently for the left and right layers. It should be noted that the choice of those parameters is based on a proper absorption in the layers. A rigours analysis of the optimal parameter values is left for future research.

The (x, t) diagrams are presented in figure 4.6. We conclude that the reflections observed in the previous case are related to the boundary conditions. The modified system (4.35) gives the desired behaviour on the boundaries, since the amplitudes of outgoing waves decay. The results are presented again in logarithmic scale; the evolution of $h(t, x)$ and $\eta(t, x)$ are plotted for the interval $[5, 15]$ in order to see the correspondence with the cases studied previously. The waves propagate into the layers without reflection.

4.5 Energy estimation

We show now that the use of PML equation leads to a dissipativity of the solution of the problem set on a bounded domain. This leads to a well-posed initial boundary value problem.

First, an energy estimation is established for the solution of the problem set on the infinite domain. We recall the original system (4.13) (primes are dropped):

$$\frac{\partial \mathbf{V}}{\partial t} + A\frac{\partial \mathbf{V}}{\partial x} = \mathbf{S}(\mathbf{V}), \tag{4.44}$$

where the matrix A and the source term S are defined earlier. According to the classical theory developed by Godunov et *al.* [56] (and also by Friedrichs and Lax), this system of conservation laws can be symmetrised using the energy conservation law. To find a symmetrizer for the matrix A, we use the nonlinear energy equation given in [49] and related directly to the Lagrangian (4.3). We obtain the positive definite matrix

$$Z = \begin{pmatrix} \dfrac{1}{F^2} + \dfrac{\lambda}{3} & 0 & -\dfrac{\lambda}{3} & 0 \\[2mm] 0 & 1 & 0 & 0 \\[2mm] -\dfrac{\lambda}{3} & 0 & \dfrac{\lambda}{3} & 0 \\[2mm] 0 & 0 & 0 & \dfrac{\mu^2}{3} \end{pmatrix}.$$

Multiplying the original system by this matrix, we have

$$Z\frac{\partial \mathbf{V}}{\partial t} + ZA\frac{\partial \mathbf{V}}{\partial x} = Z\,\mathbf{S}(\mathbf{V}), \tag{4.45}$$

where the matrix $Z_A = ZA$ is symmetric:

$$Z_A = \begin{pmatrix} \dfrac{1}{F^2} + \dfrac{\lambda}{3} & \dfrac{1}{F^2} + \dfrac{\lambda}{3} & -\dfrac{\lambda}{3} & 0 \\[2mm] \dfrac{1}{F^2} + \dfrac{\lambda}{3} & 1 & -\dfrac{\lambda}{3} & 0 \\[2mm] -\dfrac{\lambda}{3} & -\dfrac{\lambda}{3} & \dfrac{\lambda}{3} & 0 \\[2mm] 0 & 0 & 0 & \dfrac{\mu^2}{3} \end{pmatrix}.$$

Multiplying (4.45) by $V^\top$, one finds the following energy conservation law:

$$\frac{1}{2}\frac{\partial}{\partial t}\mathbf{V}^\top Z\mathbf{V} + \frac{1}{2}\frac{\partial}{\partial x}\mathbf{V}^\top Z_A\mathbf{V} = 0. \tag{4.46}$$

Moreover, the source terms in (4.46) naturally vanish, indeed,

$$Z\,\mathbf{S}(\mathbf{V}) = \big(-\lambda w/3, 0, \lambda w/3, -\lambda(\eta - h)/3\big),$$

which gives $\mathbf{V}^\top Z\,\mathbf{S}(\mathbf{V}) = 0$.

The energy $E(\mathbf{V})$ given by:

$$E(\mathbf{V}) = \frac{1}{2}\mathbf{V}^\top Z\mathbf{V}.$$

is conserved for the problem set on whole space. However, it should dissipate for the one set on a finite interval $[x_\ell, x_r]$. When boundary conditions are imposed at $x = x_\ell$, $x = x_r$ the following condition must be satisfied:

$$\frac{1}{2}\frac{\partial}{\partial t}\int_{x_\ell}^{x_r}\mathbf{V}^\top Z\mathbf{V}\, dx = -\frac{1}{2}\mathbf{V}^\top S\mathbf{V}\Big|_{x_\ell}^{x_r} < 0.$$

It induces restrictions for the boundary conditions choice. For example one of the ways to satisfy this energy inequality is to define the boundary conditions concerning the Riemann invariants found above together with Dirichlet boundary conditions. We can rewrite this inequality as

$$\frac{1}{2}\int_{x_\ell}^{x_r} E(\mathbf{V}(t,x))\, dx \leq \frac{1}{2}\int_{x_\ell}^{x_r} E(\mathbf{V}(0,x))\, dx \tag{4.47}$$

Once we have this estimation for the energy in the interval $[x_\ell, x_r]$, we recall the definition of the solution to the modified PML equations:

$$\mathbf{V}_{PML} = \frac{\mathbf{V}}{\kappa(x)}, \tag{4.48}$$

where $\kappa(x)$ is defined as

$$\kappa(x) = \begin{cases} exp\left\{\int_{x_\ell}^{x_\ell+\delta_x}\sigma(\xi)\, d\xi\right\}, & x_\ell < x < x_\ell + \delta_x, \\[2mm] 1, & x_\ell + \delta_x < x < x_r - \delta_x, \\[2mm] exp\left\{\int_{x_r-\delta_x}^{x_r}\sigma(\xi)\, d\xi\right\}, & x_r - \delta_x < x < x_r. \end{cases} \tag{4.49}$$

The energy estimation in the computational interval $[x_\ell + \delta_x, x_r - \delta_x]$ for the modified solution comes directly. Using the definitions (4.48), (4.49)

$$\int_{x_\ell+\delta_x}^{x_r-\delta_x} E(\kappa(x)\mathbf{V}_{PML}(t,x))\, dx = \int_{x_\ell+\delta_x}^{x_r-\delta_x} E(\mathbf{V}(t,x))\, dx \leq \int_{x_\ell}^{x_r} E(\mathbf{V}(t,x))\, dx \leq$$

$$\leq \int_{x_\ell}^{x_r} E(\mathbf{V}(0,x))\, dx = \int_{x_\ell}^{x_r} E(\kappa(x)\mathbf{V}_{PML}(0,x))\, dx = \int_{x_\ell+\delta_x}^{x_r-\delta_x} E(\kappa(x)\mathbf{V}_{PML}(0,x))\, dx.$$

Positivity of the energy $E(\mathbf{V}(t,x))$ gives the very first inequality, then the estimation (4.47) is used. Because the initial data are compactly supported, we established the last equality. The estimation provides dissipative properties of the PML approach for the linear boundary value problem.

4.6   Toward the nonlinear case: weak nonlinearity

The main issue in the PML construction for the nonlinear case is that the eigenstructure depends on the solution. Therefore it is more complicated to decompose the solution into left and right propagating waves. Thus, in what follows the equations for the absorbing layers in the nonlinear case are written without strict demonstration. However, the construction

of the nonlinear PML equations will be guided by the considerations given next. Let us consider the first equation of the linear system (4.11) (tildes denote the perturbations from the equilibrium state again)

$$\tilde{h}_t + \nu \tilde{h}_x + \tilde{u}_x = -\sigma^{L+R}\tilde{h},$$

where we denote by σ^{L+R} the sum $\sigma^L + \sigma^R$. For the passage to the nonlinear case we suppose that $\nu = 0$, that is to say, the system is linearized at a steady state $h = 1 + \tilde{h}$, $u = 0 + \tilde{u}$. We set $h = 1$ in the equilibrium since we consider nondimensional equations. Thus this equation can be rewritten as

$$(1 + \tilde{h})_t + ((1 + \tilde{h})\tilde{u})_x = -\sigma^{L+R}\tilde{h},$$

where we add the term $\tilde{h}\tilde{u}$, considered relatively small. Hence in the original variables one obtains

$$h_t + (hu)_x = -\sigma^{L+R}(h - 1).$$

Application of such a procedure to the rest of the equations gives finally

$$\begin{cases} h_t + (hu)_x = -\sigma^{L+R}(h - 1), \\[2mm] (hu)_t + \left(hu^2 + \dfrac{h^2}{2F^2} + \dfrac{\lambda}{3}\left(\dfrac{\eta}{h} - 1\right)\eta\right)_x = -\sigma^{L+R}hu, \\[2mm] (h\eta)_t + (hu\eta_x) = hw, \\[2mm] (hw)_t + (huw)_x = -\dfrac{\lambda}{\mu^2}\left(\dfrac{\eta}{h} - 1\right). \end{cases} \tag{4.50}$$

The assumption $\nu = 0$ leads to the absence of modifications in two last equations.

Numerical tests

For the nonlinear case the classical benchmark test for Green-Naghdi equations is solitary wave propagation. Following [49] we use a classical Green-Naghdi solitary wave solution written in the non-dimensional form as initial data,

$$h_{ex} = 1 + \varepsilon \operatorname{sech}^2\left(\frac{\sqrt{3\varepsilon}}{2\mu F S}(x - St - D)\right),$$

$$u_{ex} = S\left(1 - \frac{1}{h_{ex}}\right), \tag{4.51}$$

where F is the Froude number, $\mu = H_0/L$ the dispersive parameter introduced before, $\varepsilon = a/H_0$ the nonlinearity parameter, a the wave amplitude, H_0 the characteristic water depth, and S is a characteristic speed defined as

$$S = \frac{1}{F}\sqrt{1 + \varepsilon}.$$

After $\eta(t, x)$, $w(t, x)$ are initialized as in (4.39). This solution is only an approximate solution of the extended system (4.4). However, the tests in [49] have shown that for
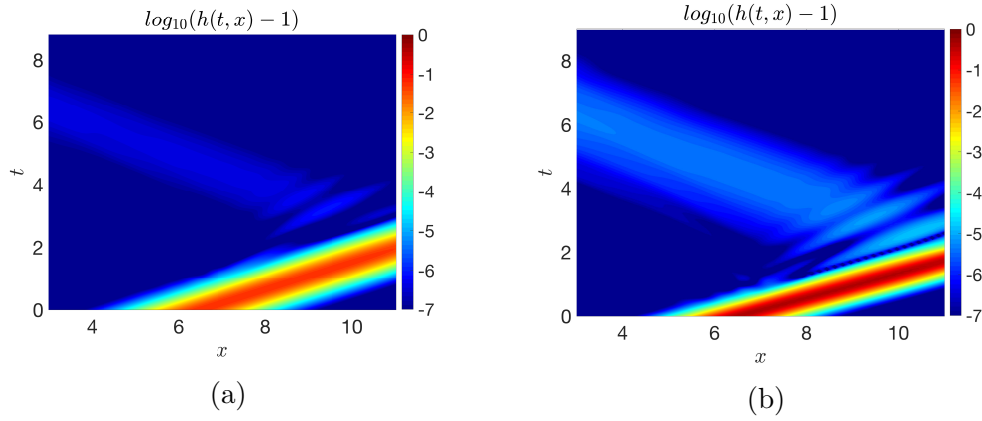
Figure 4.7: Evolution of $log_{10}(|\, h(t,x)-1\, |)$ for solitary wave propagation with nonlinearity parameter (a) $\varepsilon = 0.3$, (b) $\varepsilon = 0.7$.

$\lambda = 1000$ the solution of (4.4) with initial data (4.51) is in good agreement with the Green-Naghdi solitary wave (only a small phase difference has been observed). However, the current model admits a solitary wave solution as well; it will be shown in the Annex, Chapter A.

We perform the test for different initial nonlinearities of the solitary wave. The resulted plots are given in the Figure 4.7 for the intermediate value of nonlinearity ($\varepsilon = 0.3$) and a strongly nonlinear wave ($\varepsilon = 0.7$). For this two tests, we consider the following set of parameters

$\varepsilon = 0.3$	$\varepsilon = 0.7$
$x_\ell = 0$	$x_\ell = 0$
$x_r = 20$	$x_r = 20$
$\delta_x^\ell = 3$	$\delta_x^\ell = 3$
$\delta_x^r = 6$	$\delta_x^r = 8$
$D = 6.5$	$D = 6.5$
$\delta x = 0.02$	$\delta x = 0.02$
$CFL = 0.1$	$CFL = 0.1$
$\mu = 0.1$	$\mu = 0.1$

The different widths of the left and right layers are chosen as soon as the wave is propagating to the right. We observe a small reflection which is more intensive if the case of the strong nonlinearity. For $\varepsilon = 0.3$ the reflection reaches the order of $10^{-6} - 10^{-7}$, and $10^{-5} - 10^{-6}$ for $\varepsilon = 0.7$.

We perform a comparison of the proposed approach with direct application of Neumann boundary conditions. The results are presented in Figure 4.8. We consider the propagation of a solitary wave initially located at $x = 11$ with nonlinearity $\varepsilon = 0.5$. In the first case (Figure 4.8, (a)), we consider a wave propagation interval $[0, 17]$, while the equations are modified in the right interval $[11, 17]$ according to the proposed approach. The second test (Figure 4.8, (b)) is performed on the interval $x \in [0, 11]$ with Neumann boundary condition at $x = 11$. Reflection is observed when the PML equations are used, with an amplitude of

order 0.004, which ranges about 0.8% of initial amplitude. The reflection obtained in the second case is of order 0.12, which corresponds to 24%.

4.7 Wave generation

In this section, we are interested in the application of the obtained PML equations to the simulations of the incoming waves. This question was considered in the previous chapter for the transparent boundary conditions. We follow similar considerations here.

We initially focus on the linear system (4.11) written in the scalar form as

$$
\begin{cases}
h_t + h_x + u_x = 0, \\[2mm]
u_t + \left(\dfrac{1}{F^2} + \dfrac{\lambda}{3} \right) h_x + u_x - \dfrac{\lambda}{3}\eta_x = 0, \\[2mm]
\eta_t + \eta_x = w, \\[2mm]
w_t + w_x = -\dfrac{\lambda}{\mu^2}(\eta - h).
\end{cases}
\tag{4.52}
$$

We decompose $\mathbf{V} = (h, u, \eta, w)^\top$ as $\mathbf{V} = \chi(x)\mathbf{V}_{ex} + \bar{\mathbf{V}}$. Where $\mathbf{V}_{ex} = (h_{ex}, u_{ex}, \eta_{ex}, w_{ex})^\top$ is a profile which enters in the domain and supposed to be an exact solution of the system. The cut-off function $\chi(x)$ is defined as $\chi(x < x_\ell) = 1$, $\chi(x > x_r) = 0$. It is assumed that this function is smooth and its derivatives is compactly supported. The new unknown vector function $\bar{\mathbf{V}} = (\bar{h}, \bar{u}, \bar{\eta}, \bar{w})^\top$ is compactly supported and satisfies the equations with the source terms

$$
\begin{cases}
\bar{h}_t + \bar{h}_x + \bar{u}_x = -\chi'(x)(h_{ex} + u_{ex}), \\[2mm]
\bar{u}_t + \left(\dfrac{1}{F^2} + \dfrac{\lambda}{3} \right) \bar{h}_x + \bar{u}_x - \dfrac{\lambda}{3}\bar{\eta}_x = -\chi'(x)\left(\left(\dfrac{1}{F^2} + \dfrac{\lambda}{3} \right) h_{ex} + u_{ex} - \dfrac{\lambda}{3}\eta_{ex} \right), \\[2mm]
\bar{\eta}_t + \bar{\eta}_x = \bar{w} - \chi'(x)\eta_{ex}, \\[2mm]
\bar{w}_t + \bar{w}_x = -\dfrac{\lambda}{\mu^2}(\bar{\eta} - \bar{h}) - \chi'(x)w_{ex}.
\end{cases}
$$

It implies that for this system we can construct the PML equations in exactly the same way as before (i.e. the strategy used to obtain (4.35)). The right propagating incoming wave is chosen as an exact profile, this leads to the modification of the terms corresponding to the left layer. We obtain

$$
\begin{cases}
\bar{h}_t + \bar{h}_x + \bar{u}_x = -\chi'(x)(h_{ex} + u_{ex}) - \sigma^{L+R}\bar{h}, \\[2mm]
\bar{u}_t + \left(\dfrac{1}{F^2} + \dfrac{\lambda}{3} \right) \bar{h}_x + \bar{u}_x - \dfrac{\lambda}{3}\bar{\eta}_x = -\chi'(x)\left(\left(\dfrac{1}{F^2} + \dfrac{\lambda}{3} \right) h_{ex} + u_{ex} - \dfrac{\lambda}{3}\eta_{ex} \right) - \sigma^{L+R}\bar{u}, \\[2mm]
\bar{\eta}_t + \bar{\eta}_x = \bar{w} - \chi'(x)\eta_{ex} - \sigma^R\bar{\eta}, \\[2mm]
\bar{w}_t + \bar{w}_x = -\dfrac{\lambda}{\mu^2}(\bar{\eta} - \bar{h}) - \chi'(x)w_{ex} - \sigma^R\bar{w}.
\end{cases}
$$

It remains to go back to the original variables $\mathbf{V}$ using the decomposition $\mathbf{V} = \chi(x)\mathbf{V}_{ex} + \bar{\mathbf{V}}$.
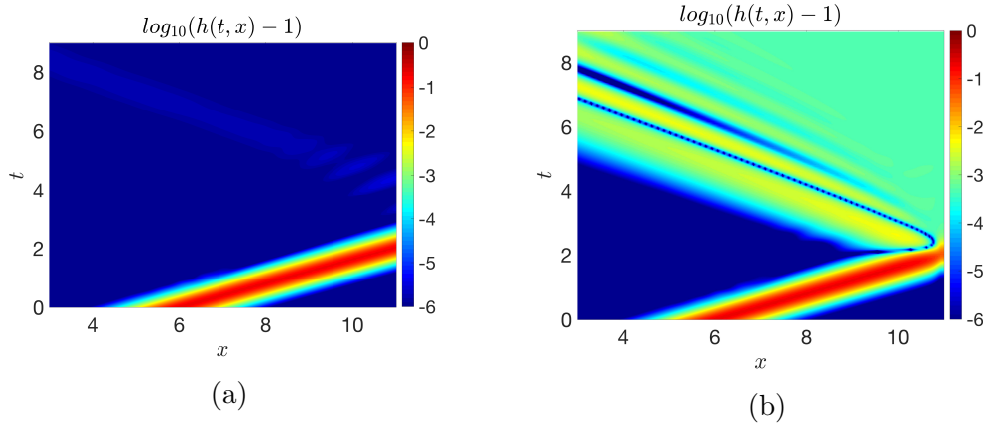
Figure 4.8: Comparison of the PML approach (a) with direct application of Neumann boundary conditions (b).

One obtains:

$$
\begin{cases}
h_t + h_x + u_x = -\sigma^L(h - \chi(x)h_{ex}) - \sigma^R h, \\[2mm]
u_t + \left(\dfrac{1}{F^2} + \dfrac{\lambda}{3}\right) h_x + u_x - \dfrac{\lambda}{3}\eta_x = -\sigma^L(u - \chi(x)u_{ex}) - \sigma^R u, \\[2mm]
\eta_t + \eta_x = w - \sigma^R \eta, \\[2mm]
w_t + w_x = -\dfrac{\lambda}{\mu^2}(\eta - h) - \sigma^R w.
\end{cases}
\tag{4.53}
$$

The same considerations for the nonlinear case, together with idea explained in subsection 4.6 lead to the system

$$
\begin{cases}
h_t + (hu)_x = -\sigma^L((h - \chi(x)h_{ex}^{NL}) - 1) - \sigma(h - 1), \\[2mm]
(hu)_t + \left(hu^2 + \dfrac{h^2}{2F^2} + \dfrac{\lambda}{3}\left(\dfrac{\eta}{h} - 1\right)\eta\right)_x = -\sigma^L(hu - \chi(x)h_{ex}u_{ex}^{NL}) - \sigma^R hu, \\[2mm]
(h\eta)_t + (hu\eta_x) = hw, \\[2mm]
(hw)_t + (huw)_x = -\dfrac{\lambda}{\mu^2}(\dfrac{\eta}{h} - 1).
\end{cases}
\tag{4.54}
$$

Here $\mathbf{V}_{ex} = (h_{ex}^{NL}, u_{ex}^{NL})$ defines a perturbation from the constant state $h = 1$ of the incoming solution profile.

Let us turn to the numerical validations of the introduced equations for incoming waves. First of all, one should construct the exact solution for the linear problem (4.52) in order to define $\mathbf{V}_{ex}$. We seek for plane wave solutions of the form

$$
\begin{pmatrix} h \\ u \\ \eta \\ w \end{pmatrix} = \begin{pmatrix} \tilde{h} \\ \tilde{u} \\ \tilde{\eta} \\ \tilde{w} \end{pmatrix} exp\{i(kx - \omega t)\}.
$$

The phase speeds are defined as the relation of the frequency ω to the wave number k: $c_i = \omega/k$ and can be determined as eigenvalues of the following matrix:

$$L = \begin{pmatrix} 1 - \dfrac{\omega}{k} & 1 & 0 & 0 \\ \dfrac{1}{F^2} + \dfrac{\lambda}{3} & 1 - \dfrac{\omega}{k} & -\dfrac{\lambda}{3} & 0 \\ 0 & 0 & 1 - \dfrac{\omega}{k} & \dfrac{i}{\mu k} \\ \dfrac{i\lambda}{\mu k} & 0 & -\dfrac{i\lambda}{\mu k} & 1 - \dfrac{\omega}{k} \end{pmatrix}. \tag{4.55}$$

This matrix is very to close to the matrix (4.12). The only difference is that the source terms are included in order to construct an exact solution to the complete system (4.11).

The matrix is complex, but the characteristic polynomial is real

$$\left(1 - \frac{\omega}{k}\right)^2 \left(\left(1 - \frac{\omega}{k}\right)^2 - \frac{\lambda}{k^2} - \frac{1}{F^2} - \frac{\lambda}{3}\right) + \frac{\lambda}{F^2 k^2} = 0.$$

The eigenvalues $c_i = \omega/k$ might be calculated explicitly. However the expressions are cumbersome, and moreover, the construction of the solution requires computing the eigenvectors. For the numerical tests, we will calculate both the eigenvalues and eigenvectors numerically. We denote $\mathbf{p}$ the eigenvector of the matrix L corresponding to the maximal eigenvalue $\max\limits_i c$ to guarantee that the wave propagating to the right is chosen. The exact solution is defined as

$$\mathbf{V}_{ex} = \mathcal{R}(\mathbf{p}) \cos(kx - \omega t) - \mathcal{IM}(\mathbf{p}) \sin(kx - \omega t). \tag{4.56}$$

Since we consider the linear system (4.52), the real part of the solution is a solution again, here $\mathcal{R}$, $\mathcal{IM}$ denote real and imaginary parts of the eigenvectors.

The initial data are given as follows

$$\mathbf{V}_{ini} = \chi(x) \left(\mathcal{R}(\mathbf{p}) \cos(kx) - \mathcal{IM}(\mathbf{p}) \sin(kx)\right).$$

Once the wave number k is chosen, the frequency is calculated with respect to the maximal eigenvalue $\omega(k) = k \max\limits_i c$. We recall that the smooth function $\chi(x)$ satisfies the conditions

$$\chi(x < x_\ell) = 1, \quad \chi(x > x_r) = 0,$$

and its derivative is compactly supported.

We first perform a test with the initial conditions presented in Figure 4.9. The second test represents an incoming wave generation over the zero initial profile. The results of the numerical tests for the depth $h(t, x)$ are presented in Figure 4.10 for $k = 2\pi$.

For the generation of a solitary wave in the nonlinear case, we use the approximate solution (4.51) as an exact incoming profile $(h_{ex}^{NL}, u_{ex}^{NL})$ again. The parameters are defined as

$$\varepsilon = 0.1,$$
$$x_\ell = 0, \quad x_r = 15, \quad \delta_x^\ell = 5, \quad \delta_x^r = 5,$$
$$D = -5,$$
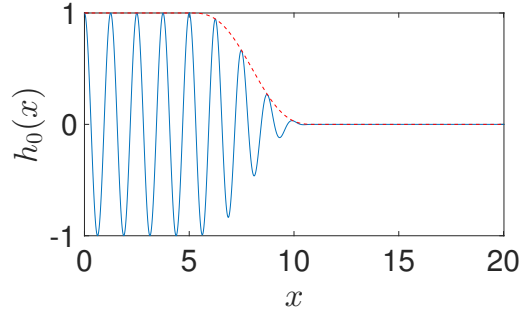$$\delta x = 0.02, \quad CFL = 0.1, \quad \mu = 0.25.$$

Figure 4.9: Initialization of an incoming wave profile: solid line – initial function $h(0, x) = h_0(x)$, dashed line – cut-off function $\chi(x)$.
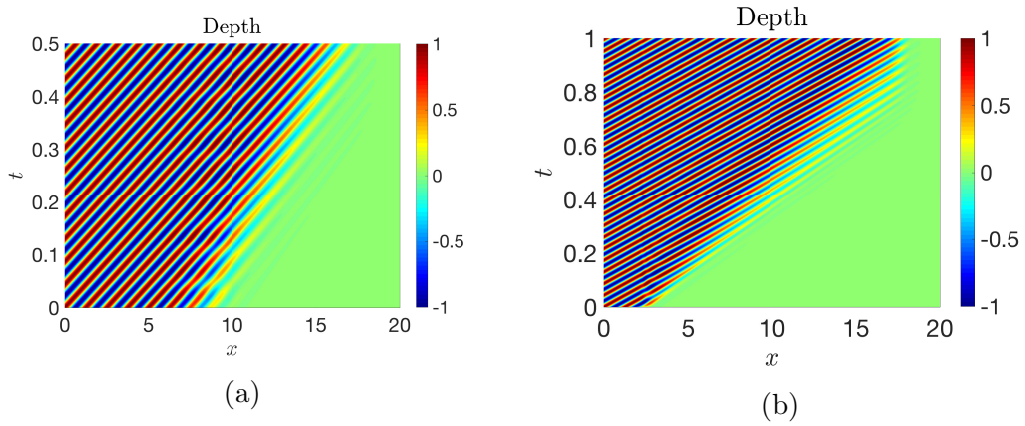

(a)

(b)

Figure 4.10: PML application to the incoming wave simulation: Linear case. Evolution of $h(t, x)$ for dispersive problem ($\lambda = 1000$) (a) non-zero initial profile, (b) zero initial profile.
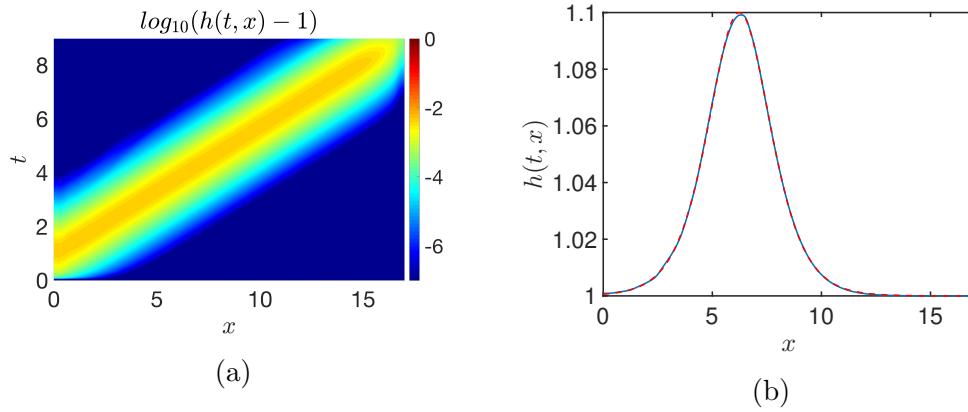
Figure 4.11: PML application to the incoming solitary wave simulation: (a) evolution of $h(t, x)$ evolution for dispersive problem ($\lambda = 1000$), (b) numeric (solid) and exact (dashed) incoming profile.

The negative shift of the initial position D means that initially the wave is not located in the domain $[x_\ell, x_r]$. The results are shown in logarithmic scale in Figure 4.11. The profile of the incoming solitary wave is slightly different (1% of the amplitude of the solitary wave solution) from the exact solution (4.11, b).

The difference comes into particular prominence for the strongly nonlinear wave. We perform another numerical test with the following parameters

$$\varepsilon = 0.6,$$
$$x_\ell = 0, \quad x_r = 20, \quad \delta_x^\ell = 8, \quad \delta_x^r = 6,$$
$$D = -5,$$
$$\delta x = 0.02, \quad CFL = 0.1, \quad \mu = 0.25.$$

The incoming solitary wave has a smaller amplitude than the exact profile and then propagates with a small deformation (see Figure 4.12). There might be several explanations. Firstly, the parameters for the PML equations are probably not optimal. Moreover, the solution (4.51) is just an approximate solution of the system (4.4) and the relaxation parameter λ probably needs to be calibrated with respect to the value of dispersive parameter μ. Since the source term responsible for the dispersive effects has a factor λ/μ. Finally, the proposed numerical scheme might be improved to a scheme of the higher order. This question requires a more precise investigation.

The last test concerns the interaction of a pair of solitary waves. We use the PML equations to generate a relatively fast moving solitary wave, while an initial slow moving solitary wave is already imposed inside the domain. During the propagation, two waves interact elastically. After the collision, the faster one propagates ahead. Both waves are absorbed after in the right layer. Results are plotted for the water depth in Figure 4.13. Again an optimisation of the PML parameter and the relaxation parameter λ might be required here. Indeed, we observe small reflections in the generation layer and both solitary waves propagate with small defects. Also, a small perturbation propagating to the left from the solitary wave initially situated inside the domain is observed.
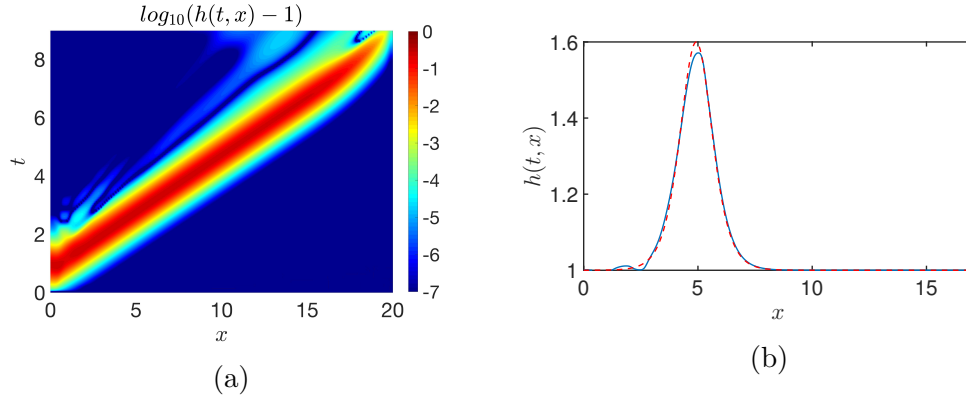
(a)

(b)

Figure 4.12: PML application to the incoming solitary wave simulation: (a) evolution of $h(t,x)$ evolution for dispersive problem ($\lambda = 1000$), (b) numeric (solid) and exact (dashed) incoming profile.
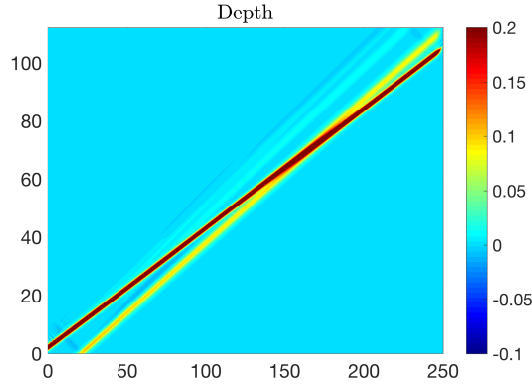

Figure 4.13: Interaction of a pair of solitary waves. One is situated inside the domain initially, another generated using PML equations, both absorb on the left layer.

The incoming solitary wave profile $(h_{ex}^{NL}, u_{ex}^{NL})$ is constructed with following parameters

$$\varepsilon = 0.5,$$
$$D = -5,$$
$$\mu = 0.7.$$

The second solitary wave are defined by

$$\varepsilon = 0.1,$$
$$D = 21,$$
$$\mu = 0.3.$$

The widths of the layers are chosen as $\delta_x^r = 8$, $\delta_x^l = 8$. The computational domain is chosen large enough $[0, 250]$ to include a collision before absorption in the right layer. The space step is defined as $\delta_x = 0.05$, and for the stability, $CFL = 0.1$ is chosen.

4.8   Conclusion

In this chapter, we proposed a strategy for the boundary condition setting for the hyperbolic generalization of the Green-Naghdi system proposed in [49]. The Perfectly Matched Layer approach is used. The derivation of the modified equations is rigours for the linear case. We have shown the dissipative properties of the solution of the PML system, which guarantee that the problem is well-possessed.

The application of the PML approach to a dispersive system may lead to a sophisticated form of additional terms, including the derivatives of the solution, and additional equations to solve. The hyperbolic structure of the system leads to simple PML equations. The final structure of the modified equations is similar to the one used in the sponge layer approach discussed earlier. However, the procedures are different, the PML approach is based on the separation of the solution components to guarantee the amplitude decays, whereas the sponge layer approach provides a forcing of the solution to a target one, which is more close to the relaxation technique.

In practice, we have to deal with non-linear equations. The main advantage of the proposed approach is that the derived equations can be applied for the nonlinear case successfully in weakly nonlinear case. For the strongly nonlinear case, the further analysis is needed for both the relaxation and PML equations parameters. However, the outgoing and incoming solitary waves are simulated only with small defects.

In this chapter, we performed several test cases for the simulations of outgoing and incoming waves in both linear and nonlinear cases. A natural perspective of this work is to apply this approach for real test cases, coming from experimental studies. Another direct perspective is a generalization of the obtained PML equations to the classical dispersive Green-Naghdi model or models derived in Part I.

Conclusions
and Outlook

In the present thesis, modelling and numerical issues of the dispersive wave theory were investigated. To sum up, the question of including additional complex physical effects in the classical models was considered in the first part; the second part was devoted to special numerical techniques designed to overcome the difficulties appearing when dispersive models are solved numerically. The classical Green-Naghdi system has been extended in the first part with vorticity effects and studied from a numerical point of view in the second part.

The first part of the present study concerns the turbulent motion modelling. Chaotic turbulent flow is a complex phenomenon which is hard to describe with a simplified model. However, using previously found simplifications ([29], [119]), in Chapter 1, we have managed to construct a model of $2D$ coastal breaking waves in the context of $1D$ depth-average settings. The turbulence in the surf zone is taken into account through an additional variable which is governed by a transport equation with empirical source terms responsible for the vorticity creation. This empirical law was justified by classical turbulent hypothesis on the turbulent scales and energy dissipation. A numerical algorithm for the model validation has been constructed, and comparison with experiments in the context of mild sloping beach was performed. One set of experimental data allowed to define the closure relations for empirical parameters and another one permitted the verification of the founded closure. The preliminary results from [116] showed that the obtained relation prescribed well the parameter values for complex $1D$ and $2D$ test cases. Additionally, a breaking criterion was proposed, in order to initiate the breaking process only when needed. In the end, breaking waves are described with a unified model of propagation which has the same dispersive properties as the Green-Naghdi equation.

In Chapter 2, a two-layer model for internal wave propagation is derived rigorously from the Euler equations in a conservative framework. The vorticity effects were taken into account in a similar manner as in the previous chapter. The pressure was supposed non-hydrostatic, and a non-uniform velocity profile was considered. The equations for the vorticity evolution in each layer close the system. The model is written in two different formulations, allowing for future numerical validations with existing approaches for dispersive systems.

Both models are reduced to the classical Green-Naghdi equations in the case of vanishing vorticity.

The second part was devoted to the boundary conditions construction. When dispersive models are solved numerically, establishing a proper procedure for incoming and outgoing waves is a fundamental concern. We proposed two different approaches, which allow for the justification of a boundary conditions procedure in linear and weakly nonlinear cases. In the context of dispersive wave propagation in a coastal zone, we considered the classical Green-Naghdi equation and its hyperbolic extension proposed recently.

In Chapter 3, we have obtained continuous and discrete artificial boundary conditions for the Green-Naghdi system linearized around a steady state. Two different discretizations were investigated. In both cases, the discrete initial-boundary problem is proved to be stable, convergent and consistent with the continuous one. Numerical tests have been constructed to validate the proposed approach, for different initial data. It has been shown that a similar technique can be adapted to the incoming wave generation, and numerical tests illustrating this method were performed.

However, the approach proposed in Chapter 3 requires a more sophisticated strategy for applications to the nonlinear case. In order to deal with nonlinear equations, we turned our attention to a recently proposed hyperbolic formulation of the Green-Naghdi equations. In Chapter 4, a different procedure for the boundary treatment was considered. We applied the Perfectly Matched Layers (PML) technique to this new system. The PML equations were constructed for the linear case first, and numerical implementation was performed. A partial justification of the method is possible for the weakly nonlinear case. Numerical tests were performed, implying weakly and strongly nonlinear waves. We observed small, but non-negligent reflections for strongly nonlinear waves. Also, a further analysis of the problem parameters is needed. Using the same arguments, the PML equations can be constructed to handle incoming waves. Numerical tests of incoming plane linear waves and solitary waves were proposed. A further systematic analysis is required to determine the range of parameter values ensuring the stability of the method.

A natural perspective opened by $1D$ investigations of boundary conditions is a $2D$ extension. In real-life applications, it is essential to ensure a detailed description of nearshore dynamics, including wave-breaking and swash motion, for example. For this reason, the transfer to $2D$ simulations for the dispersive models is a crucial concern. Dispersive terms issues aside, there is an essential need for a proper boundary conditions treatment. The extension of transparent boundary conditions to the $2D$ case requires an elaborate study and may be difficult. The PML approach seems to be a more promising one since it is possible to apply the splitting strategy. Therefore, the extension of the PML equations to the second dimension should be similar to the $1D$ case.

Brought together, the results of both parts may constitute a promising basis for future application in coastal engineering. In well-known methods dedicated to coastal wave propagation, wave breaking is modelled in a more sophisticated way than the one proposed in Chapter 1 (changing of the model propagation, or including artificial terms). Moreover, some cases can be modelled directly without any breaking criteria using the obtained model. These early successes may bring hope to resolve one day this issue in the context of a simple universal model without any criteria. Turbulent motions seem have significant responsibility for the coastal erosion. In the context of the proposed model, the analysis of the enstrophy behaviour may allow a deeper understanding and description of this phenomenon. Concerning the mathematical analysis of the obtained model, one of the interesting research directions is the study of existence and stability of solutions when turbulent viscosity is added. The internal wave propagation in the presence of vorticity may lead to very different flow regimes, as it was shown for the surface waves in previous research on the one-layer model in (see [84]). The proposed model from Chapter 2 has not been investigated numerically yet, and it is one of the open perspectives related to this result.

The boundary conditions implementation is another weakness of existing approaches in coastal wave propagation. Providing a well-posed boundary-initial problem is essential for stable numerical calculations. The conditions obtained in Part II, which are partially justified, open perspectives toward applications to more complex physical situations. Applications of the transparent boundary conditions found in 3 to the nonlinear case might be complicated, but possible using a fixed point strategy. The generalization of the proposed approaches to the model derived in Chapter 1 is an immediate aim, since it allows for the

model validation on more advanced tests cases, as discussed above. A direct application of the PML technique to the dispersive Green-Naghdi equation is likely possible, at least in the linear case, and stands for another perspective of this work. The hyperbolicity of the model proposed in [49], coupled with the boundary condition approach found in Chapter 4, could lead to considerable practical advances in coastal engineering. However, to extend these applications to real phenomenon in coastal zones, energy dissipation is still needed, but it is likely that this will not influence the proposed boundary treatment.

Appendices

On the existence of a solitary wave solution

We consider the extended hyperbolic system derived in [49] which approximates the dispersive Green-Naghdi equations. This model is considered in Chapter 4 with a more detailed explanation of the derivation procedure. The equations are written as follows

$$\frac{\partial \mathbf{U}}{\partial t} + \frac{\partial \mathbf{F}(\mathbf{U})}{\partial x} = \mathbf{S}(\mathbf{U}), \tag{A.1}$$

where the vector functions are defined as follows

$$\mathbf{U} = (h, hu, h\eta, hw)^{\top}, \quad \mathbf{F}(\mathbf{U}) = \left(hu, hu^2 + gh^2/2 - \frac{\lambda}{3}\left(\frac{\eta}{h} - 1\right), h\eta u, hwu \right)^{\top}$$

$$\mathbf{S}(\mathbf{U}) = \left(0, 0, hw, -\lambda\left(\frac{\eta}{h} - 1\right) \right)^{\top}.$$

Here, $h(t,x)$ is the water depth, $u(t,x)$ is the fluid velocity and $\eta(t,x)$, $w(t,x)$ are non equilibrium variables added to extend the system to a hyperbolic one. The relaxation parameter λ is chosen large enough in order to have a good approximation of the original Green-Naghdi equations.

Two effects are essential for the dispersive wave propagation: nonlinearity, which tends to steepen the wave form, and dispersion, which leads to the dependence of the phase speed on wave frequencies. The equilibrium between these two effects results in the existence of solitary wave solutions, which is observed in nature as well (firstly by Russell [79]).

In this Annex A, we consider the question whether the extended system inherits this property from the Green-Naghdi equations.

A.1 Theorem. The system (A.1) *admits a solitary wave solution for relatively large value of the parameter* λ *and* $F \neq 0$:

$$\lambda > \max\left(3\left(1 + \frac{1}{2F^2}\right)^2, \sqrt{\frac{54(1 + 2F^2)}{F^4 \min(1, H_1)}} \right),$$

where $H_1 = -\frac{1}{2} + \frac{\sqrt{1 + 8F^2}}{2}.$

Proof. From a physical point of view, the solitary wave is a wave that propagates without changing its form; mathematically a travelling wave solution is expressed by functions depending only on $\xi = x - ct$, where c is the constant speed of propagation.

Reduced dimensionless system

We start by setting $\mathbf{U}(x,t) = \mathbf{U}(\xi) = \mathbf{U}(x - ct)$, namely

$$h(t,x) = H(\xi), \quad u(t,x) = U(\xi), \quad \eta(t,x) = E(\xi), \quad w(t,x) = W(\xi).$$

The equations reduce to the following system of ordinary differential equations (ODEs) (prime denotes the derivative with respect to ξ)

$$\begin{cases} (H(U-c))' = 0, \\ \left(HU(U-c) + \dfrac{gH^2}{2} - \dfrac{\lambda}{3}\left(\dfrac{E}{H} - 1\right)E \right)' = 0, \\ (HE(U-c))' = HW, \\ (HW(U-c))' = -\lambda\left(\dfrac{E}{H} - 1\right), \end{cases}$$

with boundary conditions at the infinity (we suppose $E = H$ at the infinity, which corresponds to the assumptions made in the model derivation [49])

$$\begin{cases} H(x = \infty) = H_\infty, \\ U(x = \infty) = 0, \\ E(x = \infty) = H_\infty, \\ U(x = \infty) = 0. \end{cases}$$

Without loss of generality, the system can be rewritten in a simpler form if we refer to a Cartesian coordinate system moving with a constant speed c. This leads to a simple change $U = U - c$ (tildes are immediately dropped):

$$\begin{cases} (HU)' = 0, \\ \left(H(U-c)U + \dfrac{gH^2}{2} - \dfrac{\lambda}{3}\left(\dfrac{E}{H} - 1\right)E \right)' = 0, \\ (HEU)' = HW, \\ (HWU)' = -\lambda\left(\dfrac{E}{H} - 1\right), \end{cases}$$

with the modified boundary condition $U(x = \infty) = -c$.

We introduce dimensionless variables, the dispersion parameter μ and the Froude number F:

$$\xi = L\bar{\xi}, \quad U = c\bar{U}, \quad H = H_\infty\bar{H}, \quad E = H_\infty\bar{E}, \quad W = \frac{cH_\infty}{L}\bar{W}, \quad \mu = \frac{H_\infty}{L}, \quad F^2 = \frac{c^2}{gH_\infty}.$$

The dimensionless equations take the form (bars are omitted)

$$
\begin{cases}
(HU)' = 0, \\[2mm]
\left(HU^2 + \dfrac{H^2}{2F^2} - \dfrac{\lambda}{3}\left(\dfrac{E}{H} - 1\right)E \right)' = 0, \\[2mm]
(HEU)' = HW, \\[2mm]
(HWU)' = -\dfrac{\lambda}{\mu^2}\left(\dfrac{E}{H} - 1\right).
\end{cases}
$$

The two first equations are simply integrated taking into account the conditions at the infinity for dimensionless variables:

$$
\begin{aligned}
H(x = \infty) &= 1, \\
U(x = \infty) &= -1, \\
E(x = \infty) &= 1.
\end{aligned}
$$

We have

$$
\begin{cases}
HU = 1, \\[2mm]
\dfrac{1}{H} + \dfrac{H^2}{2F^2} - \dfrac{\lambda}{3}\left(\dfrac{E}{H} - 1\right)E = 1 + \dfrac{1}{2F^2}, \\[2mm]
E' = HW, \\[2mm]
W' = -\dfrac{\lambda}{\mu^2}\left(\dfrac{E}{H} - 1\right).
\end{cases}
\tag{A.2}
$$

The first equation defines the dimensionless velocity $U = 1/H$. If we go back to the dimensional variables one finds in the fixed coordinate system $U = c(1 - 1/H)$, which corresponds precisely to the velocity definition of the classical Green-Naghdi solitary wave. The second equation is an algebraic equation which relates H and E. Indeed,

$$
\left(\frac{E}{H}\right)^2 - \left(\frac{E}{H}\right) - \frac{3(H-1)(H^2 + H - 2F^2)}{2\lambda F^2 H^2} = 0,
$$

choosing the positive root, one obtains the expression for E as a function of H

$$
E(H) = \frac{H}{2} + \frac{1}{2}\sqrt{H^2 + \frac{6(H-1)(H^2 + H - 2F^2)}{\lambda F^2}}.
\tag{A.3}
$$

In order to prove that the square root is real for $H > 0$, we need to show that the radicand is positive, we denote

$$
f(H) = \frac{6(H-1)(H^2 + H - 2F^2)}{\lambda F^2},
\tag{A.4}
$$

and consider $H^2 + f(H)$. First, the function $f(H)$ has three roots,

$$
H_0 = 1, \quad H_{1,2} = -\frac{1}{2} \pm \frac{\sqrt{1 + 8F^2}}{2},
\tag{A.5}
$$

H_2 is always negative, while H_1 is always positive if $F \neq 0$. Moreover, we have

$$f(H) \leq 0, \text{ if } H \in (-\infty, H_2],$$

$$f(H) \geq 0, \text{ if } H \in [H_2, \min(1, H_1)],$$

$$f(H) \leq 0, \text{ if } H \in [\min(1, H_1), \max(1, H_1)],$$

$$f(H) \geq 0, \text{ if } H \in [\max(1, H_1), \infty).$$

Therefore the sign of $H^2 + f(H)$ is defined simply everywhere for $H > 0$, except in the interval $[\min(1, H_1), \max(1, H_1)]$ (see Figure A.1). It follows that the square root $\sqrt{H^2 + f(H)}$ is real for $H \in [0, H_0] \cup [H_1, \infty]$. We now analyse the derivative of $H^2 + f(H)$ with respect to H for $H \in [H_0, H_1]$ to define a sign,

$$H^2 + f(H)\Big|_{H=H_0} = \min(1, H_1)^2 > 0, \quad (H^2 + f(H))'_H = 2H + \frac{6}{\lambda F^2}\left(3H^2 - (1 + 2F^2)\right).$$

In order to allow a definite conclusion on the sign of the derivative, we solve the following quadratic equation

$$\frac{18}{\lambda F^2}H^2 + 2H - \frac{3}{\lambda F^2}(1 + 2F^2) = 0. \tag{A.6}$$

The roots $r_{1,2}$ are defined as

$$r_{1,2} = -\frac{\lambda F^2}{18} \pm \frac{\lambda F^2}{18}\sqrt{1 + \frac{108(1 + 2F^2)}{F^4}\frac{1}{\lambda^2}}. \tag{A.7}$$

If the positive root r_1 is smaller than $min(1, H_1)$, the derivative of $H^2 + f(H)$ is positive $\forall H > min(1, H_1)$. The expansion for r_1 with respect to the small parameter $1/\lambda^2$ is written as

$$r_1 = -\frac{\lambda F^2}{18} + \frac{\lambda F^2}{18}\left(1 + \frac{54(1 + 2F^2)}{F^4}\frac{1}{\lambda^2}\right) + O\left(\frac{1}{\lambda^4}\right). \tag{A.8}$$

One has $r_1 < \min(1, H_1)$ for all relatively large values of λ. A rough estimation reads

$$\lambda > \sqrt{\frac{54(1 + 2F^2)}{F^4 \min(1, H_1)}}.$$

This inequality is verified since for a good approximation of the initial Green-Naghdi equations by the system (A.1), the value for the parameter λ should be chosen of order 1000. Finally, we have shown that

$$(H^2 + f(H))\Big|_{H=H_0} = \min(1, H_1)^2 > 0,$$

$$(H^2 + f(H))'_H > 0 \quad \forall H > r_1, \, r_1 < \min(1, H_1),$$

which means that the square root $\sqrt{H^2 + f(H)}$ is real $\forall H > 0$.

We turn back to the system (A.2); the two last equations are rewritten taking into account the notation (A.3)

$$\begin{cases} H' = \dfrac{HW}{dE(H)/dH}, \\ W' = -\dfrac{\lambda}{\mu^2}\left(\dfrac{E(H)}{H} - 1\right). \end{cases} \tag{A.9}$$
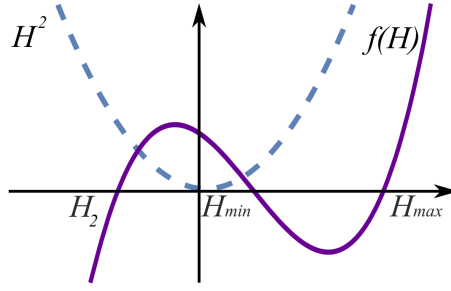
Figure A.1: Curves representing the two terms of the square root expression $\sqrt{H^2 + f(H)}$, here $H_{min} = \min(1, H_1)$, $H_{max} = \min(1, H_1)$.

Number of stationary points

We determine the stationary points for the system

$$W = 0, H = H_{(i=0,1,2)},$$

where H_i are the roots of the equation

$$\frac{E(H)}{H} = 1,$$

which coincide with the ones defined by (A.5). If $dE(H)/dH \neq 0 \ \forall H > 0$, there are no other stationary points.

Let us consider the explicit expression for $dE(H)/dH$,

$$dE(H)/dH = \frac{1}{2} + \frac{2H + f'_H(H)}{4\sqrt{H^2 + f(H)}}, \tag{A.10}$$

where the function $f(H)$ is defined by (A.4). One has $dE(H)/dH = 0$ if

$$2H + f'_H(H) = -2\sqrt{H^2 + f(H)}. \tag{A.11}$$

First, we denote the left- and right-hand sides of this equation as

$$f^\ell(H) = 2H + f'_H(H), \quad f^r(H) = -2\sqrt{H^2 + f(H)}.$$

The function $\sqrt{H^2 + f(H)}$ is always positive for a relatively large value of λ and $H > 0$. As a consequence $f^r(H)$ is always negative. On the other hand $f^\ell(H) > 0$, $\forall H > r_1$, where r_1 is a small positive value defined by (A.7). We conclude that the equation (A.11) has no roots for all $H > r_1$.

Moreover, we note that

$$f^\ell(0) = -\frac{12}{\lambda}\left(1 + \frac{1}{2F^2}\right) \quad > \quad f^r(0) = -2\sqrt{\frac{12}{\lambda}}, \qquad \forall \lambda > 3\left(1 + \frac{1}{2F^2}\right)^2.$$

We analyse now the behaviour of $f^\ell(H)$, $f^r(H)$ in the interval $H \in (0, r_1)$. There are two possible cases presented in Figure A.2. The functions $H^2 + f(H)$ and $f^r(H)$ have the local extremum at $H = r_1$ since $f^\ell = (H^2 + f(H))'_H$. In a favourable case there are no roots
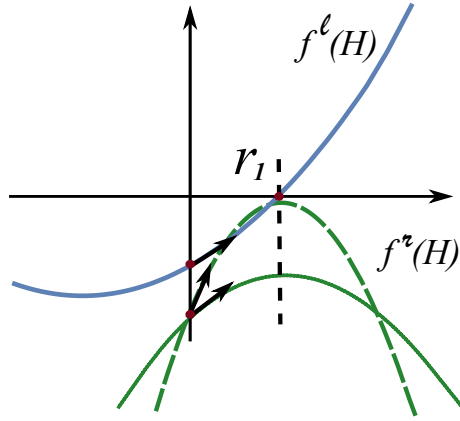
Figure A.2: Possible characteristic behaviour

in the interval $(0, r_1)$. To prove this we analyse the functions $f^\ell(H)$, $f^r(H)$. First, the function f^ℓ is strictly convex, indeed

$$(f^\ell)''_H = \frac{36}{\lambda F^2} > 0.$$

We establish now that the function f^r is concave in the interval $(0, r_1)$ using that $H^2 + f(H) > 0 \ \forall H \in (0, r_1)$. We calculate directly the second derivative

$$(f^r)''_H = -\frac{1}{\sqrt{H^2 + f(H)}^{3/2}} \left((2 + f''_H(H))(H^2 + f(H)) - (2H + f'_H(H))^2 \right).$$

The expression in the parenthesis,

$$\mathcal{D}(H) = (2 + f''_H(H))(H^2 + f(H)) - (2H + f'_H(H))^2$$

is positive for a relatively large value of λ since

$$\mathcal{D}(0) = \frac{48}{\lambda} - \frac{36}{\lambda^2 F^4} \left(1 + 2F^2 \right)^2 > 0, \quad \forall \lambda > 3 \left(1 + \frac{1}{2F^2} \right)^2,$$

and

$$\mathcal{D}'_H(H) = \frac{64}{\lambda F^2}(H^2 + f(H)) > 0, \quad \forall H > 0.$$

Subsequently, the derivative $(f^r)''_H$ is negative and f^r is concave in the interval $(0, r_1)$.

Finally, we have a convex function f^ℓ and a concave function f^r with the following property for $H = 0$, $f^\ell(0) > f^r(0)$. Then it suffices to show that $(f^r)'_H(0) < (f^\ell)'_H(0)$ in order to establish $dE(H)/dH \neq 0$ for $H > 0$. We have

$$(f^\ell)'_H(0) = 2 \quad > \quad (f^r)'_H(0) = \frac{\sqrt{3}}{\sqrt{\lambda}} \left(1 + \frac{1}{2F^2} \right) \qquad \forall \lambda > 3 \left(1 + \frac{1}{2F^2} \right)^2.$$

Since there are no roots of the equation (A.11), the only stationary points of the system (A.9) in the positive half plane $H > 0$ are defined by

$$(H_s^1, W_s^1) = (1, 0) \quad \text{and} \quad (H_s^2, W_s^2) = \left(-\frac{1}{2} + \frac{\sqrt{1 + 8F^2}}{2}, 0 \right). \qquad (A.12)$$

These two points can permute, depending on the flow regime (supercritical flow $F > 1$, subcritical flow $F < 1$).
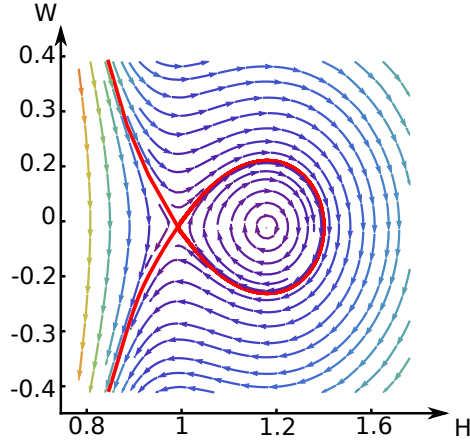
Figure A.3: Phase portrait for the system (A.9) for $F = 1.3$, $\mu = 0.4$, $\lambda = 1000$. Red curve corresponds to the solitary wave solution.

Integral curves: existence of homoclinic orbit

The system (A.9) admits the first integrals,

$$\int_{H_{min}}^{H} \mathcal{N}(\lambda, \tilde{H}) d\tilde{H} + \frac{W^2}{2} = C = \text{const}, \tag{A.13}$$

where we denote $H_{min} = \min(1, H_1)$ and

$$\mathcal{N}(\lambda, \tilde{H}) = \frac{\lambda}{\mu^2} \frac{1}{\tilde{H}} \left(\frac{E(\tilde{H})}{\tilde{H}} - 1 \right) \frac{dE(\tilde{H})}{d\tilde{H}}. \tag{A.14}$$

The integral curves described by (A.13) are shown in Figure A.3 for the parameters values $F = 1.3$, $\mu = 0.4$, $\lambda = 1000$. The solitary wave solution is a homoclinic solution to the stationary point $(\min(1, H_1); 0)$ which is implicitly described by (A.13) for chosen initial conditions. To show that this homoclinic solution exists, in what follows we show that H_{min} is a multiple root of $\mathcal{F}(H, 0)$ and there exists another root $H^* > H_{min}$. First, we note that the implicit function

$$\mathcal{F}(H, W) = \int_{H_{min}}^{H} \mathcal{N}(\lambda, \tilde{H}) d\tilde{H} + \frac{W^2}{2},$$

is equal to zero for $H = H_{min}$, $W = 0$. Moreover, its derivatives are equal to zero for $H = H_{min}$,

$$\frac{\partial \mathcal{F}}{\partial H} = \mathcal{N}(\lambda, H), \tag{A.15}$$

since $\mathcal{N}(\lambda, H) = 0$ has the roots defined by (A.5) as shown above. Therefore $H = H_{min}$ is a multiple root, and then a saddle point in the phase plane.

The behaviour in the interval $H \in (H_{min}, \infty)$ is determined by the sign of the derivative (A.15). As shown above $dE(H)/dH \neq 0$ for $H > 0$. Moreover it is easy to see that $dE(H)/dH > 0$ for $H \to \infty$. As consequence $dE(H)/dH > 0$ for $H > 0$. Then the sign of $\mathcal{N}(\lambda, H)$ is defined by $(E(H)/H - 1)$. The function $(E(H)/H - 1)$ has the same roots as
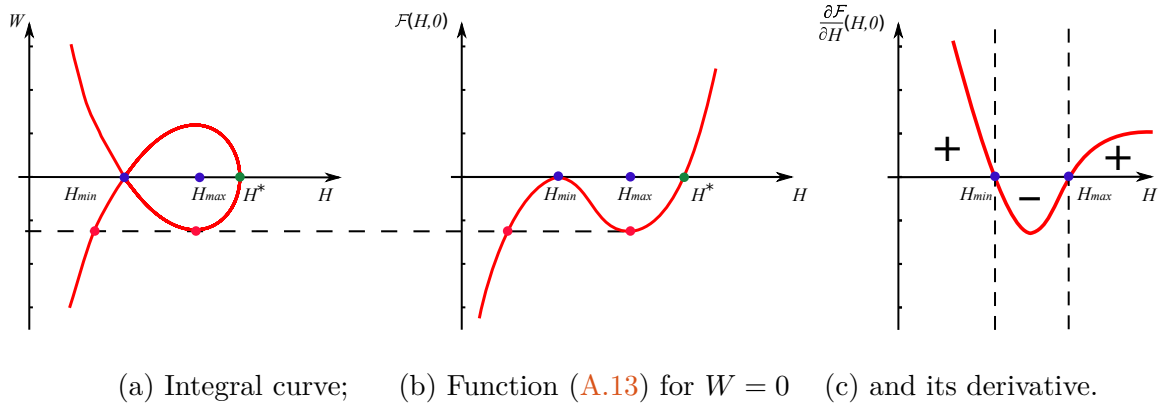
(a) Integral curve;   (b) Function (A.13) for $W = 0$ (c) and its derivative.

Figure A.4: Analysis of the characteristic behaviour of (A.13).

$f(H)$, defined by (A.5). Furthermore, $(E(H)/H - 1) > 0$ when $H \to \infty$. From all has been said it follows that the function (A.13) reaches its local minimum $H = H_{max} \equiv \max(1, H_1)$ and then increases in the interval (H_{max}, ∞) (see Figure A.4). In order to show the existence of another root $H^* : \mathcal{F}(H^*, 0) = 0$, it suffices to note that the integral in (A.13) diverges for $H \to \infty$. Indeed, the rough analysis for $H \to \infty$ gives

$$\left(\frac{E(H)}{H} - 1 \right) \sim \sqrt{H}, \quad \frac{E(H)}{H} \sim \sqrt{H}. \tag{A.16}$$

It implies that

$$\frac{\lambda}{\mu^2} \frac{1}{H} \left(\frac{E(H)}{H} - 1 \right) \frac{dE(H)}{H} \sim \frac{\lambda}{\mu^2}, \tag{A.17}$$

whereas the integration limit $H \to \infty$.

Therefore the limit value of $\mathcal{F}(H, 0)$ is positive, and there exists another root H^*. It implies the existence of bounded periodic solutions, as a consequence H^* is the stationary point.

We conclude that there exists a homoclinic orbit which corresponds to the solitary wave solution. $\qquad \square$

A.1 Remark. Equilibrium points (A.12) coincide with the stationary points of the original Green-Naghdi system.

Indeed, the same considerations for travelling wave solutions of the original Green-Naghdi equations lead to the system of ODEs:

$$\begin{cases} \dfrac{H'}{H} = Y, \\[2mm] Y' = -\dfrac{3}{H^2} \dfrac{(H-1)(H^2 + H - 2F^2)}{2F^2}. \end{cases} \tag{A.18}$$

Indeed, we obtain the same stationary point in the phase plane (H, H') as the one defined before by (A.12).
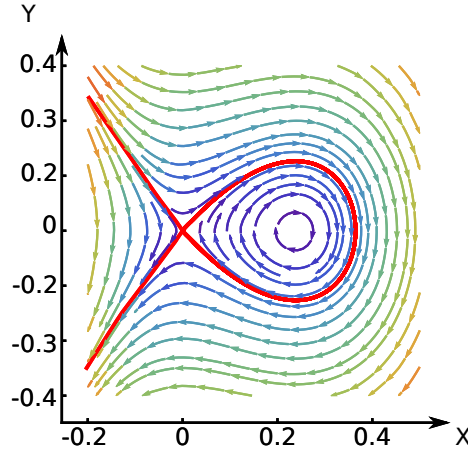
Figure A.5: Phase portrait for the original Green-Naghdi system $F = 1.3$. Red curve corresponds to the solitary wave solution.

In order to remove the singularity we introduce the new variable $X = \ln(H)$. The system takes the form

$$\begin{cases} X' = Y, \\ \\ Y' = -\dfrac{3}{e^{2X}} \dfrac{(H-1)(e^{2X} + e^X - 2F^2)}{2F^2}. \end{cases} \tag{A.19}$$

Similarly, the definition of the first integrals reads as

$$\int_1^H \frac{3}{\tilde{H}^2} \frac{(\tilde{H} - 1)(\tilde{H}^2 + \tilde{H} - 2F^2)}{2F^2} d\tilde{H} + \frac{Y^2}{2} = C = \text{const.} \tag{A.20}$$

The phase portrait in the plane (X, Y) is given in Figure A.5.

Bibliography

[1] S. Abarbanel and D. Gottlieb. A mathematical analysis of the PML method. *J. Comp. Phys.*, 134, 1997.

[2] S. Abarbanel, D. Gottlieb, and J. S. Hesthaven. Well-posed Perfectly Matched Layers for advective acoustics. *J. Compu. Phys.*, 154(2):266–283, 1999.

[3] N. B. Abdallah, F. Méhats, and O. Pinaud. On an open transient Schrödinger-Poisson system. *Mathematical Models and Methods in Applied Sciences*, 15:667, 2005.

[4] B. Alvarez-Samaniego and D. Lannes. Large time existence for 3D water-waves and asymptotics. *Inventiones mathematicae*, 171(3):485–541, 2008.

[5] X. Antoine, A. Arnold, C. Besse, M. Ehrhardt, and A. Schädle. A review of transparent and artificial boundary conditions techniques for linear and nonlinear Schrödinger equations. *Commun. Comput. Phys.*, 4:729–796, 2008.

[6] J. S. Antunes Do Carmo. Boussinesq and Serre type models with improved linear dispersion characteristics: Applications. *Journal of Hydraulic Research*, 51(6):719–727, 2013.

[7] J. S. Antunes Do Carmo, F. J. Seabra Santos, and A. B. Almeida. Numerical solution of the generalized Serre equations with the MacCormack finite-difference scheme. *International Journal for Numerical Methods in Fluids*, 16(8):725–738, 1993.

[8] M. Antuono and M. Brocchini. Beyond Boussinesq-type equations: semi-integrated models for coastal dynamics. *Phys. Fluids*, 25:016603, 2013.

[9] A. Arnold. Numerically absorbing boundary conditions for quantum evolution equations. *VLSI Design*, 6:313–319, 1998.

[10] A. Arnold, M. Ehrhardt, and I. Sofronov. Discrete transparent boundary conditions for the Schrödinger equation: Fast calculation, approximation, and stability. *Commun. in Math. Sci.*, 3:501–556, 2003.

[11] V. I. Arnold. *Mathematical Methods of Classical Mechanics*. Springer-Verlag, 1989.

[12] E. Audusse, F. Bouchut, M.-O. Bristeau, R. Klein, and B. Perthame. A fast and stable well-balanced scheme with hydrostatic reconstruction for shallow water flows. *SIAM J. on Sci. Comp.*, 25(6):2050–2065, 2004.

[13] P. Bacigaluppi, M. Ricchiuto, and P. Bonneton. Stabilized finite element model for non-hydrostatic wave breaking and run-up. In *Finite Volumes for Complex Applications VII*, volume 77 of *Springer Proceedings in Mathematics and Statistics*. Springer, 2014.

[14] R. Barros, S. L. Gavrilyuk, and V. M. Teshukov. Dispersive Nonlinear Waves in Two-Layer Flows with Free Surface. I. Model Derivation and General Properties. *Studies in Applied Mathematics*, 119(3):191–211, 2007.

[15] E. Barthélemy. Nonlinear Shallow Water Theories for Coastal Waves. *Surveys in Geophysics*, 25(3):315–337, 2004.

[16] J. P. Bérenger. A perfectly matched layer for the absorption of electromagnetic waves. *J. Comput. Phys.*, 114:185–200, 1994.

[17] C. Besse, M. Ehrhardt, and I. Lacroix-Violet. Discrete artificial boundary conditions for the linearized Korteweg–de Vries equation. *Num. Meth. for PDE*, 32(5):1455–1484, 2016.

[18] C. Besse, B. Mésognon-Gireau, and P. Noble. Artificial boundary conditions for the linearized Benjamin–Bona–Mahony equation. *Numerische Mathematik*, 139(2):1–34, 2016.

[19] C. Besse, P. Noble, and D. Sanchez. Discrete transparent boundary conditions for the mixed KDV–BBM equation. *J. Comp. Phys.*, 345:484–509, 2017.

[20] J. L. Bona, D. Lannes, and J.-C. Saut. Asymptotic models for internal waves. *Journal de Mathématiques Pures et Appliquées,*, 89(6):538–566, 2008.

[21] P. Bonneton, E. Barthelemy, F. Chazel, R. Cienfuegos, D. Lannes, F. Marche, and M. Tissier. Recent advances in Serre–Green Naghdi modelling for wave transformation, breaking and runup processes. *European Journal of Mechanics - B/Fluids*, 30(6):589 – 597, 2011. Special Issue: Nearshore Hydrodynamics.

[22] P. Bonneton, F. Chazel, D. Lannes, F. Marche, and M. Tissier. A splitting approach for the fully nonlinear and weakly dispersive Green–Naghdi model. *J. Comp. Phys.*, 230(4):1479–1498, 2011.

[23] J. Boussinesq. Théories de ondes et des remous qui se propagent le long d'un canal-rectangulaire, en communiquant au liquide contenu dans ce canal, des vitesses sensiblementpareilles de la surface au fond. *J. Math. Pures Appl. 2ème Sér.*, 17:55–108, 1872.

[24] R. Briganti, R. E. Musumeci, G. Bellotti, M. Brocchini, and E. Foti. Boussinesq modeling of breaking waves: Description of turbulence. *Journal of Geophysical Research: Oceans*, 109(C7), 2004.

[25] M. Brocchini and N. Dodd. Nonlinear shallow water equation modeling for coastal engineering. *J. Wtrwy., Port. Coast. and Oc. Engrg.*, 134(2):104–120, 2008.

[26] M. Brocchini and D. H. Peregrine. The dynamics of strong turbulence at free surfaces. Part 2. Free-surface boundary conditions. *J. Fluid Mech.*, 449:255–290, 2001.

[27] R. Camassa, W. Choi, H. Michallet, P.-O. Rusas, and J. K. Sveen. On the realm of validity of strongly nonlinear asymptotic approximations for internal waves. *J. Fluid Mech.*, 549:1–23, 2006.

[28] R. Camassa, D. D. Holm, and C. D. Levermore. Long-time effects of bottom topography in shallow water. *Physica D*, 98:258–286, 1996.

[29] A. Castro and D. Lannes. Fully nonlinear long-wave models in the presence of vorticity. *J. Fluid Mech.*, 759:642–675, 2014.

[30] F. Chazel, D. Lannes, and F. Marche. Numerical simulation of strongly nonlinear and dispersive waves using a Green–Naghdi Model. *J. Sci. Comp.*, 48(1):105–116, 2011.

[31] Q. Chen, J. T. Kirby, R. A. Dalrymple, F. Shi, and E. B. Thornton. Boussinesq modeling of longshore currents. *Journal of Geophysical Research*, 108(11), 2003.

[32] A. Chesnokov. Introduction to hydrodynamics. *Lecture Notes. (NSU)*, 2014.

[33] W. Choi and R. Camassa. Weakly nonlinear internal waves in a two-fluid system. *J. Fluid Mech.*, 313:83–103, 1996.

[34] W. Choi and R. Camassa. Fully nonlinear internal waves in a two-fluid system. *J. Fluid Mech.*, 396:1–36, 1999.

[35] R. Cienfuegos, E. Barthélemy, and P. Bonneton. A fourth-order compact finite volume scheme for fully nonlinear and weakly dispersive Boussinesq-type equations. Part I: model development and analysis. *International Journal for Numerical Methods in Fluids*, 51(11):1217–1253, 2006.

[36] R. Cienfuegos, E. Barthélemy, and P. Bonneton. A fourth-order compact finite volume scheme for fully nonlinear and weakly dispersive Boussinesq-type equations. Part II: boundary conditions and validation. *International Journal for Numerical Methods in Fluids*, 53(9):1423–1455, 2007.

[37] R. Cienfuegos, E. Barthélemy, and P. Bonneton. Wave-breaking model for Boussinesq-type equations including roller effects in the mass conservation equation. *J. Wtrwy., Port. Coast. and Oc. Engrg.*, 136(1):10–26, 2010.

[38] G. Cohen and S. Imperiale. Perfectly Matched Layer with Mixed Spectral Elements for the Propagation of Linearized Water Waves . *Commun. Comput. Phys.*, 11(2):285–302, 2012.

[39] A. J. C. de Saint Venant. Théorie du mouvement non-permanent des eaux, avec application auxcrues des rivières et à l'introduction des marées dans leur lit. *C.R. Acad. Sc. Paris*, 73:147–154, 1871.

[40] A. A. Dimas and A. S. Dimakopoulos. Surface roller model for the numerical simulation of spilling wave breaking over constant slope beach. *Journal of Waterway, Port, Coastal, and Ocean Engineering*, 135(5):235–244, 2009.

[41] H. Dong and M. Li. A reconstructed central discontinuous Galerkin-finite element method for the fully nonlinear weakly dispersive Green–Naghdi model. *Applied Numerical Mathematics*, 110:110–127, 2016.

[42] V. Duchêne. Asymptotic shallow water models for internal waves in a two-fluid system with a free surface. *SIAM Journal on Mathematical Analysis*, 42(5):2229–2260, 2010.

[43] A. Duran and F. Marche. Discontinuous-Galerkin discretization of a new class of Green-Naghdi equations. *Commun.Comput. Phys.*, 17(3):721–760, 2015.

[44] A. Duran and F. Marche. A discontinuous Galerkin method for a new class of Green–Naghdi equations on simplicial unstructured meshes. *Applied Mathematical Modelling*, 45:840–864, 2017.

[45] D. Dutykh, D. Clamond, P. Milewski, and D. Mitsotakis. Finite volume and pseudo-spectral schemes for the fully nonlinear 1D Serre equations. *European Journal of Applied Mathematics*, 24(5):761–787, 2013.

[46] M. Ehrhardt. *Discrete artificial boundary conditions*. PhD thesis, Technische Universität Berlin, 2001.

[47] M. Ehrhardt. Absorbing boundary conditions for hyperbolic systems. *Numer. Math. Theor. Meth. Appl.*, 3(3):295–337, 2010.

[48] B. Engquist and A. Majda. Absorbing boundary conditions for the numerical simulation of waves. *Math. Comput*, 31:629–651, 1977.

[49] N. Favrie and S. Gavrilyuk. A rapid numerical method for solving Serre–Green–Naghdi equations describing long free surface gravity waves. *Nonlinearity*, 30(7):2718–2736, 2017.

[50] A. G. Filippini, M. Kazolea, and M. Ricchiuto. A flexible genuinely nonlinear approach for nonlinear wave propagation, breaking and run-up. *J. Comp. Phys.*, 310:381–417, 2016.

[51] J. C. Freeman and B. Le Méhauté. Wave breakers on a beach and surges on a dry bed. *J. Hydr. Engre.*, 90(2):187–216, 1964.

[52] H. Fuchs and W. H. Hager. Solitary impulse wave transformation to overland flow. *J. Wtrwy., Port, Coast., and Oc. Engrg.*, 141(5):237–246, 2015.

[53] S. Gavrilyuk. *Variational models and methods in solid and fluid mechanics. CISM Courses and Lectures*, volume 535. Springer, 2011. (ed. F. dell'Isola and S. Gavrilyuk).

[54] S. L. Gavrilyuk, N. I. Makarenko, and S. V. Sukhinin. *Waves in Continuous Media*. Springer International Publishing, 2017.

[55] D. Givoli. High-order local non-reflecting boundary conditions: A review. *Wave Motion*, 39:319–326, 2004.

[56] S. K. Godunov and E. I. Romenskii. *Elements of Continuum Mechanics and Conservation Laws.* Springer, 2003.

[57] A. E. Green and P. M. Naghdi. A derivation of equations for wave propagation in water of variable depth. *J. Fluid Mech.*, 78(2):237–246, 1976.

[58] S. T. Grilli, I. A. Svendsen, and R. Subramanya. Breaking criterion and characteristics for solitary waves on slopes. *J. Waterw. Port Coast.*, 123:102–112, 1997.

[59] H. J. Hafsteinsson, F. M. Evers, and W. H. Hager. Solitary wave run-up: wave breaking and bore propagation. *J. Hydraulic Res.*, 55(6):237–246, 2017.

[60] T. Hagstrom. Asymptotic Expansions and Boundary Conditions for Time-Dependent Problems. *SIAM J. Numer. Anal.*, 23(5):948–958, 1986.

[61] K. L. Heitner and G. W. Housner. Numerical model for tsunami runup. *J. Wtrwy., Port, Coast., and Oc. Engrg.*, 96:701–719, 1970.

[62] S. Hibbert and D. H. Peregrine. Surf and runup on a beach: a uniform bore. *J. Fluid Mech.*, 95:323–345, 1979.

[63] C. Higgins, M. B. Parlange, and C. Meneveau. *Atmospheric turbulence and mesoscale meteorology*, chapter Energy dissipation in large-eddy simulation: dependence on flow structure and effects of eigenvector alignments., pages 51–69. Cambridge University Press. Cambridge., 2004. (ed. E. Fedorovich, R. Rotunno & B. Stevens).

[64] S. C. Hsiao, T. W. Hsu, T. C. Lin, and Yu H. Chang. On the evolution and run-up of breaking solitary waves on a mild sloping beach. *Coast. Engrg*, 55(12):975–988, 2008.

[65] M. Israeli and S. A. Orszag. Approximation of radiation boundary conditions. *J. Comp.Phys.*, 41:115–135, 1981.

[66] T. Iwasaki and H. Togashi. On the shoreline and leading front conditions of tsunami waves in the light of the method of characteristic. *Coast. Engrg. in Japan*, 13:113–125, 1970.

[67] S. Jin and Z. Xin. The relaxation schemes for systems of conservation laws in arbitrary space dimensions. *Communications on Pure and Applied Mathematics*, 48(3):235–276, 1995.

[68] E. I. Jury. *Theory and Application of the Z-Transform Method.* Wiley & Sons, New York, 1964.

[69] M. Kazolea, A. I. Delis, and C. E. Synolakis. Numerical treatment of wave breaking on unstructured finite volume approximations for extended Boussinesq-type equations. *J. Comput. Phys.*, 271:281–305, 2014.

[70] M. Kazolea and M. Ricchiuto. On wave breaking for Boussinesq-type models. *Ocean Modelling*, 123:16–39, 03 2018.

[71] A. B. Kennedy, J. T. Kirby, Q. Chen, and R. A. Dalrymple. Boussinesq-type equationswith improved nonlinear performance. *Wave Motion*, 33:225–243, 2001.

[72] O. Kimmoun and H. Branger. A particle image velocimetry investigation on laboratory surf-zone breaking waves over a sloping beach. *J. Fluid Mech.*, 588:353–397, 2007.

[73] J. T. Kirby, G. Wei, Q. Chen, and A. B. Kennedy. FUNWAVE 1.0: fully nonlinear Boussinesq wave model: Documentation and user's manual. *RA Dalrymple research report NO. CACR-98-06*, 1998.

[74] N. Kobayashi, D. T. Cox, and A. Wurjanto. Irregular wave reflection and run-up on rough impermeable slopes. *J. Wtrwy., Port. Coast. and Dc. Engrg.*, 116(6):708–726, 1990.

[75] N. Kobayashi, G. S. DeSilva, and K. Wattson. Wave transformation and swash oscillations on gentle and steep slopes. *J. Geophys. Res.*, 94(CI):951–966, 1989.

[76] N. Kobayashi, A. K. Otta, and I. Roy. Wave reflection and runup on rough slopes. *J. Wtrwy., Port, Coast. and Dc. Engrg.*, 113(3):282–298, 1987.

[77] A. N. Kolmogorov. The local structure of turbulence in incompressible viscous fluids for very large Reynolds numbers. *Dokl. Akad. Nauk SSSR*, 30:299–303, 1941.

[78] A. N. Kolmogorov. The equations of turbulent motion in an incompressible fluid. *Izvestia Akad. Sci. USSR Phys.*, 6:56–58, 1942.

[79] H. Lamb. *Hydrodynamics.* Cambridge University Press, 1932.

[80] L. D. Landau and E. M. Lifshitz. *Fluid mechanics. (translated from russian by Sykes, J.B. and Reid, W. H.).* Pergamon Press, 1959(reprinted 1975).

[81] D. Lannes. *The water waves Problem, Mathematical Analysis and Asymptotics.* Mathematical surveys and monographs. American Mathematical Society, 2013.

[82] D. Lannes and P. Bonneton. Derivation of asymptotic two-dimensional time-dependent equations for surface water wave propagation. *Physics of Fluids*, 21, 2009.

[83] D. Lannes and F. Marche. A new class of fully nonlinear and weakly dispersive Green–Naghdi models for efficient 2D simulations. *J. Comp. Phys.*, 282:238–268, 2015.

[84] D. Lannes and F. Marche. Nonlinear wave–current interactions in Shallow Water. *Studies in applied mathematics*, 136(4):382–423, 2016.

[85] J. W. Lavelle and W. C. Thacker. A pretty good sponge: Dealing with open boundaries in limited-area ocean models. *Ocean Modelling*, 20:270–292, 2008.

[86] O. Le Metayer, S. Gavrilyuk, and S. Hank. A numerical scheme for the Green–Naghdi model. *J. Comp. Phys.*, 229(6):2034–2045, 2010.

[87] N. N. Lebedev. Special Functions and their Applications. *Selected Russian Publications in the Mathematical Sciences*, 1965. Prentice–Hall.

[88] R. J. Leveque. *Finite-Volume Methods for Hyperbolic Problems.* Cambridge Texts in Applied Mathematics, 2002.

[89] D. K. Lilly. The representation of small-scale turbulence in numerical simulation experiments. In *IBM Scienthic Computing Symp. on Environmental Sciences (ed. H. H.Goldstine)*, pages 195–210. Yorktown Heights, NY:IBM, 1967.

[90] P. Lin and P. L.-F. Liu. A numerical study of breaking waves in the surf zone. *J. Fluid Mech.*, 359:239–264, 1998.

[91] P. L.-F. Liu, C. E. Synolakis, and H. H. Yeh. Report on international workshop on long-wave run-up. *J. Fluid Mech.*, 229:675–688, 1991.

[92] P. A. Madsen, R. Murray, and O. R. Sorensen. A new form of the Boussiensq equations with improved linear dispersion characteristics. *Coastal Engineering*, 15:371–388, 1991.

[93] P. A. Madsen and H. A. Schäffer. A review of Boussinesq-type equations for surface gravity waves. *Advances in Coastal and Ocean Engineering*, 5:1–94, 1999.

[94] P. A. Madsen and O. R. Sorensen. A new form of the Boussinesq equations with improved linear dispersion characteristics. Part II: A slowly varying bathymetry. *Coast. Engrg.*, 18:183–204, 1992.

[95] P. A. Madsen, O. R. Sorensen, and H. A. Schäffer. Surf zone dynamics simulated by a Boussinesq-type model. Part I: Model description and cross-shore motion of regular waves. *Coast. Engrg.*, 32:255–287, 1997.

[96] A. Majda and S. Osher. Reflection of singularities at the boundary. *Communications on Pure and Applied Mathematics*, 28(4):479–499, 1975.

[97] N. Makarenko. A second long-wave approximation in the Cauchy–Poisson problem (in russian). *Dyn. Contin. Media*, 77:56–72, 1986.

[98] R. E. Meyter and A. D. Taylor. Waves on Beaches and Resulting Sediment Transport. *New York: Academic Press.*, pages 357–411, 1972.

[99] M.H. Alford, T. Peacock, J.A. Mackinnon, J. D. Nash, M.C. Buijsman et *al.* The formation and fate of internal waves in the South China Sea. *Nature*, 521:65, April 2015.

[100] E. Mignot and R. Cienfuegos. On the application of a Boussinesq model to riverflows including shocks. *Coast. Eng*, 56:23–31, 2009.

[101] D. Mitsotakis, B. Ilan, and D. Dutykh. On the Galerkin/Finite-Element Method for the Serre Equations. *J. Sci. Comp.*, 61, 06 2014.

[102] D. Mitsotakis, C. Synolakis, and M. McGuinness. A modified Galerkin/finite element method for the numerical solution of the Serre-Green-Naghdi system. *International Journal for Numerical Methods in Fluids*, 83(10):755–778, 2016.

[103] R. E. Musumeci, I. A. Svendsen, and J. Veeramony. The flow in the surf zone: a fully nonlinear Boussinesq-type of approach. *Coast. Eng.*, 52:565–598, 2005.

[104] O. K. Nwogu. Alternative form of Boussinesq equations for near shore wave propagation. *J. Wtrwy., Port, Coast., and Oc. Engrg.*, 119(6):618–638, 1993.

[105] O. K. Nwogu. Numerical prediction of breaking waves and currents with a Boussinesq model. In Billy L. Edge, editor, *Coastal Engineering 1996, Proc. 25th Int. Conf.*, volume 25, pages 4807–4820, 1996.

[106] L. V. Ovsjannikov. Cauchy problem in a scale of Banach spaces and its application to the shallow water theory justification. *Appl. Meth. Funct. Anal. Probl. Mech. (IUTAM/IMUSymp.,Marseille, 1975), Lecture Notes in Mathematics*, 503:426–437, 1976.

[107] L. V. Ovsjannikov. *Lectures on the fundamentals of gas dynamics.* Nauka, Moscow, (in Russian), 1981.

[108] A. R. Packwood and D. H. Peregrine. Surf and runup on beaches: models of viscous effects. *Rep. AM-81-07, Univ. of Bristol*, 1981.

[109] N. Panda, C. Dawson, Y. Zhang, A. B. Kennedy, J. J. Westerink, and A. S. Donahue. Discontinuous Galerkin methods for solving Boussinesq–Green–Naghdi equations in resolving non-linear and dispersive surface water waves. *J. Comp. Phys.*, 273:572–588, 2014.

[110] M. Plancherel. Contribution à l'étude de la représentation d'une fonction arbitraire par les intégrales définies. *Math. Annalen*, 76:315–326, 1915.

[111] S. B. Pope. *Turbulent Flows.* Cambridge University Press. Cambridge., 2000.

[112] S. Popinet. A quadtree-adaptive multigrid solver for the Serre–Green–Naghdi equations. *J. Comp. Phys.*, 302:336–358, 2015.

[113] L. Prandtl. Über ein neues Formelsystem für die ausgebildete Turbulenz. *Nachr. Akad. Wiss. Göttingen Math-Phys.*, pages 6–19, 1945.

[114] J. W. S. Rayleigh. On waves. *Phil. Mag.*, 5:257–279, 1876.

[115] O. Reynolds. The Sub-Mechanics of the Universe. *Collected Papers*, 3, 1903.

[116] G. L. Richard and A. Duran. A new model of shoaling and breaking waves: Toward two dimensional applications. Unpublished.

[117] G. L. Richard and S. L. Gavrilyuk. A new model of roll waves : comparison with Brock's experiments. *J. Fluid Mech.*, 698:374–405, 2012.

[118] G. L. Richard and S. L. Gavrilyuk. The classical hydraulic jump in a model of shear shallow-water flows. *J. Fluid Mech.*, 725:492–521, 2013.

[119] G. L. Richard and S. L. Gavrilyuk. Modelling turbulence generation in solitary waves on shear shallow water flows. *J. Fluid Mech.*, 773:49–74, 2015.

[120] L. F. Richardson. *Weather prediction by numerical process.* Cambridge University-Press. Cambridge, 1922.

[121] J. S. Russell. Report on waves. *Br. Assoc. Adv. Sci.*, 14:311–390, 1844.

[122] R. Salmon. *Lectures on Geophysical Fluid Mechanics.* Oxford University Press, 1998.

[123] A. A. Samarskii and E. S. Nikolaev. *Numerical Methods for Grid Equations.* Birkhauser, 1989.

[124] F. Serre. Contribution á l'étude des écoulements permanents et variables dans les canaux. *Houille Blanche*, 6:830–872, 1953.

[125] F. Shi, J. T. Kirby, J. C. Harris, J. D. Geiman, and S. T. Grilli. A high-order adaptive time-stepping TVD solver for Boussinesq modeling of breaking waves and coastal inundation. *Ocean Modelling*, 43-44:36–51, 2012.

[126] J. Smagorinsky. General circulation experiments with the primitive equations: I. The basic equations. *Mon. Weather Rev.*, 91:99–164, 1963.

[127] J. J. Stocker. *Water Waves.* Interscience Publishers, New York, 1971.

[128] G. G. Stokes. On the theory of oscillatory waves. *Transactions of the Cambridge Philosophical Society*, 8:441–455, 1847.

[129] G. Strang. On the construction and comparison of difference schemes. *SIAM Journal on Numerical Analysis*, 5.3:506–517, 1968.

[130] C. H. Su and C. S. Gardner. Korteweg-de Vries equation and generalizations, III. Derivation of the Korteweg-de Vries equation and Burgers equation. *J. Math. Phys.*, 10:536–539, 1969.

[131] I. A. Svendsen. Mass flux and undertow in a surf zone. *Coastal Engineering*, 8(4):347–365, 1984.

[132] I. A. Svendsen and P. A. Madsen. A turbulent bore on a beach. *J. Fluid Mech.*, 148:73–96, 1984.

[133] I. A. Svendsen, K. Yu, and J. Veeramony. A Boussinesq breaking wave model with vorticity. *Proc., 25th Int. Conf. Coastal Engrg., ASCE*, 229:1192–1204, 1996.

[134] C. E. Synolakis. Discussion of "Wave Reflection and Run-Up on Rough Slopes" by N. Kobayashi, A. K. Otta, and I. Roy (May, 1987, Vol. 113, No. 4). *J. Wtrwy., Port. Coast. and Oc. Engrg.*, 115:139–143, 1989.

[135] C. E. Synolakis and J. E. Skjelbreia. Evolution of maximum amplitude of solitary waves on plane beaches. *Journal of Waterway, Port, Coastal, and Ocean Engineering*, 119(3):323–342, 1993.

[136] A. Taflove. *Advances in Computational Electrodynamics.* Artech House, 1998.

[137] V. M. Teshukov. Gas-dynamics analogy for vortex free-boundary flows. *J. Appl. Mech. Tech.Phys.*, 48(3):303–309, 2007.

[138] L. H. Thomas. Elliptic Problems in Linear Difference Equations over a Network. *Watson Sc. Comp. Lab. Rep.*, 1949.

[139] F. C. K. Ting. Large-scale turbulence under a solitary wave. *Coast. Eng.*, 53:441–462, 2006.

[140] M. Tissier, P. Bonneton, F. Marche, F. Chazel, and D. Lannes. A new approach to handle wave breaking in fully non-linear Boussinesq models. *Coastal Engineering*, 67:54–66, 2012.

[141] V. Titov and C. Synolakis. Modeling of Breaking and Nonbreaking Long-Wave Evolution and Runup Using VTCS-2. *J. Wtrwy., Port. Coast. and Dc. Engrg.*, pages 308–317, 1995.

[142] M. Tonelli and M. Petti. Simulation of wave breaking over complex bathymetries by a Boussinesq model. *Journal of Hydraulic Research*, 49(4):473–486, 2011.

[143] E. F. Toro. *Riemann solvers and numerical methods for fluid dynamics.* Springer,Berlin, 1997.

[144] J. Veeramony and I. A. Svendsen. The flow in surf-zone waves. *Coast. Eng.*, 39:93–122, 2000.

[145] A. Viviano, R. E. Musumeci, and E. Foti. A nonlinear rotational, quasi-2DH, numerical model for spilling wave propagation. *Applied Mathematical Modelling*, 39(3):1099–1118, 2015.

[146] G. Wei and J. Kirby. Time-dependent numerical code for extended Boussinesq equations. *J. Wtrwy., Port. Coast. and Oc. Engrg.*, 121:251–261, 1995.

[147] G. Wei, J. T. Kirby, S. T. Grilli, and R. Subramanya. A fully nonlinear Boussinesq model for surface waves. Part 1. Highly nonlinear unsteady waves. *J. Fluid Mech.*, 294:71–92, 1995.

[148] G. Wei, J. T. Kirby, and A. Sinha. Generation of waves in Boussinesq models using a source function model. *Coast. Engrg.*, 36:271–299, 1999.

[149] X. Wen, C. Zheng, and H. Han. Numerical Solution to a Linearized KdV Equation on Unbounded Domain. *Numer. Meth. Part. Diff. Eqs.*, 24:383–399, 2008.

[150] V. E. Zakharov. Stability of periodic waves of finite amplitude on the surface of a deepfluid. *J. Appl. Mech. Tech. Phys.*, 9:190–194, 1968.

[151] J. A. Zelt. The run-up of nonbreaking and breaking solitary waves. *Coast. Engrg.*, 15:205–246, 1991.

[152] Y. Zhang, A. B. Kennedy, A. S. Donahue, J. J. Westerink, N. Panda, and C. Dawson. Rotational surf zone modeling for $O(\mu^4)$ Boussinesq-Green-Naghdi systems. *Ocean Model.*, 79:43–53, 2014.

[153] Y. Zhang, A. B. Kennedy, N. Panda, C. Dawson, and J. J. Westerink. Generating–absorbing sponge layers for phase-resolving wave models. *Coastal Engineering*, 84:1 – 9, 2014.

[154] B. B. Zhao, W. Y. Duan, and R. C. Ertekin. Application of higher-level GN theory to some wave transformation problems. *Coastal Engineering*, 83:177–189, 2014.

[155] A. Zisowsky. *Discrete Transparent Boundary Conditions for Systems of Evolution Equations*. PhD thesis, Technische Universität Berlin, 2004.